



HAL
open science

Tectonostratigraphic evolution of the Western Niger Delta from the Cretaceous to Present

Kelvin Ikenna Chima

► **To cite this version:**

Kelvin Ikenna Chima. Tectonostratigraphic evolution of the Western Niger Delta from the Cretaceous to Present. Tectonics. Sorbonne Université, 2020. English. NNT : 2020SORUS053 . tel-03793820

HAL Id: tel-03793820

<https://theses.hal.science/tel-03793820>

Submitted on 2 Oct 2022

HAL is a multi-disciplinary open access archive for the deposit and dissemination of scientific research documents, whether they are published or not. The documents may come from teaching and research institutions in France or abroad, or from public or private research centers.

L'archive ouverte pluridisciplinaire **HAL**, est destinée au dépôt et à la diffusion de documents scientifiques de niveau recherche, publiés ou non, émanant des établissements d'enseignement et de recherche français ou étrangers, des laboratoires publics ou privés.



TECTONOSTRATIGRAPHIC EVOLUTION OF THE WESTERN NIGER DELTA FROM THE CRETACEOUS TO PRESENT

Thesis submitted for the degree of Doctor of Philosophy of the Sorbonne Université

By

Kelvin Ikenna CHIMA

Institut des Sciences de La Terre de Paris (IStEP),
Sorbonne Université, Paris

Advisers: Prof. Christian Gorini, Prof. Marina Rabineau and Dr. Didier Granjeon

Date of defence: 30th September, 2020.

Before the jury composed of:

| | | |
|--------------------------|--------------------------|----------------------|
| Prof. Andrea Moscariello | (University of Geneva) | (Rapporteur) |
| Prof. Thierry Mulder | (University of Bordeaux) | (Rapporteur) |
| Dr. Sylvie Leroy | (Sorbonne Université) | (President de jury) |
| Dr. Vincent Riboulot | (IFREMER) | (Examineur) |
| Dr. Nick Hoggmascall | (Shell Brunei) | (Guest Invité) |
| Dr. Patrick Zaugg | (Total Nigeria) | (Guest Invité) |
| Prof. Christian Gorini | (Sorbonne Université) | (Directeur de thèse) |
| Dr. Estelle Leroux | (IFREMER) | (Tuteur) |
| Dr. Damien Do Couto | Sorbonne Université) | (Tuteur) |

THESIS DECLARATION

I certify that this thesis is my original work and was carried out under the supervisions of Prof. Christian Gorini, Prof. Marina Rabineau and Dr. Didier Granjeon with the help of Dr. Estelle Leroux and Dr. Damien Do Couto. Full citation and adequate referencing of previous works have been provided throughout the thesis. No part of this work has been previously submitted to this or any other academic institution for a degree or diploma, or any other qualification.

COPYRIGHT

The copyright of this thesis rests with the author and is made available under a Creative Commons Attribution Non-Commercial No Derivatives licence. Researchers are free to copy, distribute or transmit the thesis on the condition that they attribute it, that they do not use it for commercial purposes and that they do not alter, transform or build upon it. For any reuse or redistribution, researchers must make clear to others the licence terms of this work.

DEDICATION

This thesis is dedicated to God Almighty for His unmerited grace and favours all through the course of this research.

Lack of self-confidence is a prerequisite for the infection FEAR, which if not conquered early enough, is capable of shattering dreams and aspirations...Kelvin Ikenna Chima.

ACKNOWLEDGEMENTS

I would like to thank my academic advisers, collaborators and industrial mentors for their support and contributions towards the success of this research. Prof. Christian Gorini (Sorbonne Université), for his innovative ideas in seismic stratigraphy and sequence cyclicity. Prof. Marina Rabineau (CNRS/UBO/UBS), for enlightening discussions and contributions in sequence stratigraphy and sequence cyclicity. Dr. Didier Granjeon (IFPEN), for invaluable discussions, support in sedimentation rate estimation and swift responses/feedbacks. Dr. Silvia Gardin (UMR), for professional coaching in biostratigraphic analysis and interpretation. Dr. Estelle Leroux (IFREMIER), for her guidance in seismic stratigraphy, sequence cyclicity as well as thorough and prompt feedbacks. Dr. Damien Do Couto (Sorbonne Université), for his assistance in 3D seismic geomorphology and software skills. Dr. Nick Hoggmascall (Shell Brunei), for his invaluable support, mentorship, insightful discussions/feedbacks and assistance in data access. Dr. Miguel Mora-Glukstad for insightful discussions and assistance in velocity modelling and time-depth conversions of seismic lines and interpretations. Dr. Jean Letouzey (Sorbonne Université), for his coaching on structural interpretations and parental support. Mr. Alexandre Lethiers and Mr. Philippe Resson (Sorbonne Université) are thanked for their assistance in the preparation of some figures and Information Technology (IT) support respectively.

I am indebted to the Federal Republic of Nigeria for funding this research under the auspice of the Petroleum Technology Development Fund (PTDF) Scholarship Scheme. I am ever grateful to Shell Nigeria Exploration Companies (SNEPCo) and Shell Exploration and Production Companies (SPDC), not only for graciously providing data, but also the permission to publish this study.

I am grateful to the members of the examination committee: Prof. Andrea Moscariello (University of Geneva), Prof. Thierry Mulder (University of Bordeaux), Prof. Christian Gorini (Sorbonne Université), Dr. Sylvie Leroy (Sorbonne University), Dr. Vincent Riboulot (IFREMIER), Dr. Patrick Zaugg (Total) and Dr. Damien Do Couto (Sorbonne University), whose valuable comments, helped to improve the scientific content of this research.

Remy Deschamps and Vincent Riboulot are thanked for chairing the PhD progress committee (comité de suivi) in 2018 and 2019, respectively, and providing valuable suggestions that helped to improve and focus this research. I would also like to express my gratitude to Prof. Bilal U. Haq (visiting Professor of the Sorbonne Université), for enlightening discussions in the

course this research. I am indebted to the management of Alex Ekwueme Federal University Nudfu-Alike Ikwo (AE-FUNAI), Ebonyi State, Nigeria for granting me study leave to undertake this research.

Many thanks to Mr. Olusegun Obilaja, Mrs. Adekemi Afolayan, Mr. Babatope Atitebi (SNEPCo), Mr. Richard Streatfield and Mr. Timi Tralagba (SPDC), for their great assistance in data access.

My profound gratitude goes to Colette, Izzy, Rosie and Billy Hogmascall, as well as Dominique and Maryvonne Preteseille for their warm friendship and support during this research.

This journey would not have been easy without the friendship and support of ISTE^P colleagues and friends: Alberto M. Cruz, Julien Danzelle, Roohola N. Rad, Dia Ninkabou, Camille Godbillot, Elijah N. Nkitnam, Thomas Munier, Sepideh Pajan, Sylvain Gartel and Guillaume Charbonnier. A big thanks for all the apéros, memorable *déjeuners* and *team GUIGUI*.

And off course (*pourquoi pas?*), to all my ERASMUS, Collège Néerlandais and Cite Universitaire de Paris friends, thank you for your warmth companionship. I remember with great nostalgia those awesome moments that we shared together.

To my fellow countrymen and women, whom our parts crossed in Paris, Europe and America (Gloria I. Ngene, Ugochukwu Onwudebelu, Igwe M. Nweke, Agwu J. Abuchi, Ikenna C. Okwara, Adekunle Ajayi, Muhammadu Sabiu, Ebenge Usip, Benjamin Eboh, Chigozie O. Ochulor and many others too numerous to be listed here), thank you for your support and encouragement. I wish you good luck in your research and future endeavours.

The last but not the list, I would like to thank in a very special way my beloved family for her endearing love and support, which greatly inspired me throughout the period of this research.

EXTENDED SUMMARY

Located in the Gulf of Guinea along the equatorial Atlantic margin of West Africa, the Niger Delta is the twelfth largest petroleum province in the world. The unique geodynamical and stratigraphic setting of the Cenozoic Niger Delta has continued to attract both the industry and the academia over the past 6 decades as a natural laboratory to study (i) regional/global climate dynamics; (ii) sea-level variation (iii); gravity-tectonics; (iv) sediment supply etc., that control the geometry of a large progradational delta located on a passive margin.

Regional seismic interpretation, calibrated with well data and detailed 3D seismic geomorphological analysis, allowed me to investigate in detail the tectonostratigraphic evolution of the western Niger Delta from the Cretaceous to present as summarised below.

Paleo-topographies associated with (i) the Fernando Po, (ii) the Charcot and (iii) Chain Fracture Zones, developed during the Cretaceous oceanic spreading of the South Atlantic, controlled the geometry of the Niger Delta from the Cretaceous to the Serravallian, acting as sediment transfer zones. However, delta top tectonostratigraphic processes controlled the architectural evolution of the margin from the Serravallian to present.

Tilting of the western Niger Delta early during its evolution in the Cretaceous, resulted in the development of basin centre-dipping regional seismic surface, which facilitated sedimentary wedge deformation mainly by gravity gliding from the Cretaceous to the Serravallian. An overall increase in sedimentation rates occurred in the western Niger Delta onwards from the Serravallian to the Pliocene and most of the Pleistocene, favouring sedimentary wedge deformation by gravity spreading.

The extensional, translational and contractional zones of the western Niger Delta, evolved through time and space in response to variation in sedimentation and gravity collapse of sedimentary the wedge. Overall low sedimentary wedge deformation over the late Eocene-Serravallian, probably marks the period, when the defunct extensional zone was located up-dip in the onshore. However, the overall increase in delta wedge deformation from the Tortonian to the Pliocene-Pleistocene, mark the basinward migration of the extensional and the contractional zones, probably in response to the overall increase in sedimentation over the Pliocene and the Pleistocene.

Previous studies opined that mobile shales in the Niger Delta initiated during the late Miocene and were buried during the Pliocene. However, this research shows that mobile shales

have been active in the western Niger Delta for at least the Burdigalian, and controlled submarine channels morphology, distribution and depositional patterns up to the Pliocene and the Pleistocene. Two major types of mass-transport deposits were identified on the western Niger Delta slope (i) regional MTDs that are generally triggered by failures at the shelf margin/upper slopes, and (ii) local MTDs that are generally derived from mobile shales.

The Pliocene and Pleistocene stratigraphy of the western Niger Delta intraslope basins were controlled by the interplay between allocyclic forcing linked to glacio-eustatic sea-level oscillations and basin tectonics associated with shale tectonics. Shale tectonics was generally more active in the Pliocene and the middle Pleistocene

The Pliocene and Pleistocene stratigraphy of the western Niger Delta intraslope basins were controlled by orbital (Milankovich) forcing of 400 ka and 100 ka eccentricity over the Messinian-middle Pleistocene and the middle Pleistocene-present respectively.

The dominance of actively subsiding basinward dipping normal faults on the western Niger Delta continental shelf since the early Pliocene facilitated the overall increase in sediment thickness within the extensional zone. Despite the relatively lower sedimentation rates estimated on the western Niger Delta continental shelf and slope regions since the early Pliocene, the overall increase in gravity collapse/accommodation, sediment thickness and distribution from the shelf to the deep basin, suggest an overall increase in sedimentation in this region. However, in the eastern Niger Delta, the actively subsiding counter regional normal faults and inferred delta lobe migration are thought to have contributed to the ongoing reduction in sedimentation notably in the deep basin since the Pleistocene. Given the spatio-temporal variation in gravity deformation and sediment partitioning across the western and the eastern Niger Delta since the early Pliocene, a more regional seismic and well data are needed for a complete source-to-sink (isopach mapping) of the former for a more quantitative comparison of these regions.

This PhD research not only improves our understanding of the tectonostratigraphic evolution of the western Niger Delta, highlighting the complex structural and stratigraphic trapping styles notably in the underexplored deepwater systems, but also shows the presence of syn-rift deposits that may host the Cretaceous-Paleogene petroleum play in the offshore western Niger Delta.

TABLE OF CONTENTS

| | | | | | | | | | | | |
|--|---|---|---|---|---|---|---|---|---|---|-----|
| THESIS DECLARATION | - | - | - | - | - | - | - | - | - | - | i |
| COPYRIGHT | - | - | - | - | - | - | - | - | - | - | ii |
| DEDICATION | - | - | - | - | - | - | - | - | - | - | iii |
| ACKNOWLEDGEMENT | - | - | - | - | - | - | - | - | - | - | iv |
| EXTENDED SUMMARY | - | - | - | - | - | - | - | - | - | - | vi |
| LIST OF FIGURES | - | - | - | - | - | - | - | - | - | - | xiv |
| LIST OF TABLES | - | - | - | - | - | - | - | - | - | - | xxv |
| | | | | | | | | | | | |
| General Introduction, Aim and Thesis Structure | - | - | - | - | - | - | - | - | - | - | 1 |
| | | | | | | | | | | | |
| Chapter 1 | - | - | - | - | - | - | - | - | - | - | 4 |
| GEODYNAMICAL AND SEDIMENTOLOGICAL SETTING | | | | | | | | | | | |
| 1.1 Geodynamical setting | - | - | - | - | - | - | - | - | - | - | 5 |
| 1.1.1 Evolution of the Niger catchment | - | - | - | - | - | - | - | - | - | - | 6 |
| 1.1.2 Gravity tectonics | - | - | - | - | - | - | - | - | - | - | 9 |
| 1.2. Sedimentological setting | - | - | - | - | - | - | - | - | - | - | 11 |
| 1.2.1 Lithostratigraphic successions | - | - | - | - | - | - | - | - | - | - | 11 |
| 1.2.2 Niger Delta and shale tectonics | - | - | - | - | - | - | - | - | - | - | 13 |
| 1.2.3 Sediment budget of the Niger Delta- | - | - | - | - | - | - | - | - | - | - | 15 |
| 1.2.4 Deepwater Sedimentation | - | - | - | - | - | - | - | - | - | - | 18 |
| 1.2.4.1 Mass-transport deposits | - | - | - | - | - | - | - | - | - | - | 18 |
| 1.2.4.2 Turbidity current | - | - | - | - | - | - | - | - | - | - | 18 |
| 1.2.4.3 Slope equilibrium profile, control on submarine channels and depositional patterns | - | - | - | - | - | - | - | - | - | - | 20 |
| - | - | - | - | - | - | - | - | - | - | - | 20 |
| | | | | | | | | | | | |
| Chapter 2 | - | - | - | - | - | - | - | - | - | - | 23 |
| SEISMIC STRATIGRAPHY AND DEPOSITIONAL ARCHITECTURE OF NEOGENE INTRASLOPE BASINS, OFFSHORE WESTERN NIGER DELTA | | | | | | | | | | | |
| 2.1 Introduction | - | - | - | - | - | - | - | - | - | - | 25 |

| | | | | | | | | | | |
|--|---|---|---|---|---|---|---|---|---|----|
| 2.2. Geological setting | - | - | - | - | - | - | - | - | - | 26 |
| 2.3. Dataset and methods | - | - | - | - | - | - | - | - | - | 29 |
| 2.3.1 Dataset | - | - | - | - | - | - | - | - | - | 29 |
| 2.3.1.1 Seismic data | - | - | - | - | - | - | - | - | - | 30 |
| 2.3.1.2 Borehole data | - | - | - | - | - | - | - | - | - | 30 |
| 2.3.2 Methods | - | - | - | - | - | - | - | - | - | 30 |
| 2.3.2.1 Seismic and sequence stratigraphic analysis | - | - | - | - | - | - | - | - | - | 30 |
| 2.3.2.2 Well logs, lithofacies and depositional environment | - | - | - | - | - | - | - | - | - | 31 |
| 2.3.2.3 Bio- and chronostratigraphic analyses | - | - | - | - | - | - | - | - | - | 33 |
| 2.3.2.4 3D Seismic geomorphology | - | - | - | - | - | - | - | - | - | 33 |
| 2.4 Results and interpretation | - | - | - | - | - | - | - | - | - | 33 |
| 2.4.1 Seismic facies analysis and seismic stratigraphic units | - | - | - | - | - | - | - | - | - | 34 |
| 2.4.1.1 Seismic facies analysis | - | - | - | - | - | - | - | - | - | 34 |
| 2.4.1.2 Seismic stratigraphic units | - | - | - | - | - | - | - | - | - | 34 |
| 2.4.2 Lithofacies and depositional environment | - | - | - | - | - | - | - | - | - | 40 |
| 2.4.3 Bio-chronostratigraphic analyses and correlation with seismic data | - | - | - | - | - | - | - | - | - | 40 |
| 2.4.4. 3D seismic geomorphology and depositional architecture | - | - | - | - | - | - | - | - | - | 46 |
| 2.5. Discussion | - | - | - | - | - | - | - | - | - | 50 |
| 2.5.1 Interaction between shale tectonics and submarine channel complex | - | - | - | - | - | - | - | - | - | 51 |
| 2.5.2 Reservoir distribution in filled ponded basins | - | - | - | - | - | - | - | - | - | 56 |
| 2.5.3 Shale tectonics vs MTD types and distribution | - | - | - | - | - | - | - | - | - | 57 |
| 2.5.4 Control of depositional systems in filled ponded basins | - | - | - | - | - | - | - | - | - | 58 |
| 2.6 Conclusions of Chapter 2 | - | - | - | - | - | - | - | - | - | 60 |

Chapter 3 - - - - - 61

PLIOCENE AND PLEISTOCENE STRATIGRAPHIC EVOLUTION OF THE WESTERN
NIGER DELTA INTRASLOPE BASINS: A RECORD OF GLACIO-EUSTATIC SEA-LEVEL
AND BASIN TECTONIC FORCINGS

3.1 Introduction - - - - - 63

3.2 Regional Setting - - - - - 65

3.3 Dataset and Methods - - - - - 67

3.3.1 Dataset - - - - - 67

3.3.1.1 Seismic data - - - - - 67

3.3.1.2 Well data - - - - - 69

3.3.2 Methods - - - - - 69

3.3.2.1 Seismic stratigraphy - - - - - 69

3.3.2.2 3D seismic geomorphology - - - - - 69

3.3.2.3 Allostratigraphic partitioning and dating of the Pliocene and the Pleistocene
stratigraphy - - - - - 70

3.4 Results and Interpretations - - - - - 70

3.4.1. Seismic facies analysis - - - - - 70

3.4.2 Facies association - - - - - 71

3.4.3 Mobile shale, Mud volcanoes and Bottom Simulating Reflector (BSR) - - - - - 72

3.4.4 3D seismic geomorphology and sedimentary architecture - - - - - 75

3.4.4.1 Lower part of SS1 (horizon A) - - - - - 75

3.4.4.2 Middle part of SS1 (horizons G and I) - - - - - 76

3.4.4.3 Upper part of SS1 (horizon K) - - - - - 79

| | | | | | | | | | | |
|--|---|---|---|---|---|---|---|---|---|-----|
| 3.4.4.4 Base of SS2 (horizon P) | - | - | - | - | - | - | - | - | - | 81 |
| 3.4.4.5 Middle part of SS2 (horizon R) | - | - | - | - | - | - | - | - | - | 84 |
| 3.4.4.6 Upper part of SS2 (horizons V and W) | - | - | - | - | - | - | - | - | - | 86 |
| 3.4.5 Sequence stratigraphic interpretation and age assignment (SS2) | - | - | - | - | - | - | - | - | - | 93 |
| 3.4.6 Sequence stratigraphic interpretation (SS1)- | - | - | - | - | - | - | - | - | - | 93 |
| 3.4.7 Sequence set duration and sedimentation rates | - | - | - | - | - | - | - | - | - | 94 |
| 3.5 Discussion- | - | - | - | - | - | - | - | - | - | 95 |
| 3.5.1 Allocyclic (glacio-eustatic) sea-level forcing | - | - | - | - | - | - | - | - | - | 95 |
| 3.5.2 Basin tectonics | - | - | - | - | - | - | - | - | - | 97 |
| 3.5.3 Depositional model | - | - | - | - | - | - | - | - | - | 99 |
| 3.5.3.1 Forced regression | - | - | - | - | - | - | - | - | - | 100 |
| 3.5.3.2 Early lowstand | - | - | - | - | - | - | - | - | - | 100 |
| 3.5.3.3 Late lowstand/early transgression | - | - | - | - | - | - | - | - | - | 100 |
| 3.5.3.4 Late transgression/Highstand | - | - | - | - | - | - | - | - | - | 102 |
| 3.6 Conclusions of Chapter 3 | - | - | - | - | - | - | - | - | - | 103 |
| Chapter 4 | - | - | - | - | - | - | - | - | - | 105 |
| Tectonostratigraphic evolution of the western Niger Delta since the Cretaceous: Implication of paleo-topographies and delta top tectonostratigraphic dynamics on gravity deformation of the margin | | | | | | | | | | |
| 4.1 Introduction | - | - | - | - | - | - | - | - | - | 107 |
| 4.2 Gravity tectonics | - | - | - | - | - | - | - | - | - | 110 |
| 4.3 Data and methodology | - | - | - | - | - | - | - | - | - | 111 |

| | | | | | | | | | |
|--|---|---|---|---|---|---|---|---|------|
| 4.3.1 Seismic and well data | - | - | - | - | - | - | - | - | -112 |
| 4.3.2 Methodology | - | - | - | - | - | - | - | - | -112 |
| 4.3.2.1 Seismic stratigraphy | - | - | - | - | - | - | - | - | -112 |
| 4.3.2.2 Sedimentation rates estimation | - | - | - | - | - | - | - | - | -113 |
| 4.4 Results and observation | - | - | - | - | - | - | - | - | -114 |
| 4.4.1 Tectonostratigraphic units | - | - | - | - | - | - | - | - | -114 |
| 4.4.1.1 The Cretaceous-late Eocene Unit | - | - | - | - | - | - | - | - | -116 |
| 4.4.1.2 The late Eocene-Serravallian | - | - | - | - | - | - | - | - | -123 |
| 4.4.1.3 The Serravallian-Tortonian (12.8 Ma-9.5 Ma). | - | - | - | - | - | - | - | - | -125 |
| 4.4.1.4 The Tortonian-Pliocene Unit (9.5-4.9 Ma) | - | - | - | - | - | - | - | - | -126 |
| 4.4.1.5 The Pliocene-middle Pleistocene Unit (4.9 to ~1 Ma) | - | - | - | - | - | - | - | - | -131 |
| 4.4.1.6 The middle Pleistocene-present (~1-0 Ma) | - | - | - | - | - | - | - | - | -133 |
| 4.5 Sedimentation rates (shelf and slope regions) | - | - | - | - | - | - | - | - | -134 |
| 4.5.1 Sedimentation rate (shelf region) | - | - | - | - | - | - | - | - | -134 |
| 4.5.2 Sedimentation rate (slope region) | - | - | - | - | - | - | - | - | -134 |
| 4.6 Discussion- | - | - | - | - | - | - | - | - | -135 |
| 4.6.1 Tectonostratigraphic evolution of the western Niger Delta- | - | - | - | - | - | - | - | - | 136 |
| 4.6.2 Controls of paleo-topography and delta top tectonostratigraphic dynamics on gravity deformation of the western Niger Delta | - | - | - | - | - | - | - | - | -141 |
| 4.6.3 Pliocene and Pleistocene stratigraphy of the western vs eastern Niger Delta | - | - | - | - | - | - | - | - | -141 |
| 4.7 Conclusions of Chapter 4 | - | - | - | - | - | - | - | - | -144 |
| Chapter 5 | - | - | - | - | - | - | - | - | -147 |

GENERAL CONCLUSIONS, LIMITATIONS AND PERSPECTIVES

| | | | | | | | | | |
|--------------------------|---|---|---|---|---|---|---|---|------|
| 5.1 General conclusions | - | - | - | - | - | - | - | - | 147 |
| 5.2 Research limitations | - | - | - | - | - | - | - | - | -149 |
| 5.3 Perspectives | | | | | | | | - | -149 |
| References cited | - | - | - | - | - | - | - | - | -150 |
| Appendix | - | - | - | - | - | - | - | - | -171 |

LIST OF FIGURES

- 1.1.** Superposed regional relief and bathymetric maps of Niger Delta, illustrating the main physiographic features, structural zones and sedimentary wedges (explained in detail in the next section). Inset map at the top right corner shows the location of the Niger Delta in the Gulf of Guinea (modified after Morley and Guerin, 1996). - - - - - 3
- 1.2.** Paleotectonic map of the African and South American rift systems at (ca 120 Ma) during the break-up of the African and South American plates. Note the location of the future Niger Delta in the equatorial Atlantic (modified after Frizon de la Motte *et. al.*, 2015). - - - 5
- 1.3.** The West African relief showing the modern Niger catchment (dashed white line). Rivers are indicated in black lines, that are dashed, where aridified (modified after Chardon *et al.*, 2016). 7
- 1.4.** Schematic illustration of the evolution of the West African relief: Mid-Eocene (~45 Ma) is a period of tectonic quiescence, characterized by maximum flooding of paleomarginal upwarp, which marked the continental divide; the late Eocene-early Oligocene (~34-29 Ma) is characterized by the Hoggar uplift, the establishment of the modern Niger catchment and an increase in sediment supply to alluvial fans on the Hoggar's piedmont and the Niger Delta; the Quaternary is characterized by the incision of alluvial fans, decrease in slopes of the High Niger and Sourou Rivers following the deposition of inland deltas, and eventual capture of the later by the Volta River (modified after Chardon *et al.*, 2016). - - - - - 8
- 1.5.** Schematic diagram illustrating gravity spreading and gravity gliding. (A) Gravity gliding down an inclined slope on a thin detachment; (B) Sediment loading causing gravity spreading above a thick detachment zone on a flat detachment surface; (C) Mixed gravity spreading and gravity gliding above a thick décollement zone with onshore and offshore dipping detachment surfaces (modified after Morley *et al.*, 2011). - - - - - 10
- 1.6.** Structural map of the Niger Delta. (A) Schematic illustration of the extensional, transitional and compressional zones of the Niger Delta. Note the distribution of coastal rivers/tidal channels

across the shoreline from east to west; (B) Seismic line drawing (X-Y) along the depositional dip showing the structural and stratigraphic styles from the shallow offshore to deep basin (redrawn after Corredor *et al.*, 2005). - - - - - 12

1.7. Schematic illustration of the lithostratigraphic units underlying the Niger Delta (left). Deepwater seismic reflection data showing the reflection patterns of the Agbada and Akata Formations (right) (modified after Corredor *et al.*, 2005). - - - - - 14

1.8. Physiography of the Niger Delta. (A) Sediment supply and distributive agents in the Niger Delta (redrawn after Allen, 1965). (B) Sketch map illustrating the prevailing wind (Gulf of Guinea current) (redrawn after Burke, 1972).- - - - - 17

1.9. Schematic diagram illustrating slides, slumps, debris-flow and turbidity current evolution from the shelf-edge to the deep basin (from Shanmugam, 2016).. - - - - - 21

1.10. Schematic illustration of deepwater depositional model. Note the evolution of turbidity deposits from unconfined at the upper slope through partially confined at the slope-basin transition to unconfined at the basin floor, where turbidites accumulate (from Sprague *et al.*, 2005). - 20

1.11. Schematic diagram illustrating the model of the equilibrium profile in deepwater settings. Note the occurrence of a knickpoint on a topographic high, characterized by erosion and high-depth-to-width ratio, and deposition within negative topography (intraslope basin), characterized by low a depth-width ratio (modified after Ferry *et al.*, 2005) - - - - - 22

2.1. A: Superposed relief and bathymetric map of the Niger Delta showing the extensional, translational and compressional zones. B: Schematic map showing progradation of the delta from the Late Eocene to the present-day. The red box in inset map B shows the location of the Niger Delta in the Gulf of Guinea. Red box and black circles in A show the limit of the 3-D block we studied and the locations of the boreholes, respectively. Yellow arrow points to the downstream section of the submarine channel complex that crossed the study area. A, B modified after (Rouby *et al.*, 2011). - - - - - 27

2.2. Schematic diagram (not drawn to scale) of the three lithostratigraphic units underlying the Niger Delta (redrawn after Brownfield, 2016, on the right). Representative deep borehole (FM-1 well) that penetrated more than 4 km into the deeper Neogene sedimentary records in the Akata Formation and the bio-chronostratigraphically dated intervals in this study (on the left). - 29

2.3. Physiography of the study area. A, B: Uninterpreted and interpreted time slice (at 4.9 seconds twt) showing mobile shales and filled-ponded basins in the block studied. C: Time-structure map near the level of time slice illustrating the same features as in panels A and B. D: Variance attribute map of the seabed showing the presence of mud volcanoes and submarine channel complex. Black dots show the location of the boreholes. - - - - 32

2.4: Overview of the seismic facies observed in this study, corresponding line drawings and interpretations of the depositional environment - - - - 35

2.5. A, B: Uninterpreted and interpreted seismic lines showing the stratigraphic architecture of the study area. Note the lateral discontinuities (erosional truncations) and the juxtaposition of different seismic facies. - - - - 38

2.6. A, B, C: Isochron maps of the lower, middle and upper MTD showing respective spatial variations in sediment thickness. D: Horizon slice at the top of the amalgamated channel levee deposits underlying the lower MTD showing the presence of sinuous channel. E-G: Seismic lines illustrating the architecture of the MTDs. Variations in the thickness of the middle MTD on the footwall and hanging wall blocks are indicated by double-headed arrows (panel F). - 39

2.7: Representative borehole (FM-1 well) drilled to a total depth of 4.15 km down to the Neogene series. The identified fossil markers, data and estimated ages are shown on the left. The well logs used for lithology, facies and depositional environment analysis are shown on the right. Note the vertical succession of facies from channel axis, overbank and/or hemipelagic deposits. - 42

2.8. Chronostratigraphic chart showing standard stages, long-term and short-term sea-level curves (after Haq *et al.*, 1987); the Late Miocene-Quaternary cycles according to Haq *et al.*, (1987) curve

recalibrated by Gorini *et al.* (2014). The Plio-Pleistocene cycles according to Miller *et al.* (2005).
- - - - - 44

2.9. A: RMS amplitude map at 3.3 seconds (twf) in the Cbh facies showing channel architectural patterns. B: Corresponding seismic line illustrating the associated seismic facies. C, D: Core data from the FM-1 and FM-3ST1 wells showing the lithological content - - - 45

2.10. A: Uninterpreted horizon (variance attribute) slice of the erosional event at the base of Unit 6. B: RMS amplitude extraction on the base of Unit 6 draped on panel A. The main submarine channel complex (labelled 1) and channel levee systems (labelled CLSs 2, 3 and 4) are illustrated. C, D: Interpreted seismic line and line drawing showing the architecture of the channels. Yellow arrow (panel B points to paleo-flow direction), while red arrow (part D) points to the level of amplitude extraction. - - - - - 47

2.11. A: Uninterpreted RMS amplitude map of a channel levee system near the top of Unit 7 draped on the horizon (variance attribute) slice. B: Interpretation of panel A illustrating narrow, erosional low sinuosity submarine channel complex 1 and moderate sinuosity CLSs (labelled 2, 3 and 4). C: Seismic line and line drawing illustrating the architectures of the channels. The red arrow (panel C) points to the level of amplitude extraction. Note the presence of bifurcating, bypass CLS that incised older amalgamated channel/lobe deposits in the NW corner of the map and the truncation of amalgamated channel levee deposits by the lower and middle MTDs. - - - 48

2.12. A: Horizon (variance attribute) slice at the base of the high reflectivity seismic packages above the base of Unit 7 (blue line). Note the presence of wide, highly sinuous submarine channel complex (labelled 1 in panels B and C), and highly sinuous CLSs (labelled 2 and 3). Note also the erosional character and northward shift of the main submarine channel complex 1 toward the mobile shale zone in the NE and its NE-SW orientation. - - - - - 52

2.13. A: Uninterpreted RMS amplitude map at 1.9 seconds (twf) draped on horizon (variance attribute) slice. B: 3D geomorphological interpretation of panel A showing the architectures of submarine channel complex (labelled 1), CLSs 2 to 5 and faults. C: Seismic line and line drawing

illustrating the complex cut and fill architecture/lateral aggradation of the main submarine channel complexes 1. Note: (I) The erosive nature of the main channel complex compared to the aggrading CLSs 3 to 5. (II) The presence of abandoned meander loops associated with the meandering CLS 2. (III) The presence of an avulsion channel downstream of levee deposit adjacent to CLS 4. (IV) The overall decrease in RMS amplitude downstream along the CLS 4 and the corresponding increase upstream along the avulsion channel - - - - - 53

2.14. A, B: Uninterpreted and interpreted horizon (variance attribute) slice at 1.8 seconds (twt) showing the presence of submarine channel complexes (yellow arrow), sinuous CLSs, mobile shales, radial faults and lineated scars associated with mobile shale-derived MTDs. C: Seismic lines illustrating the erosional character and rough edges of the submarine channel complex. D: Seismic line showing the conformable/slightly deformed, high amplitude seismic packages associated with mobile-derived MTDs. Note the E-W orientation, presence HARPs (panel C), terraces and entrenched CLS in the main submarine complex. - - - - 54

2.15. Shale tectonics and submarine channel complex evolution from Middle Pliocene to present-day. Note E-W orientation of the channel complex during the Middle Pliocene-Early Pleistocene (purple polygon; Unit 6); the NE-SW orientation during the Early-Middle Pleistocene (green polygon; Unit 7) and the E-W orientation from the Middle Pleistocene to present-day (brown polygon; Unit 7). Note the confinement of mobile shales in the NE of the study area during the Plio-Pleistocene intervals. See text for more a more detailed explanation - - - -
- - - - - 55

3.1. Location of the study area. A: superimposed relief and bathymetric map showing the extensional zone (EZ), transitional zone (TZ) and contractional zone (CZ) of the Niger Delta (adapted from Rouby *et al.*, 2011). B: Schematic progradation map of the Niger Delta since the Eocene. C: Seismic line drawing (AAI) showing the structural zones of the Niger Delta (adapted from Bellingham *et al.*, 2014). D: Dip of the seafloor showing the physiographic features of the transitional zone (TZ) (from Jobe *et al.*, 2016). E: Depth structure map of the modern seafloor showing the mobile shales, mud volcanoes, pockmarks and mud-draped sub-marine channel in the

study area (from Chima *et al.*, 2019). Black circles in panels A, D (labelled W1-W5) in panel E indicate well locations. - - - - - 66

3.2. A: Seismic facies analysis. A: Facies description and interpretation (modified after Chima *et al.*, 2019). B: Representative facies succession on the western Niger Delta intraslope basins. See Figs. 3.3C and 3.5A for the locations panels B, C, and text for a more detailed - - 68

3.3. Pliocene and Pleistocene stratigraphic architecture of the western Niger Delta intraslope basins. A, B: Uninterpreted north-south seismic line and line drawing (CCI) showing the depositional geometries within seismic SS1 and SS2 (modified after Chima *et al.*, 2019). Note the lateral thickening in stratigraphy of SS1 away from mobile shale. Yellow arrow points to the base of the hemipelagic drape (horizon M) dated at 5.5 Ma. Letters (M-X) in panel B represent the seismic markers. Note the changes in sedimentary architecture from turbidite-dominated at the lower part of SS1 through a mix of MTDs and turbidites at the upper part of SS1 to hemipelagites and turbidites at the transition between SS1 and SS2. Note lateral truncations of seismic reflections within SS1 compared to SS2. Note also the occurrence slide/slump scars below the modern seafloor (panel A) and inverted fault (labelled Z in panel B). C, D: Interpreted RMS amplitude map of (horizons A and P), draped on variance attribute extractions at the lower parts of SS1 and SS2 illustrating changes in depositional elements. - - - - - 75

3.4 Sedimentary architecture of the middle part of SS1. A: Interpreted RMS amplitude map of horizon G draped on variance attribute map at the middle of SS1 showing the presence of sinuous channel levee systems labelled 1a, 2 in the NW, and (3, 4) in the SE of the study area. B: Seismic line (DD¹) through channel 1a, shows its relatively shallow incision (1 km wide, 120 m deep). - - - - - 79

3.5. Sedimentary architecture of the upper part of SS1. A: Interpreted RMS amplitude map of horizon K draped on variance attribute map, showing the presence of 1.8 km wide bifurcating channel, characterized by moderate RMS amplitude and a terrace on its outer bend (see yellow arrow in panel B for the stratigraphic level). B: Interpreted north-south seismic line (FF¹) shows the incisional character of the channel (90 m deep), infilled by partially confined, turbidite feeder

channels/meandering channel levee complex that are truncated by the overlying MTDs. See Fig. 11A for the location of erosional channel 1c in the northern part of the study area - - 81

3.6. Sedimentary architecture of the upper part of SS1. A: Interpreted RMS amplitude map of horizon K draped on variance attribute map, showing the presence of 1.8 km wide bifurcating channel, characterized by moderate RMS amplitude and a terrace on its outer bend (see yellow arrow in panel B for the stratigraphic level). B: Interpreted north-south seismic line (FFI) shows the incisional character of the channel (90 m deep), infilled by partially confined, turbidite feeder channels/meandering channel levee complex that are truncated by the overlying MTDs. See Fig. 11A for the location of erosional channel 1c in the northern part of the study area -. - 83

3.7. Sedimentary architecture at the middle part of SS2 A, B: Uninterpreted and interpreted RMS amplitude map of horizon R draped on variance attribute extraction shows the presence of a 2.5 km wide channel, characterized by moderate RMS amplitude and turbidite feeder channels/meandering channel levee complexes (CLCs) within the channel axis (see yellow arrow in panel C for stratigraphic level). C: An interpreted north-south seismic line (GGI) illustrates the complex cut and fill architecture of the channel (185 m deep) with overall vertical aggradational patterns (panels D, E). Note the dominance of channel fills by turbidite feeder channels/meandering CLCs and slide/slump deposits. Note the upward decrease in the thicknesses of slide/slumps and external levee deposits. - - - - - 86

3.8. Sedimentary architecture at the upper part of SS2. A, B: Uninterpreted and interpreted RMS amplitude map of horizon V draped on variance attribute map shows the presence of 2.1 km wide, sinuous channel, characterized by moderate amplitude and turbidite feeder channels/meandering CLCs (see yellow arrow in part C for the stratigraphic level). Note the upward decrease in the thicknesses of slide/slumps and external levee deposits. The chaotic, wedge-shaped area to the north is interpreted as MTDs. C: Interpreted NW-SE seismic line (HH¹) shows the complex cut and fill architecture of the channel (panels D, E). Note the upward decrease in the thicknesses of side/slumps and external levee deposits. A, B, C after Chima *et al.* (2019). - - - 88

3.9. Sedimentary architecture of the upper part of SS2. A: Interpreted RMS amplitude map of horizon W draped on variance attribute map, shows the presence of MTDs trapped behind mobile shale in the north, a 2.5 km wide erosional channel in the central part of the study area and transient fan/lobe deposits, characterized by high RMS amplitudes in the south. B: Interpreted E-W seismic line (JJ¹) illustrates the high reflectivity and onlapping geometry of the transient fan deposits. Note in panel A, the presence of mobile shale, fluid escape features and long linear scars associated with mobile shale-derived MTDs, which underlie the level of interest (horizon V) - - 90

3.10: Sequence stratigraphic interpretation. A, B: Uninterpreted and interpreted E-W seismic and line drawing (KKI), showing the Pliocene and Pleistocene stratigraphic architecture of the western Niger Delta intraslope basins (panel C for a detailed view). Note the tentative correlation between seismic markers at (M/A, G/I and K/P) transitions with the sea-level and 18O isotope curves. Note also the lateral variation in stratigraphic thickness of SS1 compared to SS2. - - 93

3.11. Shale tectonics vs submarine channel morphology and distribution on the western Niger Delta intraslope basins over the last 5.5 Ma. A (SS1): Migration of erosional channels from the NW to SE in (stages 1a-c in Figs. 4-6). B (SS2): Absence of erosional channels in the northern part of the study area and increase in the slope of channel levee system (CLS) downdip of mobile shale. See text for a more detailed explanation. Note the spatio-temporal variation in the orientation of erosional channels in panels A and B (labelled 1, 2 and 3). Modified after Chima *et al.* (2019). - - - - - 99

3.12. Schematic illustration of the proposed long-term evolution of depositional elements on the western Niger Delta intraslope basins with respect to 4/5th-order variations in relative sea-level, locally influenced by shale tectonics. A: Forced regression marks the development of erosionally confined (bypass channels on the slope) that are locally associated with thin MTDs ('lower MTDs'), compared to the thick MTDs that supposedly accumulated on the basin floor. B: Early lowstand marks the infilling of the erosionally confined channels by turbidite feeder channels/meandering channel levee complexes. C: Late lowstand/early transgression marks the development of the MTDs ('upper MTDs') or with slides/slump deposits. D: Highstand marks hemipelagic sedimentation/muddy turbidites and punctuation of deepwater sedimentation - 102

3.12 E: Schematic illustration of slope depositional model. - - - - - 103

4.1. Location of the study area. A: Superposed relief and bathymetry map showing the extensional zone (EZ), translational zone (TZ) and contractional zone (CZ) of the Niger Delta. B: Inset map of Africa showing the location of the Niger Delta on the Atlantic coast of West Africa. C: Schematic progradation map of the Niger Delta since the Eocene. A, B and C (modified after Rouby *et al.*, 2011). D: Seismic and well data coverage (see section 3). E: Regional seismic line showing the structural styles of the western Niger Delta (modified after Bellingham *et al.*, 2014)
- - - - - 109

4.2. A plot of TWT (ms) versus measured depth (m) showing the time-depth relationship used in the depth conversion of seismic interpretation. - - - - - 115

4.3. An Overall decrease in sediment porosity with depth due to compaction- - - 116

4.4. A, B: Interpreted and uninterpreted seismic line drawing [(two-way-travel time (TWT)], about 5 km west of Fig. 2, shows similar structural styles in the eastern part of the study area (see Fig. 1A). Note the overall uniform sediment thickness between the late Eocene-Serravallian and a lateral variation in sediment thickness from Serravallian-present. Note also the overall relative higher sediment thickness within the extensional zone (the early Pliocene-present)- - 119

4.5. A, B: Regional two-way-travel time (TWT) seismic line (interpreted and line drawing), showing the structural styles in the eastern part of the study area (see Fig. 4.1A). Note the overall uniform stratigraphic thickness between the Late Eocene-Serravallian and lateral variation in thickness from Serravallian-present. Note also the relative higher sediment thickness from the early Pliocene to the present within the extensional zone compared to the other structural zones. Letters P-S and T-Z represent normal and reverse faults respectively. - - - 120

4.5. C, D: Interpreted and seismic line drawing showing detailed tectonostratigraphic architecture of the extensional and translational zones. Note the detachment of faults at the base of the upper dark grey unit. - - - - - 121

4.5 E, F: Interpreted and seismic line drawing showing detailed tectonostratigraphic architecture of the contractional zone. Note also the detachment of faults at the base of the upper dark grey unit. - - - - - 122

4.5 G: Line drawing (the depth equivalent of panel A, B displayed with the same scale). Note the overall decrease in sediment thickness on this panel compared to panels A, B. Although vertically exaggerated, this depth section enabled us to build a more reliable tectonostratigraphic evolution of the western Niger Delta from the Cretaceous-present as presented in the discussion - 123

4.6 A, B: Regional two-way-travel time (TWT) seismic line (interpreted and line drawing), about 40 km west of Fig. 2, shows the structural styles in the western part of the study area (see Fig. 1A). Note the overall uniform sediment thickness between the Late Eocene-Serravallian and a lateral variation in sediment thickness from Serravallian-present. Note also the overall increase in sediment thickness within the extensional zone (Pliocene-present). - - - - 127

4.7A, B: Delta-wide seismic strike line, showing the eastern, central and western Niger Delta lobes (see Fig. 4.1A). The structural high at the central part of the line corresponds to the Charcot Fracture Zone (CFZ), which divides the delta into the eastern and western lobes (see Fig. 4.1A). Note the tilt in the basement in the western Niger Delta lobe and the occurrence of listric normal faults that offset basin centre-dipping seismic reflections (dashed blue polygon in Fig. 4.7A-D). Note the non-uniform nature of the basement, the variation is stratigraphic thickness from the eastern to the western Niger Delta lobes, the overall thinning of the Cretaceous to Serravallian stratigraphy above the Charcot Fracture Zone compared to the Serravallian to present-day Unit. Note the overall thinning of the early Pliocene to present-day Unit to the western part of the delta compared to the eastern part, the reflection-free character of the Cretaceous-Serravallian Unit (Fig. 4.7C, E below) and the presence of syn-rift deposits in the western Niger Delta. - - 128

4.7 C, D: Interpreted seismic and line drawing of the western Niger Delta lobe illustrating the syn-rift deposits and stratigraphic interval dominated by gravity gliding (dashed blue polygon) above the tilted basement. - - - - - 129

4.7 E, F. Central Niger Delta. Zoomed seismic and line drawing illustrating the overall thinning of the Cretaceous-Serravallian stratigraphy (red interval) above the CFZ (green interval) compared to the Serravallian-present (purple, orange, yellow and pink) intervals respectively- -

- - - - - - - - - - - - - - 130

4.8. Sedimentation rates. A (shelf region); B (slope) region. See text for a detailed explanation.

- - - - - - - - - - - - - - 136

4.9. Schematic illustration of the tectonostratigraphic evolution of the western Niger Delta-

- - - - - - - - - - - - - - 140

4.10. Line drawing of the Pliocene and Pleistocene stratigraphic architecture of the western Niger Delta (A) and the eastern Niger Delta (B). Note the dominance of the western Niger Delta extensional and contractional zones by basinward dipping normal faults and imbricated faults folds respectively (Fig. 4.10A). Note the presence of actively subsiding counter regional normal faults at the eastern Niger Delta shelf/slope boarder and minor buckling in the contractional zone (Fig. 4.10B). Note also the overall distribution of sediment from the continental shelf to the abyssal plain in the western Niger Delta since the Pliocene (Fig. 4.10A), compared to the eastern part of the delta, where sediment is generally sequestered within collapsing normal faults with little or no deposition in the deep basin (Fig. 4.10B) - - - - - - - - - 144

LIST OF TABLES

Table 2.1: Summary of statistical measurements on MTDs - - - - - 50

General Introduction, Aim and Thesis Structure

The Niger Delta is located in the Gulf of Guinea along the equatorial margin of West Africa (Fig. 1.1). With sub-aerial and sub-marine sediments covering an area of ~140,000 km² and ~12 km in thickness (Allen, 1965; Evamy *et al.*, 1978; Doust and Omatsola, 1990), the Niger Delta is the twelfth largest petroleum province in the world (Tuttle *et al.*, 1999). The unique tectonostratigraphic setting of this Cenozoic delta renders it an exceptional natural laboratory for the study of depositional systems and stratigraphy of a large, progradational deltas located on passive margins (Allen, 1965; Evamy *et al.*, 1978; Avbovbo, 1978; Doust and Omatsola, 1990; Reijers, 1997; Jermannaud *et al.*, 2010). Shale tectonics, gravity-driven deformation of a sedimentary wedge, absolute sea-level changes, global and regional climate dynamics, drainage evolution, control on sediment supply and distribution (Jermannaud *et al.*, 2010; Rouby *et al.*, 2011; Chardon *et al.*, 2016; Grimaud *et al.*, 2017).

Compared to the western Niger Delta where the present study is focused, majority of publications over the last decade have been focused in the eastern Niger Delta, where most of the currently producing deepwater fields are located (Hooper *et al.*, 2002; Corredor *et al.*, 2005; Fatoke and Bhattacharya, 2010; Wiener *et al.*, 2010; Jermannaud *et al.*, 2010; Rouby *et al.*, 2011; Riboulot *et al.*, 2012; Sapin *et al.*, 2012; Jolly *et al.*, 2016; Appendix 1). The offshore eastern Niger Delta has been reported to have recorded relatively low sedimentation rates and low gravity-driven deformation of its sedimentary wedge from the Oligocene (34 Ma) to the Tortonian (9.3 Ma), when deposition was focused in the onshore domain (e.g. Billotti and Shaw, 2005; Wiener *et al.*, 2010; Jolly *et al.*, 2016). However, an overall increase in sedimentation rate from the Tortonian (9.3 Ma) to the Messinian (5.7 Ma) is reported to have triggered significant basinward progradation of the eastern Niger Delta's sedimentary wedge, an overall increase in gravity-driven deformation (Billotti and Shaw, 2005; Wiener *et al.*, 2010; Jolly *et al.*, 2016), and a general reduction in sediment supply and gravity-driven deformation over the Plio-Pleistocene (2.5 Ma), when regional delta lobe migration is proposed to have switched fluxes to the western Niger Delta (Jermannaud *et al.*, 2010; Rouby *et al.*, 2011).

Despite the numerous stratigraphic studies in the western Niger Delta over the last decade (Cohen and McClay, 1996; Morley and Guerin, 1996; Chapin *et al.*, 2002; Deptuck *et al.*, 2003; 2012; Davies *et al.*, 2003; Adeogba *et al.*, 2005; Bakare *et al.*, 2007; Heiniö and Davies, 2007;

Briggs *et al.*, 2009; Maloney *et al.*, 2010; Clark and Cartwright, 2012; Bellingham *et al.*, 2014; Benjamin *et al.*, 2015; Jobe *et al.*, 2015; 2016; 2017; Benjamin and Huuse, 2017, Hansen *et al.*, 2017), no study has investigated at a source-to-sink scale, the tectonostratigraphic evolution of the western Niger Delta from the Cretaceous-present. Hence, this PhD aims to investigate at a regional scale the, tectonostratigraphic evolution of the western Niger Delta from the Cretaceous-present with a view to understanding its controlling factors in comparison with the well-studied eastern Niger Delta.

In order to achieve the aim of this PhD, the project is sub-divided into 5 chapters as briefly described below;

Chapter 1 presents an overview of the regional geodynamical and tectonostratigraphic framework of the Niger Delta, and dataset.

Chapter 2 (paper 1): *Seismic stratigraphy and depositional architecture of Neogene intraslope basins*. The chapter presents the sequence stratigraphic evolution of the western Niger Delta from the Burdigalian (18.5 Ma) to the Messinian (5.5 Ma), based on detailed 3D seismic interpretation calibrated with well and biostratigraphic data.

Chapter 3 (paper 2): *Pliocene and Pleistocene stratigraphic evolution of the western Niger Delta intraslope basins: A record of glacio-eustatic sea-level and basin tectonic forcings*. This chapter addresses the interplay between allocyclic and basin tectonic forcings on the sequence stratigraphic evolution of the western Niger Delta over the Pliocene and the Pleistocene.

Chapter 4 (paper 3): *Tectonostratigraphic evolution of the western Niger Delta since the Cretaceous: Implication of paleo-topographies and delta top tectonostratigraphic dynamics on gravity deformation of the margin*. This chapter investigates the control of paleo-topographies and delta-top tectonostratigraphic processes on gravity deformation of the western Niger Delta's sedimentary wedge. Chapter 4 also presents a comparison of the stratigraphic evolution of the western and eastern Niger Delta over the Pliocene and the Pleistocene.

Chapter 5 (General conclusions, limitations and perspectives), highlights the key findings/contributions of this PhD research to knowledge, limitations and future studies.

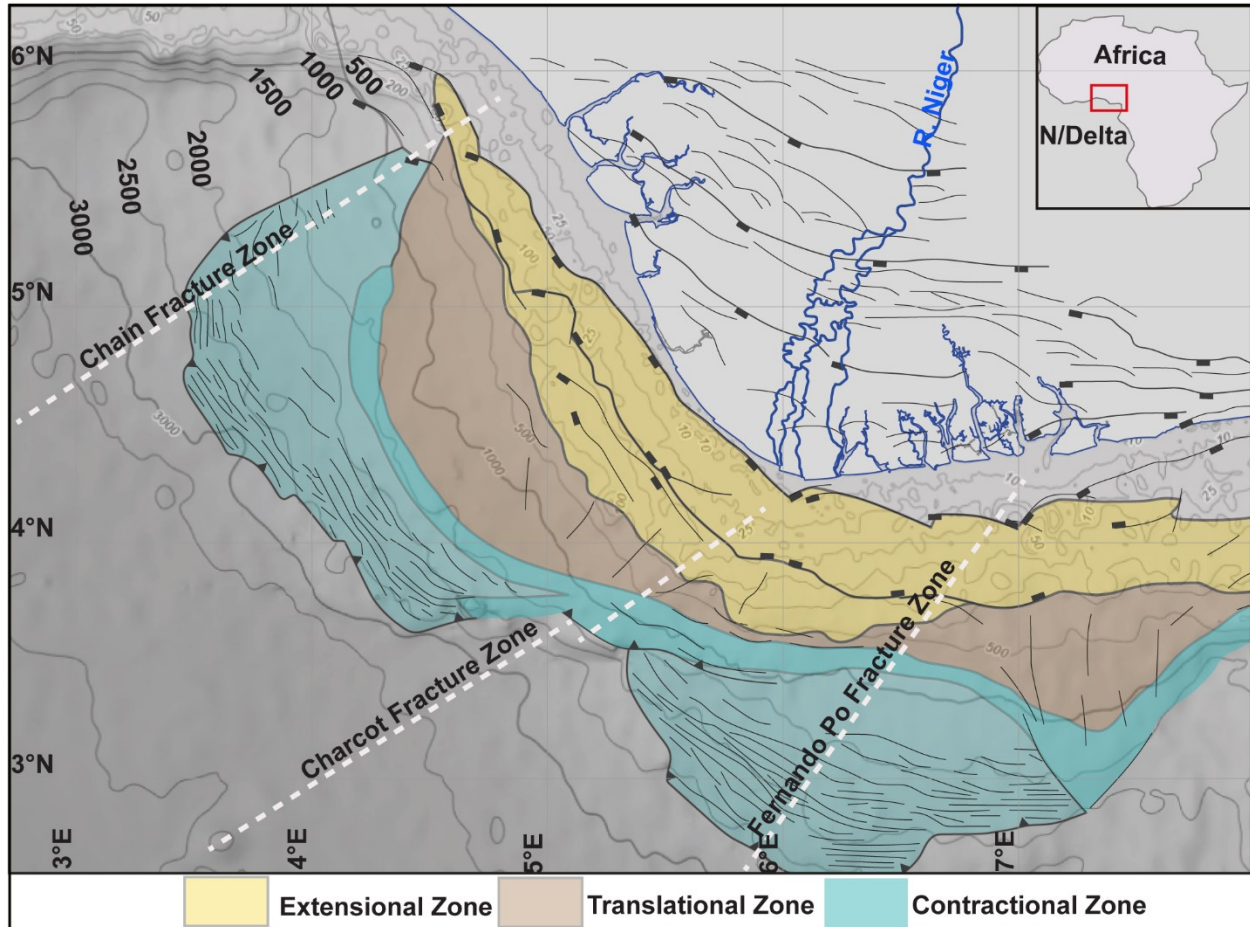


Fig. 1.1. Superposed regional relief and bathymetric maps of Niger Delta, illustrating the main physiographic features, structural zones and sedimentary wedges (explained in detail in the next section). Inset map at the top right corner shows the location of the Niger Delta in the Gulf of Guinea (modified after Morley and Guerin, 1996).

CHAPTER 1

Geodynamical and Sedimentological Setting

1.1 Geodynamical setting

The Niger Delta is located in the Gulf of Guinea (Fig. 1.1), which developed during the separation of the African and American lithospheric plates in the Cretaceous (Burke, 1972; Lehner and De Ruiter, 1977; Whiteman, 1982; Fig. 1.2). Although rifting initiated as early as the Tithonian (150 Ma) near the Falkland-Agulhas fracture zones in the south, and spread northwards (Le Pichon and Hayes, 1971; Rainbowitz and Labrecque, 1979; Nurnberg and Muller, 1991; (Fig. 1.2), seafloor spreading occurred in the equatorial Atlantic later, between the early and late Cretaceous (Nurnberg and Muller, 1991; Genik, 1993; Moulin *et al.*, 2010). The opening of Equatorial Atlantic produced Cretaceous, asymmetrical rifted sedimentary basins over which a drift sedimentary sequence was deposited, building out from the newly defined continental margin over the early oceanic crust dissected by transform faults and fracture zones (e.g. the Chain, Charcot and Fernando Po Fracture zones; Figs. 1.1; 1.6A). These fracture zones played a part in controlling accommodation on the oceanic crust (Short and Stauble, 1967; Evamy *et al.*, 1978; Doust and Omatsola, 1990; Smith and Sandwell, 1997).

After rifting ended in the equatorial Atlantic in the late Cretaceous, sub-Saharan West Africa remained tectonically stable until the Paleogene (~34-29 Ma), when it experienced long-wavelength lithospheric uplift and deformation following the uplift of the Hoggar Mountain (Burke *et al.*, 2003; Chardon *et al.*, 2016; Grimaud *et al.*, 2017; Ye *et al.*, 2017; Fig. 1.4). The proper Niger Delta was installed following the uplift of the Hoggar, which marks the onset of delta progradation across the margin (Burke *et al.*, 2003). According to Reijers (2011), a paleo-Niger Delta could have developed in the Benue region (Fig. 1.3) during the Paleocene, but the actual progradation of the delta started around the late Eocene (Doust and Omatsola, 1990).

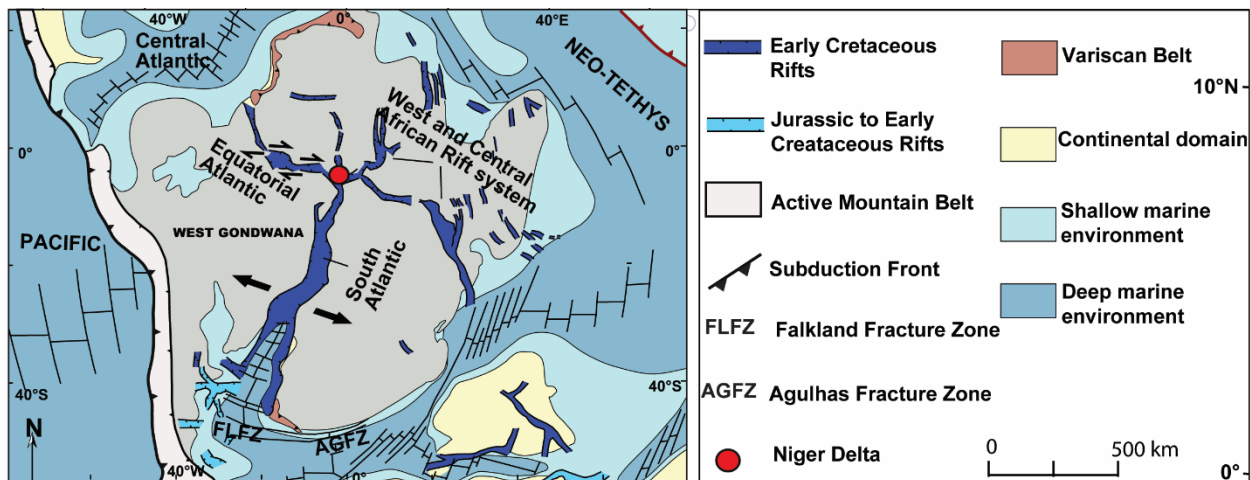


Fig. 1.2. Paleotectonic map of the African and South American rift systems at (ca 120 Ma) during the break-up of the African and South American plates. Note the location of the future Niger Delta in the equatorial Atlantic (modified after Frizon de la Motte *et al.*, 2015).

1.1.1 Evolution of the Niger catchment

The modern Niger River distributes mud to gravel-size sediment onto the delta from a drainage area of $\sim 1.2 \times 10^6 \text{ km}^2$, with an overall mean annual discharge of $6,140 \text{ m}^3/\text{s}$ and sediment load of $1,270 \text{ kg/s}$, (Mulder and Syvitski, 1995; Fig. 1.3). The Niger River drains the Guinea Rise (located in the northwest) and the Jos Plateau (in the northcentral), while its tributary (the Benue River), drains the Cameroon region in the east (Allen; 1965; Fig. 1.3). The evolution of the Niger catchment has been a subject of debate over the last decade. An earlier study by Goudie (2005), opines that the stepped longitudinal profile and elbow pattern between the High and Lower Niger catchments (Fig. 1.3), are Quaternary features of aggressive coastal erosion following the capture of intracratonic rivers (Fig. 1.3). Regional geometries of dated paleolandscapes in West Africa by Chardon *et al.* (2016), show that the evolution of the modern Niger catchment (Fig. 1.4) dates for at least the early Oligocene ($\sim 29 \text{ Ma}$), and possibly the late Eocene ($\sim 34 \text{ Ma}$). Grimaud *et al.* (2017) corroborate Chardon's work and show that the initiation and stabilization of the modern Niger catchment follow the long-wavelength ($>700 \text{ km}$) hot-spot swell associated with the uplift of the Hoggar Mountain at least since the early Oligocene ($\sim 29 \text{ Ma}$). According to Chardon *et al.* (2016), the Niger catchment experienced tectonic quiescence during the early Paleogene ($\sim 45 \text{ Ma}$), characterized by overall high sea-level and low clastic sedimentation in the offshore Niger Delta (Fig. 1.4). However, the uplift of the Hoggar around the late Eocene-early Oligocene (34-29 Ma), led to the expansion and connection of the Niger catchment to the Equatorial Atlantic (Fig. 1.4).

The capture of the Upper Niger by the Lower Niger in the Plio-Pleistocene was linked to a tectonic event (Urvoy, 1942; Voute; 1962; Allen; 1965; Figs. 1.3, 1.4). Goudie (2005), also opines that tectonic rearrangement in the Niger catchment during the Quaternary could explain the increase in sediment supply to the Niger Delta over the same period. However, recent studies link the increase in sediment supply to the Niger Delta during the Pliocene and early Pleistocene to climatically enhanced precipitation rather than catchment reorganization (Jermannaud *et al.*, 2010; Robin *et al.*, 2011; Chardon *et al.*, 2016; Grimaud *et al.*, 2017).

Prior to the uplift of the Hoggar around (34-29 Ma), the Niger was confined to a small catchment completely isolated from the Equatorial Atlantic (Burke, 1996; 2003; Grimaud *et al.*, 2014; Chardon *et al.*, 2016; Fig. 1.4). At that time, the Sourou River, which initially flowed northeast into the High Niger was captured by the Volta River in the Quaternary due to the reduction in slope following the deposition of the Niger inland delta (Chardon *et al.*, 2016; Figs. 1.3, 1.4). The capture of the Sourou River and the deposition of the Niger inland delta mark the onset of an overall decrease in sediment supply to the offshore Niger Delta (Chardon *et al.*, 2016). Furthermore, Grimaud *et al.* (2017), showed that sediment accumulation rates in the Niger Delta increased steadily between 45-16 Ma following the uplift of the Hoggar, doubled between 5.3 to 1.8 Ma (now 2.6 Ma; in Gibbard *et al.*, 2014), and then decreased onwards (see also Jermannaud *et al.*, 2010; Rouby *et al.*, 2011). The ongoing reduction in sediment supply to the Niger Delta is linked to the aridification of the rivers that initially drained the southern part of the Hoggar (Chardon *et al.*, 2016; Fig. 1.3).

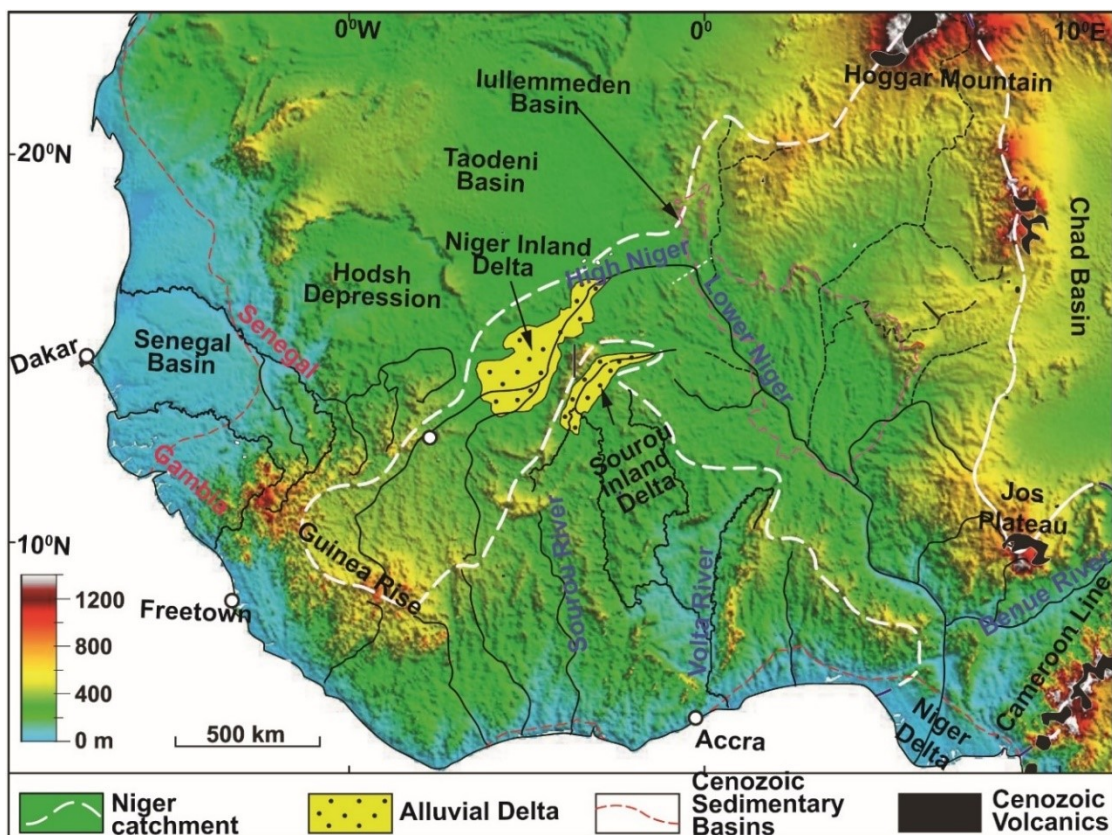


Fig. 1.3. The West African relief showing the modern Niger catchment (dashed white line). Rivers are indicated in black lines, that are dashed, where aridified (modified after Chardon *et al.*, 2016).

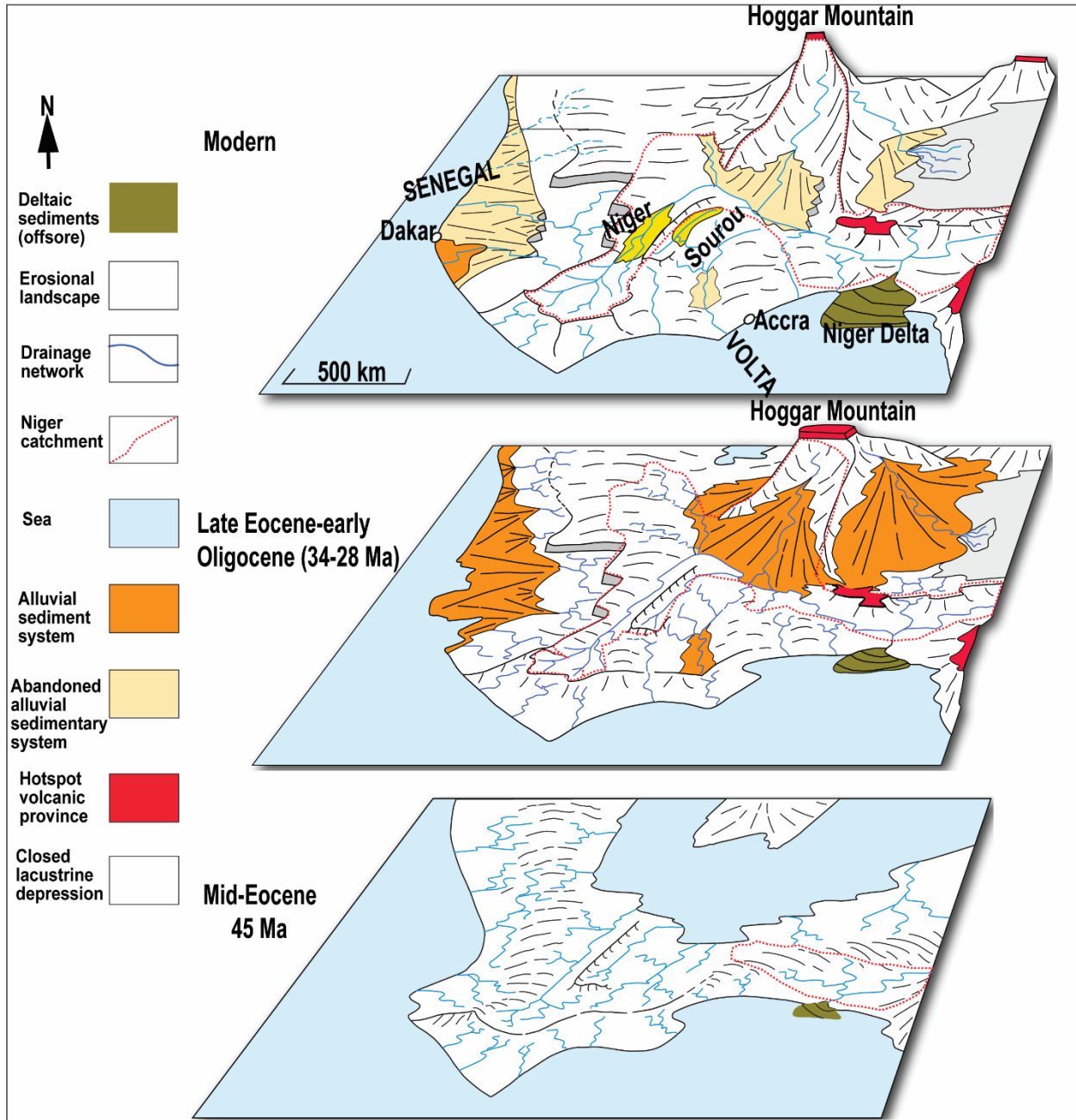


Fig. 1.4. Schematic illustration of the evolution of the West African relief: Mid-Eocene (~45 Ma) is a period of tectonic quiescence, characterized by maximum flooding of paleomarginal upwarp, which marked the continental divide; the late Eocene-early Oligocene (~34-29 Ma) is characterized by the Hoggar uplift, the establishment of the modern Niger catchment and an increase in sediment supply to alluvial fans on the Hoggar's piedmont and the Niger Delta; the Quaternary is characterized by the incision of alluvial fans, decrease in slopes of the High Niger and Sourou Rivers following the deposition of inland deltas, and eventual capture of the later by the Volta River (modified after Chardon *et al.*, 2016).

1.1.2 Gravity tectonics

Gravity tectonics describes gravity-driven deformations that affect either (i) the sedimentary layers above basal detachments in passive margins (e.g. the Niger Delta, Gulf of Mexico, the Brazilian Margin, Angola and Congo Basins), or (ii) the crust/the entire lithosphere in accretionary prisms and collision belts (e.g. the Makran Delta, the Baram-Campion Delta and Cyprus Arc) (Morley *et al.*, 2011). Although not limited to passive margins, the presence of (1) consistent regional slope into the deep basin; (2) a weak detachment (shale or salt), and (3) triggering mechanisms (e.g. crustal uplift or delta progradation), are critical for gravity tectonics (e.g. Cobbold and Szatmari, 1991; Duval *et al.*, 1992; Maudit *et al.*, 1997; Tari *et al.*, 2003; Rowan *et al.*, 2004). Gravity spreading and gravity gliding are the two main aspects of gravity tectonics that deform seaward dipping sedimentary successions in passive margins and accretionary wedges (Ramberg, 1981; Dejong and Sholten, 1973; Morley *et al.*, 2011; Fig. 1.5). Gravity spreading results from flattening and lateral spreading of a rock mass under its weight. It hardly affects the entire sedimentary column and is often limited to mobile substrates (overpressured shale or salt) at the base of gravity-driven system (Morley *et al.*, 2011). Gravity gliding is characterized by the rigid translation of a rock mass down a slope (Ramberg, 1981; Dejong and Sholten, 1973). It is generally associated with the linkage of the extensional zone in the up-dip and the compressional zone in the downdip through a décollement unit and extends over a wider spatio-temporal scale (Morley *et al.*, 2011). Although gravity gliding in passive margins can be triggered by instantaneous geological events such as storms, submarine landslides, earthquake, hurricanes and torrential rain (e.g. Embly, 1976; Canal *et al.*, 2004; Gee *et al.*, 2007), long-term geological processes associated with high sedimentation rates and uplift of adjacent margins are the common triggering mechanisms (Morley *et al.*, 2011). Although gravity spreading and gravity gliding are generally superimposed (Brun and Merle, 1985), the former predominates where a thick mobile substrate is present (e.g. Morley and Guerin, 1996; Vendeville, 2005).

In the Niger Delta, gravity tectonics became the dominant control of the structural and stratigraphic styles, following the cessation of rifting in the equatorial Atlantic in the late Cretaceous (e.g. Whiteman, 1982; Doust and Omatsola, 1990). Gravity deformation in the Niger Delta is controlled by the combination of (i) seaward-dipping slope at the shelf-slope break; (ii) deeply buried overpressured marine shales and (iii) high sedimentation/progradation of delta wedge (Whiteman, 1982; Doust and Omatsola, 1990; Damuth, 1994; Cohen and McClay, 1996;

Morely and Guerin, 1996; Graue, 2000; Corredor *et al.*, 2005; Cobbold *et al.*, 2009; Briggs *et al.*, 2009; Wiener *et al.*, 2010; Sapin *et al.*, 2012; Wu *et al.*, 2015; Fig. 1.5). The over 10 km thick sediment wedge of the Niger Delta and its loading effect locally induce the landward inclination of the basal detachment (e.g. Kehle, 1989; Morley and Guerin, 1996; Fig. I.5).

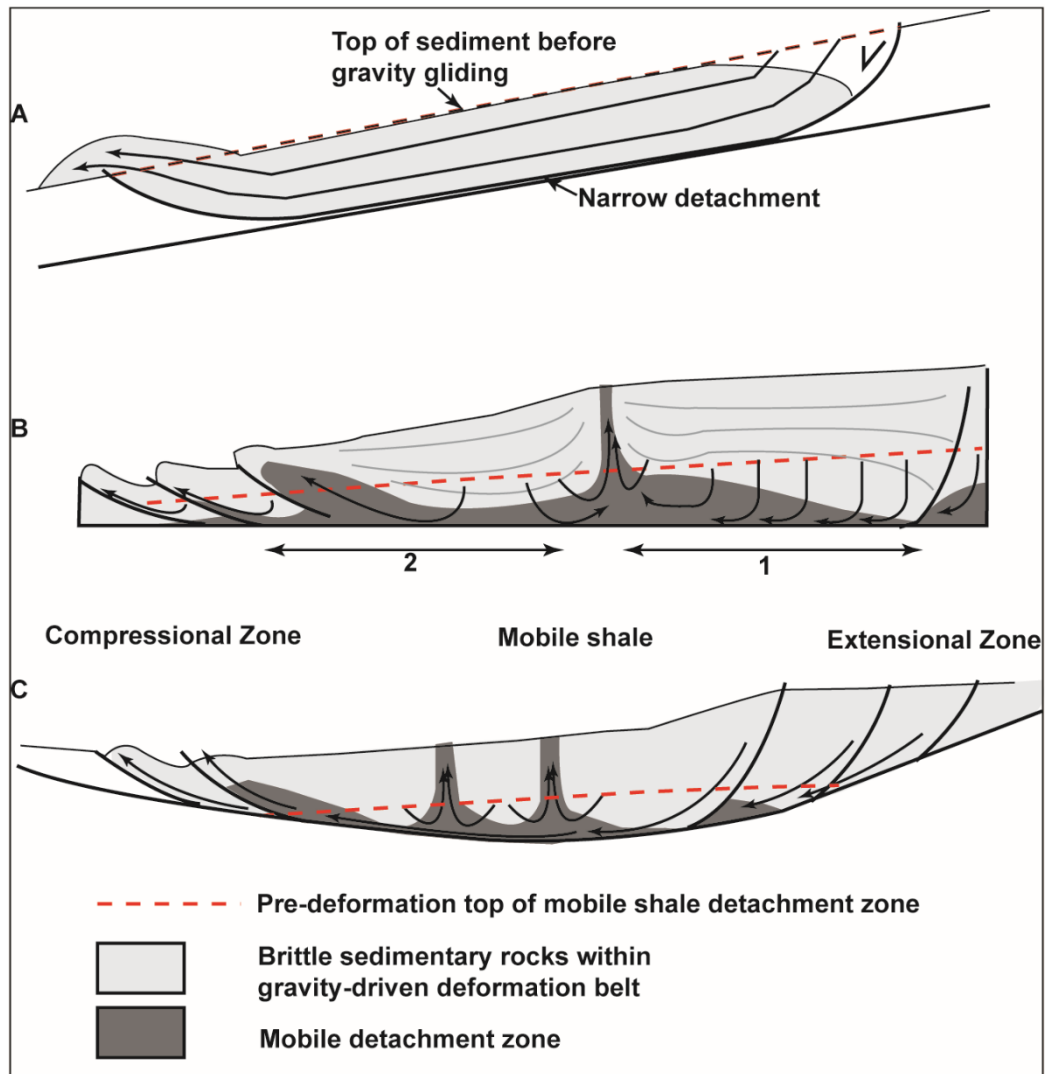


Fig. 1.5. Schematic diagram illustrating gravity spreading and gravity gliding. (A) Gravity gliding down an inclined slope on a thin detachment; (B) Sediment loading causing gravity spreading above a thick detachment zone on a flat detachment surface; (C) Mixed gravity spreading and gravity gliding above a thick décollement zone with onshore and offshore dipping detachment surfaces (modified after Morley *et al.*, 2011).

The repeated seaward progradation of the Niger Delta up to 300 km since the Eocene gave rise to the development of three structural zones namely: (i) an extensional zone below the continental shelf; (ii) a transitional zone below the upper slope, and (iii) a compressional zone located at the toe of the slope (Doust and Omatsola, 1990; Damuth, 1994; Cohen and McClay, 1996; Connors *et al.*, 1998; Morgan, 2004; Billoti *et al.*, 2005; Wiener *et al.*, 2010; Fig. 1.6). Corredor *et al.* (2005), further subdivided the Niger Delta into five structural zones (Fig. 1.6) namely: (1) an extensional zone below the continental shelf, characterized by seaward normal and landward dipping counter-regional faults; (2) a mobile shale zone below the upper slope, dominated by mobile shales (Morley and Guerin, 1996) that lead to shale cored ridges and massifs, shale overhangs and mobile shales that form mud volcanoes on the seafloor (Graue, 2000); (3) an inner fold and thrust belt, characterized by basinward verging imbricated thrust faults-and-folds with detachment folds; (4) a transitional detachment fold zone below the lower slope, characterized by large areas of little or no deformation interbedded with large detachment folds above thick marine shales; (5) an outer fold and thrust belt, characterized by both basinward and landward verging reverse faults. The coupling between the extensional and the compressional zones (aided by the ductile rheology of the overpressured marine shales within the transitional zone), facilitates the transfer of stress from the up-dip extensional zone downdip to the compressional zone, where deformation is accommodated by imbricated thrust sheets and associated folds (Doust and Omatsola, 1990; Damuth, 1994; Connors *et al.*, 1998; Morgan, 2004; Billoti *et al.*, 2005; Corredor *et al.*, 2005; Fig. 1.6).

1.2. Sedimentological setting

1.2.1 Lithostratigraphic successions

The lithostratigraphy of the Niger Delta consists of Cretaceous-Holocene siliciclastic marine sediments that overlie the oceanic crust (Short and Stauble, 1967; Nwachukwu, 1972; Evamy *et al.*, 1978; Avbovbo, 1978; Doust and Omatsola, 1990; Reijers *et al.*, 1997; Fig. I.7). Although the Cretaceous units have not been drilled in the Niger Delta, they have been extrapolated

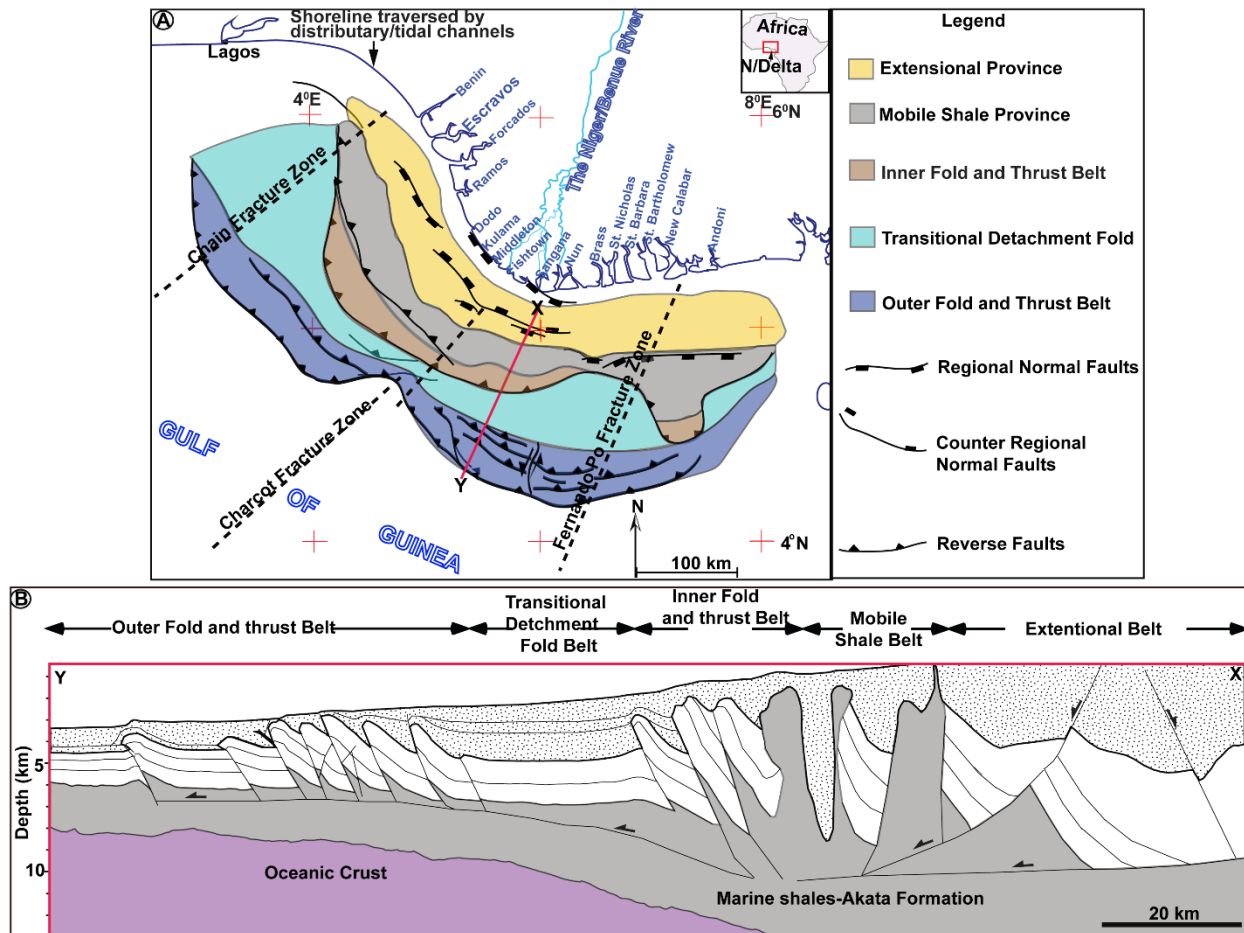


Fig. 1.6. Structural map of the Niger Delta. (A) Schematic illustration of the extensional, transitional and compressional zones of the Niger Delta. Note the distribution of coastal rivers/tidal channels across the shoreline from east to west; (B) Seismic line drawing (X-Y) along the depositional dip showing the structural and stratigraphic styles from the shallow offshore to deep basin (redrawn after Corredor *et al.*, 2005).

to the Anambra Basin in the northeast, where they are characterized by Albian-Maastrichtian shallow marine clastic deposits that are exposed along road cuts and river valleys (Nwachukwu, 1972; Reijers *et al.*, 1997). A major marine transgression in the Paleocene, referred to as ‘the Sokoto’ (Reijers, 1997), initiated the deposition of the Akata Formation in the Niger Delta (Fig. 1.7). The late Eocene marks the onset of paralic deposition in the Niger Delta and the overall southward progradation of the delta into the Gulf of Guinea (Nwachukwu, 1972; Doust and Omatsola, 1990; Fig. 1.4). The lithostratigraphy of the Niger Delta consist an overall regressive siliciclastic wedge, described and characterized from bottom to top as the Akata, the Agbada and

the Benin Formation (Short and Stauble, 1967; Evamy *et al.*, 1978; Avbovbo, 1978; Doust and Omatsola, 1990; Kulke, 1995; Fig. 1.7). The Akata Formation comprises marine shales that reach maximum thickness of 7,000 m in the inboard and decreases to 2,000 m in the outboard setting (Doust and Omatsola, 1990). The repeated occurrence of thrust ramps in the deep fold-and-thrust belt accounts for ~5,000 m thick portion of the Akata Formation in this area (Wu and Bally, 2000; Corredor *et al.*, 2005). The Agbada Formation constitutes paralic sands and shales that reach maximum thickness of 3,500 m (Evamy *et al.*, 1978; Avbovbo, 1978; Doust and Omatsola, 1990). The Benin Formation is dominated by alluvial to upper coastal plain sediment that reaches thickness of 2,000 m (Avbovbo, 1978). Marine shales and turbiditic sands within the Akata Formation respectively act as petroleum source rocks and deepwater reservoirs, while the shallow marine sands and shales within the Agbada Formation respectively act as reservoir and regional seal/or source (Ekweozor and Daukoru, 1994; Tuttle, 1999; Brownfield, 2016). Seismic data (displayed to the right of Fig. 1.7), illustrates the seismic reflection configuration of the Agbada and the Akaka Formations until approximately 8 km deep. These lithostratigraphic successions are underlain by syn-rift sediment and carbonates, that are generally poorly imaged by seismic data (e.g. Fig. 1.7).

1.2.2 Niger Delta and shale tectonics

The movement of fine-grained sediments as intrusive injectites or as extrusive eruptive sand blows has been described in different continental margins as mobile shales and mud volcanoes respectively: e.g. Trinidad (Birchwood, 1965); Markran Delta (Snead *et al.*, 1972; Azerbaijan (Guliev, 1992); Niger Delta (Graue, 2000); the Amazon Delta (Cobbold *et al.*, 2004; see also review in Wood *et al.*, 2010; Morley *et al.*, 2011). In pursuance to improving the understanding of argilokinesis from grain to basin-gravity scale, the term ‘shale tectonics’ was unanimously adopted by the geoscience community during the AAPG Hedberg Conference on Mobile Shale Basins (see Wood *et al.*, 2010; and references therein). Unlike in shale tectonic basins, where mobility is driven by porepressure, in halokinetic systems, the extrusive flow of salt result from the differences in density of the material and the surrounding sediments (e.g. Jackson and Vendeville, 1994; Prather *et al.*, 1998; Booth *et al.*, 2000).

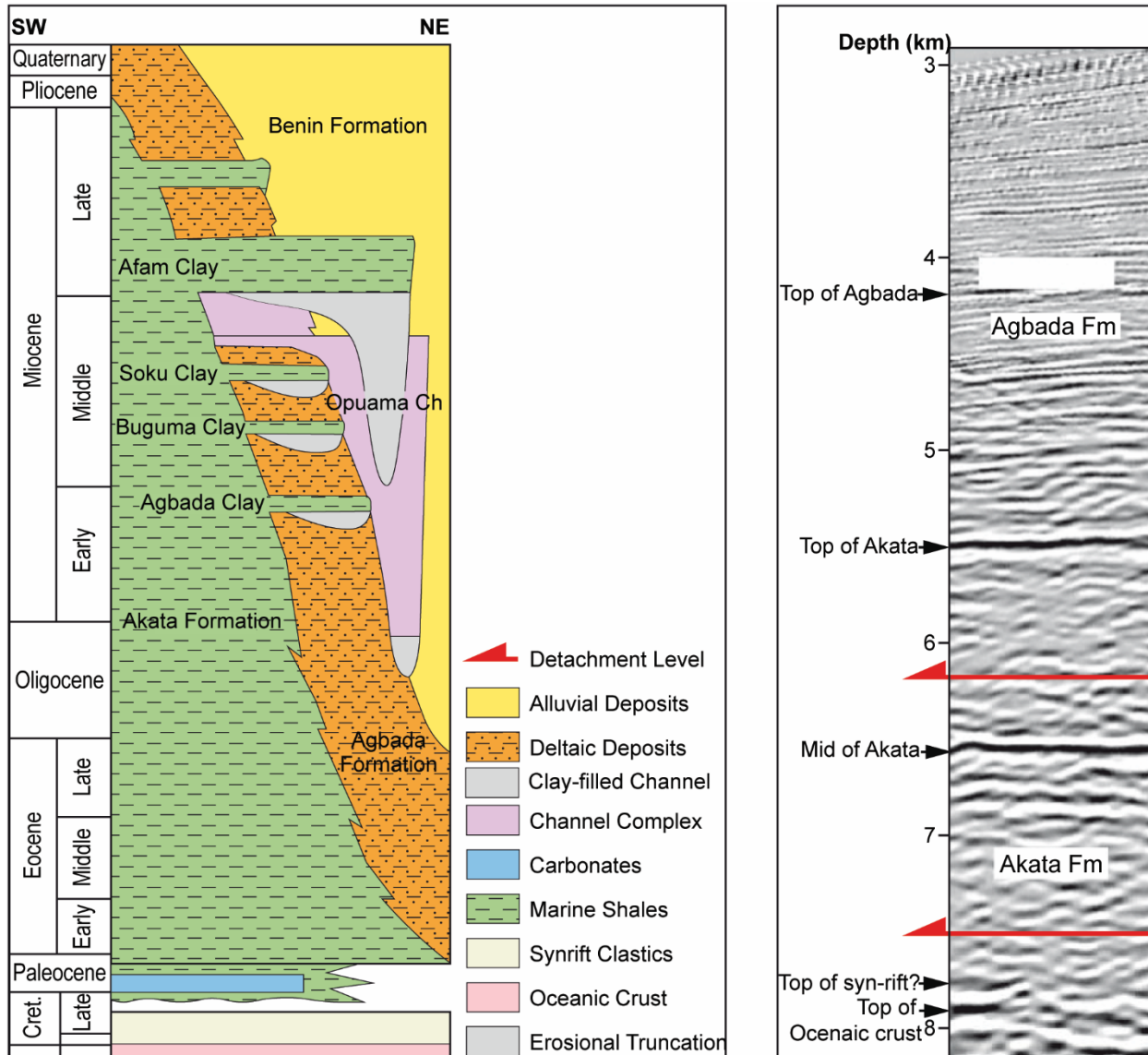


Fig. 1.7. Schematic illustration of the lithostratigraphic units underlying the Niger Delta (left). Deepwater seismic reflection data showing the reflection patterns of the Agbada and Akata Formations (right) (modified after Corredor *et al.*, 2005).

Mobile shale is any manifestation of clay constituents (indurated or not), which shows evidence of microscopic-scale fluid or plastic deformation (Wood, 2010; Fig. 1.6). It is mostly associated with zones of deep-seated overpressured shale or mudrock, which exhibit either a macroscopically ductile or a mixed brittle and ductile rheology (Wood, 2010). Mobile shale is generally characterized by seismic wipeout, low velocity/density and ductile deformation (Wiener *et al.*, 2010). Structural styles associated with mobile shales include detachment folds, shale domes with crestal normal faults, minibasins and thrust-shear-fault-bend and fault-propagation folds

(Costa and Vendeville, 2002; Fig. 1.6B). Previous studies in shale tectonic basins show that overpressure at depths between 4,000-6,000 m, results in the weakening and deformation of mud-rich sediments (e.g. Morley and Guerin, 1996, Van Rensbergen *et al.*, 1999; Graue, 2000; Rowan *et al.*, 2004).

In the Niger Delta, the primary mechanism of overpressure generation is linked to differential compaction, which results from the rapid burial of mud-rich sediments that lack sufficient permeability to transmit fluid (Morley and Guerin, 1996; Cohen and McClay, 1996; Graue, 2000; Cobbold *et al.*, 2009; Wiener *et al.*, 2010; Sapin *et al.*, 2012). Secondary mechanisms of overpressure generation may result from either hydrocarbon generation/maturation notably, cracking of oil to gas (e.g. methane-CH₄) at a higher temperature (Barker, 1990); or diagenetic transformation of clay minerals at smectite-illite transition (Bruce, 1984). While hydrocarbon maturation contributes between 50-80% increase of pore volume and shale mobility (Barker, 1990), clay diagenesis at depths ~2,164-3,322 m increases pore volume from 6-12% (Bruce, 1984).

Rapid sedimentation and progradation of the thick deltaic succession above the overpressured marine shales are the main triggering mechanism of shale mobility in the Niger Delta (Doust and Omatsola, 1990; Cobbold *et al.*, 2009; Mourgues *et al.*, 2009; Wiener *et al.*, 2010; Sapin *et al.*, 2012; Wu *et al.*, 2015). The build-up of the Niger Delta up to 4,000 m below the sea-level, coupled with the greater bulk density of the overlying delta wedge (the Agbada Formation), often result to the vertical and lateral squeezing of the overpressured marine shales (the Akata Formation) into mobile shales (Burke, 1972). Like other shale tectonic basins, mobile shale activity in the Niger Delta is often accompanied by the occurrences of fluid-flow seepages such as: bottom simulating reflector-BSR (Hovland *et al.*, 1997), mud volcanoes (Graue, 2000), gas pipes (Løseth *et al.*, 2011), pockmarks and gas hydrates (Brooks *et al.*, 2000; Ribolout *et al.*, 2011; Sultan *et al.*, 2012; Benjamin *et al.*, 2015; Benjamin and Huuse, 2017).

1.2.3 Sediment budget of the Niger Delta

The Niger catchment erodes basement complex and Cretaceous-recent sediments, that are transported down to the sea, where they are re-distributed by tides, waves, ocean currents, and finally partitioned to the deep basin by mass wasting and sediment gravity flows. The Niger

catchment is characterized by three major drainage systems: (i) the Niger-Benue (Fig. 1.3); (ii) the eastern rivers and (iii) the western rivers (Allen, 1965; Fig. 1.6A). The Niger and Benue rivers rise from the Equatorial Guinea and the Cameroon Mountains respectively (Fig. 1.3), and constitute the primary sediment supply to the Niger Delta (Allen, 1965).

The Niger-Benue drainage and their tributaries erode basement complex, Palaeozoic and Cretaceous-recent sediments in Guinea, Nigeria and Cameroon, supplying sediment directly to the Atlantic Ocean (Allen, 1965; Fig. 1.3). Of the total sand load of the Niger-Benue system, only about 35% reach the Atlantic, while about 65% is sequestered within its catchment (Allen, 1970). The Niger-Benue river bifurcates within the upper delta plain into smaller Sangana/Nun rivers that directly discharge its sediment load to the sea (Fig. 1.6A). The Niger-Benue river transports gravel and sand-sized sediments during flood periods (between September and October) and deposits fine-grained sediment within the delta plain (Nedeco, 1959).

Among the numerous rivers located in the eastern part of the Niger Delta, the New Calabar river is the most important supply system (Allen, 1965; Figs. 1.6A, 1.8A). The New Calabar River together with the rest of the eastern rivers, transport sediment directly to the Atlantic Ocean (e.g. Fig. 1.6A).

The western rivers discharge sediment partly directly and indirectly via longshore drift into the sea (Fig. 1.6A). The western and eastern coastal rivers collectively serve as distributary networks during low tides and tidal channels during the high tides (Allen, 1965; Burke, 1972; Figs. 1.6A, 1.8A). The coastal rivers generally overlie the heads of prominent canyons e.g. the Avon, Calabar and Mahin canyons, that route sediment captured from the coastal rivers to the deep basin (Burke, 1972; Fig. 1.8B).

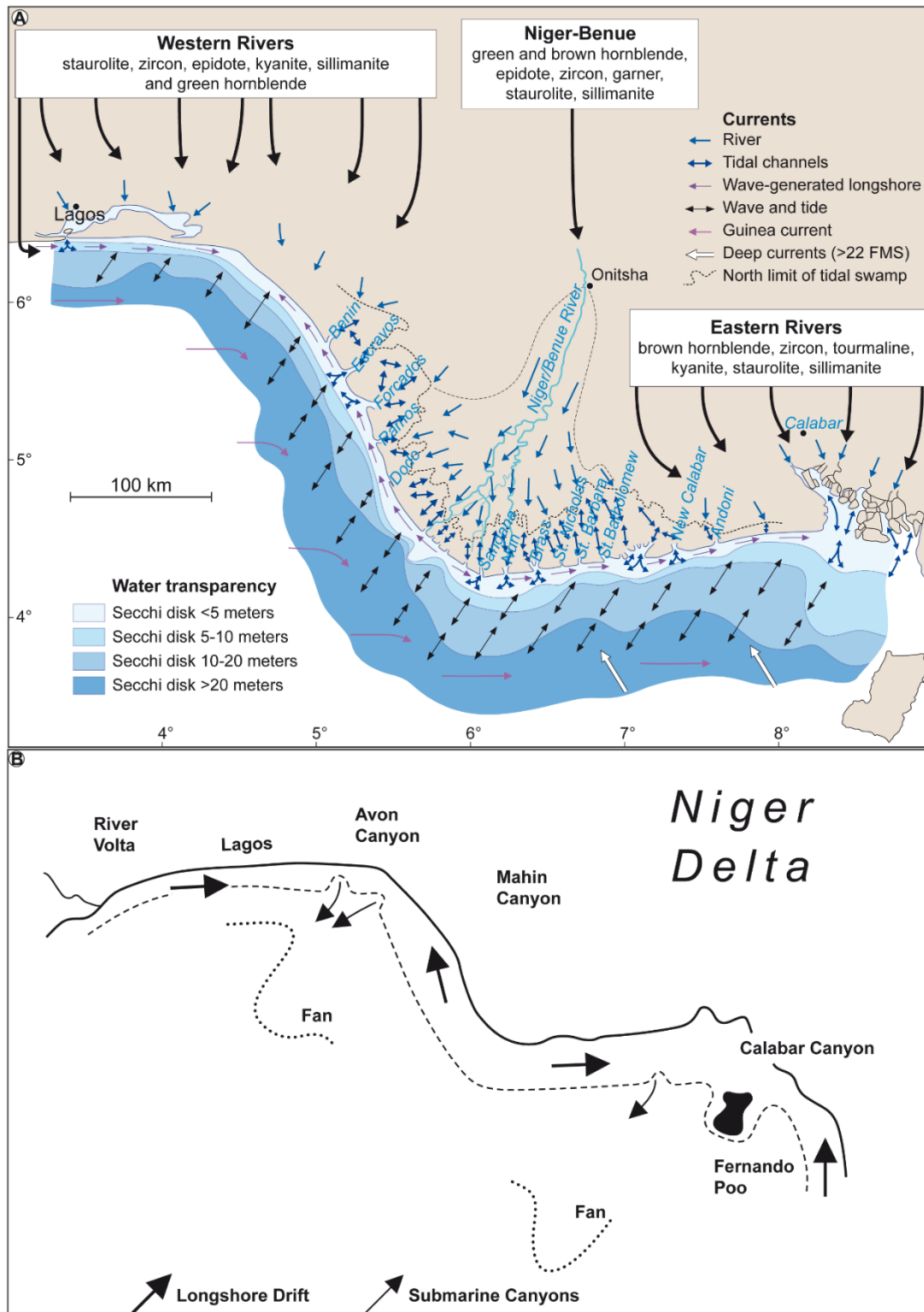


Fig. 1.8. Physiography of the Niger Delta. (A) Sediment supply and distributive agents in the Niger Delta (redrawn after Allen, 1965). (B) Sketch map illustrating the prevailing wind (Gulf of Guinea current) (redrawn after Burke, 1972).

1.2.4 Deepwater Sedimentation

Deepwater environment refers to bathyal water depths > 200 m that occur seaward of the continental shelf break, on the slope and basin floor settings (e.g. Shanmugam, 2016). The processes of sediment partitioning from the shelf to the deep basin have been studied by many authors (e.g. Middleton and Hampton, 1973; Lowe, 1982; Mutti and Normark; 1991; Hampton *et al.*, 1996; Stow and Mayall, 2000; Nelson *et al.*, 2009; Covault, 2011; McHargue *et al.*, 2011). The processes of sediment partitioning to the deep basin are subdivided into; (1) slides, (2) slumps, (3) debris-flows and (4) turbidity current (e.g. Middleton and Hampton, 1973; Lowe, 1982; Mutti and Normark; 1991; Hampton *et al.*, 1996; Stow and Mayall, 2000; Sprague *et al.*, 2005; Shanmugam, 2016; Nelson *et al.*, 2009; Covault, 2011).

1.2.4.1 Mass-transport deposits

Slides, slumps and debris-flow deposits are collectively referred to as mass-transport deposits (MTDs; Fig. 1.9). Mass-transport deposits are generally chaotic and discontinuous on seismic data (e.g. Navarre *et al.*, 2002; Posamentier and Kolla, 2003). Slides are a coherent mass of materials bound by well-defined slide plane/planar glide surface with no net internal deformation of the removed material (Middleton and Hampson, 1973; Nelson *et al.* 2009; Covault, 2011; Fig. 1.9). Slumps, on the other hand, occur if the removed materials break up into smaller blocks that rotate downslope along a concave up surface often with internal deformation (Middleton and Hampson, 1973; Nelson *et al.*, 2009; Covault, 2011; Fig. 1.9). Debris-flow is a plastic flow from which deposition occurs by freezing 'en masse' (e.g. Shanmugam, 2016; Fig. 1.9). Debris-flow deposits are generally distinguished from slides and slumps by their association with basal grooves (Posamentier and Kolla, 2003).

1.2.4.2 Turbidity current

In cases where internal deformation of mass flow is high, debris-flow may incorporate entrained seawater thereby transforming into a more turbulent, Newtonian flow know as turbidity current (Shanmugam, 2016; Figs. 1.9, 1.10). Turbidity current, as well as MTDs, are often triggered by failures of shelf-edge deltas along overstepped slopes, storms, sub-marine

earthquakes/volcanism (e.g., Shepard *et al.*, 1977; Piper *et al.*, 1985; Ricketts and Evenchick, 1999; Friedman *et al.*, 1992; Nelson *et al.*, 2009; Fatoke and Bhattacharya, 2010). Shelf-edge deltas play a significant role in sediment transfer from the shelf to the deep basin because once a delta reaches the shelf-edge (characterized by shelf-slope break geomorphic feature), sediment bypasses the topset onto canyon heads from where they are ultimately routed to the deep basin (Suter and Berryhill, 1985; Porebski and Steel, 2003; Carvajal and Steel, 2006). Dislodged materials starting off at the shelf-edge as slides, slumps or debris-flow may transform dynamically en route to the sink in the deep basin (Stow and Mayall, 2000; Covault, 2011; Fig. 1.9). When a sediment-gravity flow reaches the steeper part of the slope, its velocity increases due to the increase in gravitational pull, and the flow becomes more turbulent as ambient seawater is incorporated into the flow. The resulting turbidity current leads to the deposition of turbidites not only at the basin floor but also on the slope as flow interact with structures on the slope (Normark *et al.*, 1980; Stow and Piper, 1984; Mayall and Stewart, 2000; Wynn *et al.*, 2000; Posamentier and Kolla, 2003; Ferry *et al.*, 2005; Adeogba *et al.*, 2005; Bakare *et al.*, 2007; Mayall *et al.*, 2006; Clark and Cartwright, 2012). Turbidity currents generally evolve from (i) deeply incised, highly confined channels with bypass deposits on the slope through; (ii) partially confined channels at the slope-basin transition to; (iii) distributary channels (lobe deposits) at the basin floor (e.g. Lowe, 1982; Mutti and Normark, 1991; Sprague *et al.*, 2005; Fig. 1.10).

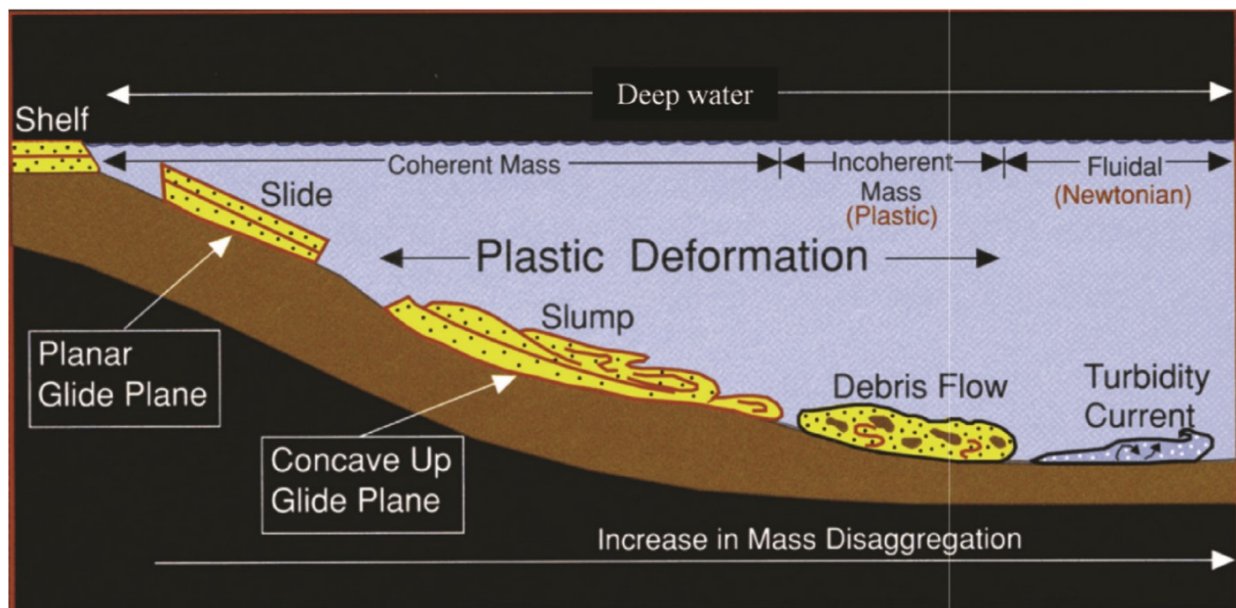


Fig. 1.9. Schematic diagram illustrating slides, slumps, debris-flow and turbidity current evolution from the shelf-edge to the deep basin (from Shanmugam, 2016).

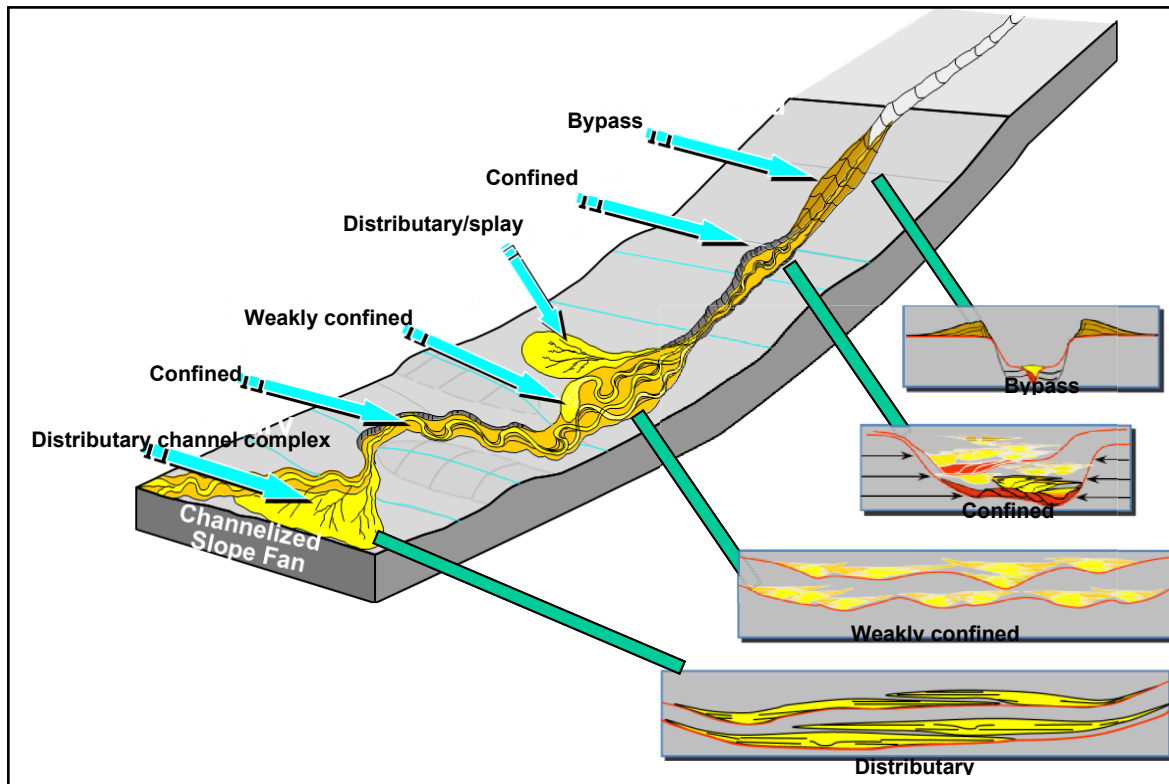


Fig. 1.10. Schematic illustration of deepwater depositional model. Note the evolution of turbidity deposits from unconfined at the upper slope through partially confined at the slope-basin transition to unconfined at the basin floor, where turbidites accumulate (from Sprague *et al.*, 2005).

1.2.4.3 Slope equilibrium profile, control on submarine channels and depositional patterns

In shale tectonic basins such as the Niger Delta, where the rate of sedimentation is often greater than the rate of mobile shale-driven subsidence, stepped equilibrium profile characterizes the depositional profile (Prather *et al.*, 2012; Fig. 1.11). The presence of folds associated with thrust/mobile shale-cored structures often creates local positive relief flanked by negative topographies (intraslope basins), that impact submarine channel morphology and depositional patterns (Adeogba *et al.*, 2005; Ferry *et al.*, 2005; Bakare *et al.*, 2007; Prather *et al.*, 2012; Clark and Cartwright, 2012; Jolly *et al.*, 2016; Fig. 1.11). Along a stepped profile, the increase in slope gradient referred to as ‘knickpoint’ develops above folds or thrust-cored anticlines (e.g. Ferry *et al.*, 2005). An imaginary line, which separates positive topographies above which erosion occurs and topographic lows, below which deposition occurs, defines hypothetical ‘equilibrium profile’ (Kneller, 2003; Huyghe *et al.*, 2004; Ferry *et al.*, 2005; Fig. 1.11). Maximum erosion of positive

topographies causes submarine channels to develop low sinuosity and high depth-to-width ratio, while deposition within the adjacent intraslope basins results to high sinuosity and low depth-to-width ratio (e.g. Prather *et al.*, 1998; Adeogba *et al.*, 2005; Ferry *et al.*, 2005; Bakare *et al.*, 2007; Clark and Cartwright, 2012; Jolly *et al.*, 2016). The presence of intraslope basins and growing structures associated with mobile shales along stepped slope generally facilitate the development of slope breaks (Garcia and Parker, 1989; Alexander and Morris, 1994). Turbidity currents generally undergo hydraulic jump at the slope breaks, decelerate and deposit the coarse fraction of its sediment load within the intraslope basins, while the fine-grained fraction of the flow is suspended further down depositional dip (Garcia and Parker, 1989; Alexander and Morris, 1994). Occasionally, the most dilute upper part of the flow, characterized by suspension cloud is able to escape basin confinement, spilling onto the adjacent topography through a process referred to as flow stripping (e.g. Covault *et al.*, 2011). Numerical studies show that the presence of slope breaks along stepped profile enhances change in the internal parameter of turbidity current from supercritical conditions (Froude number > 1) to subcritical conditions (< 1) (Komar, 1971). The decrease in the velocity of the flow and increase in thickness as a result of entrainment of ambient water, leads to a decrease in flow density (Komar, 1971). Deposition of the coarsest particles, transported by turbidity current downstream of a hydraulic jump (Komar, 1971), is the direct consequence of the change in the internal shear strength of turbidity current (Komar, 1971; Garcia, 1993). While growing structures associated with mobile shales and thrust faults constantly deform the slope and create disequilibrium conditions, submarine channels and associated sediment gravity flows constantly smooth topography in an attempt to establish equilibrium condition (Prather *et al.*, 1998; Adeogba *et al.*, 2005; Ferry *et al.*, 2005; Bakare *et al.*, 2007; Clark and Cartwright, 2012; Jolly *et al.*, 2016; Fig. 1.11).

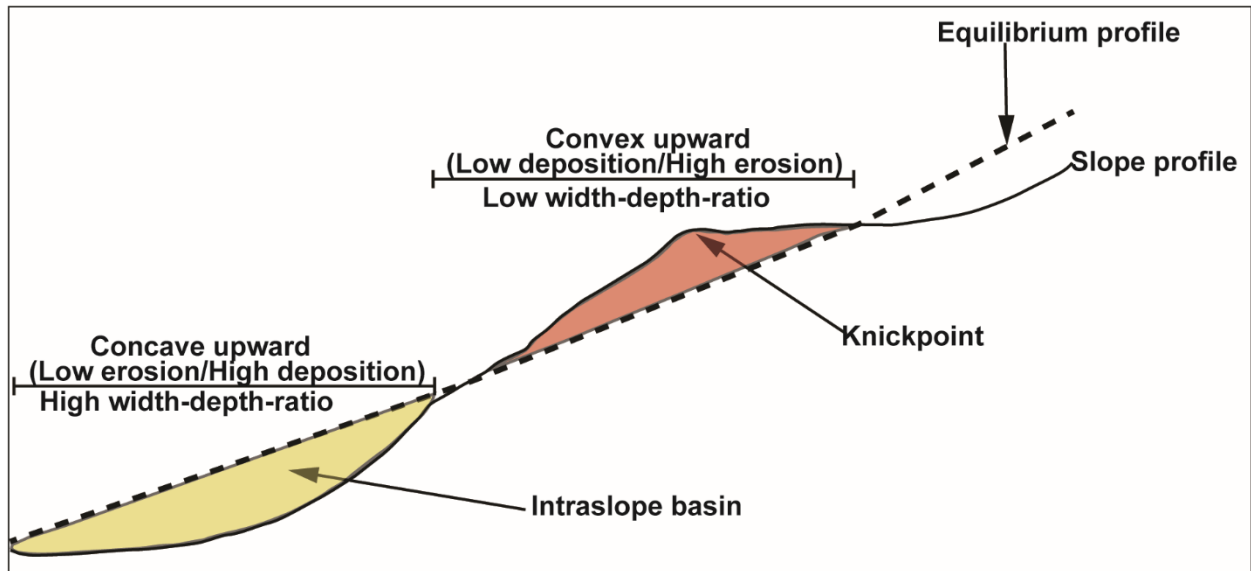


Fig. 1.11. Schematic diagram illustrating the model of the equilibrium profile in deepwater settings. Note the occurrence of a knickpoint on a topographic high, characterized by erosion and high-depth-to-width ratio, and deposition within negative topography (intraslope basin), characterized by low a depth-width ratio (modified after Ferry *et al.*, 2005)

CHAPTER 2

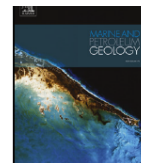
Seismic stratigraphy and depositional architecture of Neogene intraslope basins, offshore western Niger Delta



Contents lists available at [ScienceDirect](#)

Marine and Petroleum Geology

journal homepage: www.elsevier.com/locate/marpetgeo



Research paper

Seismic stratigraphy and depositional architecture of Neogene intraslope basins, offshore western Niger Delta



Kelvin I. Chima^{a,b,*}, Damien Do Couto^a, Estelle Lerpoux^c, Silvia Gardin^d, Nick Hoggmascall^e, Marina Rabineau^f, Didier Granjeon^g, Christian Gorini^a

^a Sorbonne Université-ISTeP UMR 7193, Paris, France

^b Alex Ekwueme Federal University, Ndufu-Alike Ikwo, Ebonyi State, Nigeria

^c IFREMER, ZI Pointe du Diable, Plouzane, France

^d Centre de Recherche en paléontologie Paris, UMR 7207, France

^e Shell Petroleum Development Company, Lagos, Nigeria

^f CNRS, UMR 6538, LGO (CNRS/UBO/UBS), Plouzane, France

^g IFPEN, Rueil-Malmaison, France

Abstract

Located on a divergent margin dominated by gravity tectonics above overpressured marine shales, the Niger Delta slope has been described as having a stepped profile characterized by ‘filled ponded basins’ that are prone to erosion and sediment bypass. Previous studies based on 3D seismic data have described the depositional architecture of the western Niger Delta’s upper slope, but calibration of the seismic facies is lacking and the timing of major changes in sedimentary record remains elusive. In this study, seismic sequence-stratigraphy, 3D geomorphological analyses of high-resolution 3D seismic data, and bio/chronostratigraphic analyses from four boreholes, enabled the identification and characterization of the depositional architecture in Neogene ‘filled ponded basins’. Seven major seismic units were dated as Chattian, Burdigalian, Serravallian, Tortonian, Middle Pliocene and Middle Pleistocene to the present-day. Major changes in the sedimentary record occurred in the Plio-Pleistocene, with the onset of erosive channel levee systems (CLSs) and mass-transport deposits (MTDs) generally capped by a hemipelagic drape. Amalgamated CLSs characterize the Tortonian-Late Miocene while erosive MTDs and CLSs characterize the Plio-Pleistocene units. Thick, laterally extensive MTDs are associated with regional slope instability, while active mobile shale triggered local spatially confined MTDs. Submarine channels evolved from moderate to highly sinuous. The degree of channel confinement generally decreases downstream where they are characterized by abandoned meander loops and avulsion resulting from levee breaching. Channel fills and levees/overbank deposits topped by hemipelagic drapes provide effective reservoir/seal (traps) for hydrocarbons. The alternation of channel deposits and hemipelagic layers indicate that eustasy controlled depositional patterns at a regional scale, while the spatio-temporal switches in submarine channel courses show that shale tectonics locally controlled deposition in intraslope basins.

Keywords: West Africa; Niger Delta; Seismic sequence stratigraphy; Filled ponded basins; Mass-transport deposits; Turbidite systems; Chronostratigraphy.

2.1 Introduction

The depositional architecture of the deep-water systems located on divergent margins is predominantly controlled by gravity tectonics (e.g. Doust and Omatsola, 1990; Damuth, 1994; Cohen and McClay, 1996; Morely and Guerin, 1996; Graue, 2000; Cobbold *et al.*, 2009). Gravity gliding and gravity spreading are the two main aspects of gravity tectonics that deform the sedimentary wedges that prograde into deep-water environments (Morley *et al.*, 2011). While gravity gliding is characterized by the rigid translation of a rock mass down a slope, gravity spreading results from flattening and lateral spreading of a rock mass under its weight (Ramberg, 1981; Dejong and Sholten, 1973; Alves and Lourenço, 2010; Alves, 2015). In the Niger Delta, gravity spreading driven by delta wedge progradation above overpressured marine shales has been described as the primary control of accommodation and depositional patterns (e.g. Doust and Omatsola, 1990; Damuth, 1994; Cohen and McClay, 1996; Morely and Guerin, 1996; Graue, 2000; Cobbold *et al.*, 2009).

The slope of the Niger Delta, characterized by a lower subsidence rate than its regional sedimentation rate, has been described as comprising a ‘stepped profile’, compared to the ‘above-grade slope profile’ typical of the central Gulf of Mexico-where the rate of salt driven subsidence is always greater than that of sediment supply (Prather, 2003). Consequently, ‘shallow ponded basins/perched accommodation’ described by Prather *et al.* (2012), but herein referred to as ‘filled ponded basins’, dominate the intra-slope regions of the Niger Delta (Booth *et al.*, 2000; Prather, 2000). These ‘filled ponded basins’ are dominated by healed-slope accommodation that is always overfilled or bypassed compared to the underfilled ponded basins in the central Gulf of Mexico (Prather, 2003). Although the lack of ponded accommodation in the upper-and mid-slope regions of the Niger Delta renders it susceptible to erosion and bypass, thin reservoir facies associated with channel and overbank deposits in these areas could still be good drilling targets (Prather, 2003). Furthermore, hydrocarbon traps are better developed in filled ponded systems, where reservoir facies occur directly below mud-rich pelagic/hemipelagic deposits (Prather, 2003).

Following the discovery of hydrocarbons in the deep-water Niger Delta in recent decades, exploration is now focused on understanding the control on depositional architecture and reservoir distribution in the deep-water setting of this region (e.g. Chapin *et al.*, 2002; Adeogba *et al.*, 2005). Consequently, the impact on submarine channel evolution and depositional patterns by mobile

shale structures has received considerable attention (e.g. Adeogba *et al.*, 2005; Bakare *et al.*, 2007; Clark and Cartwright, 2012; Prather *et al.*, 2012., Jobe *et al.*, 2015; Jolly *et al.*, 2016; Hansen *et al.*, 2017). The depositional architecture of the Pliocene and Quaternary filled ponded basins on the western slope of the Niger Delta has already been described and includes MTDs and turbidite systems draped by hemipelagites (e.g. Adeogba *et al.*, 2005; Bakare *et al.*, 2007). Similar depositional architectures have been described in the deep-water fold-and-thrust belt of the Niger Delta (e.g. Posamentier and Kolla, 2003; Clark and Cartwright, 2012). Recently, academic seismic-stratigraphic studies were conducted on the deeper Neogene stratigraphic records of the upper slope of the western Niger Delta, although lacking calibration (Benjamin *et al.*, 2015; Benjamin and Huuse, 2017). Industry-based study of Neogene stratigraphy reveals that highly amalgamated channel fill deposits are less compartmentalized than less amalgamated overbank deposits (Chapin *et al.*, 2002).

Despite the plethora of observations on the upper slope of the western Niger Delta, lack of published borehole and bio/chronostratigraphic data has limited seismic facies calibration and age estimates for the entire Neogene succession in this region. Similarly, no study has investigated the interactions between shale tectonics and submarine channels/reservoir distribution in the study area (Fig. 2.1). Hence, the objectives of this study are to: (1) identify and date major sequence-stratigraphic surfaces (Neogene to present-day) preserved on the upper slope of the western Niger Delta; (2) calibrate seismic facies by defining depositional environments to better the understanding of depositional patterns and their controlling factors; (3) investigate the interaction between shale tectonics and depositional patterns with a view to predicting reservoir distribution in the associated ‘filled ponded basins’. This study not only provides age constraints on the Neogene stratigraphy of the western Niger Delta, but also describes the effect of the interplay between autogenic and allogenic forcing on the depositional architecture and potential reservoir distribution in ‘filled ponded basins’.

2.2. Geological setting

The Niger Delta is located along the Equatorial Atlantic margin of West Africa (Fig. 2.1). The delta is underlain by sub-aerial and submarine sediments covering an area of ~140,000

km²; and its thickness reaches 12 km (Allen, 1965; Evamy *et al.*, 1978; Doust and Omatsola, 1990). The progradation of this siliciclastic wedge since the Late Eocene has been estimated as ~300 km (Doust and Omatsola, 1990; Fig. 2.1). Known oil and gas resources rank the delta the twelfth largest petroleum province in the world (Tuttle *et al.*, 1999). The Niger Delta is sub-divided into three major structural domains: (i) an extensional zone below the continental shelf, (ii) a transitional zone below the upper slope, and (iii) a compressional zone located at the toe of the slope (Doust and Omatsola, 1990; Damuth, 1994; Connors *et al.*, 1998; Morgan, 2004; Billoti and Shaw, 2005; Fig. 2.1).

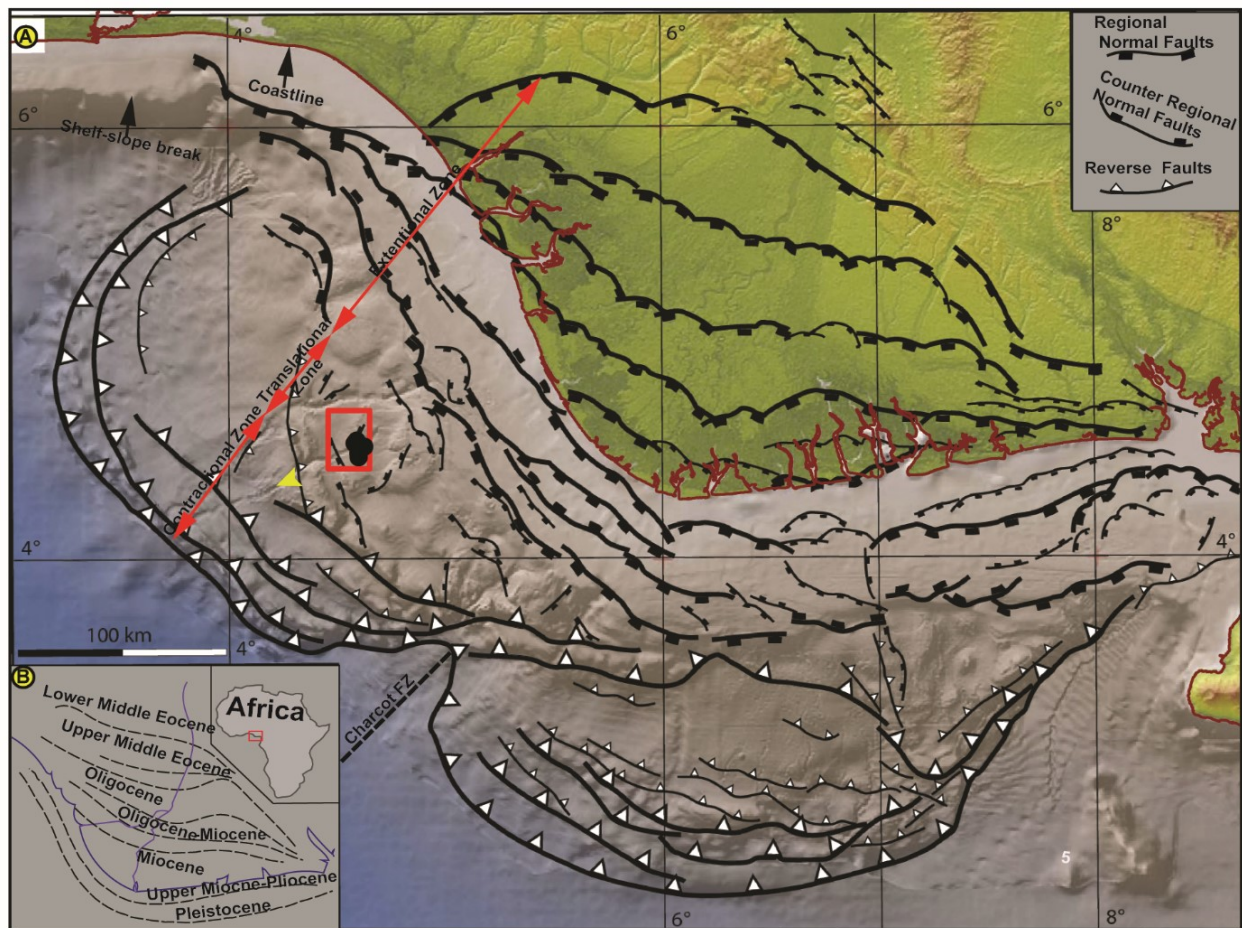


Fig. 2.1. A: Superposed relief and bathymetric map of the Niger Delta showing the extensional, translational and compressional zones. B: Schematic map showing progradation of the delta from the Late Eocene to the present-day. The red box in inset map B shows the location of the Niger Delta in the Gulf of Guinea. Red box and black circles in A show the limit of the 3-D block we studied and the locations of the boreholes, respectively. Yellow arrow points to the downstream

section of the submarine channel complex that crossed the study area. A, B modified after (Rouby *et al.*, 2011).

The stratigraphy of the Niger Delta is dominated by three major lithostratigraphic units: the Akata, Agbada and Benin Formations (Short and Stauble, 1967; Evamy *et al.*, 1978; Avbovbo, 1978; Doust and Omatsola, 1990; Fig. 2.2). The Akata Formation comprises marine shales that range in thickness from 7,000 m beneath the continental shelf to 2,000 m in the distal portion (Doust and Omatsola, 1990). Its thickness reaches 5,000 m in the deep fold-and-thrust belt due to the repeated occurrence of thrust ramps (Wu and Bally, 2000; Corredor *et al.*, 2005). The Agbada Formation constitutes the deltaic unit of the Niger Delta. The thickness of this paralic unit reaches 3,500 m (Evamy *et al.*, 1978; Avbovbo, 1978; Doust and Omatsola, 1990). The depositional setting of this lithostratigraphic unit ranges from delta-front, delta-topset to fluvio-deltaic environments (Avbovbo, 1978). The Benin Formation consists of alluvial to upper coastal plain deposits up to 2,000 m thick (Avbovbo, 1978). The Agbada and Benin Formations are associated with clay-filled channels that were incised during the Late Miocene and Plio-Quaternary (Fig. 2.2).

The present study is focused on the mobile shale belt located on the upper continental slope downward the transition between the extensional and compressional belts, offshore western Niger Delta (Fig. 2.1; red square). It covers 638 km² at a distance of ~120 km from the present-day coastline (Fig. 2.1), at depths ranging from 900 to 1,150 m within the Akata Formation, which is located at water depths between ~810 to ~3240 m. The area is characterized by 'filled ponded basins' located at the flanks of mobile shales and ~3 km wide NE-SW trending submarine channel complex extending more than 25 km into the 3D block studied (Fig. 2.3). The reservoir compartmentalization of the block has already been investigated by Chapin *et al* (2002) and seabed mounds and pockmarks by Benjamin *et al.* (2015); Benjamin and Huuse (2017).

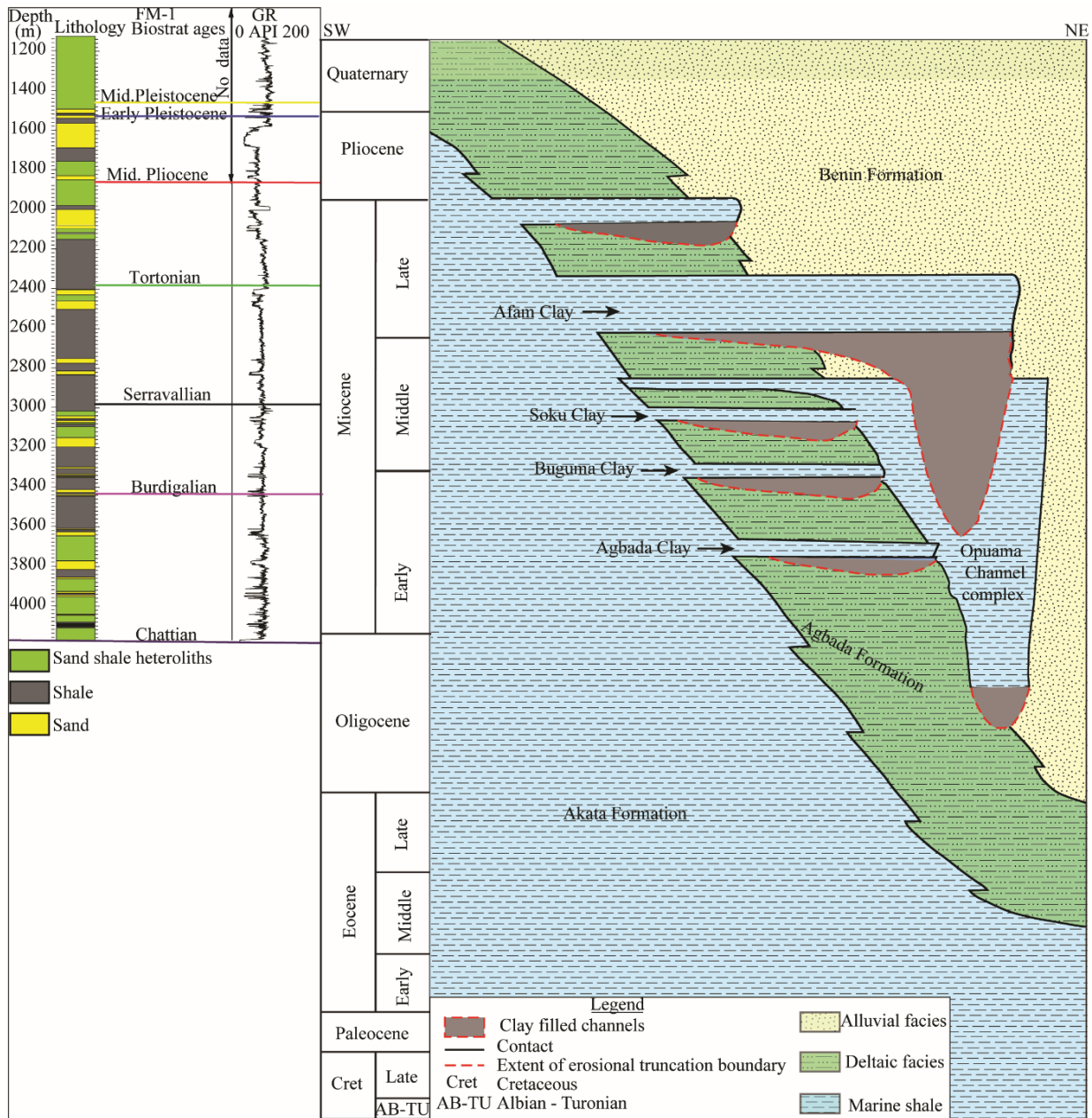


Fig. 2.2. Schematic diagram (not drawn to scale) of the three lithostratigraphic units underlying the Niger Delta (redrawn after Brownfield, 2016, on the right). Representative deep borehole (FM-1 well) that penetrated more than 4 km into the deeper Neogene sedimentary records in the Akata Formation and the bio-chronostratigraphically dated intervals in this study (on the left).

2.3. Dataset and methods

2.3.1 Dataset

The dataset used in this study includes high-resolution 3D seismic and borehole data, comprising well logs, core and biostratigraphic data.

2.3.1.1 Seismic data

The 3D seismic data were processed as a zero-phase source wavelet in American reverse standard polarity. Thus, an increase in acoustic impedance corresponds to a trough (blue loop) in the wavelet, while a decrease in acoustic impedance is represented by a peak (red loop) in the wavelet. The horizontal resolution of the data is characterized by a stacking bin spacing of 25 m x 25 m (in-line and cross-line spacing), and a seismic recording sampling interval of 4 milliseconds two-way travel time (TWT). The dominant frequency of the data is 30 Hz over the first 3 seconds (TWT) but decreases between 20-25 Hz below a depth of 3 km. Using average interval seismic velocity of 1,639.4 m/s and applying the velocity-wavelength equation ($\lambda/4$; Brown, 1999), the vertical resolution of the data was ~13.7 m over the Pliocene-Quaternary intervals but decreased between 25 and 30 m at depths below 3 km.

2.3.1.2 Borehole data

The lithology, facies and depositional environments of five boreholes, labelled FM-1, FM-2, FM-3ST1, FM-4ST1 and FM-5 located in the southern part of the study area (Fig. 2.3), were analyzed. The wells penetrated respective total depths of 4,154 m, 3,627 m, 2,924 m, 3,458 m and 3,497 m below the seafloor. Petrophysical (gamma-ray, resistivity, neutron, density and sonic) logs were acquired mostly in the deeper stratigraphic intervals, e.g. between 1,140-4,154 m in the deepest FM-1 well and 1,718-2,119 m in the shallowest FM-3ST1 well. Four of the five boreholes contain biostratigraphic data, whereas core data were only available in two boreholes.

2.3.2 Methods

2.3.2.1 Seismic and sequence stratigraphic analysis

A standard seismic-stratigraphic analysis approach (Mitchum and Vail, 1977) was used for the 3D seismic data based on the recognition of reflection termination patterns such as onlap, erosional truncations, seismic facies/configuration and vertical stacking patterns. Previously described depositional architectures include MTDs, turbidite systems and hemipelagic drapes. In the present study, MTDs and turbidite deposits were identified based on seismic criteria and 3D geomorphology (e.g. Posamentier and Kolla, 2003; Richardson *et al.*, 2011). MTDs were recognized (i) by their basal shear zone or basal continuous surface, which delimits the overlying deformed materials and the underlying, relatively continuous materials (Frey Martinez *et al.*, 2005; Alves and Lourenço, 2010; Gamberi *et al.*, 2011; 2015) and (ii) by their top, characterized by rugose/irregular topographies (Richardson *et al.*, 2011). In terms of internal architecture, MTDs may be chaotic or transparent depending on (i) the nature of materials inherited from the source area (Masson *et al.*, 2006), and (ii) the distance from source area (e.g. Alves *et al.*, 2009; Omosanya and Alves, 2013; Rovere *et al.*, 2014; Omosanya and Harishidayat, 2019). Turbidite systems were recognized based on the presence of sandy submarine channel deposits, which are generally characterized by high to moderate seismic reflectivity and high root mean square (RMS) amplitudes on 3D paleo-geomorphological maps (see also Posamentier and Kolla, 2003; Catuneanu, 2006). Drapes were interpreted as the result of a combination of pelagic/hemipelagic suspension fall-out as well as from the fine-grained suspended portion of turbidity flows (Kneller and McCaffrey, 1999).

2.3.2.2 Well logs, lithofacies and depositional environment

The standard approach to well-log analysis (e.g. Mitchum and Vail, 1977) is the display and visual inspection of accurately scaled gamma-ray, neutron-density cross plots, resistivity and sonic logs. Integrated analysis of these logs and calibration with core data helped delineate lithofacies and associated depositional environments.

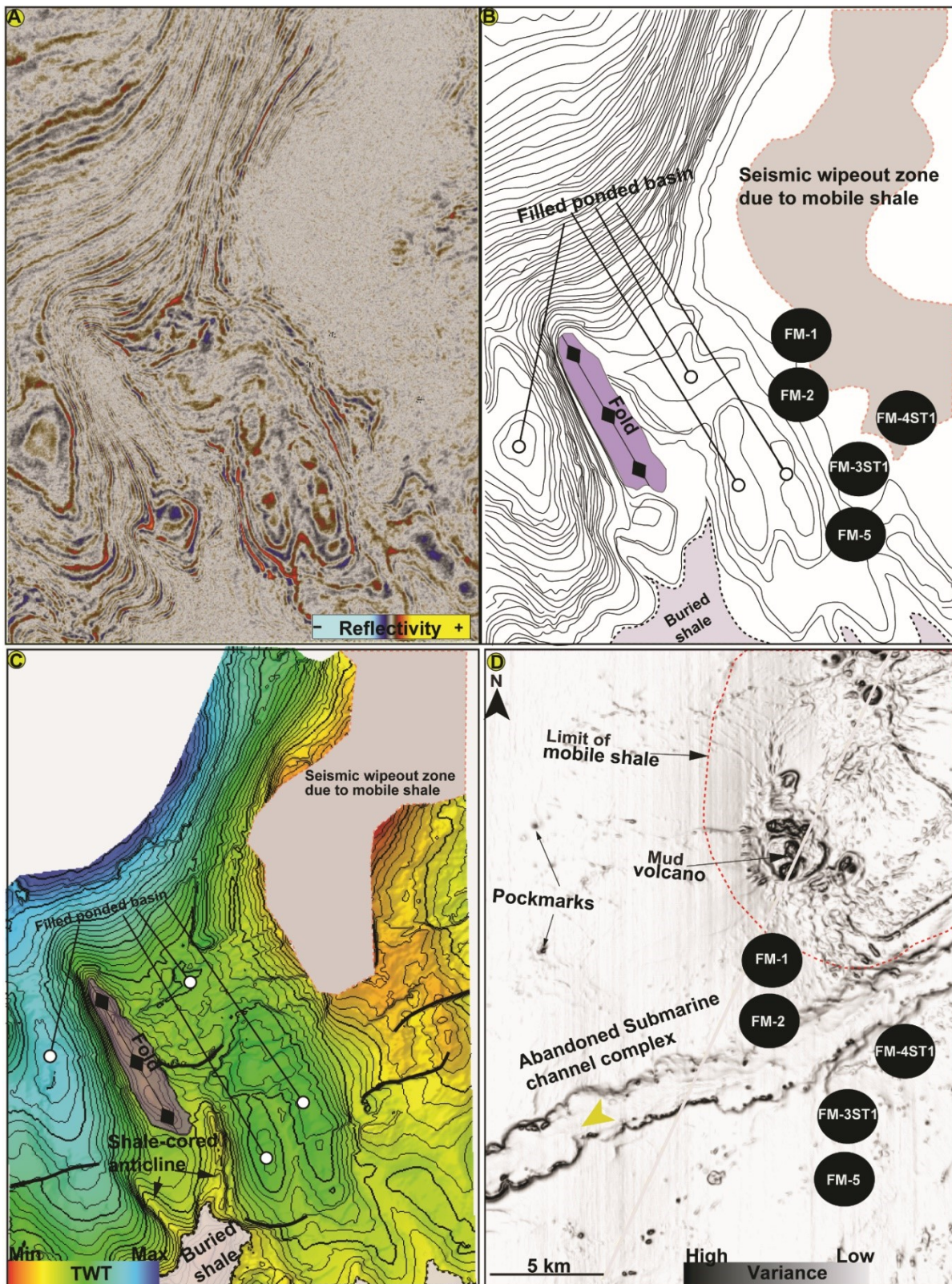


Fig. 2.3. Physiography of the study area. A, B: Uninterpreted and uninterpreted time slice (at 4.9 seconds twt) showing mobile shales and filled-ponded basins in the block studied. C: Time-

structure map near the level of time slice illustrating the same features as in panels A and B. D: Variance attribute map of the seabed showing the presence of mud volcanoes and submarine channel complex. Black dots show the location of the boreholes.

2.3.2.3 Bio- and chronostratigraphic analyses

We analyzed existing biostratigraphic data, chiefly calcareous nannofossils and planktonic foraminifera, from ditch cutting samples available in four boreholes. This allowed us to constrain the ages of Neogene stratigraphic intervals.

2.3.2.4 3D Seismic geomorphology

In addition to 2D seismic stratigraphy, we conducted 3D seismic geomorphological analyses to identify erosional features and channel architectures, and to distinguish main depositional elements (mass-flow deposits, channel deposits, overbank deposits, mud volcanoes and hemipelagic units). This was achieved through a detailed analysis of seismic attributes, horizon slices and amplitude maps (after Posamentier and Kolla, 2003; Catuneanu, 2006).

Seismic attributes are all observations extracted from seismic data that directly or indirectly facilitate hydrocarbon identification, lithological discrimination or geological interpretation (Chopra and Marfurt; 2007; Taner *et al.*, 1994). We generated RMS and Variance Edge/Coherence attributes from the original 3D seismic data using Petrel™ software. The RMS attribute computes the square root of the sum of squared amplitudes over the geological interval of interest and facilitates lithofacies discrimination (e.g. Catuneanu, 2006). The variance attribute (e.g. Fig. 2.3D) emphasizes the correlation of seismic traces by assigning light colours to areas where seismic traces correlate (low variance) and dark colours to areas where there is no correlation (high variance; Fig. 2.3D; see Catuneanu, 2006). This attribute was used to delineate structural and stratigraphic discontinuities such as faults, mobile shales, turbidite systems, MTDs etc.

2.4. Results and interpretation

This section presents the results of seismic facies analysis and lithofacies description, depositional environments and depositional architectures within the stratigraphic intervals we studied. Seismic artefacts (*sensu* Chopra and Marfurt, 2007; Alves, 2015) in the studied 3D volume is characterized by seismic wipe out in mobile shales zones (e.g. Fig. 2.3A).

2.4.1. Seismic facies analysis and seismic stratigraphic units

2.4.1.1 Seismic facies analysis

Six seismic facies were identified in the studied 3D volume (Fig. 2.4) using the seismic facies classification schemes proposed by Prather *et al.* (1998) and Hanson *et al.* (2017). These include: (1) chaotic, discontinuous low amplitude seismic facies (B_l), generally characterized by an erosive base, irregular top and deformed internal architecture interpreted as mass-transport deposits (MTDs); (2) chaotic, discontinuous, high amplitude seismic facies (B_h) interpreted as turbidite feeder channels; (3) inclined, coherent/moderately deformed, high amplitude seismic facies interpreted as slides/slump blocks; (4) parallel, continuous/convergent, high amplitude seismic facies (C_{bh}) interpreted as amalgamated channels/lobes; (5) convergent thinning high amplitude seismic facies (C_{th}) flanked by seismic packages that onlap negative topographic relief features interpreted as levees and channel fill deposits, respectively; (6) transparent, continuous seismic facies (D) interpreted as hemipelagic drapes.

2.4.1.2 Seismic stratigraphic units

Seven major seismic stratigraphic units were identified in the Neogene stratigraphic records of the upper slope of the western Niger Delta (Fig. 2.5).

Unit 1

This is the oldest stratigraphic unit identified in the study area. This unit has not been drilled. It is characterized by high amplitude seismic packages whose base corresponds to the top of the reflection-free (low reflectivity) seismic unit (Fig. 2.5). Seismic reflectivity in Unit 1 generally decreases toward the north corresponding to a vertical, irregular, seismic wipeout zone that extends upwards from 6 to 1.8 seconds (twt) deforming the overlying seabed (Fig. 2.5). This feature was interpreted as mobile shale. Unit 1 thins from north and south toward the mobile shale zone in the north (Fig. 2.5). The overall thinning of seismic Unit 1 from the south to the north toward mobile shale indicates syn-kinematic deformation linked to the movement of mobile shale during the deposition of Unit 1 (Fig. 2.5).

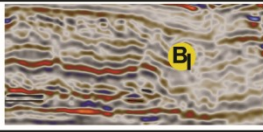
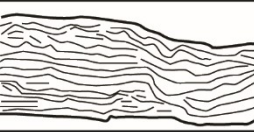
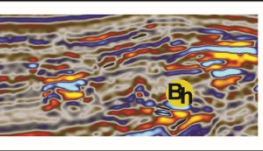
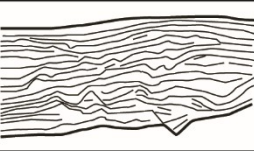
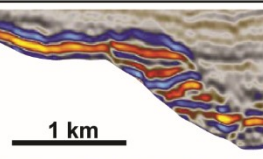
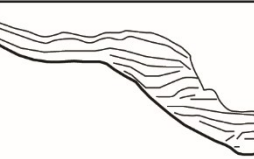
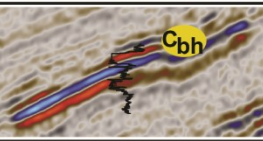
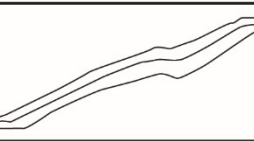
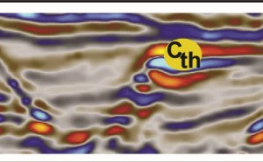
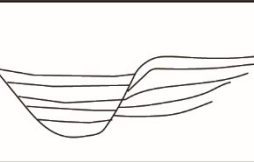
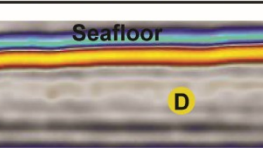
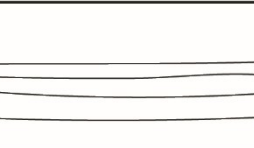
| Prather <i>et al.</i> (1998); Basin floor/slope depositional environments | Seismic facies | Line drawing | Depositional Architecture |
|---|---|--|---|
| Mass-flow deposits with variable lithology |  |  | MTD |
| Turbidite feeder channel systems, amalgamated channel sands |  |  | Turbidite feeder channels |
| Submarine slide /slumps |  |  | Slide blocks/slumps |
| Basin-floor and slope, submarine fan complexes with sand sheets and levees |  |  | Amalgamated channels/lobe deposits |
| Fine-grained suspension fallout, Muddy/overbank turbidites and hemipelagic drapes on slopes |  |  | Channel fill and levees/overbank deposits |
| Muddy turbidites to condensed section and hemipelagic drape |  |  | Hemipelagic drape |

Fig. 2.4: Overview of the seismic facies observed in this study, corresponding line drawings and interpretations of the depositional environment.

Unit 2

The base of Unit 2 shows base lap (apparent onlap) surface overlain by parallel to sub-parallel, moderate to high amplitude seismic packages that generally decrease in reflectivity northward due to the presence of mobile shale (Fig. 2.5). Seismic packages within this unit are generally subparallel and thin northward except within a landward dipping normal fault near the mobile shale zone (Fig. 2.5).

Unit 3.

The base of unit 3 is also a base lap (apparent onlap) surface overlain by parallel continuous, high amplitude seismic packages whose reflectivity decreases northward toward the mobile shale zone (Fig. 2.5). Although Unit 3 reaches a maximum thickness within a fault-controlled accommodation in the southern part, it thins northward toward the mobile shale zone (Fig. 2.5).

Unit 4

The base of unit 4 is locally erosional and marks a transition from underlying parallel, continuous high amplitude seismic packages to overlying moderate to high amplitude strata (Fig. 2.5). Unit 4 is characterized by localized high amplitude seismic packages that generally converge or thin away from their central parts toward their lateral limits (Fig. 2.5). These seismic packages are interpreted as amalgamated channel levee deposits (dashed purple circles in Fig. 2.5). Although Unit 4 also reaches a maximum thickness in fault-controlled accommodation in the southern part, it thins northward toward the mobile shale zone (Fig. 2.5).

Unit 5

Unit 5 is marked at the base by an erosional event overlain by thin, discontinuous/chaotic, low amplitude seismic packages that grade to relatively continuous, high amplitude seismic packages near the mobile shale zone (Fig. 2.5). Seismic geometries in Unit 5 vary from sub-parallel (north and south) in the mobile shale zone to convergent/thinning toward the mobile shale zone (Fig. 2.5). Unit 5 is characterized by amalgamated, high amplitude seismic packages corresponding to the channel levee deposits described above (dashed purple circles in Fig. 2.5). An over 80 m-thick transparent seismic unit interpreted as an hemipelagic drape overlies this unit

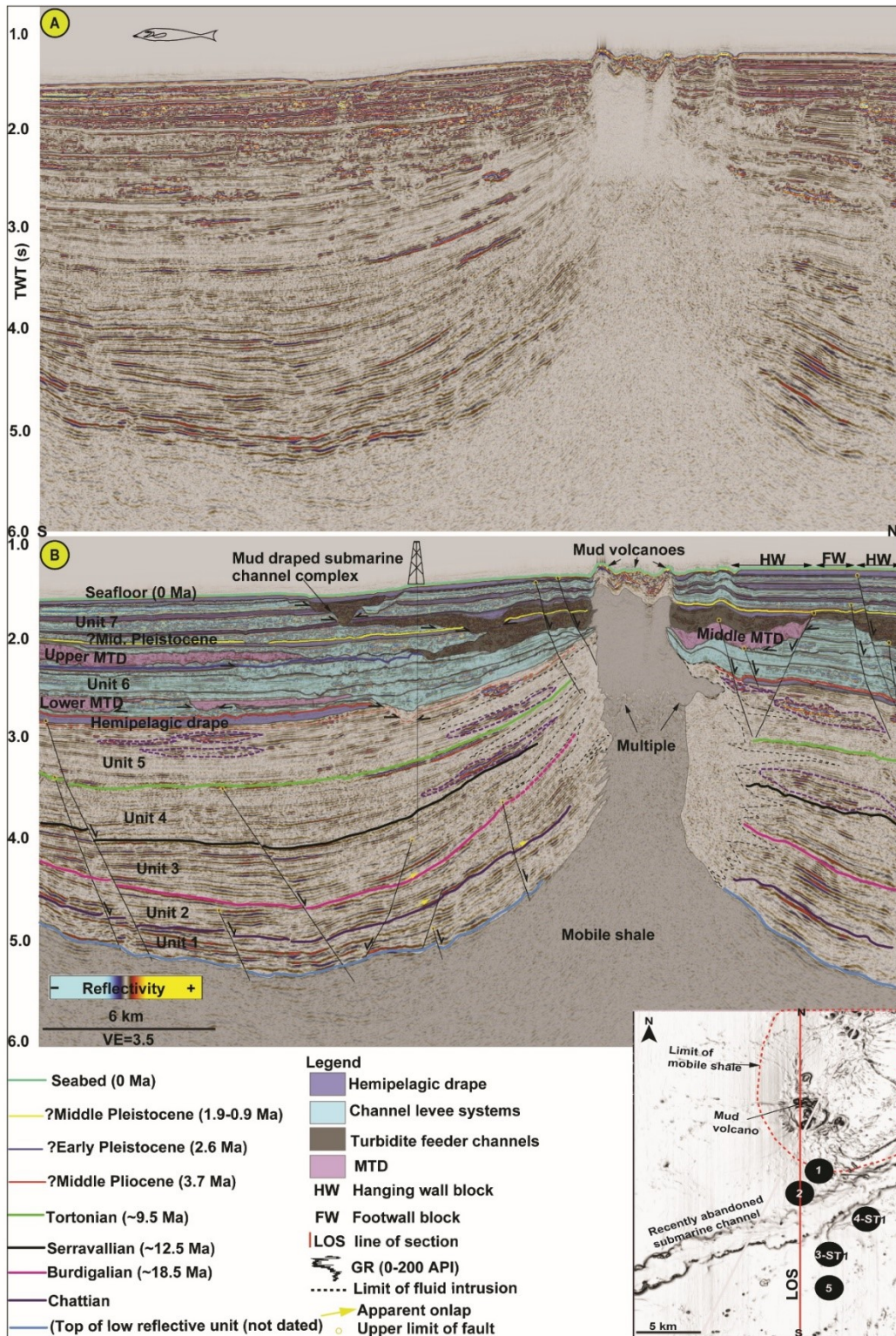


Fig. 2.5. A, B: Uninterpreted and interpreted seismic lines showing the stratigraphic architecture of the study area. Note the lateral discontinuities (erosional truncations) and the juxtaposition of different seismic facies

(Fig. 2.5). This hemipelagic layer was truncated by younger channel levee systems (CLSs) that locally incised the underlying deposits by up to 40 m (Fig. 2.5). The thickness of Unit 5 remains uniform in the south but thins northward toward the mobile shale zone.

Unit 6

The base of Unit 6 is erosional and marks a major change with the onset of erosive MTDs and CLSs (Fig. 2.5). This erosional event can be traced throughout the studied 3D block except in the northeast, where it could not be interpreted due to the combined effect of signal wipe out (artefacts) and erosion (Fig. 2.5). Three erosive mass-transport deposits labelled lower, middle and upper MTDs were identified in unit 6 (Figs. 2.5, 2.6).

The lower MTD covers an area of $\sim 155 \text{ km}^2$ and extends 3-5 km laterally with a maximum thickness of $\sim 148 \text{ m}$ (using an average interval velocity of 1,639.4 m/s). Its upper limit is relatively gentle with localized erosional scours (Fig. 2.5). This MTD truncates the underlying CLS, reaching its maximum thickness at the northern and southern flanks, but drapes the central area, where the CLS thins out (e.g. Figs. 2.5, 2.6 C, D, G).

The middle MTD covers an area of $\sim 175 \text{ km}^2$ with a lateral distance of 6-8 km and reaches a maximum thickness of $\sim 246 \text{ m}$ in the hanging-wall block bounded by normal faults labelled P, Q (see also Doust and Omatsola, 1990; Cohen McClay, 1996; Graue, 2000; Figs. 2.5, 2.6B, F). The middle MTD is followed by relatively continuous/chaotic, high amplitude seismic packages interpreted as turbidite feeder channels. Unlike the lower MTD, the middle MTD is highly deformed by synthetic and antithetic normal faults with inferred offsets of a few meters, and 20-25 m relief incised into the underlying CLS (Figs. 2.5, 2.6F).

The upper MTD is the third and most laterally extensive MTD in Unit 6 (Fig. 2.5). It covers an area of 187 km^2 with a lateral distance of 12 km and reaches a maximum thickness of $\sim 205 \text{ m}$ downstream (Fig. 2.6A, E). This MTD also incises the underlying CLS, but was truncated by younger turbidite feeder channels and affected by extensional deformation (Figs. 2.5, 2.6A, E). The upper MTD is overlain by CLSs, ultimately draped by a hemipelagic layer that was truncated by younger CLSs (Fig. 2.5).

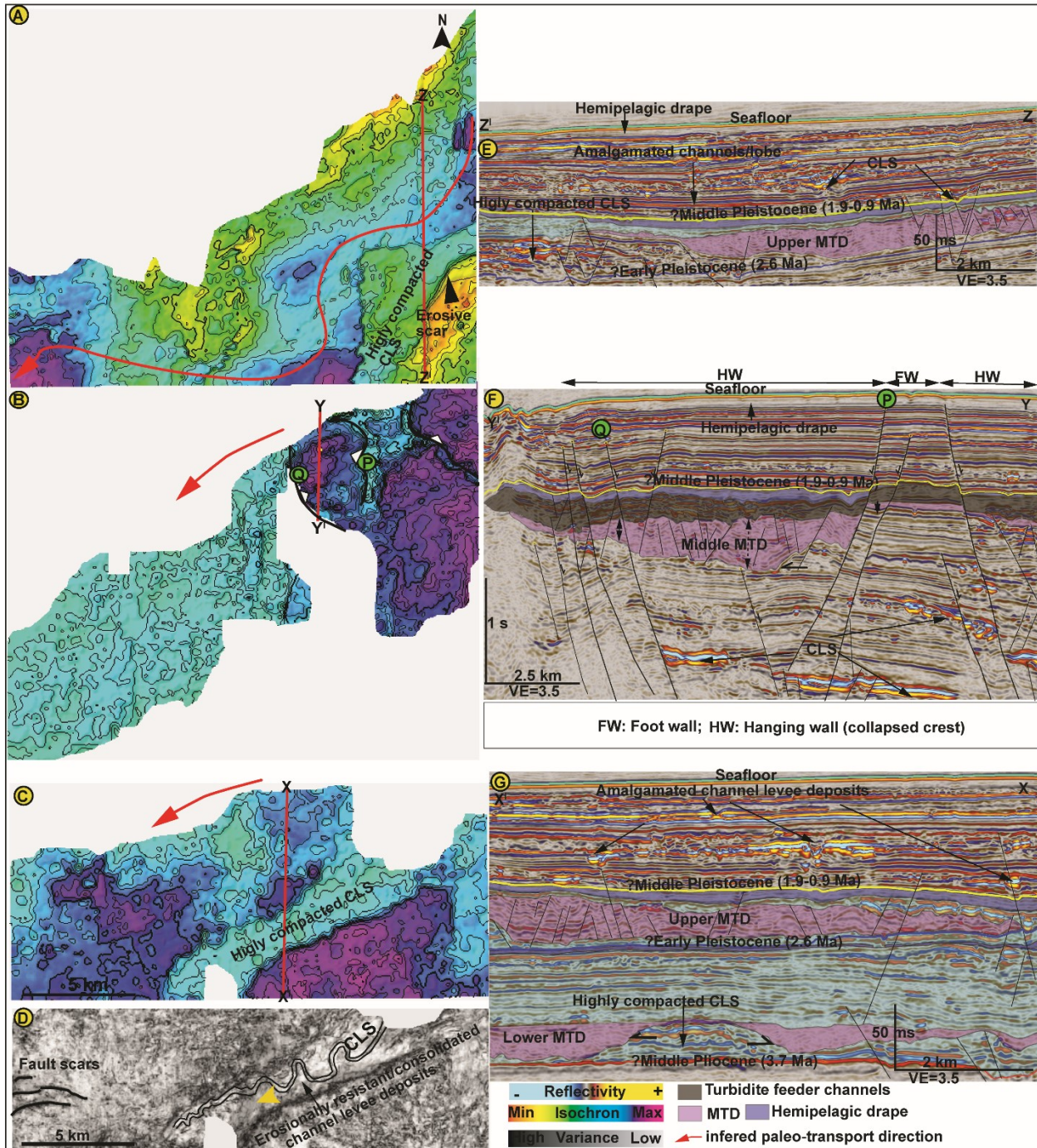


Fig. 2.6. A, B, C: Isochron maps of the lower, middle and upper MTD showing respective spatial variations in sediment thickness. D: Horizon slice at the top of the amalgamated channel levee deposits underlying the lower MTD showing the presence of sinuous channel. E-G: Seismic lines illustrating the architecture of the MTDs. Variations in the thickness of the middle MTD on the footwall and hanging wall blocks are indicated by double-headed arrows (panel F). See text for a more detailed explanation.

Unit 7

Unit 7 is the youngest seismic unit identified in the study area. Its base marks another major change in the sedimentary record, characterized by overall high-frequency and high-amplitude seismic packages (Fig. 2.5). These seismic packages are interpreted as amalgamated channel levee/lobe deposits and alternate with transparent seismic packages corresponding to hemipelagites (Fig. 2.5). The amalgamated channel levee/lobe deposits are locally truncated by turbidite feeder channels (Fig. 2.5). Unit 7 is topped by the seafloor, which is directly underlain by a thick hemipelagic deposit (Fig. 2.5).

2.4.2 Lithofacies and depositional environment

The integrated analysis of well logs in the study area shows that the intervals characterized by average to moderately high gamma-ray log values, low resistivity, high neutron-density separation and high sonic values correspond to hemipelagic layers, overbanks and/or mud-rich turbidites (e.g. Fig. 2.7). However, intervals defined by low gamma-ray, high resistivity, low neutron-density separation and low sonic values are interpreted as amalgamated channel deposits (Fig. 2.7). Facies vary from amalgamated channel sands at the base of submarine channel deposits to overbank and/or hemipelagic drape at the top (Fig. 2.7).

2.4.3 Bio-chronostratigraphic analyses and correlation with seismic data

Despite the location of the study area on the upper slope, which is prone to mass-wasting and sediment reworking, the integration of calcareous nannofossil and planktonic foraminifera biohorizons increased the reliability of the age model presented in this study.

We fixed the first occurrences (FOs), last occurrences (LOs), and the corresponding depths of key Neogene planktonic foraminifera (pf) and calcareous nannofossils (cn), in the biostratigraphic distribution sheet of the FM-1, FM-2, FM-3ST1 and FM-4 boreholes. We assigned ages to these fossil markers using equivalent ages derived from recently published studies (Anthonissen and Ogg, 2012; Backman *et al.*, 2012; Agnini *et al.*, 2014; Raffi *et al.*, 2016).

Accordingly, the FO of *Sphenolithus ciperoensis* (cn) was assigned to ~24.4 Ma; the LO of *Cyclicargolithus abisectus* (cn) to ~23.5 Ma; the FO of *Globoquadrina dehiscens* (pf) to ~22.4 Ma; the FO and LO of *Sphenolithus heteromorphus* (cn) to ~17.5 Ma and ~13.53 Ma respectively; the LO of *Neogloboquadrina acostaensis* (pf) to ~9.8 Ma; the LO of *Cartinaster coalitus* (cn) to ~9.7 Ma (Fig. 2.7).

With the aid of time-depth relationship (checkshot) data, we depth-matched this bio/chronostratigraphic information with their corresponding seismic horizons. Finally, we attributed relative ages to the identified seismic reflectors based on: (i) the presence of fossil markers in at least two wells, with the exception of the LOs of *S. ciperoensis* (24.4 Ma) and *C. abisectus* (23.5 Ma), which were only recorded in the deepest FM-1 borehole. (ii) Relative depths of the identified seismic reflectors with respect to the nearest biohorizons (Figs. 2.5, 2.7, 2.8).

The basal limit of Unit 1 has not been drilled and could not be assigned a precise age (Figs. 2.5, 2.8). It tops the transparent seismic unit previously interpreted as deep-marine shales deposited during Eocene sea-level highstand e.g. Doust and Omatsols (1990). Also, it marks a transition from the transparent seismic unit to the high amplitude seismic packages interpreted as turbidite deposits (amalgamated channels/lobes; e.g. Fig. 2.9). The base of Unit 1 could be associated with an increase in sediment supply to the Niger Delta following the regional uplift that affected the area in the Oligocene (~34-28 Ma; Chardon *et al.*, 2016; Grimaud *et al.*, 2017).

The base lap (apparent onlap) associated with the base of Unit 2 (purple line in Fig. 2.5) occurs 200 m below the FO of *Sphenolithus ciperoensis* (~24.4 Ma), which occurs at the depth of 4,017.3 m in the FM-1 borehole (Fig. 2.7). The base of Unit 2 also could not be assigned a precise age since it has not been drilled (Fig. 2.7). The geometries of successive apparent onlaps (Fig. 2.5) suggests it is associated with a non-deposition period in the deep basin probably during maximum flooding of the shelf. Also, since it lies 200 m below the 24.4 Ma biohorizon, it could be a good candidate for the sea-level transgression described in the Chattian (Haq *et al.*, 1987; Fig. 2.8).

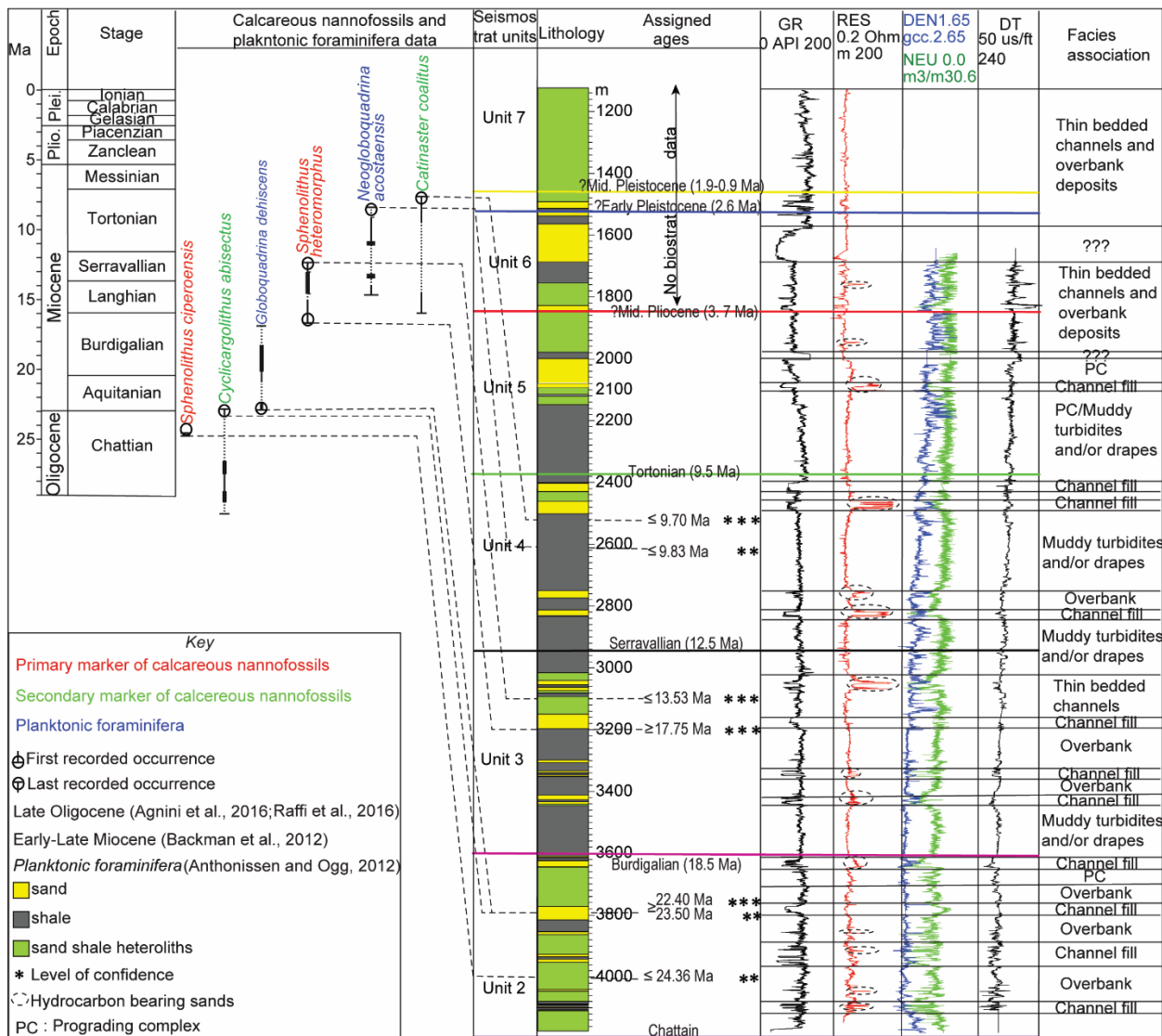


Fig. 2.7: Representative borehole (FM-1 well) drilled to a total depth of 4.15 km down to the Neogene series. The identified fossil markers, data and estimated ages are shown on the left. The well logs used for lithology, facies and depositional environment analysis are shown on the right. Note the vertical succession of facies from channel axis, overbank and/or hemipelagic deposits. See text for a detailed explanation.

The base of Unit 3 (pink in Fig. 5) occurs 195 m above the LO of *Cyclocargolithus abisectus* (~23.5 Ma) and the FO of *Globoquadrina dehiscens* (~22.4 Ma; Figs. 2.5, 2.7). The base of this unit, defined by apparent onlaps, could also be a good candidate for a sea-level transgression in the Burdigalian (Haq *et al.*, 1987; Fig. 2.8). The older fossil marker-the LO of *C. abisectus* (~23.5

Ma), which was only recorded in the FM-1 borehole, occurs at the same depth as the younger fossil marker—the FO of *G. dehiscens* (~22.4 Ma), recorded in both FM-1 and FM-2 boreholes. These fossil markers are separated by ~1.1 Ma and should not coexist. Hence, this datum may represent a condensed interval or *C. abisectus* could represent a reworked component. Since, the base of seismic Unit 3 lies 195 m above the FO of *G. dehiscens* ~22.4 Ma-Aquitainian (Figs. 2.7, 2.8), it could be related to the long-term Burdigalian sea-level transgression. It was tentatively assigned to the ~18.5 Ma (see Haq *et al.*, 1987; Fig. 2.8).

The base of seismic Unit 4 occurs 160 m above the LO of *Sphenolithus heteromorphus* (~13.53 Ma) and corresponds to a regional erosional truncation. This limit could be linked to the short-term sea-level fall in the Serravallian (~13.8 Ma) according to the Haq *et al.* (1987; Fig. 2.8), but probably occurred a little later in the Niger Delta. Since it is younger than 13.53 Ma, it was tentatively assigned to the Serravallian (~12.5 Ma).

The base of Unit 5 corresponds to a regional truncation and occurs 120 m above the LO of *Catinaster coalithus* (~9.7 Ma). Since this erosional event is younger than 9.7 Ma, it was assigned a tentative age of ~9.5 Ma on the assumption that it could be associated with the major progradation event recorded in the eastern Niger Delta during the Tortonian ~9.5 Ma (Jolly *et al.*, 2016).

On top of seismic Unit 5, we identified a transparent unit characterized in the FM-3ST1 borehole by abundant and diverse nannofossils and foraminifera. The LO of *Discoaster quinqueramus* (~5.5 Ma) allowed us to confidently date this hemipelagic layer as uppermost Messinian. At the top of this hemipelagic layer lies a barren interval, which is followed by an interval characterized by the simultaneous occurrence of *Reticulofenestra pseudoumbilicus* (cn), *Globorotalia plesiotumida* (pf), *Globorotalia miocenica* (pf), *Discoaster pentaradiatus* (cn), *Globorotalia exilis* (pf), *Discoaster brouweri* (cn) and *Gephyrocapsa spp* (cn). The co-occurrence of *D. brouweri* and *D. pentaradiatus*, whose extinction levels should be distinct in the uppermost Pliocene (Backman *et al.*, 2012), together with the Pleistocene markers such as *H. sellii* and *Gephyrocapsa spp*, suggests that the top of this interval has been affected by reworking. The presence of a regional erosional event corresponds to this interval on seismic sections (e.g. red line in Figs. 2.5, 2.9B, 2.10C, 2.11C). It is characterized by the onset of erosive CLSs and MTDs.

Although we were unable to precisely define the Messinian-Pliocene transition due to poor biostratigraphic data, the onset of sediment-gravity flows following the hemipelagic drape dated ~5.5 Ma could be associated with sea-level fall following the transgressive event of the uppermost

Messinian (Haq *et al.*, 1987). Therefore, the base of Unit 6 could be related to a sea-level fall in the Middle Pliocene (~3.7 Ma; see Haq *et al.*, 1987 curve recalibrated by Gorini *et al.*; 2014; Fig. 2.8). This interpretation seems to agree with the progradation event recorded in the eastern Niger Delta during the Middle Pliocene (3.7 Ma; Jolly *et al.*, 2016).

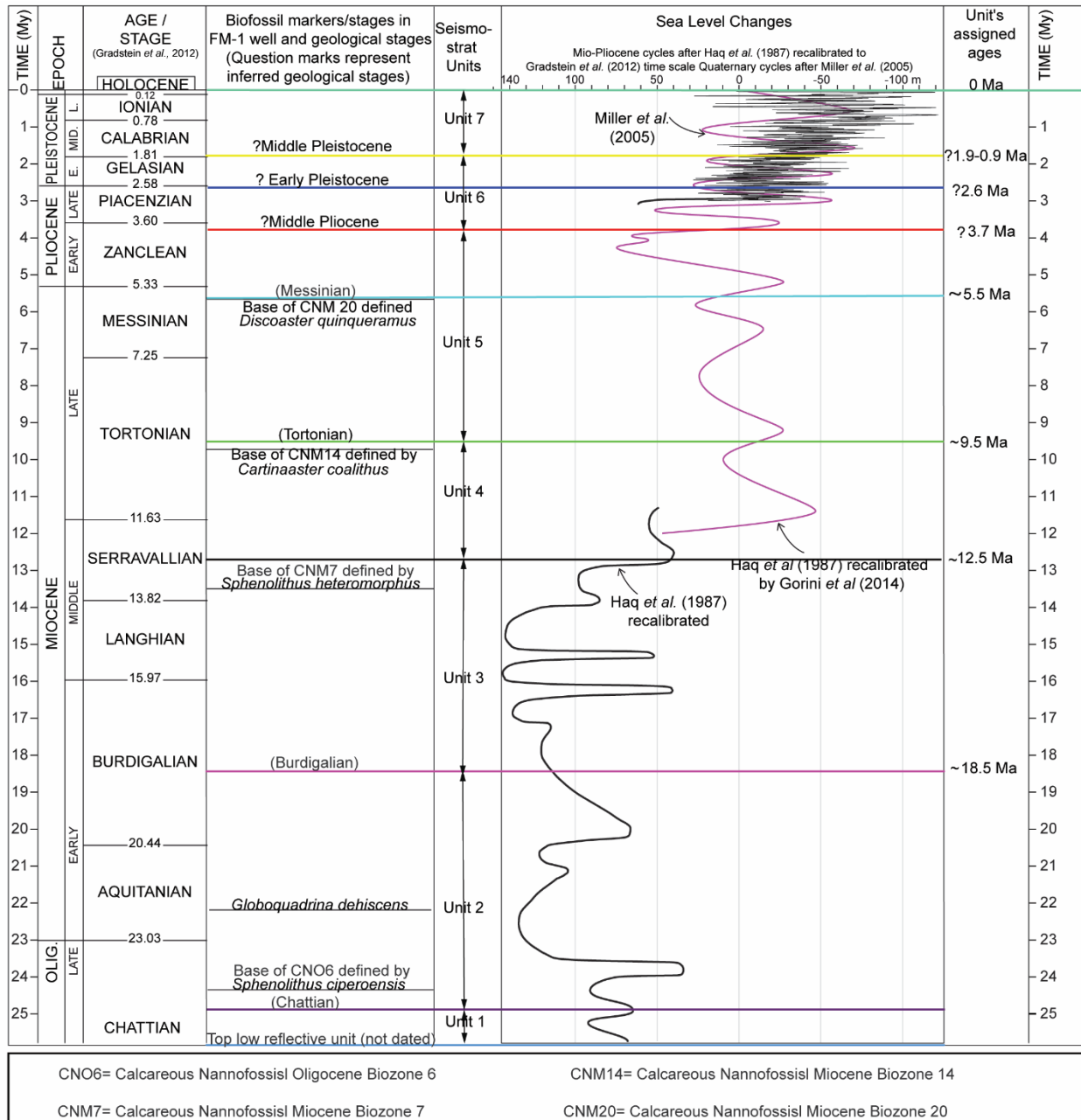


Fig. 2.8. Chronostratigraphic chart showing standard stages, long-term and short-term sea-level curves (after Haq *et al.*, 1987); the Late Miocene-Quaternary cycles according to Haq *et al.*, (1987) curve recalibrated by Gorini *et al.* (2014). The Plio-Pleistocene cycles according to Miller *et al.* (2005).

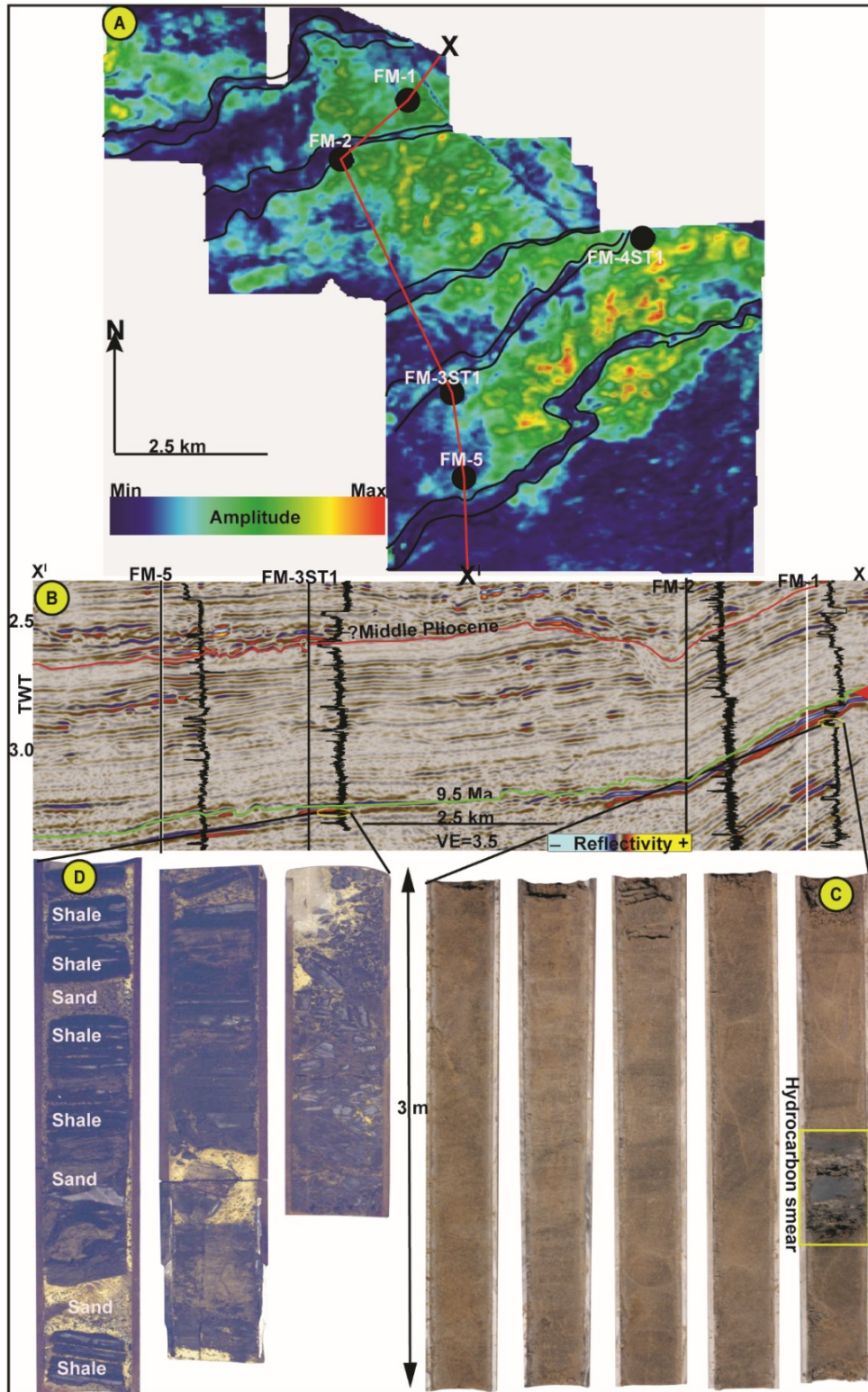


Fig. 2.9. A: RMS amplitude map at 3.3 seconds (twt) in the C_{bh} facies showing channel architectural patterns. B: Corresponding seismic line illustrating the associated seismic facies. C, D: Core data from the FM-1 and FM-3ST1 wells showing the lithological content.

Similarly, assuming that the base of the laterally extensive (upper MTD) and associated CLS, mark the onset of the major cooling event at the base of the Gelasian ~2.6 Ma (see Miller *et al.*, 2005; Fig. 2.8), the base of Unit 7, characterized by erosive CLSs and the onset of strongly reflective seismic packages could be associated with a sea-level fall during the Middle Pleistocene. It was assigned ~?1.9-0.9 Ma on the assumption that it could mark the onset of the high-frequency/high-amplitude sequence cycles (Miller *et al.*, 2005; Fig. 2.8). The assigned 1.9 Ma seems to agree with a published line located a few kilometres from our study area (see Bellingham *et al.*, 2014).

2.4.4. 3D seismic geomorphology and depositional architecture

Detailed analysis of interval attribute maps, horizon and time slices focused on Units 5, 6 and 7 (Fig. 2.5). It allowed us to characterize the depositional architecture within the younger stratigraphic units in detail. RMS amplitude extraction at 3.3 seconds (twt) at the top of parallel, continuous high amplitude seismic packages (C_{bh} facies), revealed the presence of NE-SW trending sinuous channels (Fig. 2.9A). These channels are characterized by their low amplitudes in their axes, showing high amplitudes in their overbanks (Fig. 2.9A). They are interpreted to have incised older amalgamated channel/lobe deposits but were draped with mud during their abandonment (see also Chapin *et al.*, 2002; Jobe *et al.*, 2015). A ~5 m core data retrieved in the FM-1 borehole within the (C_{bh}) facies revealed high net-to-gross channel sand, characterized by blocky gamma-ray log patterns (Fig. 2.9B). Downstream, a ~2 m core data retrieved in the FM-3ST1 borehole is characterized by interbedded sand and shales that grade downward to dominant shales characterized by irregular gamma-ray log patterns (Fig. 2.9B, D). A lateral variation in the gamma-ray log from blocky in the FM-1 borehole to irregular patterns in the FM-3ST1 borehole points to an overall decrease in grain size in this case from the channel axis to overbank deposits characterized by thin interbedded sands and shales.

The RMS amplitude map of the erosive event at the base of Unit 6 revealed the presence of a ~2 km wide, E-W oriented, low-amplitude, moderate sinuosity submarine channel complex (labelled 1; Fig. 2.10A, B) and three channel levee systems (CLSs labelled 2, 3 and 4), confined

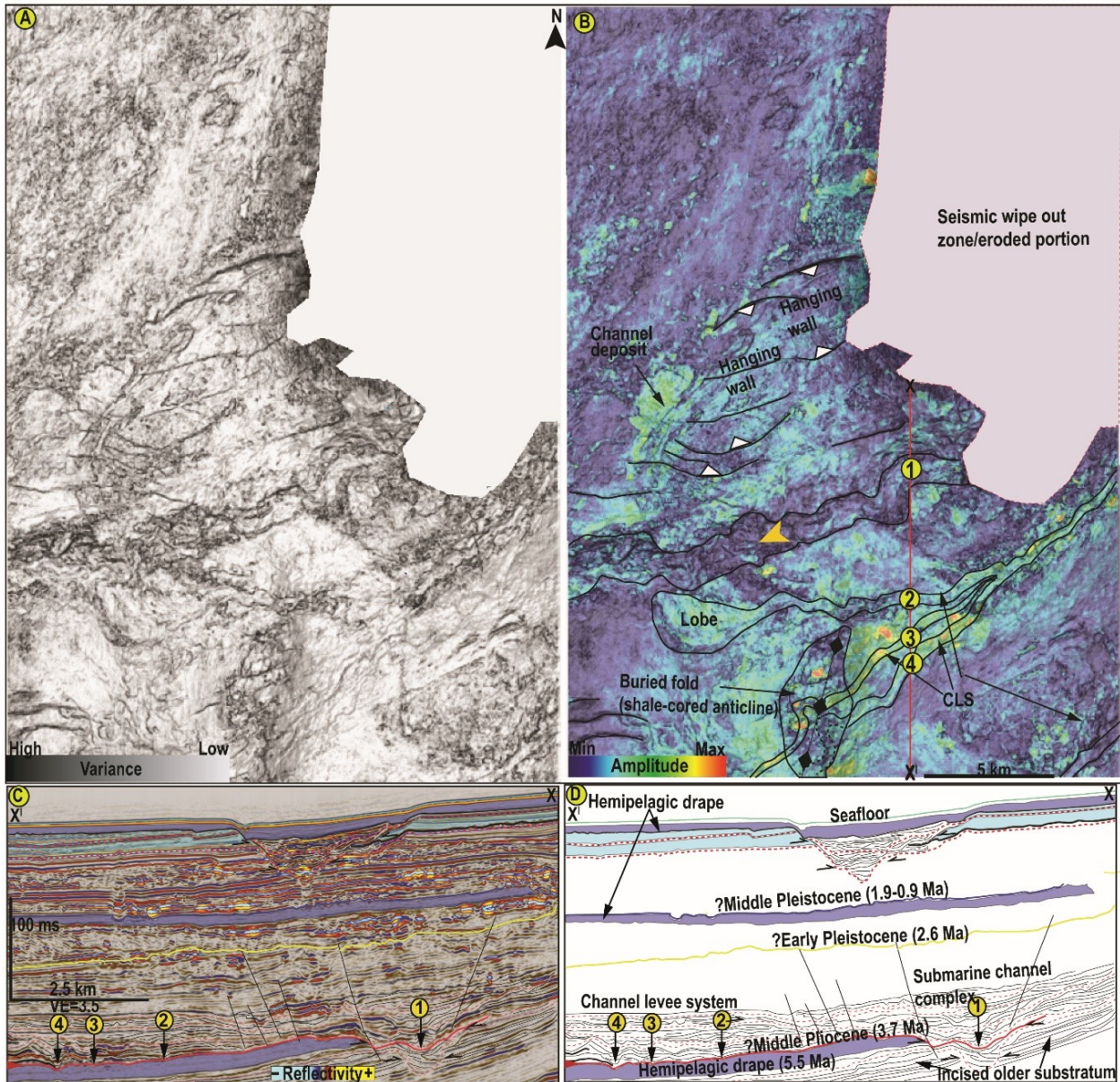


Fig. 2.10. A: Uninterpreted horizon (variance attribute) slice of the erosional event at the base of Unit 6. B: RMS amplitude extraction on the base of Unit 6 draped on panel A. The main submarine channel complex (labelled 1) and channel levee systems (labelled CLSs 2, 3 and 4) are illustrated. C, D: Interpreted seismic line and line drawing showing the architecture of the channels. Yellow arrow (panel B points to paleo-flow direction), while red arrow (part D) points to the level of amplitude extraction. Note the narrow, low sinuosity, erosional character and E-W orientation of the main submarine channel complex 1. Note also the ability of the CLSs 2 and 3 to cross paleo-relief features associated with the buried shale-cored anticline/fold.

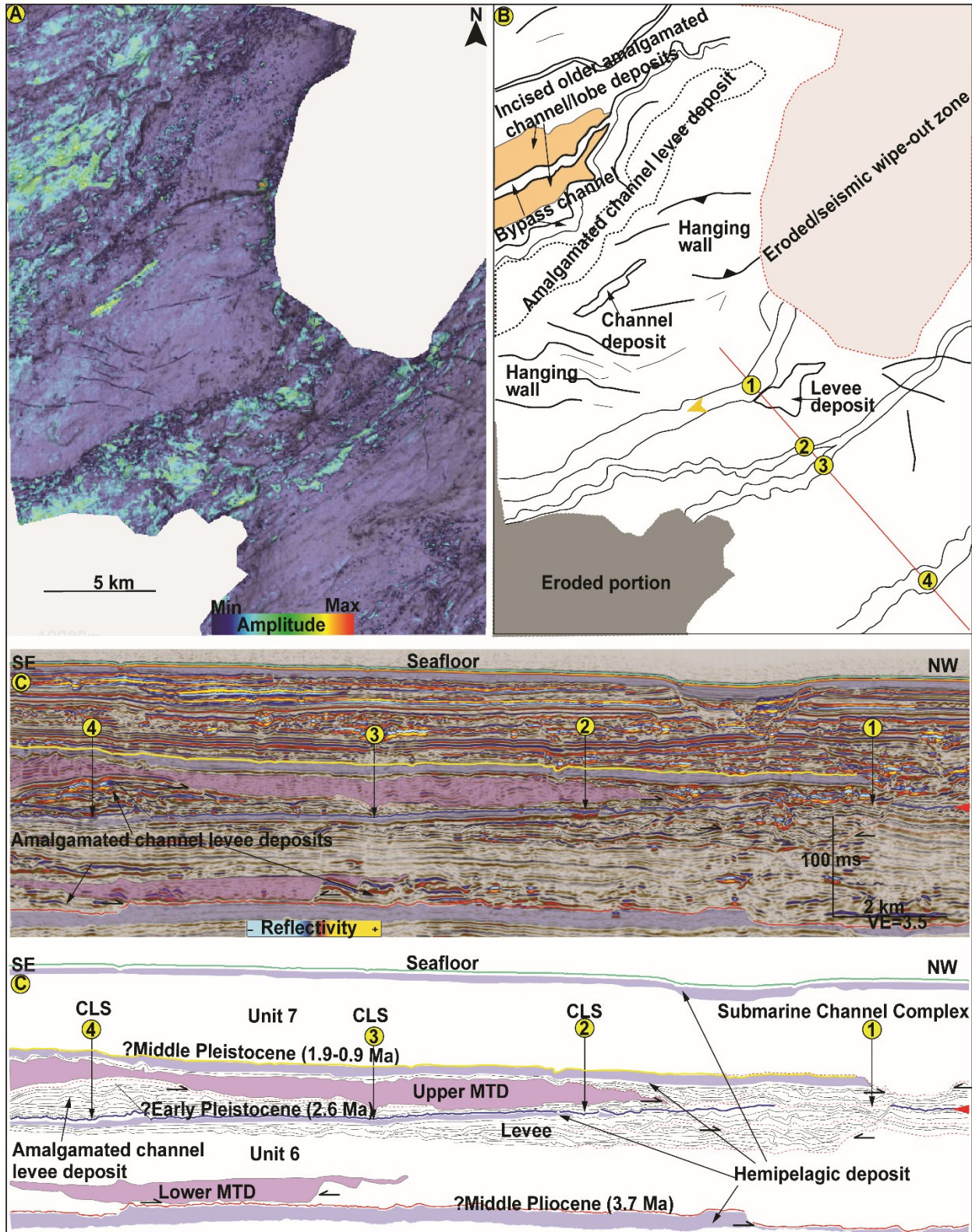


Fig. 2.11. A: Uninterpreted RMS amplitude map of a channel levee system near the top of Unit 7 draped on the horizon (variance attribute) slice. B: Interpretation of panel A illustrating narrow,

erosional low sinuosity submarine channel complex 1 and moderate sinuosity CLSs (labelled 2, 3 and 4). C: Seismic line and line drawing illustrating the architectures of the channels. The red arrow (panel C) points to the level of amplitude extraction. Note the presence of bifurcating, bypass CLS that incised older amalgamated channel/lobe deposits in the NW corner of the map and the truncation of amalgamated channel levee deposits by the lower and middle MTDs.

to the southern part of the mobile shale zone (Fig. 2.10 A, B). The main CLS developed tripartite, moderate sinuosity networks with overall E-W paleo-flow direction (Fig. 2.10A, B). CLS 1 terminated on a moderate amplitude, lobe-like feature (Fig. 2.10 B). CLSs 3 and 4 are characterized by higher amplitudes and crossed paleo-relief associated with a buried fold/shale-cored anticline (Fig. 2.10A, B).

RMS amplitude extraction at the base of Unit 7 reveals the presence of a submarine channel complex (SE in Fig. 2.11B; labelled channel 1), CLSs 2, 3 and 4 (SE in Fig. 2.11B) and bifurcating, moderate sinuosity CLSs located in the NW corner of the 3D volume (Fig. 2.11B). The NW CLSs are interpreted as bypass channels that incised older sand-rich amalgamated channels/lobe deposits. The up-dip continuity of the main submarine channel complex is obscured by mobile shale/erosion (Fig. 2.11B).

Furthermore, the horizon slice at the base of the high reflectivity seismic packages in Unit 7 reveals the presence of erosive submarine channel complex 1 and high sinuosity CLSs 2 and 3 (Fig. 2.12A, B). A seismic line through this channel complex revealed its erosive character and wide U-shaped geometry. This stage marks a significant increase in the width of the channel, the development of higher sinuosity, a northward shift toward the mobile shale zone and overall NE-SW orientation compared to the previous stages (Figs. 2.10, 2.11 and 2.12).

An RMS amplitude extraction at 1.9 seconds within the high amplitude seismic packages revealed a NE-SW trending, moderate sinuosity submarine channel complex (labelled 1; Fig. 2.13B) and four E-W oriented sinuous CLSs (labelled 2, 3, 4 and 5; Fig. 2.13B). These channels are all confined to the southern part of the mobile shale zone (Fig. 2.13). The submarine channel complex 1 captured the CLSs 2 and 3 downslope, where the latter developed abandoned meander loops (Fig. 2.13). CLS 4 is bordered by a high amplitude sediment wedge interpreted as levee deposits (Fig. 2.13). The linear, high amplitude channel-like feature located downslope of CLS 4 is interpreted as an avulsion channel (see also Posamentier and Kolla, 2003; Fig. 2.13).

The horizon slice at 1.8 seconds (below the present-day seafloor) shows the presence of irregular, low coherent seismic areas in the north, flanked by planar radial discontinuities interpreted as radial faults (Fig. 2.14A). These low coherent features were interpreted as mobile shales (Figs. 2.2, 2.5, 2.12, 2.13, 2.14). Linear scars were also observed in a hanging-wall fault block adjacent to the mobile shale zone (Fig. 2.14). A seismic line through these lineated features revealed coherent to slightly deformed high amplitude seismic packages with a somewhat erosive base. These lineaments were interpreted as scars associated with mobile shale-derived MTDs (Fig. 2.14D). This MTD shows a lateral distance, area and maximum thickness of ~2.3 km, ~13 km² and ~60 m, respectively (Table 2.1). The presence of an E-W oriented, moderate sinuosity submarine channel complex characterized by rough edges and entrenched CLSs can also be observed on this map (Fig. 2.14).

Table 2.1: Summary of statistical measurements on MTDs

| Name | Length (m) | Thickness (m) | Area (km²) |
|------------------------|-------------------|----------------------|------------------------------|
| Mud-derived MTD | 2.3 | 75 | 13 |
| Upper MTD | 12 | 205 | 187 |
| Middle MTD | 6-8 | 246 | 175 |
| Lower MTD | 3-5 | 148 | 155 |

2.5. Discussion

Here, we focus on the sedimentary processes in intraslope basins, interactions between shale tectonics and submarine channel evolution, depositional patterns and their implications for reservoir distribution. We prefer the term ‘filled ponded basins’ to ‘shallow ponded basins’ used by Prather *et al.* (2012) in the description of the depositional architecture in the intraslope basins we studied. We think this term is more appropriate as the 3D block, we studied is located in a supply-dominated deep-basin between 900-1,150 m, where deep-water processes dominate, and where the high rate of sediment supply filled the accommodation created by shale tectonics.

2.5.1 Interaction between shale tectonics and submarine channel complex

Detailed seismic and 3D geomorphological analyses (Fig. 2.15) revealed that the main submarine channel complex described in Units 6 and 7 (Figs. 2.10, 2.11, 2.12, 2.13, 2.14, 2.15), evolved in three stages from the Pliocene to the present-day. The evolution of the submarine channel from relatively moderate to high sinuosity over the Pliocene and the Pleistocene could be related to shale tectonics (Figs. 2.5, 2.10, 2.11, 2.12, 2.13, 2.14, 2.15; see also Bakare *et al.*, 2007; Clark and Cartwright, 2012; Jolly *et al.*, 2016; Hansen *et al.*, 2017).

During stage 1 (Middle Pliocene-Early Pleistocene), the channel was characterized by narrow morphology, low sinuosity and confined to the south of mobile shale in an E-W orientation (Figs. 2.10, 2.11, 2.15). The narrow low sinuosity of the channel during this stage is typical of young submarine channels with a relatively high slope gradient (see also Posamentier and Kolla, 2003; Ferry *et al.*, 2005; Heiniö and Davies, 2007; Jobe *et al.*, 2015; Jolly *et al.*, 2016; Hansen *et al.*, 2017). The E-W orientation of the channel south of the mobile shale zone suggests that the later was active from the Middle Pliocene to the Early Pleistocene, leading to the channel's confinement (Fig. 2.10, 2.11, 2.15).

Stage 2 (Early to Middle Pleistocene) marks a northward shift of the submarine channel complex toward the mobile shale zone and a transition from an E-W to a NE-SW orientation (Figs. 2.12, 2.15). Its higher sinuosity, broad U-shaped morphology are typical features of mature submarine channels with relatively gentle slope gradients (Fig. 2.12; see also Posamentier and Kolla, 2003; Ferry *et al.*, 2005; Jobe *et al.*, 2015; Heiniö and Davies, 2007; Jolly *et al.*, 2016; Qin *et al.*, 2016; Hansen *et al.*, 2017). The channel's northward adjustment toward the mobile shale zone (Figs. 2.12, 2.15) suggest relative quiescence of mobile shales.

Stage 3 (Middle Pleistocene to present-day) marks a return of the channel to its original E-W paleo-flow direction, south of the mobile shale zone (Figs. 2.1D, 2.14, 2.15). The downward shift of the submarine channel complex suggests that renewed activity of the mobile shale led to the deflection of the submarine channel complex southward away from the mobile shale zone. The presence of NE-SW oriented, high sinuosity submarine channel complexes 1 and 2 at 1.9 seconds (twt; the middle part of Unit 7; Fig. 2.13) suggests that shale tectonics and the final southward deflection of the channel complex occurred a little later than the Middle Pleistocene. The presence of mud volcanoes on the present-day seafloor supports the ongoing activity of the mobile shale

(Fig. 2.5). The presence of entrenched sinuous channel levee system within a valley (Fig. 2.14) indicates increasing confinement due to successive erosional and aggradational (depositional)

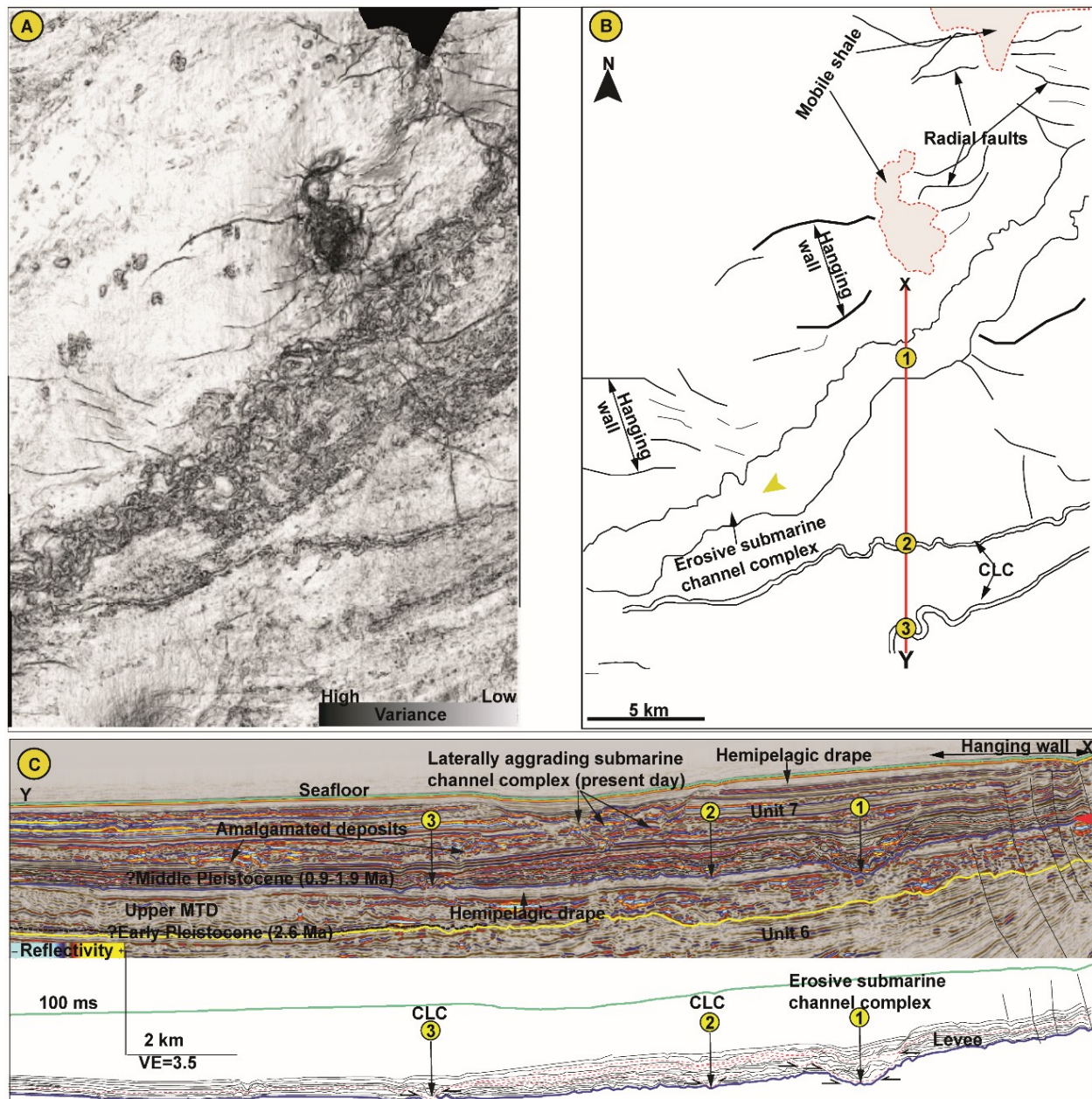


Fig. 2.12. A: Horizon (variance attribute) slice at the base of the high reflectivity seismic packages above the base of Unit 7 (blue line). Note the presence of wide, highly sinuous submarine channel complex (labelled 1 in panels B and C), and highly sinuous CLCs (labelled 2 and 3). Note also the erosional character and northward shift of the main submarine channel complex 1 toward the mobile shale zone in the NE and its NE-SW orientation.

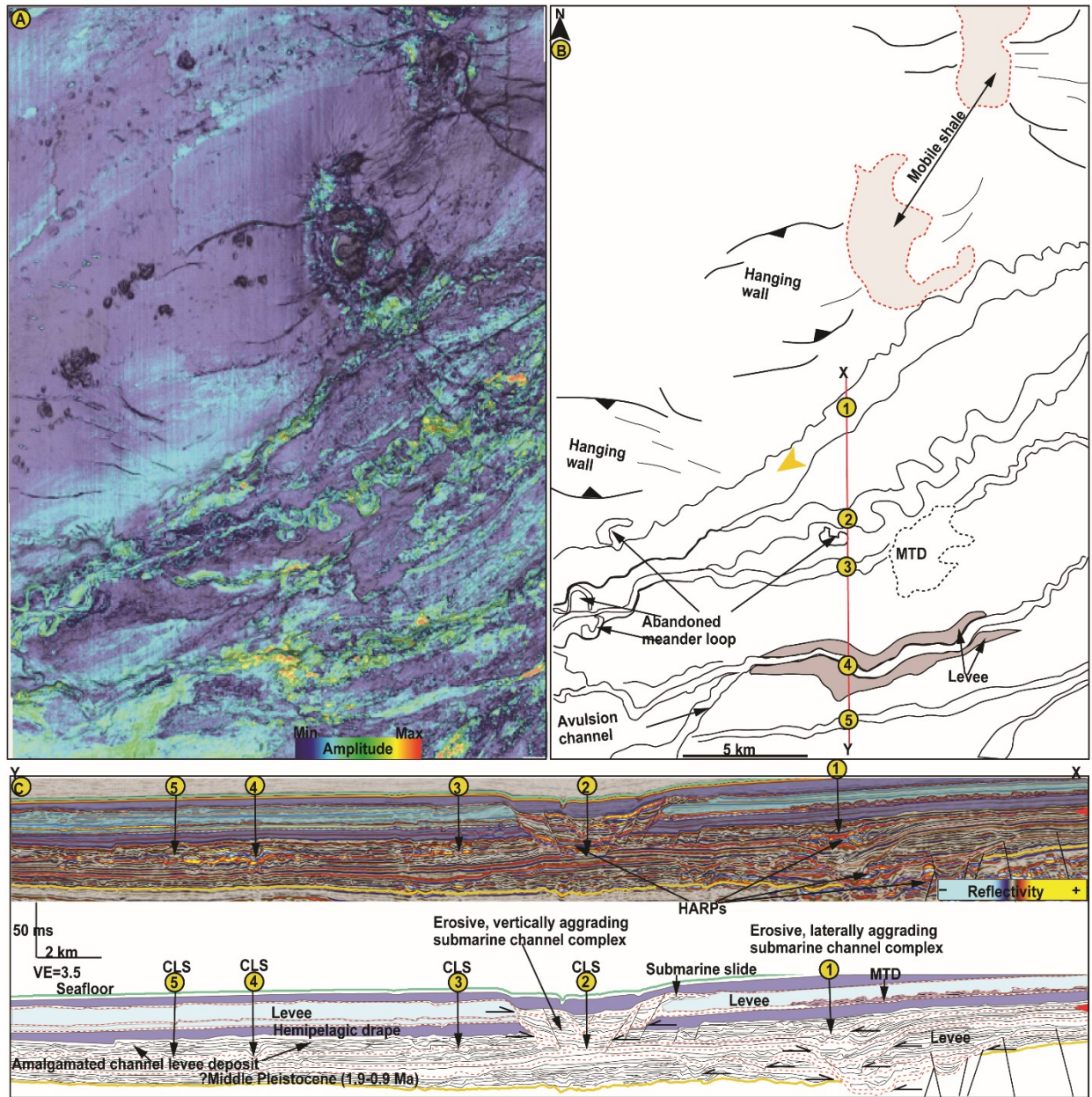


Fig. 2.13. A: Uninterpreted RMS amplitude map at 1.9 seconds (tw) draped on horizon (variance attribute) slice. B: 3D geomorphological interpretation of panel A showing the architectures of submarine channel complex (labelled 1), CLSs 2 to 5 and faults. C: Seismic line and line drawing illustrating the complex cut and fill architecture/lateral aggradation of the main submarine channel complexes 1. Note: (I) The erosive nature of the main channel complex compared to the aggrading CLSs 3 to 5. (II) The presence of abandoned meander loops associated with the meandering CLS 2. (III) The presence of an avulsion channel downstream of levee deposit adjacent to CLS 4. (IV)

The overall decrease in RMS amplitude downstream along the CLS 4 and the corresponding increase upstream along the avulsion channel.

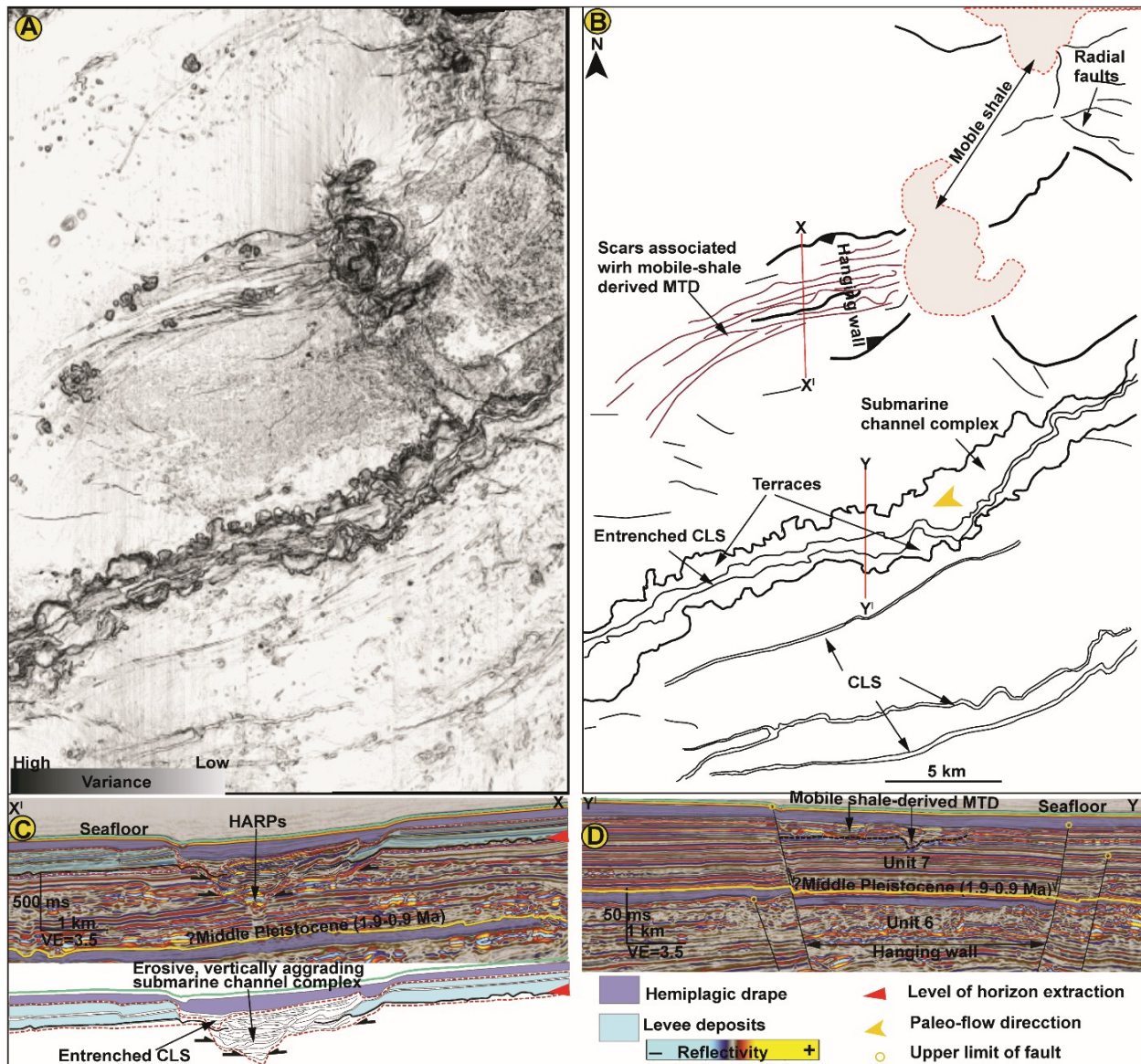


Fig. 2.14. A, B: Uninterpreted and interpreted horizon (variance attribute) slice at 1.8 seconds (tw) showing the presence of submarine channel complexes (yellow arrow), sinuous CLSs, mobile shales, radial faults and lineated scars associated with mobile shale-derived MTDs. C: Seismic lines illustrating the erosional character and rough edges of the submarine channel complex. D: Seismic line showing the conformable/slightly deformed, high amplitude seismic packages associated with mobile-derived MTDs. Note the E-W orientation, presence HARPs (panel C), terraces and entrenched CLS in the main submarine complex.

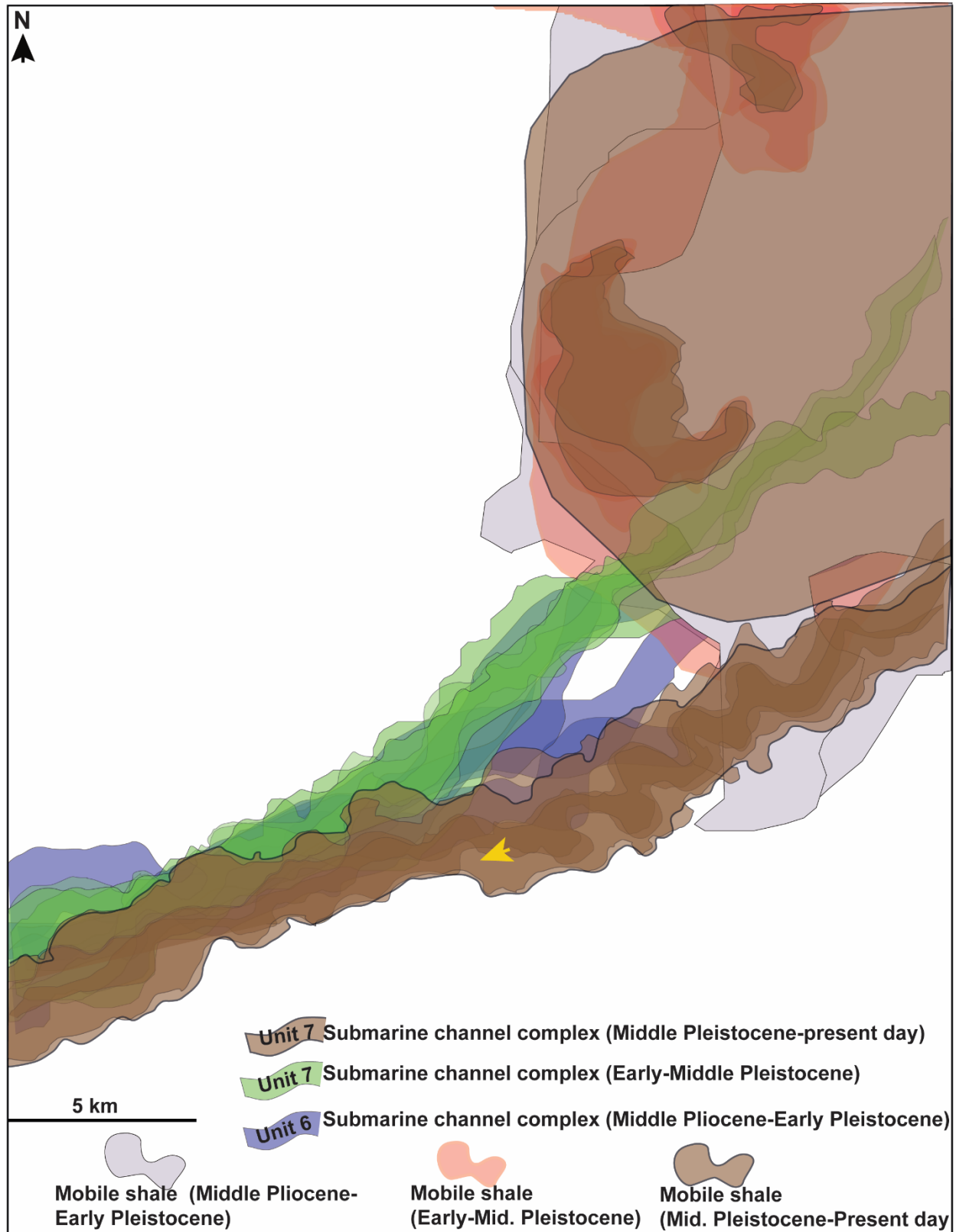


Fig. 2.15. Shale tectonics and submarine channel complex evolution from Middle Pliocene to present-day. Note E-W orientation of the channel complex during the Middle Pliocene-Early

Pleistocene (purple polygon; Unit 6); the NE-SW orientation during the Early-Middle Pleistocene (green polygon; Unit 7) and the E-W orientation from the Middle Pleistocene to present-day (brown polygon; Unit 7). Note the confinement of mobile shales in the NE of the study area during the Plio-Pleistocene intervals. See text for more a more detailed explanation.

stages (Fig. 2.13; channel complexes 1 and 2). A large valley containing the channel develops complex geometries as the valley wall becomes unstable (large scars Fig. 2.14A), with the development of inner terraces and a central sinuous channel (labelled in part B). The modification of the channel valley could result from the increasing confinement and focused energy of turbidity currents (see also Gee and Gawthorpe 2007, and others) during their activity. The present-day hemipelagic drape (Fig. 2.14 C) shows that the last channel complex described in this study was not active in the Holocene.

2.5.2 Reservoir distribution in filled ponded basins

Fig. 2.13 is a detailed example of the recent entrenched channel levee system (CLS) in Unit 7. The generally high amplitudes on the upstream bank of channel levee system (e.g. CLS 4; Fig. 2.13) suggest that sand-rich sediment was deposited both in the channel axis and on the overbank. In addition, the chaotic high amplitude reflection packages (HARPs) at the erosional base of the main submarine channel complexes (e.g. Figs. 2.13, 2.14; labelled HARPs) are interpreted as coarse-grained turbiditic channel fill deposits (after Prather *et al.*, 1998; Heiniö and Davies, 2007; Gamboa and Alves, 2016). However, the occurrence of high RMS amplitudes downstream of the channels (e.g. CLS 4 in Fig. 2.13A, B; labelled avulsion channel) show that turbidity flows periodically spilled sandy deposits on the overbank environment. The presence of high amplitudes associated with the avulsion channel (Fig. 2.13 A, B) compared to lower amplitudes in the downstream part of the main CLS 4 (Fig. 2.13), suggests that sand-rich sediment was diverted from the main channel during the avulsion event. Similar observations have been reported in the De Soto Canyon, Gulf of Mexico, where upstream avulsion due to a breached levee resulted in the

deposition of the avulsion lobe and concomitant decrease in both water and sediment discharge downstream of the main channel (Posamentier and Kolla, 2003).

As a first conclusion, these detailed images of reservoir distribution in Unit 7 are a good analogue for the Middle to Late Miocene turbidite deposits described by previous authors as amalgamated channels and overbank deposits (Chapin *et al.*, 2002). However, our study shows that reservoirs topped by hemipelagic layers and/or mud-rich turbidites are Late Oligocene to present-day in age (see Figs. 2.5, 2.7, 2.9). Our study also shows that the geometries and the distribution of reservoir could be controlled by both shale tectonics and sediment supply, with the prevalence of hemipelagic deposition during the periods of sea-level rise (see Figs. 2.7 and 2.8). Reservoir facies were confirmed by borehole data (see Fig. 2.9). Lobe-like deposits (e.g. Fig. 2.10 B) are generally rare and not discussed further in this paper due to lack of sufficient evidence to fully characterize their architecture.

2.5.3 Shale tectonics vs MTD types and distribution:

Two types of MTDs were recognized based on seismic facies, internal architecture and aerial extent (Figs. 2.5, 2.6, 2.14 D and Table 2.1): (1) Mobile shale-derived MTDs and (2) regional MTDs. Detailed analysis of kinematic indicators enabled us to infer the source area of the locally derived type 1 MTDs, but the limited size of the 3D volume we studied did not allow us to observe the headwall scars of the type 2 MTDs. However, analysis of their thickness maps helped us to infer their provenance.

Type 1 (Mobile shale-derived MTDs)

The type 1 MTDs described in seismic Unit 7 are thin and laterally confined adjacent to mobile shales (Fig. 2.14. D; Table 2.1). Their strong reflectivity distinguishes them from the type 2 MTDs, and their overall coherent internal architecture indicates that they are close to their source area (mobile shales).

Type 2 (Regional MTDs)

The type 2 MTDs described in Unit 6 (labelled lower, middle and upper MTDs; Figs. 2.5, 2.6; Table 2.1) are characterized by thick, chaotic, discontinuous low amplitude/transparent seismic packages that are bounded at the base by laterally extensive erosional scours. Their thick, lateral distribution, low amplitudes and chaotic internal architecture indicate that they were reworked far from their source areas (shelf-margin/upper slope).

The distribution of the regional MTDs could be controlled by the general slope (Fig. 2.6), syn-depositional faulting (Fig. 2.6B) and differential compaction/cementation in the underlying substratum (Fig. 2.6D).

The lower MTD increases in thickness from the NE downslope to the SW suggesting possible source area upslope (Fig. 2.6C; see also Alves *et al.*, 2009). However, the local increase in MTD thickness on both side of CLSs (Figs. 2.5, 2.6C, G), suggest that the degree of compaction/cementation in the underlying CLSs could be a controlling factor at a local scale. The differential erosion in sandy CLSs and muddy deposits could also explain the observed variation in thickness of the lower MTD (see erosional truncations at its base, Fig. 2.6G).

We observed a NE-SW decrease in thickness of the middle MTD downstream (Fig. 2.6B, F) due to its confinement within fault-bounded accommodation (Hanging-Wall; HW; Fig. 2.6F). This observation suggests that the deposition of MTD in the intraslope basins of the Niger Delta was controlled by syn-depositional normal faults (P, Q? Fig. 2.6F) that were active during the emplacement of MTD (Fig. 2.6B, F).

The thickness of the upper MTD increases downstream and was locally controlled by the degree of compaction in the underlying CLSs (Fig. 2.6A). The overall downstream increase in the thickness of this MTD suggests a response to regional accommodation development (see also Alves *et al.*, 2009). The foregoing observations strongly suggest that the type 2 MTDs originate from shelf-margin and/or upper slope.

2.5.4 Control of depositional systems in filled ponded basins:

Our results show that the depositional architecture of the filled ponded basins in the western Niger Delta is controlled by shale tectonics, sediment supply and eustasy.

At a local scale, basin tectonics is associated with mobile shale deformation and syn-depositional faults, controlling submarine channel morphology and depositional patterns in these filled ponded basins. Inferred high uplift/subsidence rates driven by the mobile shale in the Middle Pliocene and Early Pleistocene resulted in high slope gradients characterized by erosionally confined channels with low sinuosity (e.g. Figs. 2.10B, C, D; 2.11 A, C). However, relative quiescence and/or low subsidence/uplift rates from the Early to Middle Pleistocene resulted in more mature CLSs characterized by complex terraces, overbank deposits and channel avulsion (e.g. Fig. 2.13). The erosional nature of the main submarine channel complex during mobile shale deformation suggests that a dynamic equilibrium was maintained between changing local slope gradients and sedimentation rates (see also Adeogba *et al.*, 2005; Clark and Cartwright, 2012; Jolly *et al.*, 2016; Hansen *et al.*, 2017). Similar observations have been made in the adjacent Lower Congo Basin (Ferry *et al.*, 2005).

In addition, the control of the distribution of MTDs by syn-depositional faults suggests that mass-wasting was coeval with the growing faults. Equivalent observations have been reported in the lower Congo Basin (Ferry *et al.*, 2005).

At a basin scale, the depositional sequence is characterized by a succession of MTDs and turbidite deposits topped by hemipelagic layers (see Fig. 2.6G). Moreover, the Plio-Pleistocene sedimentary records show that eustasy and sediment supply could control the depositional architecture at a regional scale (e.g. Figs. 2.5, 2.6E, G, H; 2.10, 2.11, 2.12, 2.13). The absence of thick hemipelagic drape above the older submarine channel complex (e.g. CLS 1 Fig. 2.10 C, D) suggests that this hemipelagic drape could have been eroded during stage 1 of the submarine channel complexes or that the former was below resolution. However, the presence of a thick hemipelagic layer above the present-day submarine channel complex (just below the present-day seafloor; Figs. 2.5, 2.10 C, D; 2.12, 2.13, 2.14 C) indicates that it was draped and abandoned during the last postglacial sea-level rise. These observations suggest that channel complexes were most active during the low eustatic sea level but that hemipelagic sedimentation prevailed during high eustatic sea level.

2.6 Conclusions of Chapter 2

- The Neogene stratigraphy of the western Niger Delta's slope is characterized by seven major seismic units dated as Chattian, Burdigalian, Serravallian, Tortonian, Middle Pliocene, Middle Pleistocene and present-day. Major changes in the sedimentary record occurred in the Pliocene-Pleistocene, characterized by erosional MTDs, turbidites and channel levee systems draped by hemipelagites. In the Plio-Pleistocene upper sequences, we observed changes in the morphology of submarine channel complexes over time (low sinuosity/highly erosive versus high sinuosity/depositional) that were controlled by the interaction between shale tectonics (creating accommodation, and controlling the seafloor profile) and sediment supply.
- Younger sequences of the Niger Delta upper slope could be a good analogue for sedimentary processes in intraslope basins; at the margin scale, depositional architecture in the filled ponded basins on the upper slope of the western Niger Delta is controlled by the interaction between local basin tectonics, eustasy and sediment supply. Reservoir facies are characterized by amalgamated channel fills and overbank deposits. Periodic levee breaching by high-energy turbidity currents results in channel avulsion and diversion of sand-rich sediments downstream of avulsion channels. Our detailed analysis of the depositional architecture of the Tortonian and Plio-Pleistocene sedimentary units provides a useful analogue for deeper exploration of the older stratigraphic units.

CHAPTER 3

Pliocene and Pleistocene stratigraphic evolution of the western Niger Delta intraslope basins: A record of glacio-eustatic sea-level and basin tectonic forcings

K. I. Chima^{a,b*}, C. Gorini^a, M. Rabineau^c, D. Granjeon^d, D. Do Couto^a, E. Leroux^e, N. Hoggmascall^f

^a Sorbonne Université-ISTeP UMR 7193, F7500, Paris (France)

^b Alex Ekwueme Federal University, Ndufu-Alike Ikwo, Ebonyi State, Nigeria.

^c CNRS, UMR 6538, LGO (CNRS/UBO/UBS), Plouzane (France)

^d IFPEN, Rueil-Malmaison (France)

^e IFREMER, ZI Pointe du Diable, Plouzane, France (France)

^f Shell International (UK).

Abstract

Although climate proxy ($\delta^{18}\text{O}$) across worlds' ocean basins reveals that orbital forcing significantly controlled the Pliocene and the Pleistocene sediment deposition, and has been documented in seismic and outcrop studies on the continental shelves of many margins, little or no seismic stratigraphic studies have investigated orbital forcing on deepwater sediment record. In this study, we integrated detailed seismic stratigraphy and 3D geomorphological analysis of a high-resolution 3D seismic block to study in detail the stratigraphic evolution of the western Niger Delta intraslope basins over the last 5.5 Ma. Two sequence sets (SS1 and SS2) were identified.

The change in sedimentary architecture from (i) mass flows and turbidite sequences to (ii) hemipelagites and turbidite sequences at the SS1/SS2 transition coincides with significant increase in sedimentation rates (x3), and a transition from dominant 400 ka eccentricity cycles (from 5.3 Ma to 0.8-1.0 Ma) to dominant 100 ka eccentricity cycles, at the Middle Pleistocene Transition (MPT) (circa 0.8-1.0 Ma). The timing of these changes was estimated based on detailed analysis of seismic facies succession, correlation of seismic markers with high-resolution sea-level and oxygen isotope curves, and sequence set duration estimation. Further changes in sedimentary record, characterized by turbidite-dominated sequences at the lower part of SS1 to mixed mass flows and turbidite sequences at the upper part of SS1, were respectively correlated to changes occurring in the early Pliocene (circa 4.9 Ma) and the early Pleistocene (circa 2.6 Ma).

This seismic stratigraphic study demonstrates for the first-time sequence cyclicity associated with orbital (Milankovich) forcing in the deepwater Niger Delta over the last 5.5 Ma. The Pliocene and Pleistocene sedimentary records of the western Niger Delta intraslope basins were controlled by the interplay between allocyclic forcing linked to glacio-eustatic sea-level oscillations and basin tectonics associated with mobile shale activities, with the latter being more prevalent from the early Pliocene to the MPT. If calibrated with high-resolution biostratigraphic data in future studies, this study could serve as a useful analogue for further studies in the Gulf of Guinea, equatorial Atlantic and other margins feed by large deltas.

Keywords: Niger Delta; Intraslope basins; Pliocene; Pleistocene; Seismic stratigraphy; Allocyclic forcing; Eccentricity cycles.

3.1 Introduction

Deepwater sediments are important archives of the Earth's history not only because they record past climatic, geodynamic, environmental and hydrodynamic changes (e.g. Burbank, 1992; Molnar, 2004; Catuneanu, 2006; Posamentier and Kolla, 2003; Clift, 2010; Zecchin and Catuneanu, 2010), but also play host to viable hydrocarbon fields (see review in Morley *et al.*, 2011). The understanding of the complex interplay between allocyclic (e.g. eustasy, tectonics, climate and indirectly sediment supply), and autocyclic (e.g. channel avulsion) or regional forcings (e.g. delta lobe switching, shale tectonics etc.), are critical to the interpretation of deepwater sedimentary systems evolution (e.g. Elliot, 1975; Jervey, 1988; Posamentier *et al.*, 1988; Pulham, 1989; Einselle, 1991; Wiener *et al.*, 2010; Miall, 2010; Morley *et al.*, 2011; Catuneanu and Zecchin, 2013).

The Pliocene and Pleistocene are ideal time intervals to study because eustasy and climate proxies ($\delta^{18}\text{O}$) are well constrained and show significant variations both in amplitude and frequency (e.g. Ruddiman *et al.*, 1989; Imbrie *et al.*, 1993; Bassinot *et al.*, 1994; Leroy *et al.*, 1999; Shackleton, 2000; Lisiecki and Raymo, 2005; Miller *et al.*, 2005; Gibbard *et al.*, 2010; Gibbard and Lewin, 2016; Raymo *et al.*, 2018). Published climate proxies across the world's ocean basins show that the Pliocene and Pleistocene were controlled by orbital forcing (Milankovitch cycles) of three major periodicities namely: (i) precession (23 ka), (ii) obliquity (41 ka), and (iii) eccentricity (400 ka and 100 ka) (Lisiecki and Raymo, 2007). The early Pliocene from (5.3 Ma) to the early Pleistocene was dominated by obliquity cycles (41 ka), while the middle Pleistocene (circa 1.4 Ma) to present-day was dominated by eccentricity (400 to 100) (Head and Gibbard, 2015a, b; Gibbard and Lewin, 2016). Although the switch to the eccentricity cycles is poorly understood and a transition period from 1.4 to 0.4 Ma was suggested by Head and Gibbard (2015a, b), and Gibbard and Lewin (2016), a marked change to increasingly severe glacial cycles, so-called '0.8 Ma event' (Lisiecki and Raymo, 2007; Head and Gibbard, 2015a, b) or '0.9 Ma' (Miller *et al.*, 2005; Elderfield *et al.*, 2012), is usually taken as the Middle Pleistocene Transition (MPT). Sedimentary records over the world show the imprint of tectonic, climatic and glacio-eustatic cycles of different orders (Haq *et al.*, 1987). Climatic 4th-order cycles of 400 ka duration have been reported during the Pliocene e.g. on the continental shelf offshore Foz do Amazonas Basin (Brazil), with incised valleys, slope canyons and mass wasting (Gorini *et al.*, 2014). During the Pleistocene,

5th-order glacio-eustatic sea-level changes of 100 ka periodicity have also been well documented with marked shoreline progradation on the shelf and increased deepwater sedimentation during glacials e.g. in the Mediterranean Sea over the last 500 ka (Rabineau *et al.*, 2006; Ridente *et al.*, 2008). During the Pliocene in the Mediterranean Sea, sediment architecture does not seem to be much imprinted by the 400 ka cycles as shown on seismic (Rabineau *et al.*, 2014) and numerical simulation (Leroux *et al.*, 2014), probably because of an anomaly in accommodation created by the erosion of the entire margin after the Messinian Salinity Crises. The 100 ka glacio-eustatic cycles have also been described worldwide e.g. offshore Alaska (Gulick *et al.*, 2012), in the Gulf of Mexico (Galloway, 2001) and the Bengal fan (Werber *et al.*, 1997).

In the eastern Niger Delta, Jermannaud *et al.* (2010) and Rouby *et al.* (2011), documented a transition from global climate-controlled sequences from circa 4-2.5 Ma to sediment supply-controlled sequences from 2.5 Ma-present. Jermannaud *et al.* (2010) and Rouby *et al.* (2011) also demonstrated an overall progradation and increase in sedimentation rates between 4-2.5 Ma, followed by a retrogradation and decrease in sedimentation rates over the last 2.5 Ma. Furthermore, Riboulot *et al.* (2012), showed that eccentricity forcing of 100 ka periodicities controlled the stratigraphic evolution of the eastern Niger Delta continental shelf over the last 0.5 Ma.

In the western Niger Delta slope, where the present study is located (Fig. 3.1), Jobe *et al.* (2015, 2016; red box in Fig. 3.1A, D), linked changes in sedimentation rates during the last 130 ka (MIS 5e to present-day) to glacial/interglacial cycles with increased sedimentation rates during lowering of sea-level (MIS3 and MIS2) and an overall reduction in sedimentation during a rapid post-glacial sea-level rise associated with the Meltwater Pulse 1-A at (14 ka). Earlier studies e.g. Lézine *et al.* (2005); Weldeab *et al.* (2011); Collins *et al.* (2014); Govin *et al.* (2014) and Armitage *et al.* (2015), also linked the increase in sedimentation rates in the Gulf of Guinea during the Quaternary to the West African Monsoon. Recent high-resolution, 3D seismic and sequence stratigraphic study by Chima *et al.* (2019) on the western Niger Delta slope (yellow box in Fig. 3.1A, C, D, E), dated the Neogene stratigraphic record from the Burdigalian (18.5 Ma) to the late Miocene (5.5 Ma), and described the interaction between mobile shale and erosional submarine

channel over the last (5.5 Ma). However, the lack of biostratigraphic data over the Pliocene and Pleistocene poses a challenge in constraining the timing of major changes in sedimentary records.

Despite the foregoing studies on the Pliocene and Pleistocene sedimentary records of the Niger Delta, no study has investigated its control by orbital forcings from the late Messinian (5.5 Ma) to the present-day. Hence, the objective of this paper was to study in detail the stratigraphic evolution of the western Niger Delta intraslope basins over the last 5.5 Ma with a view to; (i) proposing a sequence stratigraphic framework for the Pliocene and Pleistocene intervals; and (ii) investigating their control by orbital forcings.

Pliocene and Pleistocene stratigraphy of the Niger Delta is an ideal laboratory to study climato-stratigraphy and slope depositional processes due to its location on a passive margin, where the imprints of regional/global climate dynamics, sea-level variation, gravity-tectonics, drainage evolution and sediment supply are well imaged on high-resolution 3D seismic reflection data.

3.2 Regional Setting

The Cenozoic Niger Delta is located in the Gulf of Guinea along the equatorial Atlantic margin of West Africa (Fig. 3.1A). The delta is the twelfth largest petroleum province in the world (Tuttle *et al.*, 1999), and covers an area of ~140,000 km² with a maximum sediment thickness of ~12 km (Allen, 1965; Evamy *et al.*, 1978; Doust and Omatsola, 1990). The Niger Delta is divided into the eastern and western lobes by a Cretaceous basement high [the Charcot Fracture Zone (CFZ)] (Corredor *et al.*, 2005; Fig. 3.1A). The development of the delta since the late Eocene (Fig. 3.1B, C), led to structuration in 3 major structural zones namely; (i) an extensional zone (EZ) below the continental shelf, characterized by normal faults; (ii) a translational zone (TZ) below the upper slope, dominated by mobile shales and intraslope basins, and (iii) a contractional zone (CZ) located at the toe of the slope, characterized by reverse faults and detachment folds (Doust and Omatsola, 1990; Damuth, 1994; Cohen and McClay, 1996; Connors *et al.*, 1998; Morgan, 2004; Bilotti *et al.*, 2005; Corredor *et al.*, 2005; Fig. 3.1A, C).

Based on the classification scheme of Prather *et al.* (2003), the western Niger Delta slope profile fall within 'graded slope', characterized by a seafloor whose downslope profile is elevated above the level of theoretical concave-upward, smoothed graded profile. Shale tectonics on the

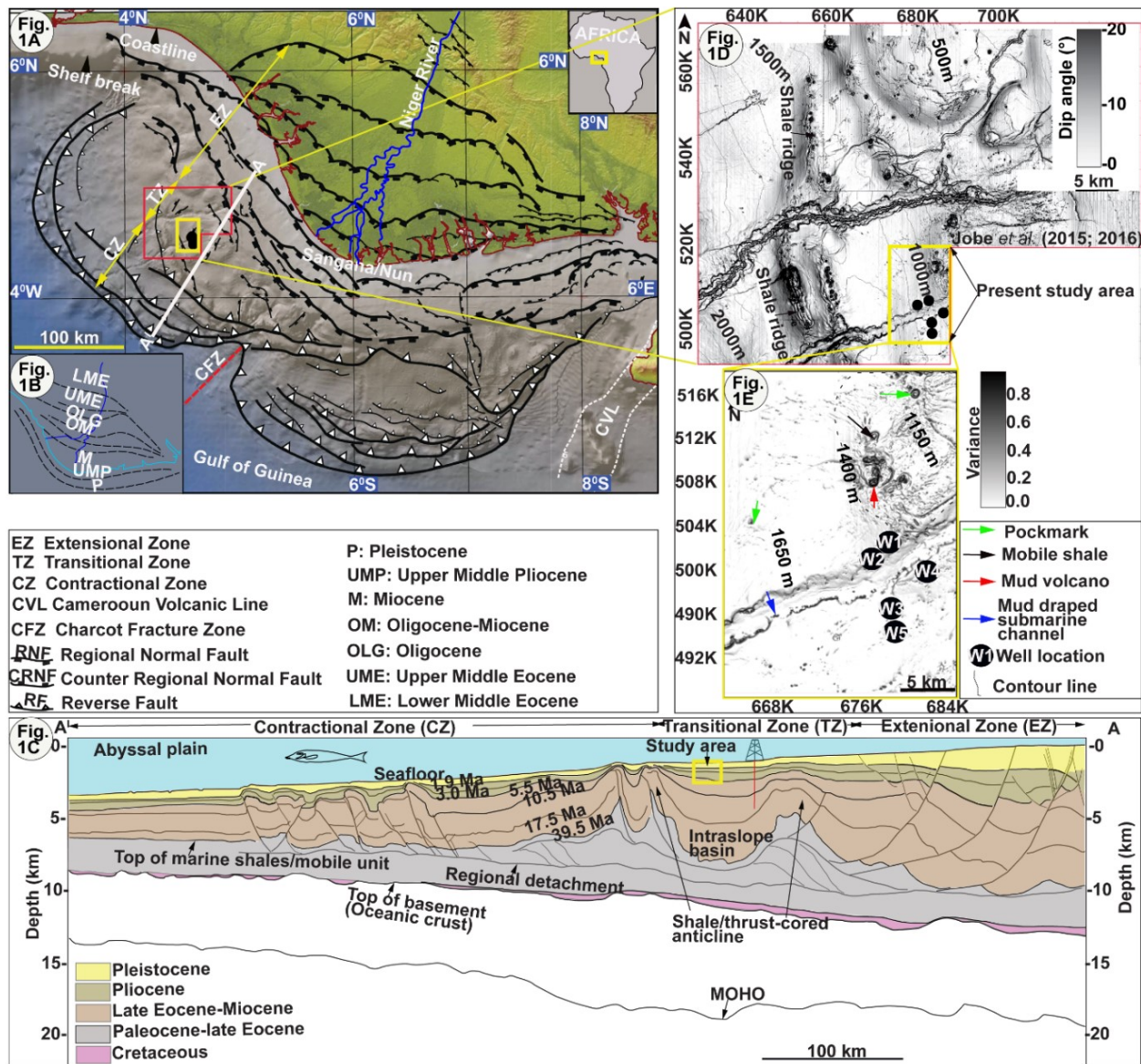


Fig. 3.1. Location of the study area. A: superimposed relief and bathymetric map showing the extensional zone (EZ), transitional zone (TZ) and contractional zone (CZ) of the Niger Delta (adapted from Rouby *et al.*, 2011). B: Schematic progradation map of the Niger Delta since the Eocene. C: Seismic line drawing (AA¹) showing the structural zones of the Niger Delta (adapted from Bellingham *et al.*, 2014). D: Dip of the seafloor showing the physiographic features of the transitional zone (TZ) (from Jobe *et al.*, 2016). E: Depth structure map of the modern seafloor showing the mobile shales, mud volcanoes, pockmarks and mud-draped sub-marine channel in the study area (from Chima *et al.*, 2019). Black circles in panels A, D (labelled W1-W5) in panel E indicate well locations.

Niger Delta slope give rise to the occurrence of shale/thrust-cored structural highs flanked by mobile shale withdrawal intraslope basins that interact with sediment-gravity flows (Doust and Omatsola, 1990; Damuth, 1994; Cohen and McClay, 1996; Connors *et al.*, 1998; Graue, 2000; Morgan, 2004; Bilotti *et al.*, 2005; Corredor *et al.*, 2005; Wiener *et al.*, 2010; Prather *et al.*, 2012; Fig. 3.1D, E). The western Niger Delta slope is constantly in dynamic equilibrium as mobile shale activities create structural highs that are in turn smoothed by sediment-gravity flows that preferentially accumulate within adjacent intraslope basins (Deptuck *et al.*, 2003; Adeogba *et al.*, 2005; Bakare *et al.*, 2007; Prather *et al.*, 2012; Clark and Cartwright, 2012; Chima *et al.*, 2019; Fig. 3.1D, E). The distribution of shale/thrust-cored structures on the western Niger Delta slope significantly control the morphology of submarine channels, depositional patterns, reservoir architecture and distribution (e.g. Adeogba *et al.*, 2005; Bakare *et al.*, 2007; Jobe *et al.*, 2015, 2016; Clark and Cartwright, 2012; Deptuck *et al.*, 2012; Prather *et al.*, 2012; Jolly *et al.*, 2016; Hansen *et al.*, 2017; Chima *et al.*, 2019). The present study is located within the translational zone of the western Niger Delta slope at the transition between the extensional and the contractional domains (Fig. 3.1A, C). It covers an area of 638 km² at ~120 km from the present-day coastline and lies at water depths between 900 to 1,755 m (Fig. 3.1E).

3.3 Dataset and Methods

3.3.1 Dataset

We integrated a high-resolution 3D seismic data and lithologic logs from 5 boreholes (see Fig. 3.1A, D, E), to study the Pliocene and the Pleistocene stratigraphic evolution of the western Niger Delta.

3.3.1.1 Seismic data

The 3D seismic data was processed as a zero-phase source wavelet in the American reverse standard polarity such that an increase in acoustic impedance corresponds to a trough (blue loop) in the wavelet, while a decrease in acoustic impedance is represented by a peak (red loop) in the

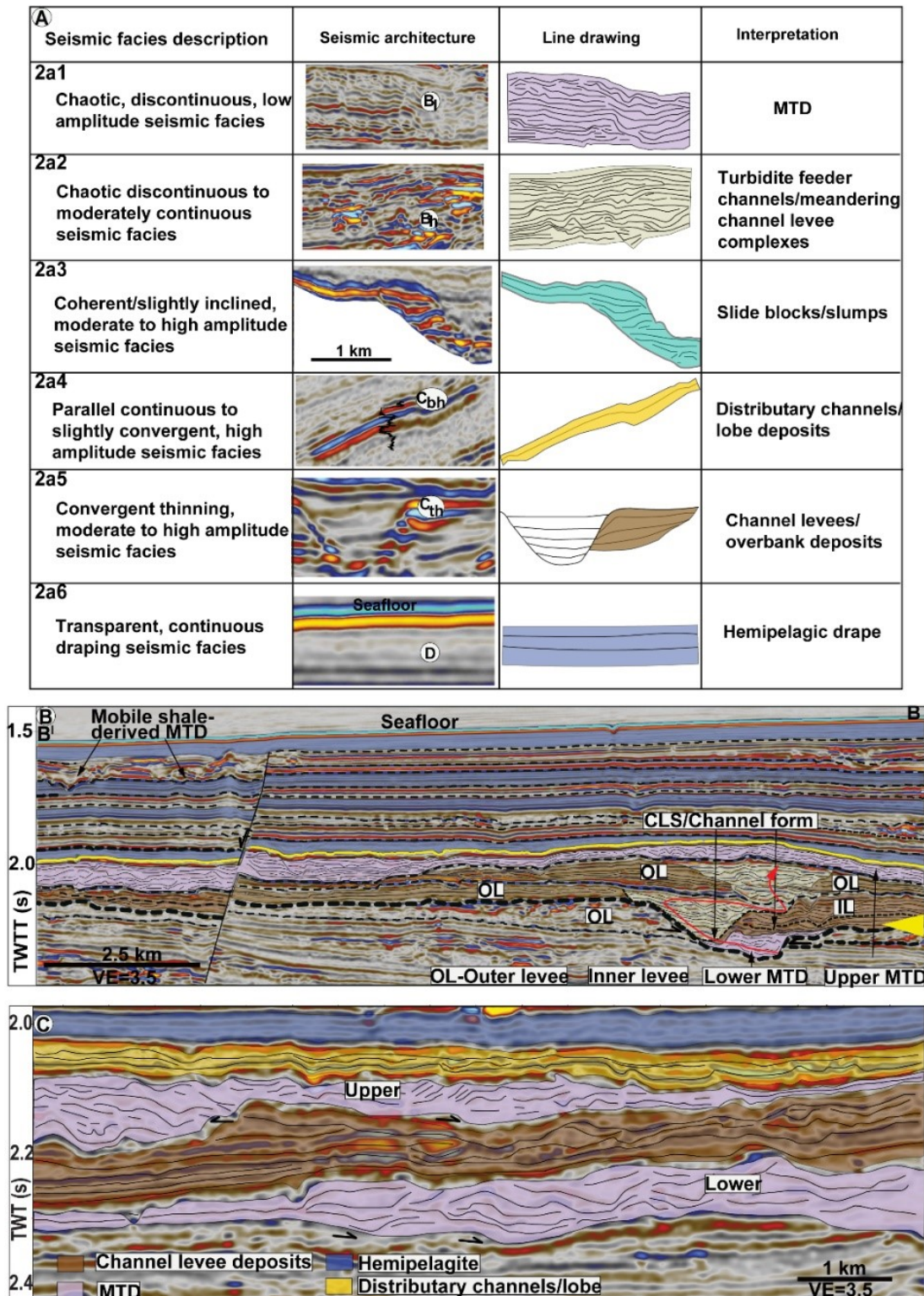


Fig. 3.2. A: Seismic facies analysis. A: Facies description and interpretation (modified after Chima *et al.*, 2019). B: Representative facies succession on the western Niger Delta intraslope basins. See Figs. 3.3C and 3.5A for the locations panels B, C, and text for a more detailed explanation.

wavelet (Fig. 3.2A, B). The horizontal resolution of the data is characterized by a stacking bin spacing of 25 m x 25 m (inline and crossline spacing), and a seismic recording sampling interval of 4 milliseconds two-way travel time (TWT). The dominant frequency of the data is 30 Hz over the first 3 seconds (TWT), which yields a vertical resolution of ~13.7 meters within the interval of interest.

3.3.1.2 Well data

The well data comprises gamma ray logs from 5 wells (labelled W1, W2, W3, W4 and W5; Fig. 3.1A, D, E). Wells W2-W5 cover only the lower part of the Pliocene whereas W1 samples Neogene to the late Pleistocene (see Chima *et al.*, 2019; Figs. 2.2; 2.7 and 2.9B). The last available biostratigraphic dating corresponds to the late Messinian (circa 5.5 Ma), based on the last recorded occurrence of *Discoaster quinquerramus* (see Chima *et al.*, 2019). Biostratigraphic data was not available within the interval of interest (the Pliocene and the Pleistocene).

3.3.2 Methods

3.3.2.1 Seismic stratigraphy

We applied the concept of seismic and sequence stratigraphy (after Mitchum and Vail, 1977) to analyse the sedimentary architecture of the Pliocene and Pleistocene sedimentary records of the western Niger Delta intraslope basins. Our seismic stratigraphic approach relied on the recognition of reflection amplitude, continuity, internal architecture, external geometry, nature of bounding surfaces and erosional truncations to delineate key seismic surfaces as well as their corresponding seismic facies association.

3.3.2.2 3D seismic geomorphology

We applied the 3D seismic geomorphological analysis technique described by Posamentier and Kolla (2003) and Catuneanu (2006) to study in detail the depositional environments

corresponding to seismic facies described above. This was achieved by detailed analysis of Root Mean Square (RMS) seismic amplitudes, that allow for lithological and depositional environments discrimination (see Chima *et al.*, 2019; and references therein). The RMS amplitudes analyses were combined to a variance seismic attributes to guide the geological interpretation of the seismic data (Chopra and Mafort, 2007; Taner *et al.*; 1994; Chima *et al.*, 2019). Three (3D) seismic geomorphological analysis allowed us to study in detail the spatio-temporal evolution of the Pliocene and the Pleistocene sedimentary records.

3.3.2.3 Allostratigraphic partitioning and dating of the Pliocene and the Pleistocene stratigraphy

The detailed analysis of RMS maps, combined with the variance analysis of seismic attributes and the 3D geomorphological interpretation of the seismic data made it possible to define 21 mappable seismic surfaces, which bound 4th-order allostratigraphic sequences as defined by Catuneanu (2006) and Catuneanu *et al.* (2011). These allostratigraphic sequences could be grouped in two sequence sets (SS1 and SS2). As there was no biostratigraphic data over the Pliocene and the Pleistocene, we used the last biostratigraphically constrained interval (the late Messinian) dated at ~5.5 Ma based on the last recorded occurrence of *Discoaster quinqueramus* (see Chima *et al.*, 2019) to define the age of the base of the lower sequence set (SS1). Then, we matched key discontinuous and conformable seismic surfaces that show significant changes in sedimentary architecture both on seismic lines and 3D geomorphological maps to the high-resolution Pliocene and Pleistocene sea-level and oxygen isotope (¹⁸O) curves derived from (Lisiecki and Raymo, 2005; Raymo *et al.*, 2018). As the SS1 and the overlying SS2 present very different seismic facies and morphology, we assumed that the limit between the SS1 and the SS2 could correspond to the Middle Pleistocene climatic Transition (MPT), and assigned it an age of 0.8-1 Ma.

3.4 Results and Interpretations

3.4.1. Seismic facies analysis

The Pliocene and Pleistocene stratigraphy of the western Niger Delta intraslope basins were subdivided into 2 sequence sets (SS1 and SS2) based on the observed changes in seismic

geometries and depositional environments, and respectively correspond to Unit 6 and Unit 7 of Chima *et al.* (2019). Although detailed seismic facies analysis of the study area has been presented by Chima *et al.* (2019) (Fig. 3.1A, C, D, E; Fig. 3.2A), the present study sheds more light on facies association in order to improve the understanding of depositional processes and sequence stratigraphy. The six seismic facies identified in the study area includes: (1) chaotic, discontinuous low amplitude seismic facies (B_l), characterized by elongate/tabular geometry, irregular tops and bases interpreted as mass-transport deposits (MTDs); (2) chaotic, discontinuous to moderately continuous, high amplitude seismic facies (B_h), characterized by blocky external form interpreted as turbidite feeder channels/meandering channel levee complexes (CLCs); (3) coherent/slightly inclined, moderate to high amplitude seismic facies that generally onlap margins of concave-upward negative relief interpreted as slides/slump blocks (MTDs); (4) parallel continuous to slightly convergent, high amplitude seismic facies (C_{bh}), with elongate geometry and irregular base interpreted as distributary channels/lobes; (5) convergent/thinning, high to moderate amplitude seismic facies (C_{th}), characterized by wedge geometry interpreted as channel levee deposits; (6) transparent, parallel continuous, draping seismic facies (D), that locally display small-scale chaotic internal architecture, bounded by conformable surfaces interpreted as hemipelagic drape (HD) and/or muddy turbidites. The foregoing seismic facies and interpretations are consistent with previous studies on the Niger Delta intraslope basins (e.g. Deptuck *et al.*, 2003; 2012; Adeogba *et al.*, 2005; Bakare *et al.*, 2007; Liu *et al.*, 2013; Hansen *et al.*, 2018; Zhao *et al.*, 2019).

3.4.2 Facies association

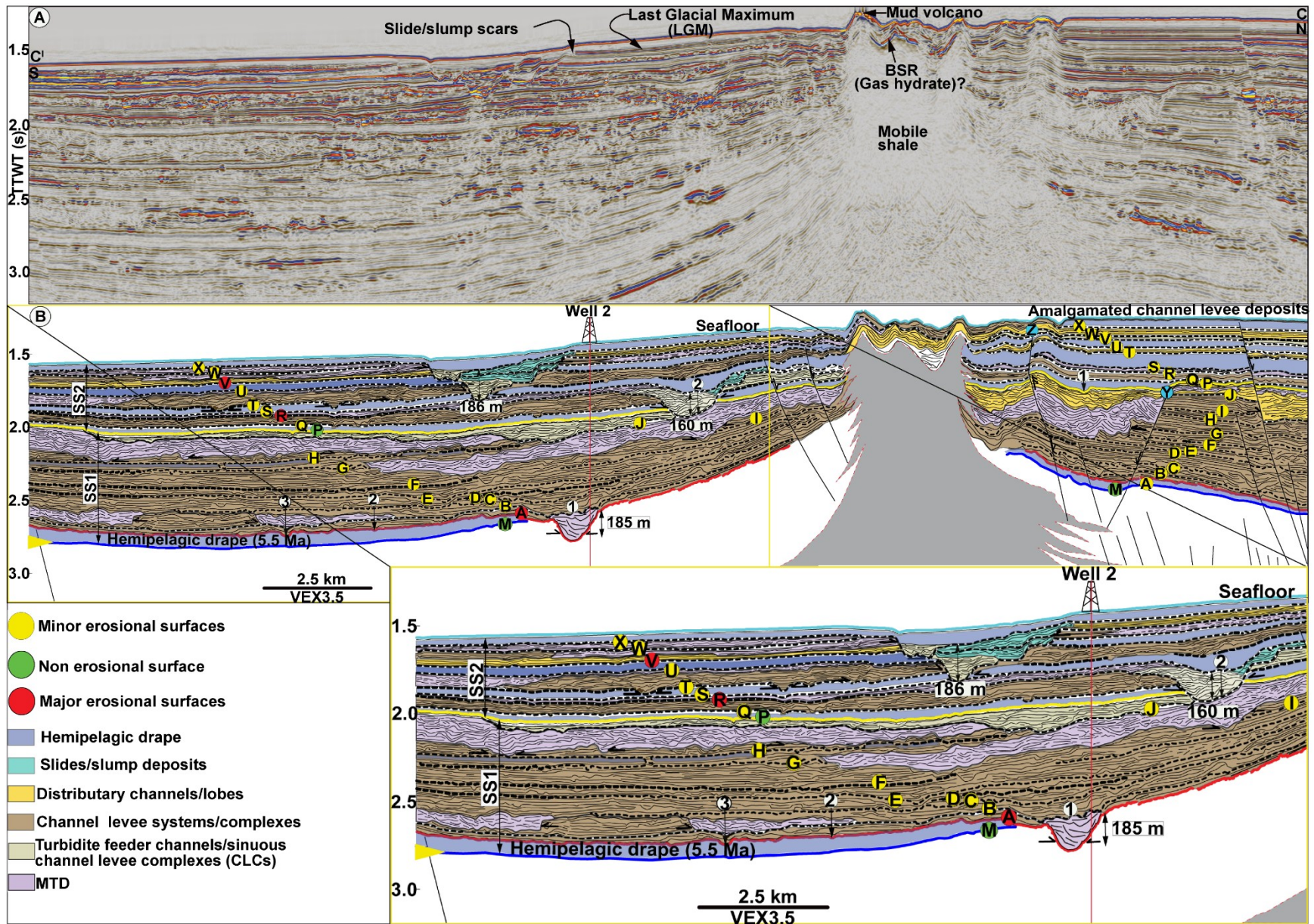
Seismic facies association on the western Niger Delta intraslope basins display complex arrangement and varied in time and space. Concave-upward negative topographies (90-185 m deep) that obstruct the lateral continuity of seismic reflections were interpreted as erosional submarine channel fairways (after Deptuck *et al.*, 2003; e.g. Fig. 3.2B). Seismic facies association within erosional submarine channels include: (i) chaotic, discontinuous low amplitude seismic facies (B_l) (MTDs) that overlie erosional channel fairway, informally referred to as lower MTDs (Fig. 3.2B). Narrow concave-upward negative topography within the main erosional channel fairway were interpreted as channel levee systems (CLSs)/channel forms (after Deptuck *et al.*, 2003; Fig. 3.2B), and were filled by (ii) turbidite feeder channels/meandering channel levee

complexes that are flanked by (iii) convergent/thinning, high to moderate amplitude seismic facies (C_{th}) within and outside the main erosional channel fairway interpreted as inner levee (IL) and outer levee (OL) respectively (e.g. Fig. 3.2B); (iv) chaotic, discontinuous low amplitude seismic facies (B_l) (MTDs) at the upper part of the erosional channel fairway (informally referred to as upper MTDs); (v) transparent, parallel continuous, draping seismic facies (D), hemipelagic drape/muddy turbidites, which covers the entire system (e.g. Fig. 3.2B). In the overlying sequence set 2 (SS2), facies association within erosional submarine channels generally includes: (i) turbidite feeder channels/meandering channel levee complexes overlain by (ii) coherent/slightly inclined, moderate to high amplitude seismic facies (slides/slump blocks) that are in turn covered by (iii) hemipelagic drape (where preserved) (e.g. Fig. 3.3B). Elsewhere laterally away from erosional submarine channels, seismic facies association within the SS1 generally includes: (i) lower MTDs; (ii) turbidite feeder channels/meandering CLSs; (iii) upper MTDs; (iv) distributary channels/lobes and (v) hemipelagic drape (Fig. 3.2C). In the overlying SS2, seismic facies association outside erosional submarine channels include: (i) amalgamated channel levee systems (CLSs) (e.g. Fig. 3.3A, B); (ii) MTDs (upper MTDs?) and (iii) hemipelagic drape (e.g. between horizons T and V towards the extreme left of Fig. 3.3B).

3.4.3 Mobile shale, Mud volcanoes and Bottom Simulating Reflector (BSR)

The Pliocene and Pleistocene stratigraphy were pierced to the by over 2.5 km wide, mounded seismic wipe-out zone with multiple deformation on the modern seafloor previously interpreted as mobile shales and mud volcanoes respectively (see Chima *et al.*, 2019; Fig. 3.3A, B). On a depth structure map of the seafloor, the mobile shale is characterized by >5 km wide relief, associated with a dark rounded summit corresponding to the mud volcano (Fig. 3.1E). Numerous, smaller dark rounded depressions a few meters to tens of meters across, scattered on the seafloor were interpreted as pockmarks (Chima *et al.*, 2019; e.g. Fig. 3.1E). Towards the upper part of the mobile shale, an over 1 km wide negative high amplitude anomaly (NHAA), with opposite polarity to the seafloor was interpreted as Bottom Simulating Reflector (BSR) (see also

Tectonostratigraphic Evolution of the western Niger Delta From Neogene to Present



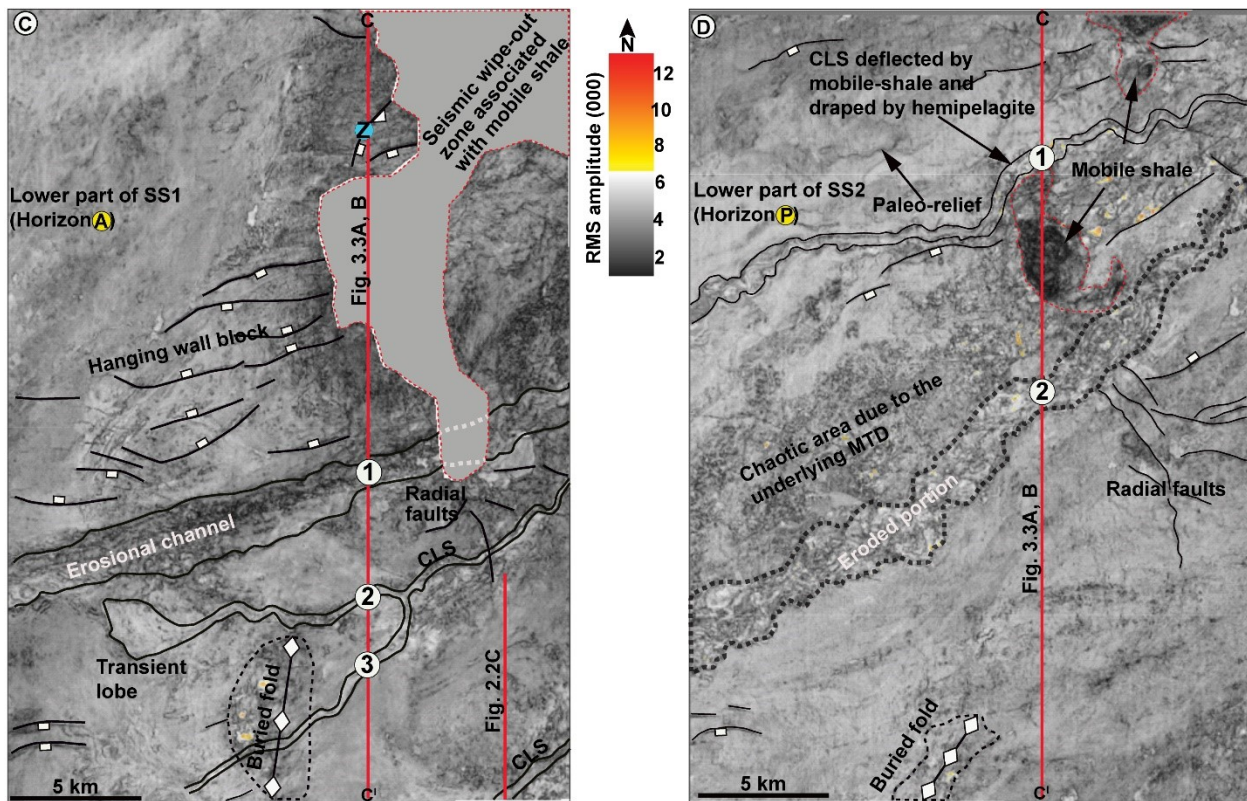


Fig. 3.3. Pliocene and Pleistocene stratigraphic architecture of the western Niger Delta intraslope basins. A, B: Uninterpreted north-south seismic line and line drawing (CC^1) showing the depositional geometries within seismic SS1 and SS2 (modified after Chima *et al.*, 2019). Note the lateral thickening in stratigraphy of SS1 away from mobile shale. Yellow arrow points to the base of the hemipelagic drape (horizon M) dated at 5.5 Ma. Letters (M-X) in panel B represent the seismic markers. Note the changes in sedimentary architecture from turbidite-dominated at the lower part of SS1 through a mix of MTDs and turbidites at the upper part of SS1 to hemipelagites and turbidites at the transition between SS1 and SS2. Note lateral truncations of seismic reflections within SS1 compared to SS2. Note also the occurrence slide/slump scars below the modern seafloor (panel A) and inverted fault (labelled Z in panel B). C, D: Interpreted RMS amplitude map of (horizons A and P), draped on variance attribute extractions at the lower parts of SS1 and SS2 illustrating changes in depositional elements. See text for a more detailed explanation..

Crutchley *et al.*, 2014; Fig. 3.3A). On the flank of the mobile shale, there is a marked lateral variation in the stratigraphic thickness of SS1 compared to SS2 (e.g. Fig. 3.3A, B).

3.4.4 3D seismic geomorphology and sedimentary architecture

A total of 21 seismic surfaces (12 within SS1 and 9 within SS2) (labelled M-X; e.g. Fig. 3.3B), were studied in detail. Only a few representative surfaces at the lower, middle and upper parts of the SS1 and SS2, that illustrate the main changes in sedimentary architecture are presented here. Throughout this section, we retain the descriptions and interpretations of seismic facies, mobile shales, mud volcanoes and pockmarks presented above to avoid unnecessary repetitions.

3.4.4.1 Lower part of SS1 (horizon A)

Description:

The base of SS1 (horizon M in Fig. 3.3B) is overlain by >80 m thick hemipelagic drape (highlighted in blue; Fig. 3.3B). The horizon M is trackable through significant part of the study area except across the overlying 185 m negative relief (horizon A; Fig. 3.3A) and the mobile shale described above (Figs. 3.1D, 3.3A, B). The 185 m deep relief associated with horizon A, marks the onset of MTDs, channel levee systems and distributary channels/lobes (Fig. 3.3A, B). An RMS amplitude map draped on variance attribute of the 185 m deep relief, shows the presence of 1.5 km wide, E-W trending straight feature (labelled 1 in Fig. 3.3C), and narrow winding features (labelled 2, 3; Fig. 3.3C), in the southern part of the study area. The narrow winding features (labelled 2 in Fig. 3.3C) is connected to a fan-shaped feature to the southwest. Linear scars with NE-SW, radial patterns and E-W orientations were observed in the northern, central and southern parts of the study area (Fig. 3.3C). A grey area (dashed red polygon) was observed in the northeast of the study area and characterized by radial features at its southern tip (Fig. 3.3C). The narrow winding feature (labelled 3 in Fig. 3.3C), crossed an oblique, elongate positive relief to the south. A north-south seismic line (CC¹) located in (Fig. 3.3C), illustrates the sedimentary architectures associated with horizon A at the lower part of SS1. The base of SS1 (horizon M) and associated hemipelagite (Fig. 3.3B) are conformable but were disrupted by the 185 m deep negative relief

associated with the overlying (horizon A; Fig. 3.3B), and mobile shale in the north (Fig. 3.3A-C). Most of the NE-SW trending linear scars offset stratigraphy normally except the one to the north (labelled Z; Fig. 3.3B, C), which offset stratigraphy normally at its lower part but inversely at its upper part.

Interpretation:

The >80 m thick seismic unit, which directly overlies the base of SS1 (horizon M), corresponds to the hemipelagic drape (HD)/muddy turbidites, dated at 5.5 Ma (see Chima *et al.*, 2019). The conformable nature of this hemipelagite suggests that it probably accumulated passively during episode of maximum flooding of the shelf and sediment starvation in the deep basin (see Chima *et al.*, 2019; and references therein). This interpretation is supported by the fact that the *D. quinqueramus* (calcareous nannofossil), which we used in dating the hemipelagite at 5.5 Ma is globally recognized as an important marker for the high sea-level during the late Miocene (e.g. Backman *et al.*, 2012). The 1.5 km wide and 185 m deep negative relief associated with horizon A (Fig. 3.3B), characterized by straight planform geometry on 3D geomorphological map was interpreted as straight erosional channel fairway (Fig. 3.3C) (after Deptuck *et al.*, 2003). The lateral discontinuity of horizon M (base of hemipelagite) adjacent the overlying horizon A, further supports the interpretation of the later as erosional surface (Fig. 3.3B). The narrow, winding features to the south of this erosional surface were interpreted as sinuous channel levee systems (CLS) or channel forms (after Deptuck *et al.*, 2003; Fig. 3.3C). The fan-shaped feature associated with the CLSs 2 was interpreted as transient fan/lobe (after Adeogba *et al.*, 2005; Fig. 3.3C). The grey area in the northeast of the study area corresponds to mobile shale, while the linear scars and oblique, elongated feature crossed by CLS, were interpreted as normal faults and buried fold respectively (see Chima *et al.*, 2019; Fig. 3.3C). The change in stratal offset patterns along the fault Z (Fig. 3.3B), from normal at lower stratigraphic section to inverse at upper part was interpreted as fault inversion probably associated with shale tectonics.

3.4.4.2 Middle part of SS1 (horizons G and I)

Description:

RMS amplitude map of horizon G draped on variance attribute extraction in the middle part of SS1 (horizon G), reveals the presence of 4 narrow, winding features (labelled 1a, 2, 3, and 4 on Fig. 3.4A), that are located in the NW and SE of the study area. Compared to the winding features 1a and 4, 2 and 3 display elongate borders of moderate RMS amplitudes (Fig. 3.4A). Linear scars exhibit different orientations with NE-SW and E-W trends dominating the north, while radial patterns dominate the central part of the study area (Fig. 3.4A). A NE-SW grey zone subdivide the study area into the northern and southern halves. An irregular-shaped, chaotic area was observed in the SE corner of the study area (Fig. 3.4A). A seismic line (DD¹) through the winding feature 1a reveals the presence of 1 km wide, 120 m deep relief, infilled by turbidite feeder channels flanked by outer levees (OLs) (Fig. 3.4B).

Furthermore, variance attribute extraction on horizon I, in the middle of SS1 (above horizon G), reveals in the northern part of the study area, a 2.5 km wide, sinuous feature (labelled 1b), characterized by smaller winding features at the centre (Fig. 3.5A). A chaotic area occurs on the outer side of this feature to the NE, marked by smaller linear or slightly curved features (Fig. 3.5A). A seismic line (BB¹) through the sinuous planform feature (Fig. 3.5A), reveals the presence of 176 m deep relief corresponding to horizon I, flanked by OL deposits (Fig. 3.5B). This relief is directly overlain by 'lower MTD' followed by turbidite feeder channel/meandering channel levee complexes that infill a smaller, narrower negative relief within the main topographic depression (Fig. 3.5B). The turbidite feeder channels/CLCs is flanked by an inner levee (IL) deposit within the main topographic depression (Fig. 3.5B). These deposits are overlain by a 1 km wide, 166 m deep negative relief, characterized by irregular base, infilled by turbidite feeder channel/CLSs, followed by laterally extensive 'upper MTDs' (Fig. 3.5B). The entire sequence is covered by hemipelagites and display an overall convex-upward geometry (Fig. 3.5B).

Interpretation:

The 4 narrow winding features associated with horizon G in (Fig. 3.4A) were interpreted as CLSs or channels forms, while the border zones that parallel the course of CLSs 2 and 3 were interpreted as channel belts (Fig. 3.4A). The NE-SW oriented grey area corresponds to the zone affected by mobile shale and erosion (Fig. 3.4A). The irregular chaotic area in the SE corner of the study area was interpreted as MTDs (Fig. 3.4A). The 1 km wide, 120 m deep relief associated with

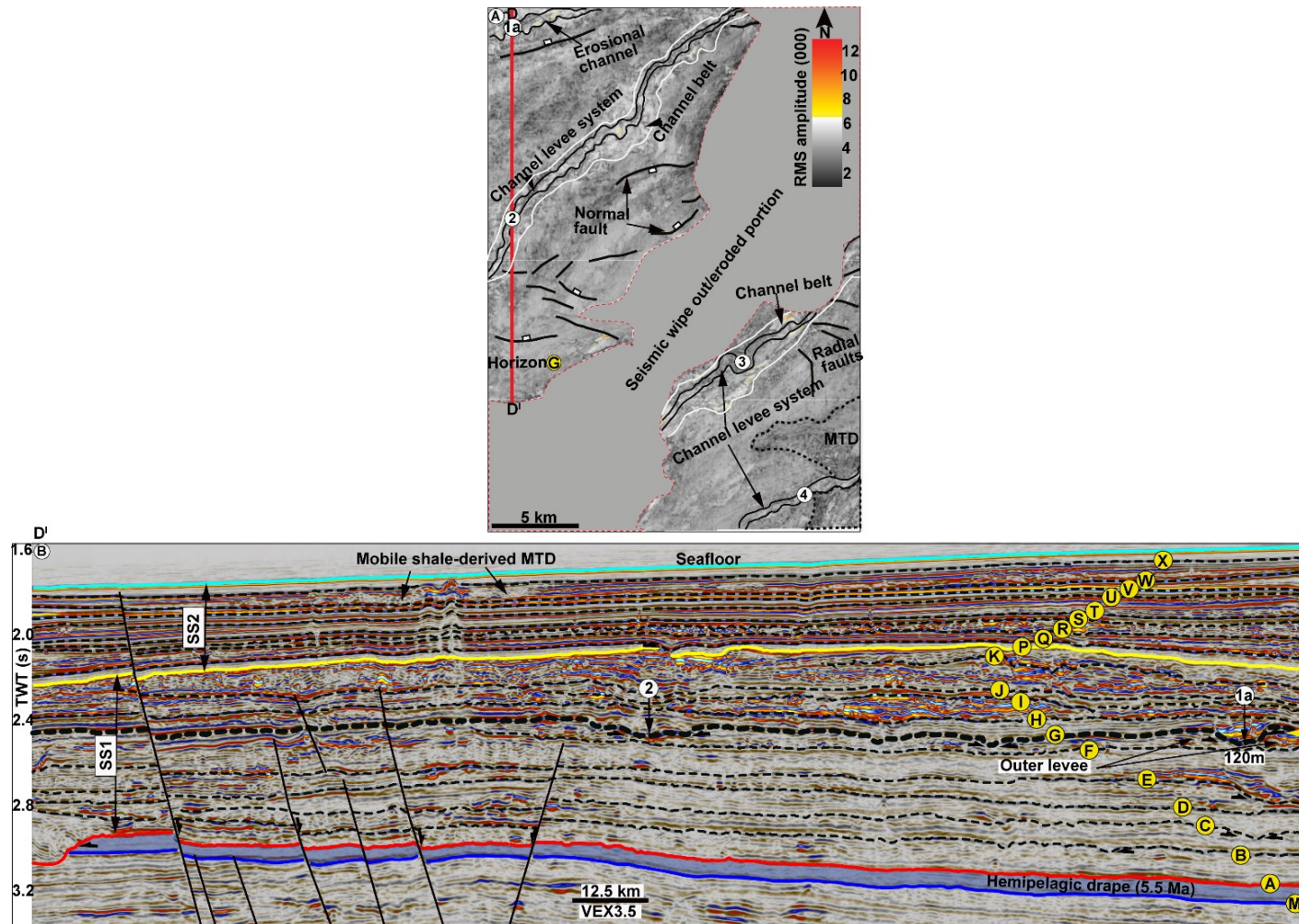


Fig. 3.4. Sedimentary architecture of the middle part of SS1. A: Interpreted RMS amplitude map of horizon G draped on variance attribute map at the middle of SS1 showing the presence of sinuous channel levee systems labelled 1a, 2 in the NW, and (3, 4) in the SE of the study area. B: Seismic line (DD¹) through channel 1a, shows its relatively shallow incision (1 km wide, 120 m deep). See Fig. 2.11A for the location of channel 1a in the northern part of the study area.

horizon G was interpreted as erosional CLS. The occurrence of OL deposits at nearly the same stratigraphic level as channel fills suggests that the erosional channel was unconfined (see Deptuck *et al.*, 2003; Fig. 3.4B).

The 2.5 km wide, sinuous feature associated with horizon I (Fig. 3.5A) was interpreted as sinuous erosional channel, while the enclosed smaller winding features were interpreted as turbidite feeder channels/meandering CLCs (Fig. 3.5B). The chaotic to slightly curved features located adjacent to the outer bank of the erosional channel to the north were interpreted as OLs (Fig. 3.5B). The presence of IL to the right side of the main erosional channel, coupled with the narrowing and lateral shifts of the enclosed channel forms (red arrow in Fig. 3.5B), were interpreted to different episodes of meandering/lateral aggradation of the system. The presence of OLs at every stage of the erosional channel suggest that sediment-gravity flows were unconfined (Fig. 3.5B). The convex-upward relief of the entire system suggests that it was overfilled.

3.4.4.3 Upper part of SS1 (horizon K)

Description:

RMS amplitude map draped on variance attribute extraction at the upper part of SS1, (labelled horizon K in Fig. 3.6A), shows the presence of a 1.8 km wide, moderately planform feature in the northern part of the study area, which bifurcates downstream (labelled 1c; Fig. 3.6A). The feature is characterized by moderate RMS amplitude and smaller, winding features with higher RMS amplitude within the main system (Fig. 3.6A). A linear relief occurs at the central outer bend of the main system (Fig. 3.6A). A north-south seismic line (FF¹) through the centre of the system reveals a 1.8 km wide, 90 m deep negative relief, infilled by turbidite feeder channel/

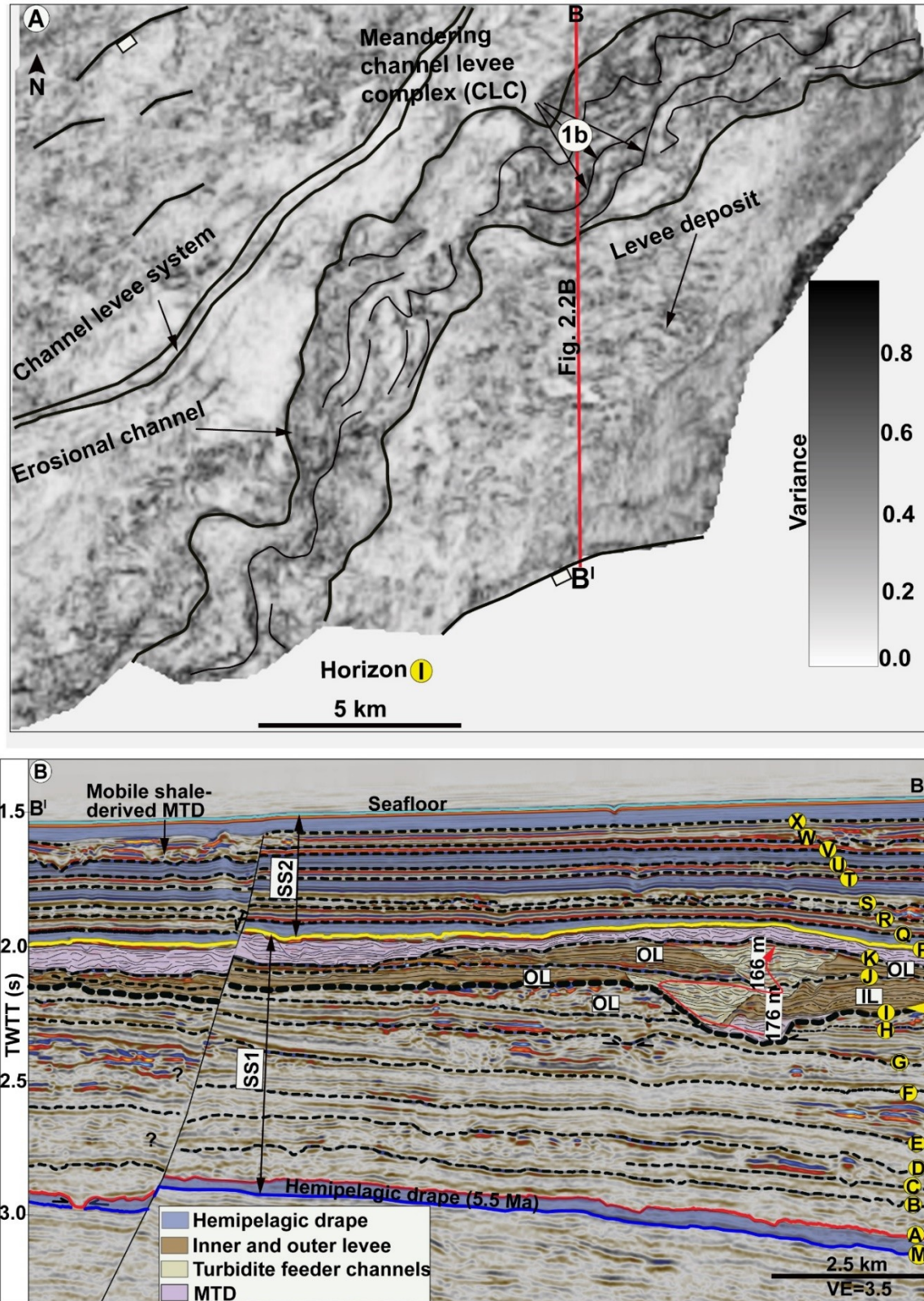


Fig. 3.5. Sedimentary architecture of the upper part of SS1. A: Interpreted RMS amplitude map of horizon K draped on variance attribute map, showing the presence of 1.8 km wide bifurcating

channel, characterized by moderate RMS amplitude and a terrace on its outer bend (see yellow arrow in panel B for the stratigraphic level). B: Interpreted north-south seismic line (FF¹) shows the incisional character of the channel (90 m deep), infilled by partially confined, turbidite feeder channels/meandering channel levee complex that are truncated by the overlying MTDs. See Fig. 11A for the location of erosional channel 1c in the northern part of the study area.

meandering CLC that were abruptly overlain by the 'upper MTD' and subsequently covered by hemipelagite (Fig. 3.6B).

Interpretation

The 1.8 km wide, 90 m deep relief, characterized by moderate RMS amplitude and the enclosed, smaller winding features of higher RMS amplitude were interpreted as erosional channel and CLC respectively (Fig. 3.6A, B). The sharp relief at the outer bend of the erosional channel fairway is interpreted as a terrace (Fig. 6A, B). The correspondence of this system to the earlier erosional channel fairways labelled 1a-c in (Figs. 3.4A, 3.5A, 3.6A), suggests that this feature has been active since the time equivalent to horizon E (Fig. 3.4A). From the early stage (labelled 1a; Fig. 3.4A) to the late stage (labelled 1c; Fig. 3.6B), the erosional channel has migrated over 10 km from NW to SE with an overall increase in width and erosional efficiency until the age equivalent to horizon K, when it was truncated by the overlying upper MTDs (Fig. 3.6B).

3.4.4.4 Base of SS2 (horizon P)

Description:

RMS amplitude map at the base of SS2 (yellow horizon labelled P in Fig. 3.3B), shows narrow winding, 2.5 km wide sinuous, NE-SW trending features (labelled 1, 2 in Fig. 3.3D), separated by a NE-SW trending chaotic zone. The narrow winding feature (labelled 1 in Fig. 3.3D) displays a relatively horizontal planform geometry up-dip of mobile

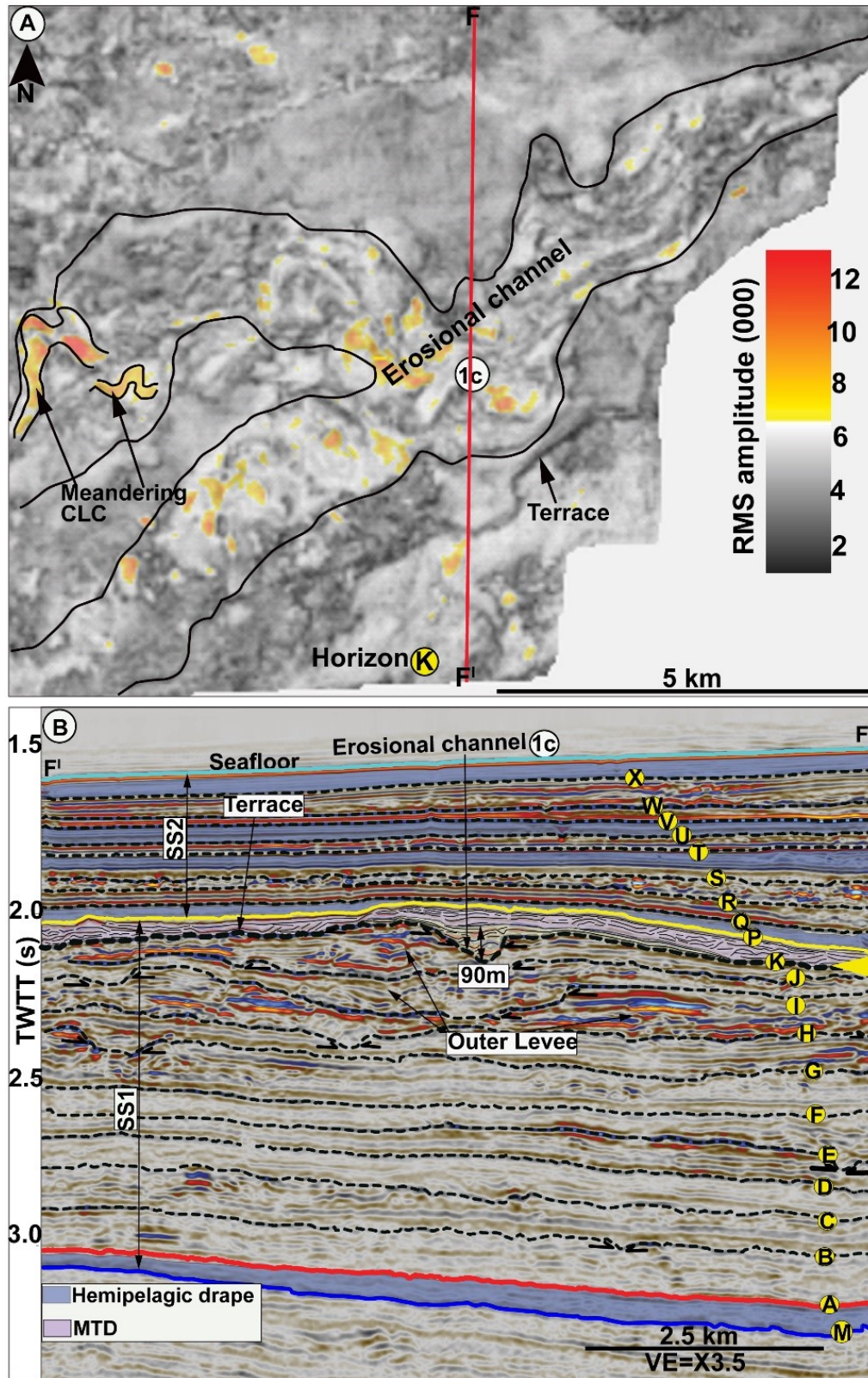


Fig. 3.6. Sedimentary architecture of the upper part of SS1. A: Interpreted RMS amplitude map of horizon K draped on variance attribute map, showing the presence of 1.8 km wide bifurcating

channel, characterized by moderate RMS amplitude and a terrace on its outer bend (see yellow arrow in panel B for the stratigraphic level). B: Interpreted north-south seismic line (FF¹) shows the incisional character of the channel (90 m deep), infilled by partially confined, turbidite feeder channels/meandering channel levee complex that are truncated by the overlying MTDs. See Fig. 11A for the location of erosional channel 1c in the northern part of the study area.

shale but becomes inclined downdip of the later (Fig. 3.3D). An over 3 km long wavy scar was observed north of the narrow winding feature (Fig. 3.3D). Radial and NE-SW trending feature were observed in the northern and eastern part of the study area (Fig. 3.3D). A north-south seismic line (CC¹), through these features shows the observed, narrow winding feature as a small negative relief just below the horizon P (labelled 1) in the northern part of (Fig. 3.3B). The wide sinuous feature (labelled 2 in Fig. 3.3B) corresponds to a 160 m deep relief (labelled 2; Fig. 3.3B), which obstructs the lateral continuity of the horizon P (Fig. 3.3B).

Interpretation:

The NE-SW trending narrow winding feature, characterized by small negative relief was interpreted as CLS and its occurrence below the stratigraphic level of horizon P indicates that the overlying hemipelagite draped the topography associated with the former (Fig. 3.3A, B). The 160 m deep negative relief (labelled 2 in Fig. 3.3B), which occurs above the stratigraphic level of interest (horizon P), corresponds to the portion of the latter, which was eroded by the younger horizon R (Fig. 3.3B). The transition of CLSs from horizontal up-dip of mobile shale to inclined platform geometry downdip of the structure suggests that relief associated with mobile shale deflected the former (see also Chima *et al.*, 2019). Linear scars (Fig. 3.3D) that offset stratigraphy on seismic line (Fig. 3.3B) were interpreted as normal faults, while wavy scar north of narrow CLS was interpreted as paleo-relief associated with abandoned CLS. The NE-SW trending, elongate topography to the south of the study area is interpreted as buried shale-cored anticline (Fig. 3.3B, D).

3.4.4.5 Middle part of SS2 (horizon R)

Description:

RMS amplitude map at the middle part of SS2 superimposed on variance attribute extraction (the level of horizon R in Fig. 7C), reveals the presence of NE-SW trending 2.5 km wide sinuous feature, characterized by low RMS amplitude (Fig. 3.7A, B). The feature displays overall increase in width downstream to the SW and is characterized by numerous, smaller winding features within the main system (Fig. 3.7A, B). Rounded relief features >300 m wide occur at the middle outer bend of the system (Fig. 3.7A, B). South of this sinuous feature, 3 narrow winding systems were observed. Radial, NE-SW and E-W trending linear scars occur in the north, central and southern part of the study area respectively. To the north, 2 mobile shales occur with the lower one flanked by small rounded features that are confined within NE-SW and E-W trending linear scars (Fig. 3.7A, B). A north-south seismic line (GG¹) through the main sinuous feature, reveals the presence of 185 m deep, negative relief with elevated margins, characterized by irregular scars to the right side (Fig. 3.7C, D, E). The 185 m deep relief was infilled by turbidite feeder channels/meandering CLCs that are in turn overlain by coherent/slightly inclined, moderate to high amplitude seismic facies (slide/slump blocks; Fig. 3.7C, D, E). The fill of this relief (horizon R) is successively overlain by 180 m and 100 m deep reliefs respectively corresponding to horizons V and W respectively, that are in turn infilled by turbidite feeder channels/meandering CLCs and slide/slump deposits (Figs. 3.7C, D, E; 3.8D, E). The entire system displays overall vertical aggradation with a minor lateral shift to the left during the final phase (red arrow in Fig. 3.7E). A thick hemipelagite, which occurs just below the modern seafloor drapes the entire system (Figs. 3.7C, D, E; 3.8D, E).

Interpretation:

The 2.5 km wide, 185 m deep sinuous feature, characterized by chaotic, discontinuous high amplitude seismic facies was interpreted as sinuous, erosional submarine channel, infilled by turbidite feeder channels/meandering CLCs (Fig. 3.7A-E). This turbidite feeder channels/meandering CLCs are similar to the highly erosive, High Amplitude Reflections (HARS), previously described on the western Niger Delta slope (e.g. Deptuck *et al.*, 2003; Heiniö and

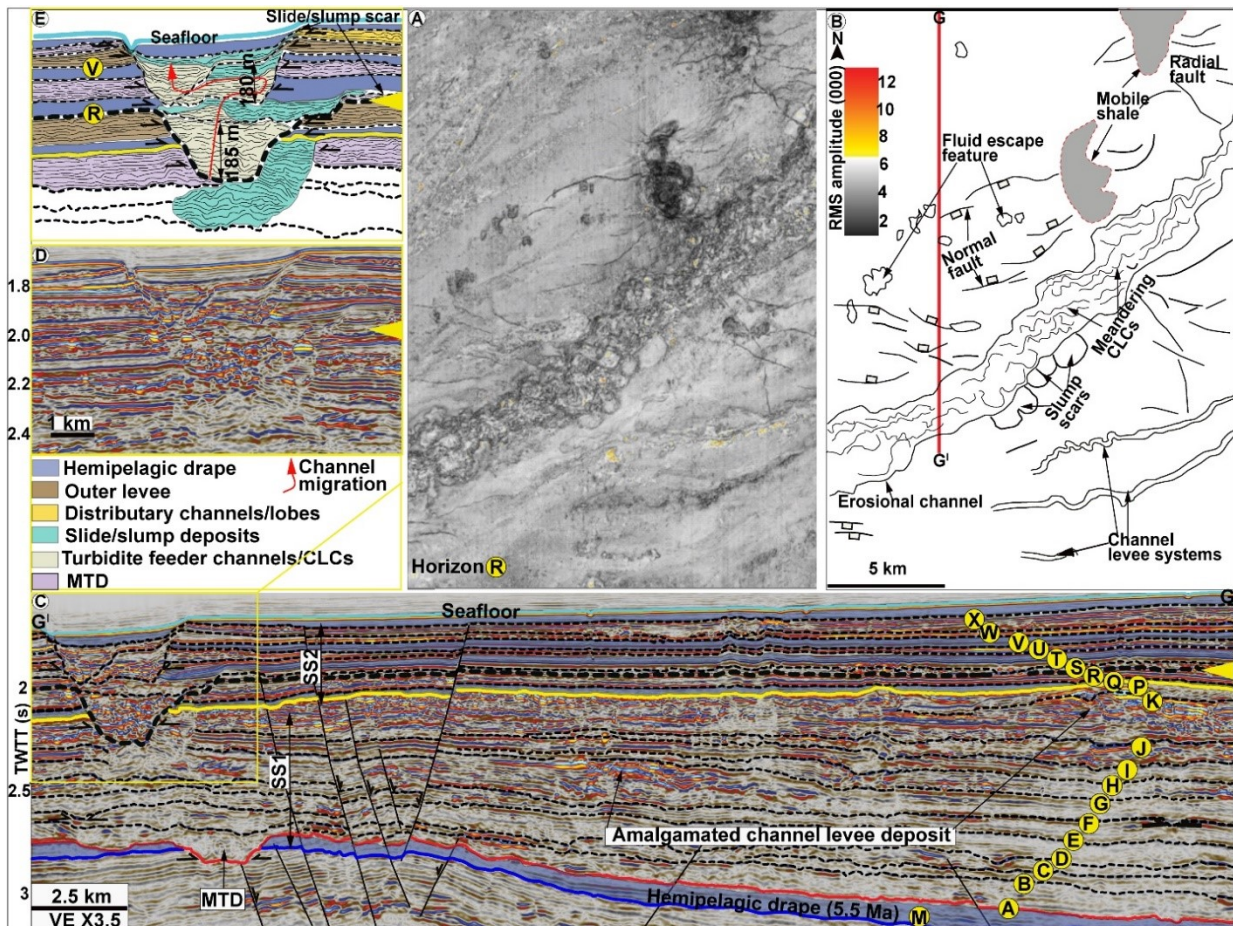


Fig. 3.7. Sedimentary architecture at the middle part of SS2 A, B: Uninterpreted and interpreted RMS amplitude map of horizon R draped on variance attribute extraction shows the presence of a 2.5 km wide channel, characterized by moderate RMS amplitude and turbidite feeder channels/meandering channel levee complexes (CLCs) within the channel axis (see yellow arrow in panel C for stratigraphic level). C: An interpreted north-south seismic line (GG¹) illustrates the complex cut and fill architecture of the channel (185 m deep) with overall vertical aggradational patterns (panels D, E). Note the dominance of channel fills by turbidite feeder channels/meandering CLCs and slide/slump deposits. Note the upward decrease in the thicknesses of slide/slumps and external levee deposits. See text for a more detailed explanation.

Davies, 2007; Hansen *et al.*, 2017); and elsewhere on the adjacent side of the equatorial Atlantic, the Rio Muni Basin (Equatorial Guinea), where their origin was linked to tropical storm events (see Jobe *et al.*, 2011). The >300 m wide, rounded features at the middle outer bend of the erosional channel fairway were interpreted as slides/slump scars (Fig. 3.7A, B). The narrow, winding

features to the south of the main erosional channel were interpreted as sinuous CLS or channel forms. The lateral discontinuity of seismic reflections (e.g. horizon P) on the either side of the erosional channel (Fig. 3.7C-E), indicates the erosivity of sediment-gravity flows, which sculpted the former. This interpretation is supported by the channel's deeply incised nature (185 m deep) and presence of terraces (multiple slide/slump scars) along its elevated margin (Fig. 3.7A-E). Hence, the presence of multiple slides/slumps, dominance of erosional channel fills by chaotic, highly reflective turbidite feeder channels/meandering CLSs and overall confined nature of erosional channels distinguish submarine channels in SS2 from SS1, where channels are generally unconfined (Fig. 3.5B). The vertical superposition of erosional channels with minor lateral migration indicates the complex cut and fill architecture of channels with overall vertical aggradation (red arrow in Fig. 3.7E). The radial, E-W and NE-SW trending linear scars distributed in the north, central and southern part of the study area were interpreted as normal faults (Fig. 3.7A-C). The small, dark rounded features that flank mobile shales were interpreted as fluid escape features (Fig. 3.7A, B). These mobile shales, mud volcanoes, fluid escape features, BSR and pockmarks (Figs. 3.1E, 3A, 8A, 9A; Appendices 2, 3, 3, 4), are indirect evidences of fluid overpressure in the study area (see also Riboulot *et al.*, 2011).

3.4.4.6 Upper part of SS2 (horizons V and W)

Description:

RMS amplitude map of horizon V draped on variance attribute extraction at the upper part of SS2, shows the presence of 2.1 km wide, sinuous planform feature, characterized by moderate RMS amplitudes and smaller winding features within the main system (Fig. 3.8A, B). Smaller winding features also occur in the northern and southern part of the study area (Fig. 3.8A, B). The borders of the main sinuous system are irregular and contain some detached curved loops at its outer bends (Fig. 3.8A, B). North of the system, a NE-SW trending, wedge-shaped chaotic area of low RMS amplitude was observed (dashed black polygon in Fig. 3.8A, B). Further north, 2 mobile shales were observed that are flanked by small, dark rounded features (Fig. 3.8A, B). The dark rounded features adjacent to the lower mobile shale were confined within roughly NE-SW

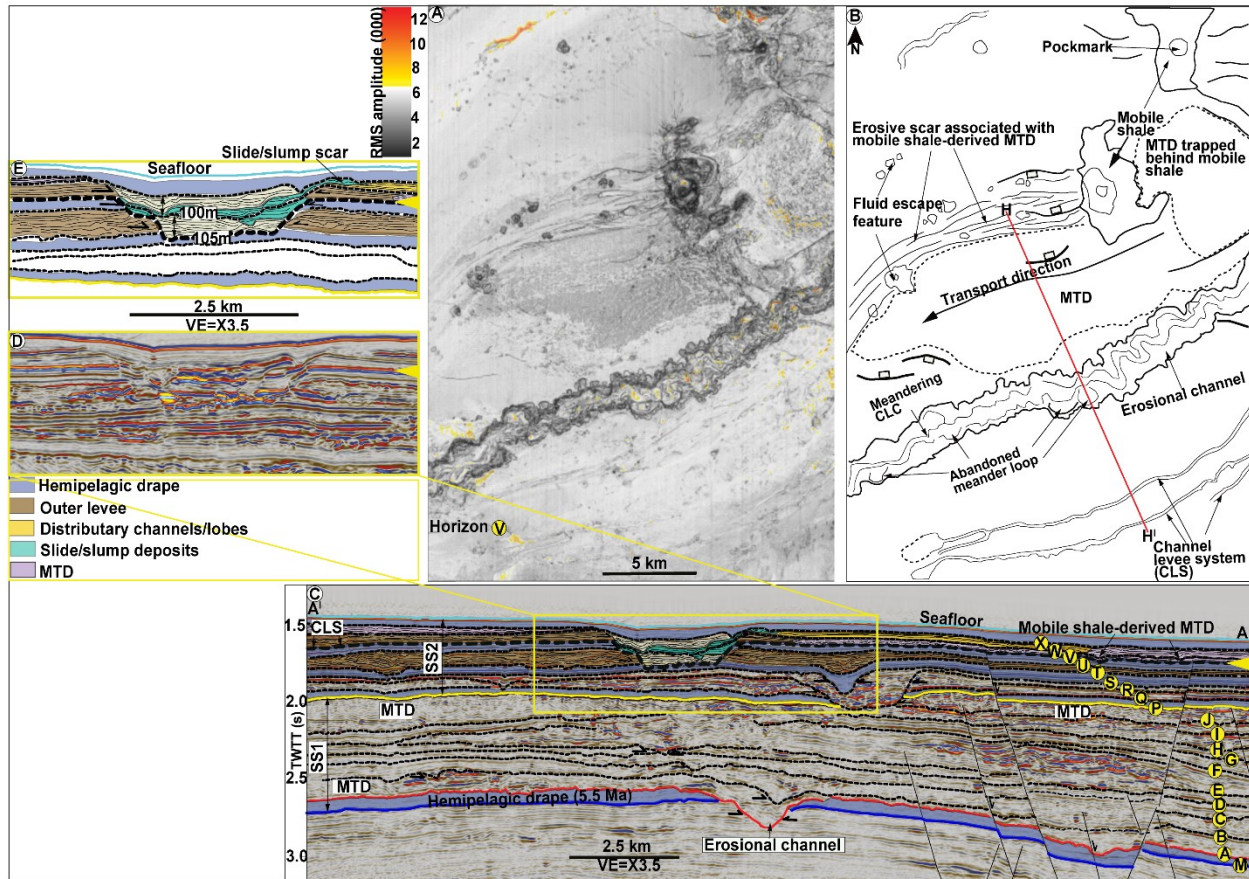


Fig. 3.8. Sedimentary architecture at the upper part of SS2. A, B: Uninterpreted and interpreted RMS amplitude map of horizon V draped on variance attribute map shows the presence of 2.1 km wide, sinuous channel, characterized by moderate amplitude and turbidite feeder channels/meandering CLCs (see yellow arrow in part C for the stratigraphic level). Note the upward decrease in the thicknesses of slide/slumps and external levee deposits. The chaotic, wedge-shaped area to the north is interpreted as MTDs. C: Interpreted NW-SE seismic line (HH¹) shows the complex cut and fill architecture of the channel (panels D, E). Note the upward decrease in the thicknesses of slide/slumps and external levee deposits. A, B, C after Chima *et al.* (2019).

trending short and long linear scars (Fig. 3.7A, B). A NW-SE seismic line (HH¹), illustrates 105 m deep negative relief associated with the 2.1 km wide sinuous feature (Fig. 3.8C-E). This feature is infilled by turbidite feeder channels/meandering CLCs that are overlain by slides/slump deposits (Fig. 3.8C-E). The fill of horizon V is abruptly overlain by another 100 m deep relief associated with the overlying horizon W (Fig. 3.8C, 9A). The topographies of horizons V and W are

respectively associated with relatively thick and thin OLs (Fig. 3.7C, 8C). Towards the east of the study area (Fig. 3.8C), thin, laterally confined, somewhat coherent, low to moderate reflectivity seismic unit overlies horizon V, above a V-shaped, depth-penetrating linear scars, that offset seismic reflections (Fig. 3.8A, B). The shallow relief associated with the youngest surface (horizon X) is covered by hemipelagite (e.g. Fig. 3.8C).

Furthermore, RMS amplitude map superimposed on variance attribute map (the level of horizon W), just above (horizon V), reveals the presence of a 2.5 km wide, sinuous feature, characterized by narrow winding features and low RMS amplitudes (Fig. 3.9A). South of the main sinuous system, 2 elongate features, characterized by high RMS amplitudes in the eastern and western parts of the study area were observed, with narrow, winding features crossing the eastern elongate feature (Fig. 3.9A). To the north, 2 mobile shales were flanked by short and long linear scars, and small, dark rounded features (Fig. 3.9A). An irregular chaotic area with low RMS amplitude (dashed black polygon in (Fig. 3.9A), occurs adjacent the mobile shales. An E-W seismic line (JJ¹) through the elongated features in the south of the study area, shows their high reflectivity and onlapping geometry within a regional negative relief (Fig. 3.9B). Although our observations in the previous seismic lines show that the fills of negative reliefs are generally chaotic and difficult to track (e.g. Figs. 3.3A, B, 7C, D), horizons X and W could be locally correlated inside negative topographies (e.g. Fig. 3.8C-E).

Interpretation:

The wide sinuous features associated with horizons V and W were interpreted as meandering erosional channels, while the narrow winding features to the north and south of these features (Figs. 3.8A, B, 9A), were interpreted as sinuous CLSs or channel forms. (Figs. 3.8A, B; 9A, B). The detached, curved loops at the outer bends of the erosional channel fairway associated with horizon V were interpreted as abandoned meander loops (Fig. 3.8A, B). The occurrences of slide/slump deposits (with lower reflectivity) above turbidite feeder channels/meandering CLCs within the fills of the erosional channels associated with horizons V and W, suggests failures of outer levees and hemipelagite/muddy turbidites that flank channel (Fig. 3.7C-E, 8C-E). The chaotic areas with overall low RMS amplitudes to north and NE of the study area (Fig. 3.8A, B) were interpreted as MTDs. The moderate RMS amplitude associated MTDs in the NE of mobile

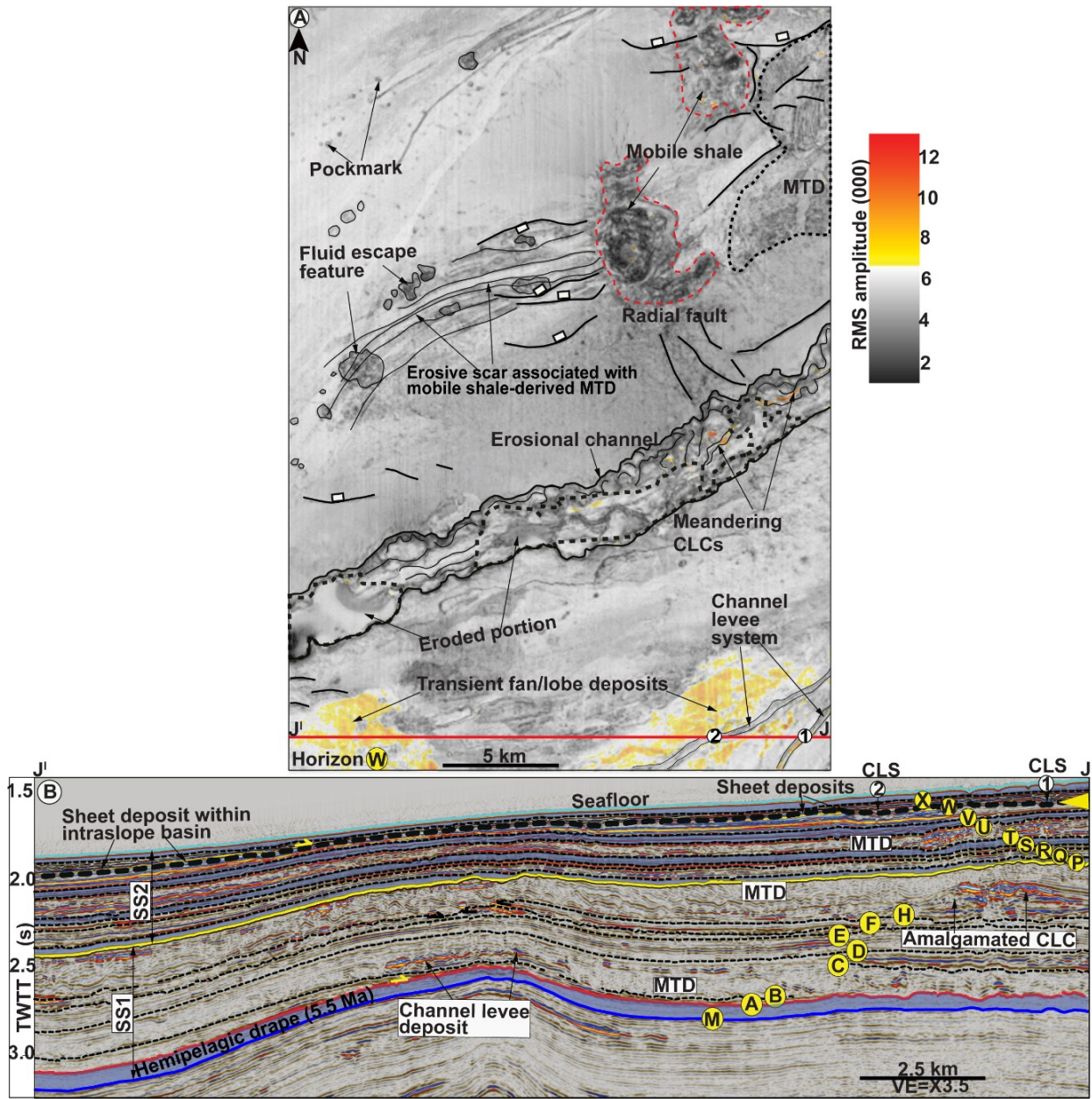
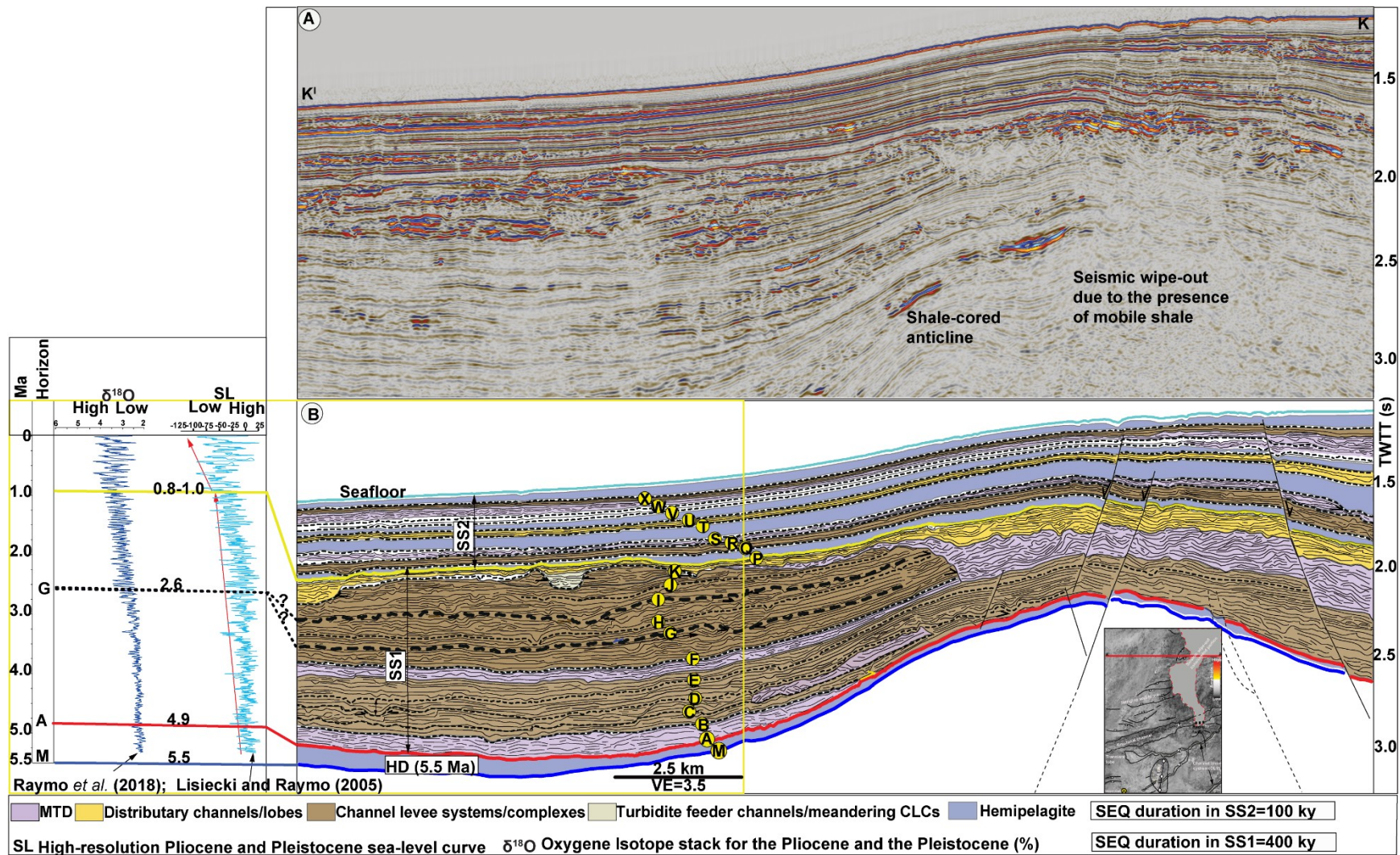


Fig. 3.9. Sedimentary architecture of the upper part of SS2. A: Interpreted RMS amplitude map of horizon W draped on variance attribute map, shows the presence of MTDs trapped behind mobile shale in the north, a 2.5 km wide erosional channel in the central part of the study area and transient fan/lobe deposits, characterized by high RMS amplitudes in the south. B: Interpreted E-W seismic line (JJ') illustrates the high reflectivity and onlapping geometry of the transient fan deposits. Note in panel A, the presence of mobile shale, fluid escape features and long linear scars associated with mobile shale-derived MTDs, which underlie the level of interest (horizon V).

shale in (Fig. 3.7A), suggests the presence of sandy sediment within MTDs that were trapped within local topography associated with mobile shale (Fig. 3.8A, B). The short E-W trending linear scars, adjacent to mobile shales and associated small, dark rounded features were interpreted as fault scars and fluid escape features respectively (Fig. 3.8A). The longer linear scars confined within fault scars that exhibit coherent/slightly deformed internal architecture with moderate to high reflectivity on seismic line (e.g. Fig. 3.2B, 5A), were interpreted as mobile shale-derived MTD (see Chima *et al.*, 2019). The lateral confinement of this MTD adjacent to mobile shale (Figs. 8A, 9A), coupled with their somewhat coherent internal architecture and moderate to high RMS amplitudes, distinguish them from the regional (lower and upper MTDs) (see Chima *et al.*, 2019). The elongate features, characterized by high RMS amplitude located in the southern part of the study area (Fig. 3.9A), were interpreted as transient fan/lobe deposits (after Adeobga *et al.*, 2005). The crossing of the eastern transient fan/lobes by sinuous CLSs, suggests sediment bypass on the former to more distal setting beyond the limit of the studied 3D block (see also Adeobga *et al.*, 2005; Fig. 3.9A). The upward decrease in the thickness of slide/slump deposits from (horizons R-W) (Figs. 3.7C-E, 9C-E), suggests an overall decrease in the incisional ability of sediment-gravity flows or gradual establishment of local slope equilibrium profile. However, the upward decrease in the thickness of OLs from (horizons R-W) (Figs. 3.8C-E, 9C-E), suggests increased confinement of sediment-gravity flows or overall decrease in mud fraction of the former. The concave upward topography associated with erosional submarine channels in SS2 suggests that they were underfilled prior to hemipelagic draping (e.g. Figs. 3.7C-E, 8C-E), compared to SS1, where channels were overfilled (e.g. Fig. 3.5B).

From the foregoing observations, three major changes occurred in the sedimentary records of the western Niger Delta intraslope basins over the last 5.5 Ma (see Figs. 3.3-3.10). These changes include: (1) lower part of SS1 at the transition from the late Messinian thick hemipelagites (5.5 Ma) (horizon M) to the overlying erosional event (horizon A), characterized by relatively confined, erosional submarine channels, thin MTDs and meandering CLSs (e.g. Fig. 3.3A, B); (2) the upper part of SS1 at the transition between horizons F and G, dominated by laterally extensive MTDs and partially confined incisional submarine channels, characterized by complex cut and architecture (e.g. Figs. 3.3A-C, 5A, B); (3) the transition between SS1 to SS2 (horizons K/P), which marks the onset of alternating hemipelagites and relatively confined, incisional, submarine channels with multiple slide/slumps within channels axes (e.g. Figs. 3.3A, B, 7C-E 8C-E).

Tectonostratigraphic Evolution of the western Niger Delta From Neogene to Present



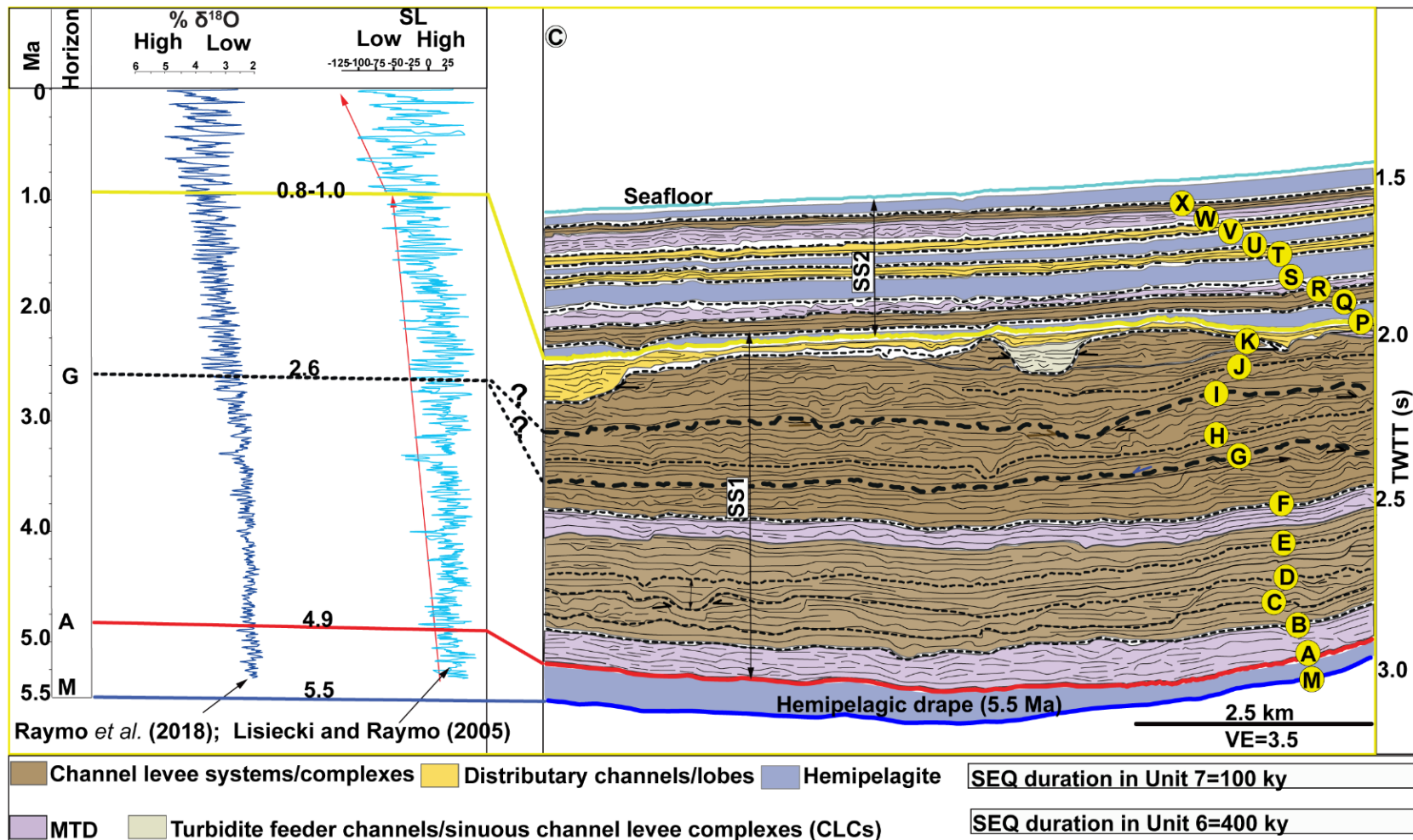


Fig. 3.10: Sequence stratigraphic interpretation. A, B: Uninterpreted and interpreted E-W seismic and line drawing (KK¹), showing the Pliocene and Pleistocene stratigraphic architecture of the western Niger Delta intraslope basins (panel C for a detailed view). Note the tentative correlation between seismic markers at (M/A, G/I and K/P) transitions with the sea-level and 18O isotope curves. Note also the lateral variation in stratigraphic thickness of SS1 compared to SS2.

3.4.5 Sequence stratigraphic interpretation and age assignment (SS2)

Using the biostratigraphically constrained late Messinian (5.5 Ma), the modern seafloor (0 Ma), and taking into account the observed changes in sedimentary architecture (Figs. 3.3-3.10), we suggest that the change in sedimentary architecture at the transition between SS1 and SS2 (K/P) boundary, could have occurred around 0.8-1.0 Ma during the Middle Pleistocene Transition (MPT) as described in the literature (0.8-0.9 Ma; Miller *et al.*, 2005; Lisiecki and Raymo; 2007; Fig. 3.10B, C). The identified 9 horizons within SS2 (P-X), could represent nine 5th-order sequences. The hemipelagic drape, which marks this transition (base of SS2; horizon P), correlates with moderate oxygen isotope (3.5‰) and moderate sea-level variations (~12.5 m) before the more pronounced sea-level cycles with amplitudes as high as 100 m (Fig. 3.10B, C). This hemipelagite like the one at the base of SS1, is inferred to have been deposited during overall highstand relative-sea level (see Chima *et al.*, 2019 and references therein). The assigned age (0.8-1.0 Ma) agrees with Benjamin *et al.* (2015), who proposed middle Pleistocene to this conformable seismic surface. The repetitive motifs consisting of vertically juxtaposed erosional channels infilled by aggrading CLSs/CLCs and MTDs, ultimately draped by hemipelagites at the uppermost part (e.g. Figs. 3.3A, B; 7C, D, E; 8D, E), seems to record regressive-transgressive cycles previously documented on the eastern Niger Delta continental shelf (e.g. Fatoke and Bhattacharya, 2010; Jermannaud *et al.*, 2010; Riboulot *et al.*, 2012). From the foregoing observations, it is reasonable to infer that the juxtaposed, highly incisional submarine channels associated with e.g. horizons R, V and W (e.g. Figs. 3.3A, B; 7C-E, 8C-E) correspond to regional erosional surfaces during forced regressions, while the infilling/aggrading turbidite feeder channels/meandering CLCs and MTDs represent lowstand deposits with hemipelagites marking transgressive/highstand deposits, probably controlled by glacio-eustatic sea-level oscillations over the last circa 0.8-1.0 Ma (see Miller *et al.*, 2005; Lisiecki and Raymo; 2007; Fig. 3.10B, C). The estimated age of the last erosional surface within SS2 (horizon X; Figs. 3.3A, 10B, C) is interpreted as the LGM, at around ~20 ka as also suggested Jobe *et al.*, (2015; 2016).

3.4.6 Sequence stratigraphic interpretation (SS1)

Based on the foregoing interpretation of SS2, SS1 could correspond to a deposition between 5.5 Ma and 0.8-1.0 Ma (seismic reflections M-P; Fig. 3.10B, C), with the 11 horizons

representing eleven 4th-order sequences of circa 400 ka duration. The transition at the lower part of SS1 (M/A interface), is an erosional surface, which correlates with high oxygen isotope value (>4.5‰) and one of the highest falls in the relative sea-level during the early Pliocene (>25 m) (Fig. 3.10B, C). We suggest an age of 4.9 Ma for this 185 m deep erosional surface reasoning that it could be correlated to the first major lowering of the sea-level just after the late Miocene (5.5 Ma) high sea-level see Miller *et al.*, 2005; Lisiecki and Raymo, 2007; Raymo *et al.*, 2018; Fig. 3.10B, C). The 4.9 Ma, which we propose for this erosional surface (horizon A in Fig. 3.10B, C), disagrees with the late Miocene proposed by Benjamin *et al.* (2015), who lacked biostratigraphic control. The occurrence of horizon A just above the hemipelagite dated at 5.5 Ma, its erosional character (Fig. 3.3A-C, 7C-E, 8C-E), and association with MTDs and CLSs, further supports its nomination as a possible candidate for a sea-level lowering during the early Pliocene around 4.9 Ma (see Miller *et al.*, 2005; Lisiecki and Raymo, 2007; Raymo *et al.*, 2018; Fig. 3.10B, C).

Furthermore, the transition at upper the part of SS1 (F/G interface), is an ~120 m deep erosional surface (e.g. Fig. 3.4B), which tentatively correlates with (>30) m fall in relative sea-level and relatively high Oxygen isotope (>3.5‰) (Fig. 3.10B, C). The erosional character of this surface coupled with its association with multiple CLSs (e.g. Fig. 3.4A, B), suggest that it could be related to a lowstand sea-level. Furthermore, horizon I, which overlies horizon G is 176 m deep (Fig. 3.5B), partially confined and characterized by complex cut and fill architecture, similar to those observed within SS2 (e.g. Figs. 3.7, 8, 9A). The observed changes in sedimentary architecture associated with horizons G and I (Figs. 3.4, 5), could be related to relative sea-level fall probably during the early Pleistocene, following the Northern Hemisphere Glaciation (NHG), which is documented in the literature to have occurred around 2.6 Ma (see Miller *et al.*, 2005; Lisiecki and Raymo, 2007; Gibbard *et al.*, 2010; Head and Gibbard, 2015a, b; Gibbard and Lewin, 2016; Raymo *et al.*, 2018). (see Miller *et al.*, 2005; Lisiecki and Raymo, 2007; Raymo *et al.*, 2018; Fig. 3.10B, C). Hence, we nominate horizons G and I as possible candidates for the early Pleistocene but favour horizon I due to its deep incision (176 m) and similar architectural patterns as those described in the deepwater western Niger Delta over the last circa 120 ka as controlled by glacio-eustatic sea-level oscillations and sediment supply (see Jobe *et al.*, 2015; 2016).

3.4.7 Sequence set duration and sedimentation rates

Sequence duration measures the ratio of the time interval for sequence set development to the number of enclosed seismic surfaces (see Zhang *et al.*, 2019). Using the estimated ages above, sequence set duration for SS1 yields $(5.5-0.8) \text{ Ma}/12 = \sim 0.4 \text{ Ma}$ ($\sim 400 \text{ ka}$) and $(0.8-0) \text{ Ma}/9 = \sim 0.1 \text{ Ma}$ ($\sim 100 \text{ ka}$) for SS2. Furthermore, using an average velocity of 1253.2 m/s obtained from Well-1 (W1) (Fig. 3.1E), estimated sedimentation rates within the non-decompacted SS1 and SS2 are 132 m/Ma and 370 m/Ma respectively.

3.5 Discussion

We discuss the Pliocene and Pleistocene stratigraphic evolution of the western Niger Delta intraslope basins over the last 5.5 Ma in relation to allocyclic (glacio-eustatic) sea-level and local basin tectonic forcings, and finally propose a deepwater depositional model.

3.5.1 Allocyclic (glacio-eustatic) sea-level forcing

Allocyclic factors are controls external to the depositional system such as climate, eustasy, tectonics and sediment supply (Einsele *et al.*, 1991). Orbital parameters, such as obliquity and eccentricity forcings control global sea-level, climate, drainage basin erosion, sediment supply, or more locally environmental energy, and thus impact the architecture of sedimentary units and their bounding surfaces (Zecchin, 2007; 2010; 2012; Catuneanu and Zecchin, 2013).

High subsidence rates (350 m/Ma) compensated by high sedimentation rates (36.5 cm/ka) have been documented to have facilitated the preservation of eccentricity cycles of 100 ka on the eastern Niger Delta continental shelf over the last circa 0.5 Ma (Riboulot *et al.*, 2012). This result is similar to that observed in the Mediterranean margin over the same interval (the last circa 0.5 Ma), where subsidence rate as high as 255 m/Ma, accompanied by high sedimentation rates led to the preservation 100 ka eccentricity sequences during the Quaternary glacio-eustatic sea-level oscillations (see Rabineau *et al.* 2006; Leroux *et al.*, 2014). Although we did not estimate subsidence rate over the last circa 5.5 Ma, the overall increase in sedimentation rates (x3) at the MPT (0.8-1.0 Ma), possibly accompanied by high subsidence rate (e.g. Goudie, 2005), is inferred to have facilitated the preservation of the 100 ka observed within SS2 (see also Rabineau *et al.*,

2006; Riboulot *et al.*, 2012; Leroux *et al.*, 2014.). Our study is also in agreement with Gulick *et al.* (2012), who documented overall increase in sedimentation rates at a source-to-sink-scale on the New Jersey margin (USA), which is largely linked to glacio-eustatic sea-level changes over the last 0.7-1.2 Ma.

Furthermore, although the eccentricity sequences of 400 ka, which we propose for SS1 has been recognized to have strongly influenced sedimentation in ocean basins (e.g. Pälike *et al.*, 2006; Boulila *et al.*, 2011; and references therein), it has rarely been described in the deep basin architecture. The estimated sequence set duration of 400 ka, the overall lateral discontinuity of seismic reflections, the preponderance of laterally extensive MTDs and erosional submarine channels, characterized by complex cut and fill architecture at the upper part of the SS1 (Fig. 3.3B, 5A,B), are similar to the 4th-order incised valleys/slope canyons that were biostratigraphically constrained and calibrated with seismic records within the Pliocene of the Foz do Amazonas continental shelf as 400 ka eccentricity sequences (see Gorini *et al.*, 2014).

The Pliocene and Pleistocene stratigraphy of the western Niger Delta intraslope basins, respectively characterized by mass-wasting and turbidites sequences, and hemipelagite and turbidite sequences (Figs. 3.3-3.10), also compares with the Pliocene and Pleistocene stratigraphy of the Ulleung Basin, East Sea (Japan), where the Pliocene and Pleistocene stratigraphy are characterized by (debris-flows and turbidite sequences), and (hemipelagites and turbidites sequences) (Yoo *et al.*, 2017). In the Ulleung Basin, the Pliocene stratigraphy is largely linked to tectonic deformation, while the Pleistocene is linked to changes in relative sea-level (Yoo *et al.*, 2017). However, the Pliocene and Pleistocene stratigraphy described in this study contrasts with that of the northern Gulf of Mexico (GOM), where thick hemipelagites/muddy turbidites and thin MTDs dominate the Pliocene compared to the Pleistocene, which is dominated by thick MTDs and thin hemipelagites (Madof *et al.*, 2017; Wu *et al.*, 20120). Madof *et al.* (2017) and Wu *et al.* (2020), argued that the stratigraphy of the northern Gulf of Mexico over last 3.7 Ma was mainly controlled by differential sedimentation and associated salt-related subsidence, while the overall increase in sedimentation rates over the Pleistocene was largely controlled by the capture of the Ohio and Missouri Rivers by the Mississippi in the late Pleistocene (see also Prather *et al.*, 1998).

In the western Niger Delta intraslope basins, the Pliocene and Pleistocene stratigraphy were controlled by a combination of glacio-eustasy and shale tectonics (see discussion below). The

observed increase in sedimentation rates at the MPT (0.8-1.0 Ma) could be related to: (i) glacio-eustatic sea-level forcing linked to the Milankovich cycles; (ii) regional climate forcing associated with the West African Monsoon, which is established to have interacted with drainage basins, erosion and sediment supply to the Niger Delta since the Plio-Quaternary (see Lézine *et al.* (2005; Weldeab *et al.*, 2011; Collins *et al.*, 2014; Govin *et al.*, 2014; Armitage *et al.*, 2015); (iii) a possible shift in sediment flux from the eastern to the western Niger Delta over the Pleistocene due either to delta lobe switching/regional climate evolution (see Jermanaud *et al.*, 2010; and references therein), or tectonic reorganization in the catchment (e.g. Goudie, 2005). Recent study by Picot *et al.* (2019) in the adjacent Congo Basin also demonstrated overall architecture of avulsions that can describe progradation/retrogradation patterns in response to climate forcing.

3.5.2 Basin tectonics

In terms of basin tectonics control of the Pliocene and Pleistocene stratigraphy of the western Niger Delta intraslope basins, Chima *et al.* (2019) showed that the main erosional submarine channel in the study area (labelled 1, 2, 3; Fig. 3.11A, B), has been active since the Pliocene, and was generally deflected to the south with E-W orientation during early and late mobile shale active periods (stages 1 and 3), and northwards with NE-SW orientation during quiescence in mobile shale (stage 2) (Fig. 3.11A, B). The present study investigated the entire submarine channel systems over the last 5.5 Ma allowing for better understanding of basin tectonics control on the evolution of deepwater depositional systems (Fig. 3.11A, B).

The progressive shift of erosional submarine channel levee systems from NW to SE in SS1 (stages 1a-c; Fig. 3.11A), could be linked to avulsion events in response to shale tectonics, changes in sediment supply or up-dip delta lobe migration. Similarly, the absence of submarine channels in the northern part of the study area in SS2 (Fig. 3.11B), could be due to; (i) up-dip channel avulsions

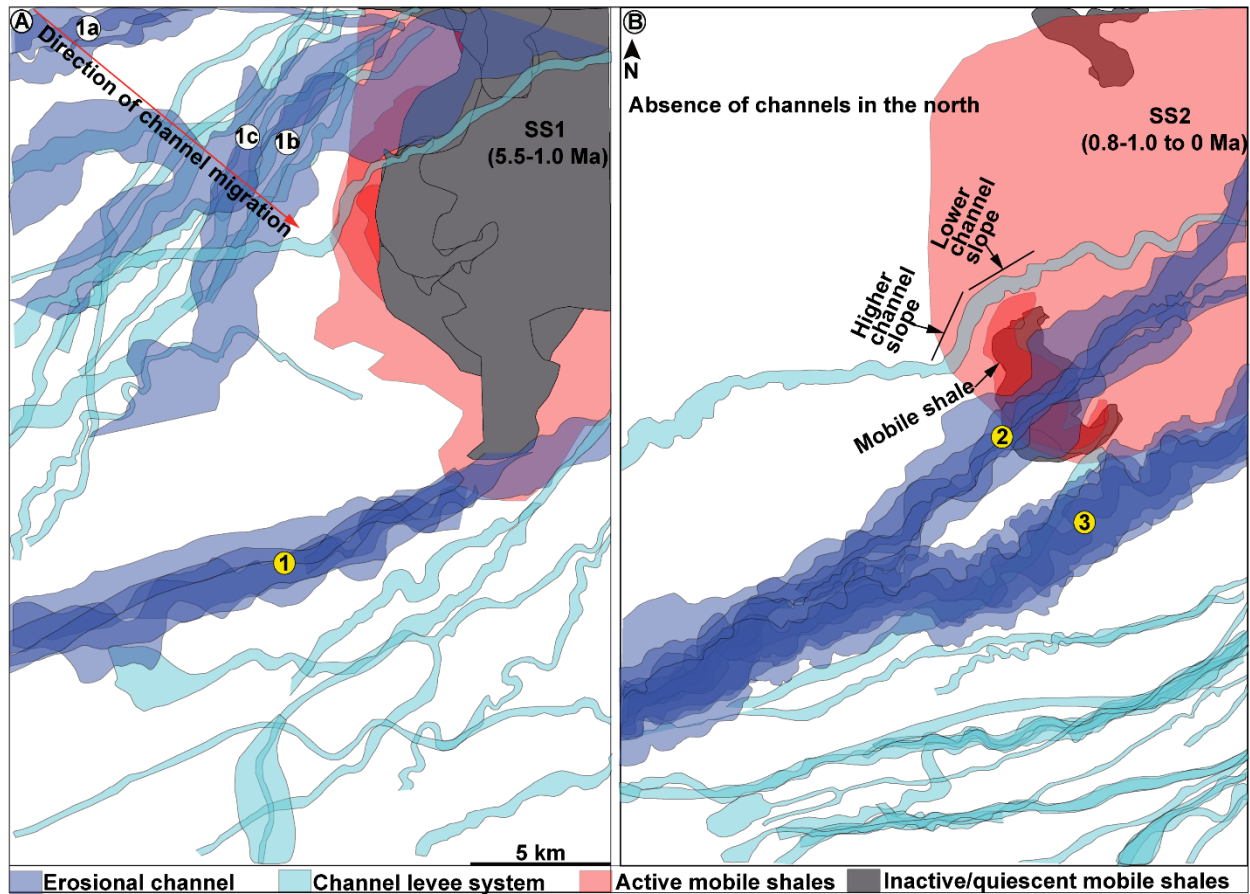


Fig. 3.11. Shale tectonics vs submarine channel morphology and distribution on the western Niger Delta intraslope basins over the last 5.5 Ma. A (SS1): Migration of erosional channels from the NW to SE in (stages 1a-c in Figs. 4-6). B (SS2): Absence of erosional channels in the northern part of the study area and increase in the slope of channel levee system (CLS) downdip of mobile shale. See text for a more detailed explanation. Note the spatio-temporal variation in the orientation of erosional channels in panels A and B (labelled 1, 2 and 3). Modified after Chima *et al.* (2019).

in response to mobile shale activities (see also Clark and Cartwright, 2012; Jolly *et al.*, 2016) or (ii) up-dip delta lobe migration/shifting of depositional axis further NW, away from the study area (see Jermannaud *et al.*, 2010). The lateral variation in stratigraphic thickness of SS1 (5.5 to 0.8-1.0 Ma), compared to SS2 (0.8-1.0 to 0 Ma), suggests that mobile shale was more active in the Pliocene than in the Pleistocene (e.g. Figs. 3.3B, 3.10B). The presence of mobile shales, mud volcanoes, pockmarks, BSR, fluid escape features and mobile shale-derived MTDs (e.g. Figs. 3.1E; 3.3A, B, 3.5A, 3.8A-C, 3.9A), support the fact that shale tectonics locally controlled slope

depositional patterns (see Chima *et al.*, 2019). The local increase in CLS gradient downdip of mobile shale (Fig. 3.11B), the inversion of some normal faults during the Pleistocene (e.g. fault Z in Fig. 3.3B), and the presence of mud volcanoes on the modern seafloor (Figs. 3.1E, 3.3A, B), further supports mobile shale activity on the western Niger Delta slope during the Plio-Quaternary (see also Chima *et al.*, 2019; Appendix 7). These observations therefore call for caution over the general assumption that mobile shales in the Niger Delta were buried during the late Pliocene (e.g. Cohen and McClay, 1996; Wiener *et al.*, 2010; Morley *et al.*, 2011).

3.5.3 Depositional model

Despite the dissimilarity in facies association within SS1 (e.g. Fig. 3.2B, C) and SS2 (Figs. 3.7C-E, 8C-E), the overall sedimentary architecture (e.g. Figs. 3.3, 3.10), suggests that similar external forcing at different scales and to a lesser extent basin tectonics, controlled the stratigraphic evolution of the western Niger Delta over the last 5.5 Ma. Hence, we propose a 4-stage depositional model in relation to 4/5th-order glacio-eustatic sea-level changes to explain the long-term depositional systems evolution of the western Niger Delta intraslope basins over the last 5.5 Ma. These include: (1) forced regression; (2) early lowstand; (3) late lowstand/early transgression and (4) late transgression/highstand stages (Fig. 3.12A-D).

3.5.3.1 Forced regression

Forced regression generally marks the forestepping of the shoreline and sediment partitioning to the deep basin via sediment-gravity flows (e.g. Catuneanu, 2006; Zhang *et al.*, 2019; Fig. 3.12A). The highly erosional submarine channels that we observed in SS1 and SS2 (e.g. Figs. 3.3, 3.5, 3.7, 3.8, 3.9A), are inferred to have developed during 4th and 5th-order forced regressions respectively. The occurrence of mass-transport deposits (lower MTD) at the base of erosional channel fairway within SS1 (Fig. 3.4B), suggests that sediment-gravity flows was mud-rich (debris-flows) and were partly sequestered on the slope en route to the deep basin (Fig. 3.12A). Similar observation has been documented in the deepwater eastern Niger Delta, where MTDs were calibrated with core data and showed to be mud-rich (debris-flows), linked to 4th-order relative sea-level fall (see Zhang *et al.*, 2019). The paucity of MTDs in SS2 (e.g. Fig. 3.3B) and its overall

absence within erosional channel fairways (e.g. Figs. 3.7C, 3.8C), could be related to changes in sediment supply/calibre, flow dynamics or reduced activity of mobile shale in the Pleistocene (e.g. Figs. 3.3B, 3.10B).

3.5.3.2 Early lowstand

The turbidite feeder channels/meandering channel levee complexes or complexes that overlie the upper MTDs within erosional channel fairway in SS1 (Fig. 3.5B) and dominate the erosional channels fairways in SS2 (Figs. 3.3B, 3.7C-E, 3.8C-E), are inferred to be early lowstand deposits that accumulated within channel axis as the relative sea-level falls (Fig. 3.12B). The high amplitude reflectivity of these turbidite deposits coupled with their erosive character suggests that they were deposited from sand-rich sediment-gravity flows (see also Chapin *et al.*, 2002; Deptuck *et al.*, 2003; Heiniö and Davies, 2007; Jobe *et al.*, 2011). We infer that the turbidite feeder channels/meandering channel levee complexes were probably deposited during early lowstand as distributary channels/lobes accumulated on the basin floor (Fig. 3.12B).

3.5.3.3 Late lowstand/early transgression

Chima *et al.* (2019), showed that the thick, laterally extensive/regional MTDs with transparent and chaotic internal architecture (e.g. Figs. 3.3A, B; 3.5B 3.8C; 3.9B; 3.10A, B), are likely to have been sourced upslope, while thin, laterally confined MTDs with coherent/slightly deformed internal architecture are locally sourced from mobile shales (Figs. 3.2A, 3.8C, 3.9A). Consequently, we infer that the regional MTDs (e.g. Figs. 3.3B, 3.8C, 3.9B, 3.10B) were likely triggered by failures at the shelf-margin/upper slope probably during 4/5th-order lowstand of the relative sea-level/early transgression. The overall truncation of CLSs inferred to be deposited during the early lowstand by the regional MTDs (Fig. 3.12C), support their interpretation as late lowstand/early transgression deposits (see also Adeogba *et al.*, 2005). Depositional patterns during this stage maybe locally influenced by mobile shale and fluid flow activities associated with e.g. pockmarks and BSR (evidence of gas hydrates) (e.g. Riboulot *et al.*, 2012; Figs. 3.1D; 3.3A, B; 3.8A, 3.9A, 3.12C).

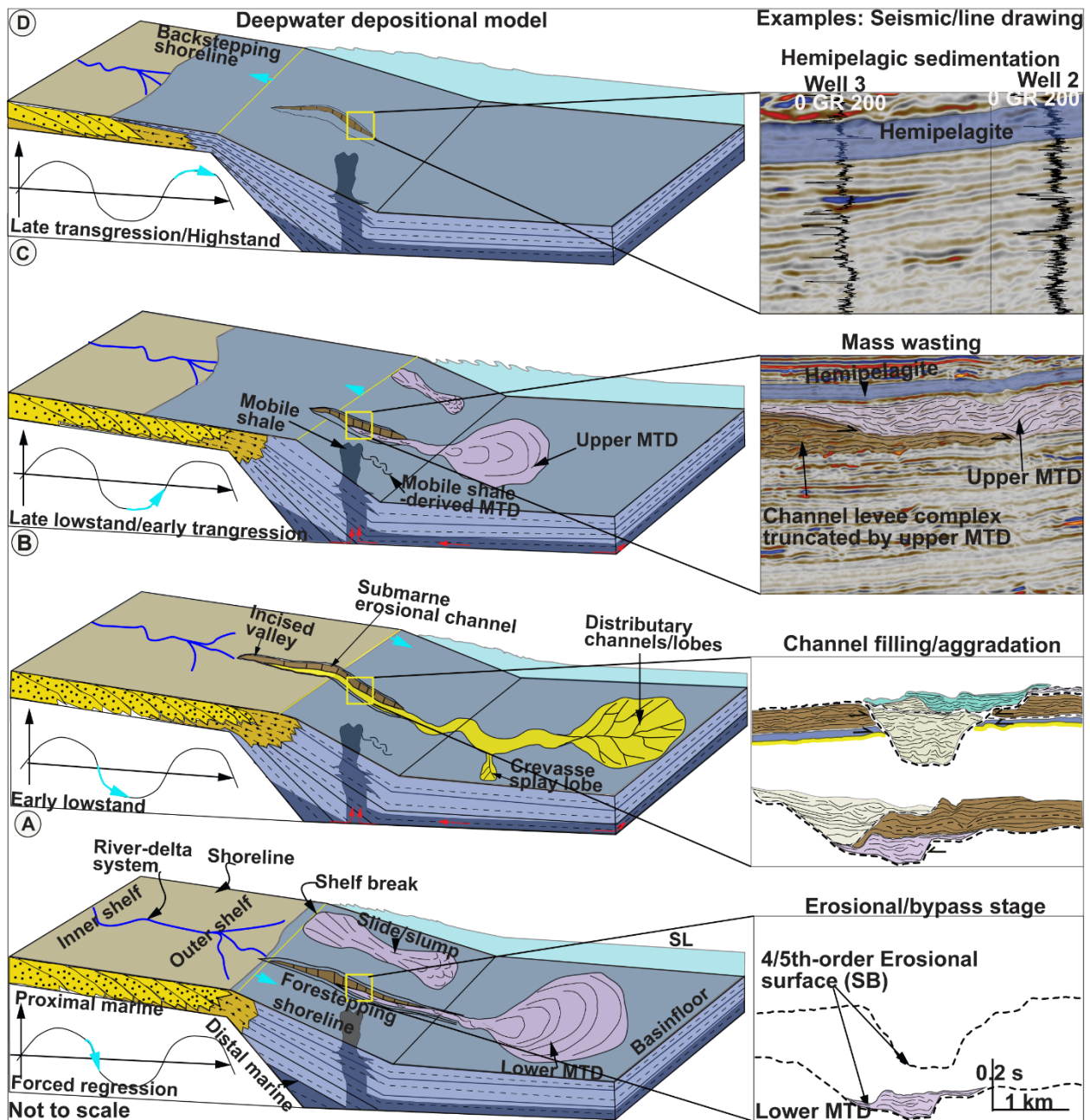


Fig. 3.12. Schematic illustration of the proposed long-term evolution of depositional elements on the western Niger Delta intraslope basins with respect to 4/5th-order variations in relative sea-level, locally influenced by shale tectonics. A: Forced regression marks the development of erosionaly confined (bypass channels on the slope) that are locally associated with thin MTDs ('lower MTDs'), compared to the thick MTDs that supposedly accumulated on the basin floor. B: Early lowstand marks the infilling of the erosionaly confined channels by turbidite feeder channels/ meandering channel levee complexes. C: Late lowstand/early transgression marks the

development of the MTDs ('upper MTDs') or with slides/slump deposits. D: Highstand marks hemipelagic sedimentation/muddy turbidites and punctuation of deepwater sedimentation.

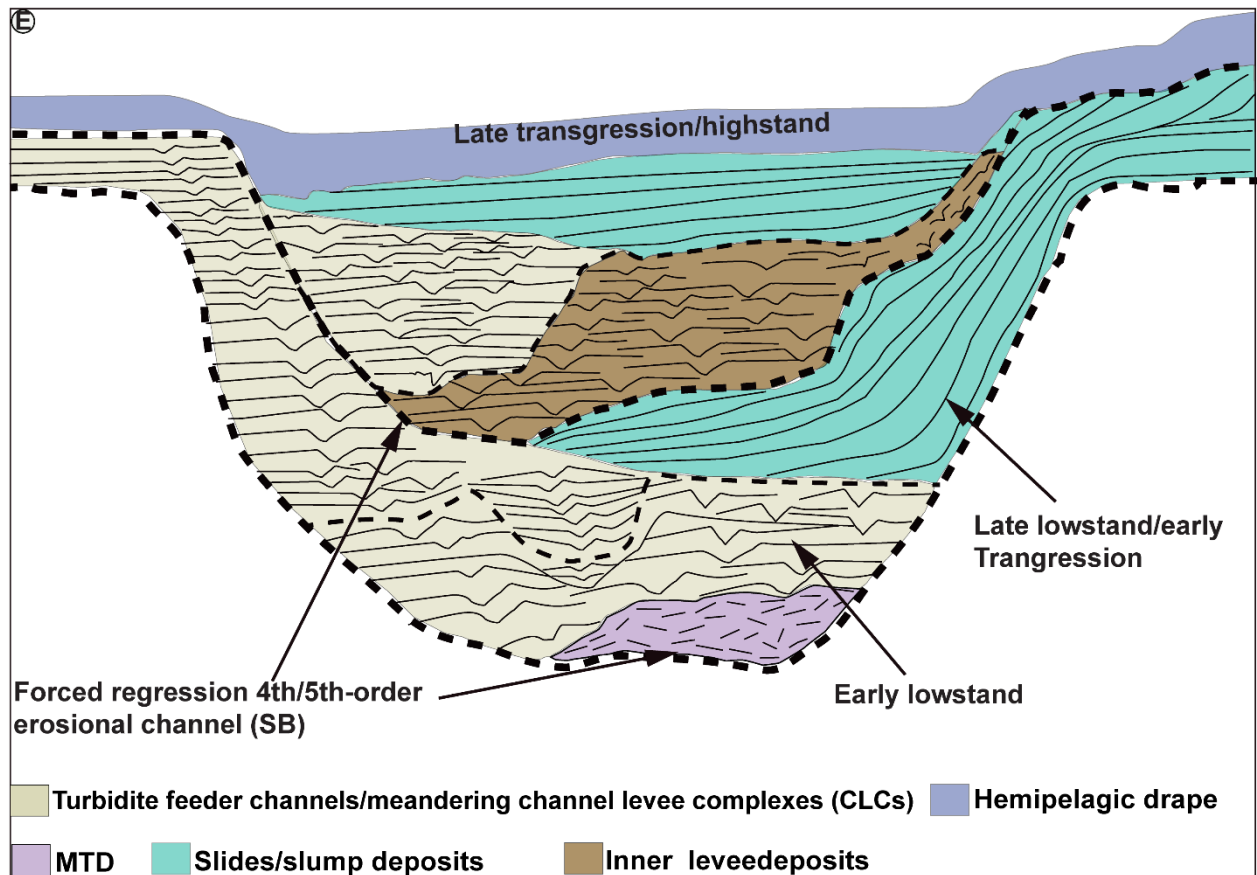


Fig. 3.12 E: Schematic illustration of slope depositional model (see text for a more detailed explanation).

3.5.3.4 Late transgression/Highstand

The thick hemipelagites that generally drape turbidite feeder channels or CLSs (e.g. Figs. 3.3B, 3.7C-E, 3.8C-E), are inferred to have been deposited during the late transgression/highstand probably during clastic sediment starvation in the deep basin (Fig. 3.12D). The conformable nature of hemipelagites (e.g. Figs. 3.3B, 3.7C-E, 3.8C-E), their mud-rich nature inferred from moderate gamma-ray log patterns (e.g. Fig. 3.12D) and their association with *Discoaster quinqueramus* recorded in Well 3 (W3) (Fig. 3.12D), support their interpretation as highstand deposits (see Chima

et al., 2019). The hemipelagites are inferred to have punctuated deepwater sedimentation by shutting down sediment-gravity flows.

The foregoing processes are inferred to have occurred 12 and 9 times respectively within SS1 and SS2 (e.g. Fig. 3.10B, C). A simplified schematic diagram illustrating the long-term (4/5th-order sea-level controlled) incision, infilling and hemipelagic draping of submarine channels on the slope is shown (Fig. 3.12E). Although the proposed model is mainly hinged on long-term changes in relative sea-level, evidences exist that show that shale tectonics locally influenced depositional patterns on the western Niger Delta intraslope basins over the last 5.5 Ma (Appendices 6, 7).

3.6 Conclusions of Chapter 3

Detailed seismic stratigraphy and 3D geomorphological analysis of a high-resolution 3D seismic data over the Pliocene and Pleistocene stratigraphic record of the western Niger Delta intraslope basins, showed that:

- Glacio-eustatic sea-level changes since the last 5.5 Ma are recorded at regional scale on the western Niger Delta intraslope basins.
- Three major seismic facies associations were recorded in the Pliocene and Pleistocene stratigraphic records, and are characterized by (i) turbidite-dominated sequences at the lower part of SS1; (ii) mass-wasting and turbidite dominated sequences at the upper part of SS1 and (iii) hemipelagite and turbidite-dominated sequences starting at the transition between SS1 and SS2. Changes from one seismic unit to the other may mark the early Pliocene (base of SS1, ~ 4.9 Ma), the early Pleistocene (upper limit of SS1, ~ 2.6 Ma), and the Middle Pleistocene Transition (MPT) (SS1-SS2 limit, ~ 0.8-1.0 Ma).
- The overall seismic facies succession characterized by: (i) Juxtaposed, highly incisional submarine channels; (ii) Infilling/aggrading turbidite feeder channels/meandering CLCs and MTDs; (iii) hemipelagites, respectively are interpreted to document forced regressive, lowstand and transgressive/highstand transits of the shoreline.

- The Pliocene and Pleistocene stratigraphy of the western Niger Delta intraslope basins were controlled by allocyclic forcing linked to glacio-eustatic sea-level oscillations and basin tectonics associated with mobile shales. The latter being more active during the Pliocene and the middle Pleistocene.
- The overall higher sedimentation rate over the MPT (0.8-1.0 Ma to present) possibly accompanied by subsidence is inferred to have facilitated the preservation of the 100 ka sequences within SS2 compared to the SS1 (5.5 to 0.8-1.0 Ma), where lower sedimentation rate is inferred to have favoured the preservation of the 400 ka sequences.
- This seismic stratigraphic study demonstrates for the first-time sequence cyclicity associated with orbital (Milankovich) forcing in the deepwater western Niger Delta and if calibrated with biostratigraphic data in future studies, could serve as a useful analogue for further studies in the Gulf of Guinea, the equatorial Atlantic and other margins fed by large deltas.

CHAPTER 4

Tectonostratigraphic evolution of the western Niger Delta since the Cretaceous: Implication of paleo-topographies and delta top tectonostratigraphic dynamics on gravity deformation of the margin

Kelvin Ikenna Chima^{a,b*}, Didier Granjeon^c, Damien Do Couto^a, Estelle Leroux^d, Christian Gorini^a, Marina Rabineau^e, Jean Letouzey^a, Nick Hoggmascall^f, Miguel-Mora Glukstad

^a Sorbonne Université-ISTeP UMR 7193, F7500, Paris (France)

^b Alex Ekwueme Federal University, Ndufu-Alike Ikwo, Ebonyi State, Nigeria.

^c IFPEN, Rueil-Malmaison (France)

^d IFREMER, ZI Pointe du Diable, Plouzane, France (France)

^e CNRS, UMR 6538, LGO (CNRS/UBO/UBS), Plouzane (France)

^f Shell International the United Kingdom (UK).

^g Shell International, Houston (USA).

Abstract

Although numerous studies have been published in the Niger Delta over the past decades, only a few of them have investigated at regional scale the interaction between paleo-topographies associated with the spreading of the margin, delta top tectonostratigraphic dynamics and gravity deformation from the Cretaceous-present. This was achieved in this study through detailed tectonostratigraphic analysis and interpretation of regional depth-penetrating 2D seismic lines, high-resolution 3D seismic and well data. Our results show that relief associated with paleo-oceanic fracture zones controlled the geometry of the western Niger Delta from the late Cretaceous to the Serravallian, when delta top tectonostratigraphic processes initiated and dominated most of the Neogene and the Quaternary. Tilting of the margin early during its evolution and the resulting delta-centre dipping surface, favoured gravity gliding from the late Cretaceous to the Serravallian. However, an increase in sedimentation rates, notably over the early Pliocene and the Pleistocene, and a corresponding increase in gravity collapse/accommodation on the continental shelf and the upper slope, favoured deformation of the margin under its weight (gravity spreading). The overall low sedimentary wedge deformation within the extensional and translational zones over the late Eocene-Serravallian, suggests the location of the defunct extensional zone up-dip in the onshore. However, the basinward propagation of deformation to the contractional zone over the Tortonian-early Pliocene, seems to record the migration of the extensional zone to its present position, basinward of the modern coastline. Although relatively high sedimentation rates on the western Niger Delta continental shelf and slope regions over the Serravallian-Tortonian seems to have triggered shale tectonics, the syn-depositional deformation of the Burdigalian-Serravallian Unit, suggests that shale tectonics could have initiated since the Burdigalian. The dominance of actively subsiding basinward dipping normal faults on the western Niger Delta continental shelf since the early Pliocene facilitated the overall increase in sediment thickness within the extensional zone. Despite the relatively lower sedimentation rates estimated on the western Niger Delta continental shelf and slope regions since the Pliocene, the overall sediment distribution from the shelf to the deep basin since the early Pliocene, suggests an overall increase in sedimentation in the region compared to the eastern Niger Delta, where actively subsiding counter regional normal faults and inferred delta lobe migration are thought to have contributed to the overall reduction sediment

fluxes in the region since the Pleistocene. Given the spatio-temporal variation in gravity deformation and sediment partitioning across the western and the eastern Niger Delta since the early Pliocene, a more regional seismic and well data are needed for a complete source-to-sink that allows for a more quantitative comparison of these regions. This study not only improves our understanding of the tectonostratigraphic evolution of the western Niger Delta, highlighting the complex structural and stratigraphic trapping styles notably in the underexplored deepwater systems, but also shows the presence of syn-rift deposits that may host the Cretaceous-Paleogene petroleum play in the offshore western Niger Delta.

Keywords: Niger Delta; Tectonostratigraphic dynamics; Paleo-topography; Gravity gliding; Gravity Spreading; sedimentation rate.

4.1 Introduction

Passive continental margins fed by large progradational deltas manifest gravity-driven deformation of their sediment wedge by a combination of gravity gliding and gravity spreading (Damuth, 1994; Cohen and McClay, 1996; Schultz-Ella, 2001; Rowan *et al.*, 2004). Unlike active margins (e.g. accretionary prisms and transform margins), where gravity-tectonics is mainly controlled by crustal deformation, high sedimentation and progradation above weak detachments/décollements drive gravity tectonics in passive margins (see review in Morley *et al.*, 2011). Detachments may be associated with overpressured shales or salts (Doust and Omatsola, 1990; Morley and Guerin, 1996; Cohen and McClay, 1996; Graue, 2000; Hooper *et al.*, 2002; Morgan, 2004; Corredor *et al.*, 2005; Briggs *et al.*, 2006; Sapin *et al.*, 2012; Wiener *et al.*, 2010; Reis *et al.*, 2016). Detachment in shales occur for example, in the Niger Delta (Doust and Omatsola, 1990; Corredor *et al.*, 2005; Briggs *et al.*, 2006; Wiener *et al.*, 2010), the Amazon Fan (e.g. Cobbold *et al.*, 2004; Rowan *et al.*, 2004), the Mexican Ridge (Weimer and Buffler, 1992; Rowan *et al.*, 2004; Morley *et al.*, 2011), the Brunei Delta (Morley and Guerin, 1996), the southern Beaufort Sea (Elsley and Tieman, 2006), the Krishna-Godavari Basin in India (Choudhuri *et al.*, 2010), the eastern offshore Trinidad (De Landro Clarke, 2010), offshore Brunei (Warren *et al.*,

2010), and along the Spanish arm of the Mediterranean Sea (Soto *et al.*, 2010). Salt detachments occur along the African Atlantic margins of Mauritania, Gabon, Congo and Angola (e.g. Tari *et al.*, 2003; Hudec and Jackson, 2004), the Brazillian Atlantic margin (Karner, 2000), Mississippi Delta and the northern Gulf of Mexico (Rowan, 2004; Madof *et al.*, 2017; Wu *et al.*, 2020).

Compared to salt, which is viscous and readily deforms under thin overburden, shale exhibits mixed plastic-brittle rheology with inherent shear strength and requires deeper burial under thick overburden to generate sufficient overpressure to trigger its mobility (Rowan *et al.*, 2004; Vendeville, 2005; Peel *et al.*, 2014; Restrepo-Pache, 2018; Goncalves *et al.*, 2020). Elevated pore fluid pressure generally weakens shale and reduces its ability to withstand deformation (Rowan *et al.*, 2004).

The Niger Delta is a linked extensional-contractional system, where the gravity-driven collapse of sediment wedge on the shelf is accommodated on the slope and the deep basin by mobile shales structures, detachment folds, imbricated thrusts and associated folds (Doust and Omatsola, 1990; Morley and Guerin, 1996; Cohen and McClay, 1996; Graue, 2000; Hooper *et al.*, 2002; Morgan, 2004; Corredor *et al.*, 2005; Briggs *et al.*, 2006; Sapin *et al.*, 2012; Wiener *et al.*, 2010; Fig. 4.1). The extensional and contractional systems are generally linked by down-to-basin listric normal faults that detach on overpressured/undercompacted shales (Fig. 4.1E).

Previous studies by Chardon *et al.* (2016) and Grimaud *et al.* (2017), opined that regional tectonic reorganization of the Niger catchment around (~34-29 Ma), marked the onset of an increase in sediment supply to the Niger Delta. Also, regional studies by Haack *et al.* (2000), Robin *et al.* (2011) and Grimaud *et al.* (2017), documented an overall increase in sediment accumulation in the offshore Niger Delta between the early Pliocene (5.3 Ma) and the early Pleistocene (1.8 Ma), now 2.6 Ma (see Gibbard *et al.*, 2014), whereas the middle and the late Pleistocene, record overall decrease in sediment accumulation rate. A switch in depositional patterns from progradation and increase in sediment supply from ~4 Ma to ~2.5 Ma, to retrogradation and decrease in sediment since the Pleistocene, has been documented in the eastern Niger Delta (Jermannaud *et al.*, 2010; Rouby *et al.*, 2011). Jermannaud *et al.* (2010) and Rouby *et al.* (2011), proposed that the overall reduction in sediment supply to the eastern Niger Delta over the Pleistocene could be due to: (i) regional migration of delta lobe and switch of sediment fluxes to the western Niger Delta or (ii) climate warming of west Africa and aridification in the Niger catchment, led to an overall decrease in sediment supply to the entire Niger Delta.

Although numerous publications exist on the western Niger Delta (Cohen and McClay, 1996; Morley and Guerin, 1996; Chapin *et al.*, 2002; Deptuck *et al.*, 2003; 2012; Davies *et al.*,

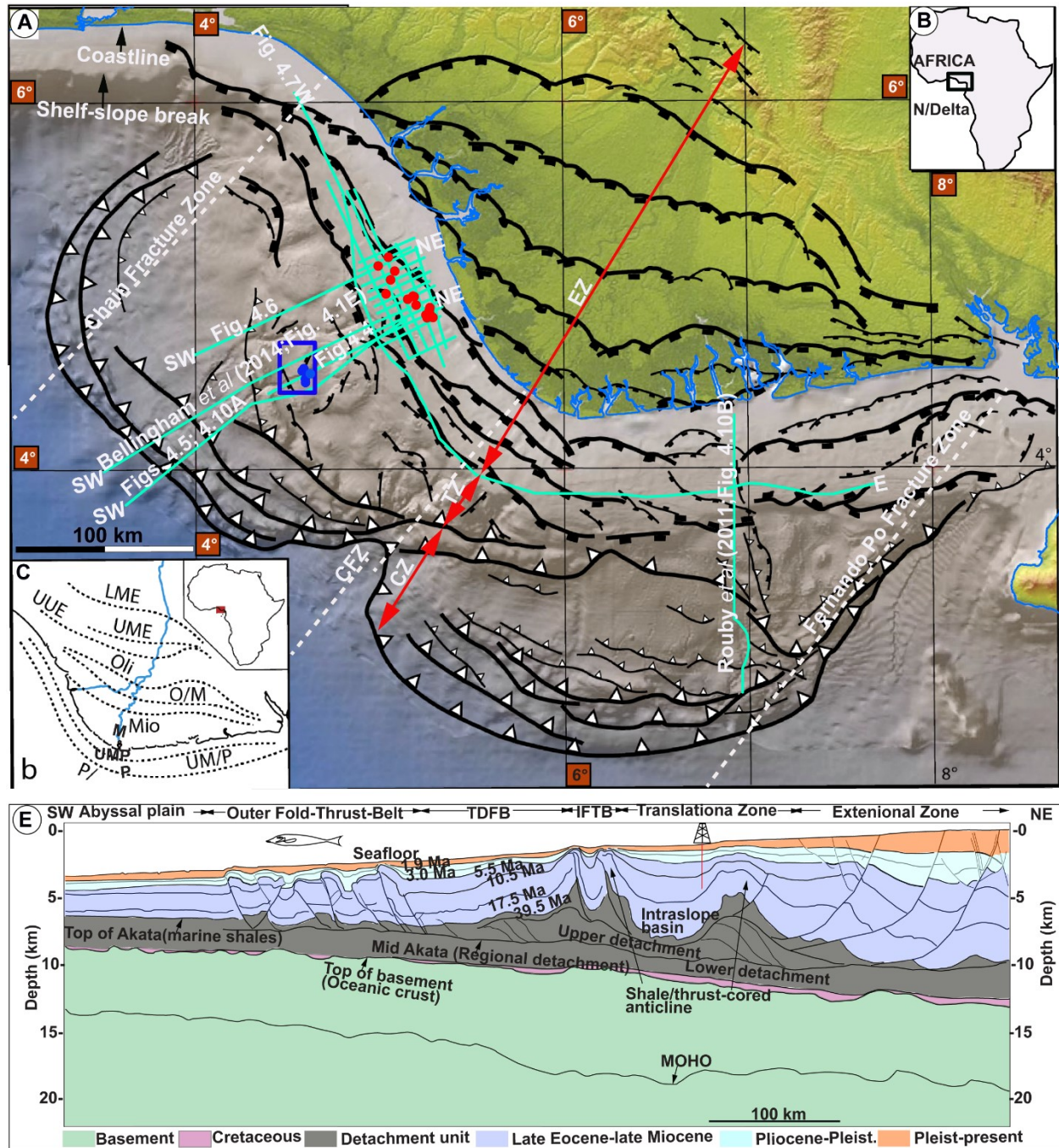


Fig. 4.1. Location of the study area. A: Superposed relief and bathymetry map showing the extensional zone (EZ), translational zone (TZ) and contractional zone (CZ) of the Niger Delta. B: Inset map of Africa showing the location of the Niger Delta on the Atlantic coast of West Africa. A and B (modified after Rouby *et al.*, 2011) C: Close up of the continental shelf wells locations (red circles) and 2D seismic data (light blue line). D: Close up of the slope 3D seismic survey

coverage (dark blue box) and wells locations (dark blue circles). E: Northeast-southwest trending regional seismic line showing the structural styles of the western Niger Delta (modified after Bellingham *et al.*, 2014). See text for a more detailed explanation.

2003; Adeogba *et al.*, 2005; Bakare *et al.*, 2007; Heiniö and Davies, 2007; Briggs *et al.*, 2009; Maloney *et al.*, 2010; Clark and Cartwright, 2012; Bellingham *et al.*, 2014; Benjamin *et al.*, 2015; Jobe *et al.*, 2015; 2016; 2017; Benjamin and Huuse, 2017, Hansen *et al.*, 2017; Chima *et al.*, 2019; Chima *et al.*, revised), only a few studies have investigated the interplay between paleo-topography, delta top tectonostratigraphic dynamics and gravity deformation of the margin. Hence, the objectives of this study are: (i) to investigate the interaction between paleo-topography, delta top tectonostratigraphic dynamics and gravity deformation of the western Niger Delta sedimentary wedge from the Cretaceous-present; (ii) compare the stratigraphic architecture of the western and the eastern Niger Delta with a view to understanding their evolution over the Pliocene and the Pleistocene.

4.2 Gravity tectonics

Gravity gliding and gravity spreading are generally used in the description of overall deformation of passive margins, such that margins with basinward-dipping detachments are termed gravity gliding margins (e.g. offshore Angola, Mauduit *et al.*; 1997; offshore Brazil; Cobbold and Szatmari, 1991; Kartner, 2000). However, passive margins, characterized by prograding deltas above landward-dipping detachments are termed gravity-spreading systems (e.g. northern Gulf of Mexico; Worrall and Snelson, 1989).

Propagation of gravity-driven systems on passive margins is triggered by the loss of gravitational potential energy (gravity potential of sediment) and is controlled by the complex interplay between gravity gliding and gravity spreading (Rowan *et al.*, 2004; Morley *et al.*, 2011; Peel *et al.*, 2014). Gravity gliding is the rigid, downward movement of sediment along a basal slip surface, while gravity spreading is the downward movement and deformation within the body of

a linked system (Dejong and Scholten, 1973; Ramberg, 1981). Schultz-Ela (2001), opines that gravity gliding and gravity spreading commonly combine in the deformation of natural systems, and are essentially difficult to discriminate. However, Rowan *et al.* (2004) and Peel *et al.* (2014), demonstrated that gravity-gliding dominates stratigraphic intervals above seaward-dipping detachments, while gravity-spreading dominates stratigraphic intervals, characterized by seaward-dipping bathymetric slope with little or no basal dip. Tilting of a margin due to thermal subsidence or isostatic loading reinforces gravity-gliding, while up-dip (sedimentation on the continental shelf and upper slope), generally fuels gravity-spreading by increasing gravity potential and seaward-dipping bathymetric slope, which facilitates the spreading of the margin under its weight (Rowan *et al.*, 2004; Peel *et al.*, 2014).

The present study is located in the western Niger Delta (Fig. 4.1). The Niger Delta is subdivided into the eastern and western lobes by a paleo-topographic feature defined as the Charcot Fracture Zone, which developed in the Cretaceous during the opening of the Atlantic ocean (Short and Stauble, 1967; Evamy *et al.*, 1978; Doust and Omatsola, 1990; Fig. 4.1A). The delta is also bound to the east and west by paleo-topographies corresponding to the Fernando Po and Chain Fracture Zones respectively (Fig. 4.1A). Gravity-driven deformation of Niger Delta's post-rift sediment since the late Eocene, resulted in the development of five structural zones, namely: (i) the extensional zone, dominated by basinward and landward dipping, normal faults; (ii) the translational zone, dominated by thrust/shale-cored anticlines and shale-withdrawal intraslope basins, and (iii) contractional zone, further sub-divided into (iiia) inner-fold-thrust belt; (iiib) transitional detachment fold belt, dominated by detachment fold and (iiic) outer fold-thrust-belt, dominated by imbricated thrusts and associated folds (Corredor *et al.*, 2005; Fig. 4.1E). Regional seismic observations and analogue models show that deformation in these structural zones is generally complicated by the presence of multiple detachments (Corredor *et al.*, 2005; Briggs *et al.*, 2006; Wiener *et al.*, 2010; Sapin *et al.*, 2012; Bellingham *et al.*, 2014; Peel *et al.*, 2014; Jolly *et al.*, 2016; Restrepo-Pace, 2018; Fig. 4.1E).

4.3 Data and methodology

4.3.1 Seismic and well data

We combined seismic and well data to study the tectonostratigraphic evolution of the western Niger Delta from Paleogene-present. Seismic data comprises of 21 closely spaced 2D lines (6 strike lines and 15 dip lines), that cover an area of $\sim 3,620 \text{ km}^2$ on the continental shelf, and a high-resolution 3D survey, which covers an area of 638 km^2 on the slope (Fig. 4.1A). The longest (delta-wide) seismic strike line extends 500 km, covering the eastern, the central and the western Niger Delta lobes, while 3 of the dip lines extend basinward with the longest ($>200 \text{ km}$), reaching the abyssal plain (Fig. 4.1A). Both the 2D seismic lines and the 3D survey have sampling interval of 4 milliseconds two-way-travel time (4 ms TWT) and were processed as zero-phase source wavelet in the American reverse standard polarity such that an increase in acoustic impedance corresponds to a trough (black loop) in the wavelet, while a decrease in acoustic impedance is represented by a peak (white loop) in the wavelet. The vertical resolution of the 3D seismic survey is $\sim 13.7 \text{ m}$ over the first 3 km but decreases between 25-30 m at depths greater than 3 km, while that of the 2D lines averages between $\sim 25\text{-}40 \text{ m}$.

We studied a total of 21 wells (16 located on the continental shelf within the 2D seismic data coverage and 5 on the slope within the 3D seismic survey (Fig. 4.1A). The continental shelf wells were designated Izaga shelf (IZSH1-IZSH15) (Fig. 4.1C), while the slope wells that were formerly labelled as FM1-FM 5 wells in Chima *et al.* (2019), were designated (FMSL1-FMSL 5) in this study (Fig. 4.1D), in order to distinguish them from their shelf equivalents (Fig. 4.1C). While the slope wells (FMSL1-FMSL5) (Fig. 4.1D) generally provide gamma ray, resistivity, neutron, density and sonic logs (e.g. Fig. 2.7), only IZSH 1, 4, 7, 13 and 15, contain gamma ray, resistivity and neutron, density or sonic logs. Furthermore, FMSL1-FMSL5 and IZSH 1, 2, 4, 6, 7, 11, 14 and 15, provide checkshot data. Biostratigraphic studies have been done on wells FMSL1-FMSL 4 (chapter 2). These data were used in dating the Neogene (Burdigalian to the Messinian) (see Chima *et al.*, 2019; Figs. 2.5; 2.7). Of the 15 wells on the shelf, only IZSH 1, 4, 7, 13 and 15, contain biostratigraphic data for the Messinian interval. Out of the seismic horizons that were dated from the Burdigalian to the Messinian on the slope 3D block (Chima *et al.*, 2019; Figs. 2.1; 2.5; 2.7), only the Serravallian, Tortonian and the Messinian seismic horizons could be correlated up-dip onto the shelf with the aid of the connecting regional 2D seismic lines (Fig. 4.1A). The candidate early Pliocene and the Pleistocene horizons were also correlated up-dip onto the shelf based on a detailed cyclostratigraphic study of the slope 3D block (see Chima *et al.*, revised; Figs. 3.3 and 3.10). Ages of the older seismic horizons (the Cretaceous and the late Eocene) that were

not penetrated by the wells available for this study, were estimated from a published study (Fig. 4.1E).

4.3.2 Methodology

4.3.2.1 Seismic stratigraphy

This study builds on the recently published sequence stratigraphic and cyclostratigraphic studies of the 3D seismic survey located on the western Niger Delta slope (Fig. 4.1A, E) (see Chima *et al.*, 2019; and Chima *et al.*, *revised*), respectively. Chima *et al.* (2019), applied the seismic and sequence stratigraphic approach described by Mitchum and Vail (1977), which consists in the recognition of seismic reflection amplitude, continuity, internal architecture, external geometry, nature of bounding surfaces, erosional truncations; and calibration with detailed 3D seismic geomorphological analysis to delineate and date key sequence stratigraphic surfaces. The older seismic units, were dated from (the Burdigalian to the Messinian), using the biostratigraphic information contained in (FMSL1-FMSL4) wells (see Chima *et al.*, 2019; Fig. 2.7). Although there was no biostratigraphic data over the early Pliocene and the Pleistocene, an integrated high-resolution cyclostratigraphy, calibrated with detailed 3D seismic geomorphology, allowed for the identification of the main surfaces in the early Pliocene, the early and middle Pleistocene (Chima *et al.*, *revised*; chapter 3; Figs. 3.3 and 3.10).

Despite the abundance of wells on the continental shelf (Fig. 4.1C), their lack of biostratigraphic data did not allow for direct age calibration in this region. The above challenge was overcome by extending the biostratigraphically and cyclostratigraphically constrained stratigraphic surfaces identified within the 3D survey area on the continental slope (see Chima *et al.*, 2019; chapter 2 and Chima *et al.*, *revised*; chapter 3), to the abyssal plain and the continental shelf with the aid of interconnected, regional 2D seismic lines (Fig. 4.1A). Also, although the overall decrease in the vertical resolution of seismic data at depths below 3.5 seconds two-way travel time (TWT), locally hampered stratigraphic correlation notably in the outer shelf, we leveraged on one of the signal processing algorithms in Petrel™ software (median filter), to improve the overall reflection continuity of the seismic data. Median filter generally smoothes and removes random noise in seismic data while preserving edges of planar features.

4.3.2.2 Sedimentation rates estimation

To estimate sedimentation rates from gridded horizon interpretations on the shelf and slope regions, we first performed velocity analyses and sediment decompaction as explained below.

Velocity analyses was achieved by plotting the TWT values derived from checkshot data of the key wells described previously on the horizontal axis against the corresponding measured depths on the vertical axis (e.g. Fig. 4.2). From this plot, we generated a time-to-depth relationship, whose mean, yield an average velocity (green circles in Fig. 4.2), which we used in the depth conversion of seismic surfaces and seismic lines.

In addition, sediment is generally deposited with high porosity and pore fluid but compacts and undergoes reduction in porosity as the depth of burial increases through time. In order to obtain actual sediment (solid grains) deposition rate, we decompacted the stratigraphic intervals that we studied. This was achieved by the estimation of average porosity from neutron logs derived from FMSL1-FMSL5 and IZSH1, 4, 7, 13, and 15 wells. The initial porosity curve showed some lateral variations due to lateral heterogeneities imposed by the presence of fine-grained sediment and the effect of pressure. Hence, we smoothed the curves to obtain mean porosity law with respect to burial depths for each stratigraphic unit (e.g. Fig. 4.3). The mean porosity/theory (green circles in Fig. 4.3), reveals an overall decrease in porosity with depth due to compaction. We applied this porosity law in the decompaction of each stratigraphic unit. Finally, we estimated solid sedimentation rates on the shelf and slope regions by dividing the average solid sediment thickness of each stratigraphic unit by its duration.

4.4 Results and observation

4.4.1 Tectonostratigraphic units

Following the stratigraphic architecture of the western Niger Delta described by Chima *et al.* (2019 and Chima *et al.*, revised), using a relatively shallow, high-resolution 3D block located

on the slope (Fig. 4.1A), this study provides a regional tectonostratigraphic evolution of the western Niger Delta (from the continental shelf to the deep basin), using regional, depth-penetrating 2D seismic lines. The stratigraphic record of the western Niger Delta was subdivided into 6 major seismic units described in details below.

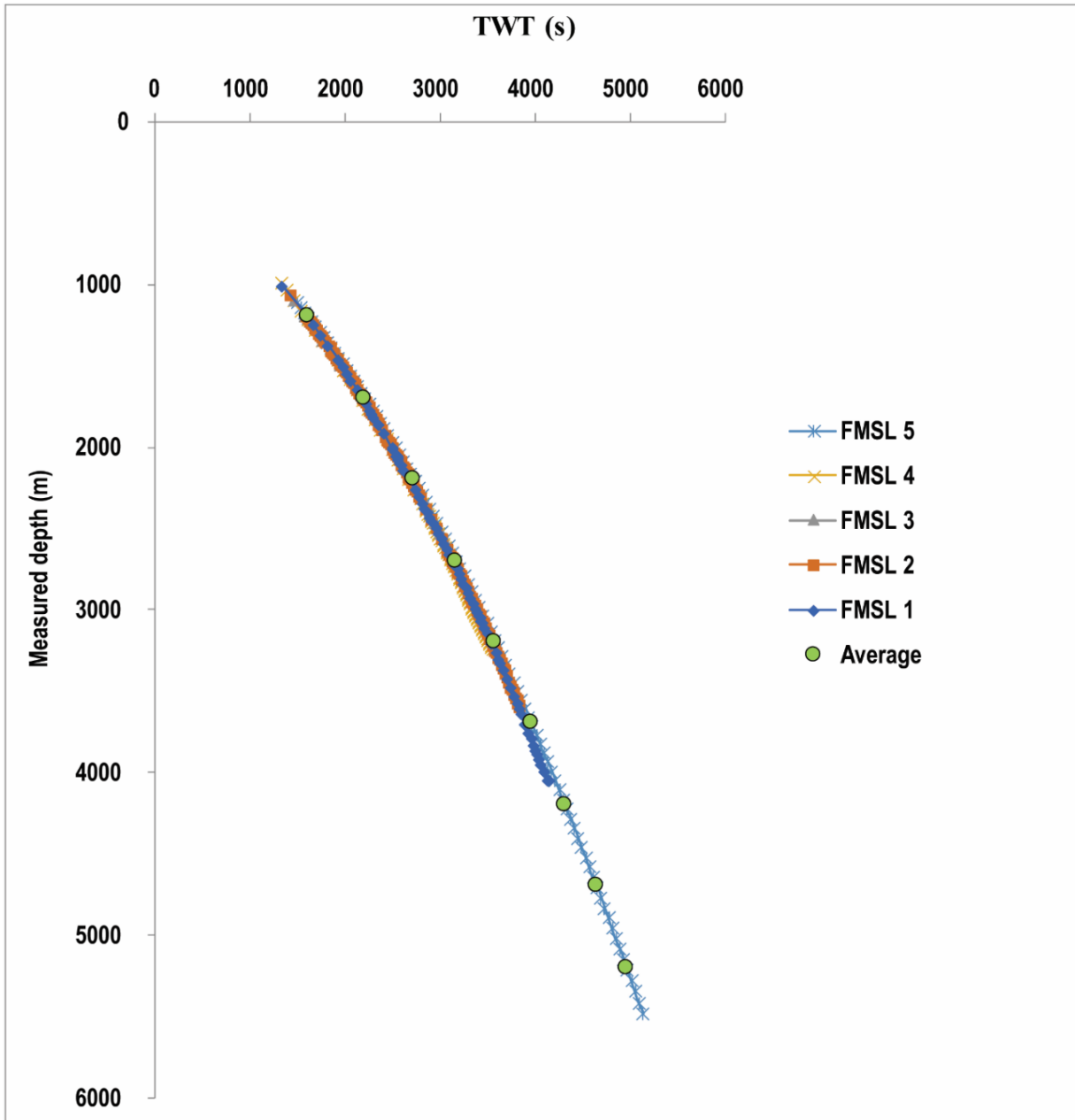


Fig. 4.2. A plot of TWT (ms) versus measured depth (m) showing the time-depth relationship used in the depth conversion of seismic interpretation.

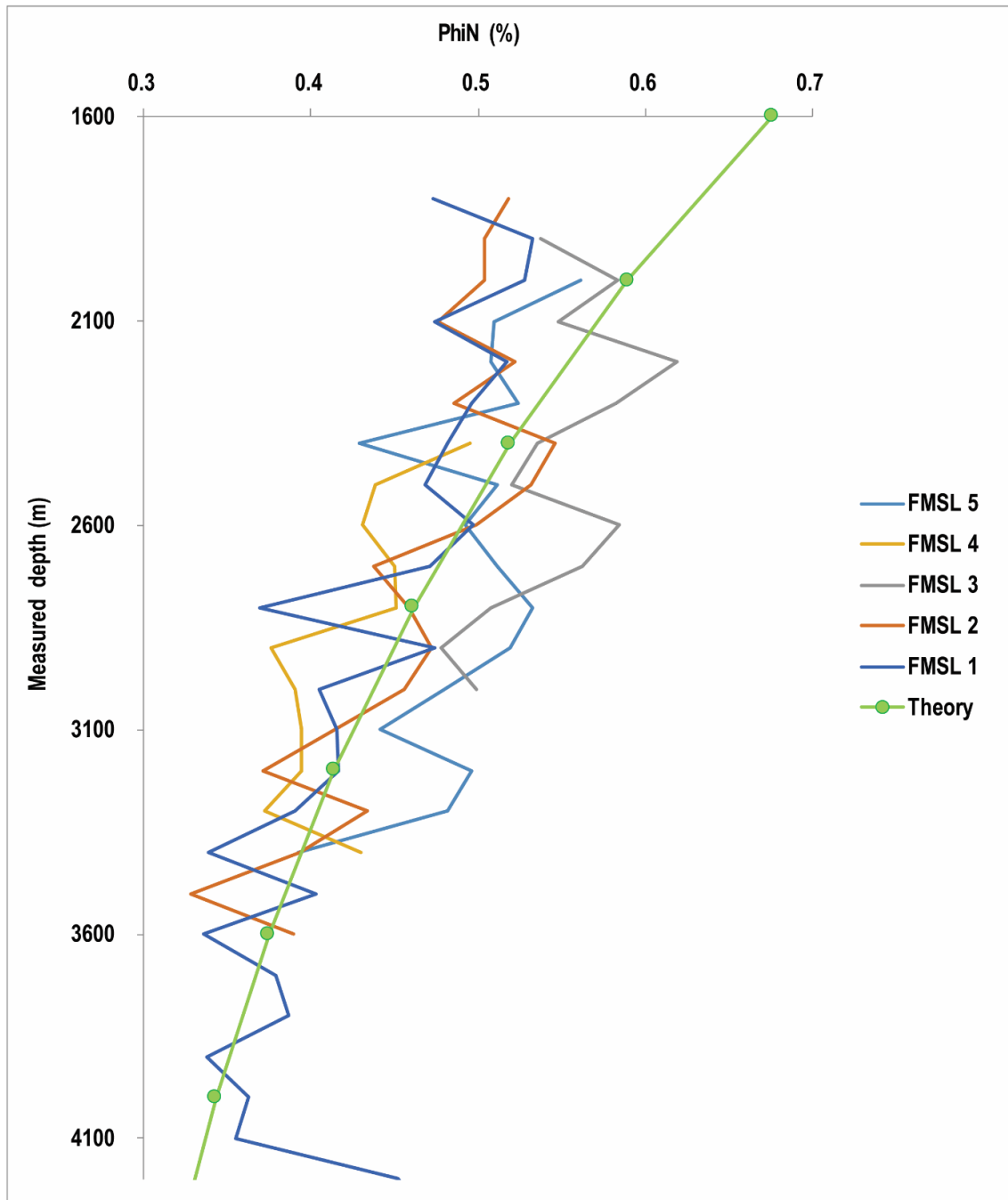


Fig. 4.3. An overall decrease in sediment porosity with depth due to compaction.

4.4.1.1 The Cretaceous-late Eocene Unit

Description:

The Cretaceous-late Eocene Unit is the oldest sedimentary deposit identified in the western Niger Delta (Figs. 4.4-4.6). It is bounded at the base and top by high amplitude seismic reflections (respectively highlighted in dark green and light blue in Figs. 4.4-4.6). The Cretaceous and late Eocene ages, assigned to these horizons were based on a comparison of our data with Bellingham *et al.* (2014) (compare Figs. 4.1E and 4.5A, B). The younger stratigraphic surfaces were dated from the Burdigalian to the Messinian, using biostratigraphic information derived from Chima *et al.* (2019; e.g. Fig. 4.4A). The late Cretaceous horizon caps the underlying seismic unit, dominated by chaotic, moderate to high amplitude seismic reflections (shaded green in Figs. 4.4-4.6). A moderate to high-amplitude seismic reflection at the middle part of the Cretaceous-late Eocene Unit (the horizon marked in black above the basement in Figs. 4.4A, 4.5E, 4.6A), sub-divides the unit into 2 reflection-free seismic sub-units (shaded light and dark-grey in Figs. 4.5A; 4.5A, C, E; 4.6A). The Cretaceous-late Eocene Unit generally decreases in thickness basinward, with its upper sub-unit, displaying remarkable thickness within the transitional zone and the inner-fold-thrust belt, where linear features, characterized by listric geometries are common (e.g. Figs. 4.4-4.6). On a delta-wide strike line located at the proximal part of the continental shelf (Figs. 4.1A; 4.7A, B), the late Eocene horizon interpreted on regional dip lines (Figs. 4.1A; 4.4-4.6), could not be tracked due to lack of seismic reflections. This poor reflectivity seismic unit (the interval shaded in red; Fig. 4.7A, B), exhibits remarkable lateral variation in thickness from the western to the eastern Niger Delta lobes (Fig. 4.7A, B). The unit reaches minimum thickness at the summits of topographic highs identified in the western, central and eastern Niger Delta lobes (Figs. 4.1A; 4.7A, B). Lineated features that offset seismic reflections, are distributed throughout the delta-wide strike line and are poorly imaged within the deeper stratigraphic intervals (Fig. 4.7A, B). Along the regional dip lines, these linear features display high angles of inclination within the younger stratigraphic intervals but develop listric geometry within the deeper stratigraphic intervals, where they terminate at the upper part of the Cretaceous-late Eocene Unit (Figs. 4.4-4.6).

Interpretation:

The chaotic, moderate-high amplitude seismic unit, bounded at the top by a high-amplitude seismic reflection was interpreted as the basement (Figs. 4.4-4.7). The topographic highs identified in the western, central and eastern Niger Delta were interpreted as the Chain, Charcot and Fernando Po Fracture Zones respectively (Short and Stauble, 1967; Evamy *et al.*, 1978; Doust and Omatsola, 1990; Figs. 4.1A, 4.7A, B). The lateral variation in thickness of the reflection-free seismic unit (shaded in red; Fig. 4.7A, B), at the summit of the Chain, Charcot and Fernando Po Fracture Zones, suggests that the relief associated with these fracture zones, controlled the deposition of the unit. On the regional dip seismic lines located downdip (Fig. 4.1A), the reflection-free sub-units that overlie the basement, were respectively interpreted as lower and upper detachments (see also Bellingham *et al.*, 2014; Figs. 4.1E; 4.4-4.6). The moderate to high-amplitude seismic reflection (the horizon marked in black above the basement in Figs. 4.4E, 4.5A and 4.6A), which delimits the lower and upper detachments, was interpreted as regional detachment (see also Bellingham *et al.*, 2014; Fig. 4.1E). This interpretation is supported by the termination on this horizon, the linear features (labelled P-Z; in Figs. 4.4, 4.5; and G-O in Fig. 4.6). The normal and reverse offsets of seismic reflections by these linear features support their interpretations as normal and reverse faults respectively (Figs. 4.4-4.7). The positive topographies, characterized by bathymetric relief on the modern seafloor, were interpreted as thrust/shale-cored anticlines, while the negative topographies that flank them were interpreted as intraslope basins (see also Adeogba *et al.*, 2005; Bakare *et al.*, 2007; Prather *et al.*, 2012., Bellingham *et al.*, 2014; Chima *et al.*, 2019; Fig. 4.4). The reflection-free interval (shaded red in Fig. 4.7A, B), where the late Eocene and the Burdigalian horizons could not be tracked suggests sediment burial beyond the resolution of our seismic data. The overall thickening of the upper detachment within the translational zone and the inner-fold-thrust belt was interpreted to have resulted from structural thickening by duplexing (e.g. Figs. 4.4, 4.6).

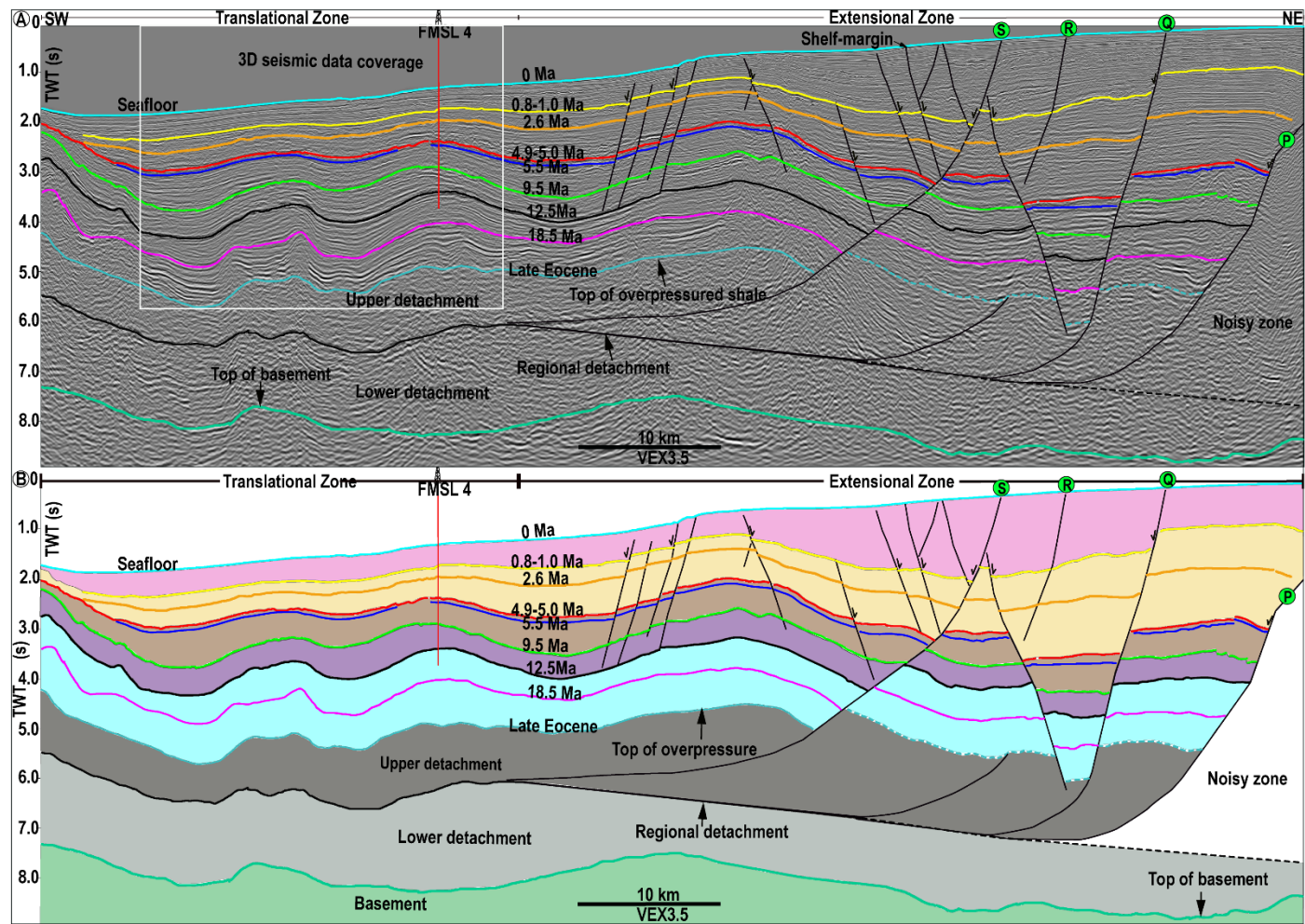


Fig. 4.4. A, B: Interpreted and uninterpreted seismic line drawing [(two-way-travel time (TWT)], about 5 km west of Fig. 2, shows similar structural styles in the eastern part of the study area. Note the overall uniform sediment thickness between the late Eocene-Serravallian and a lateral variation in sediment thickness from Serravallian-present. Note also the overall relative higher sediment thickness within the extensional zone (the early Pliocene-present). See Fig. 4.1A for location of interpreted line.

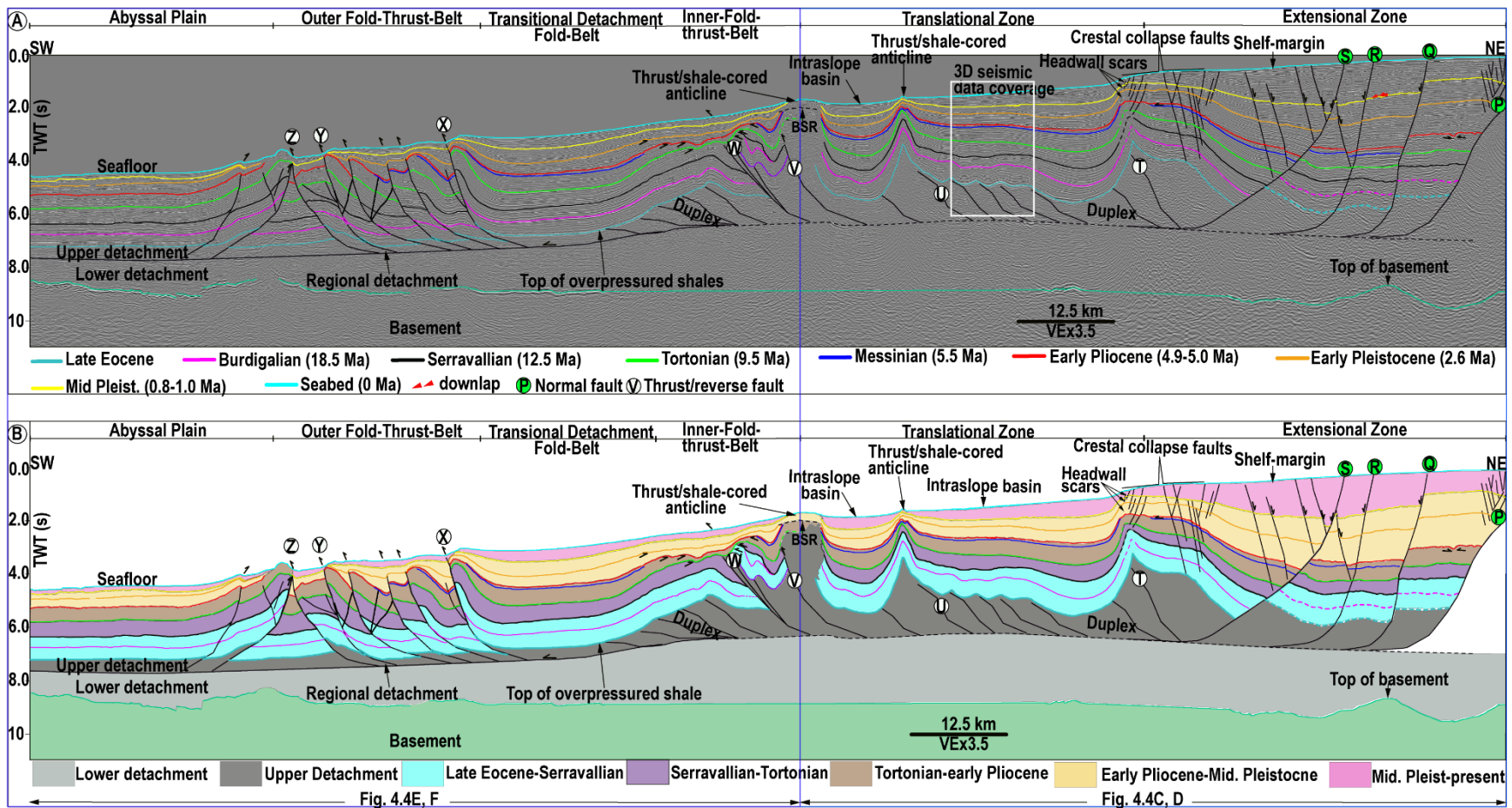


Fig. 4.5. A, B: Regional two-way-travel time (TWT) seismic line (interpreted and line drawing), showing the structural styles in the eastern part of the study area (see Fig. 4.1A). Note the overall uniform stratigraphic thickness between the Late Eocene-Serravallian and lateral variation in thickness from Serravallian-present. Note also the relative higher sediment thickness from the early Pliocene to the present within the extensional zone compared to the other structural zones. Letters P-S and T-Z represent normal and reverse faults respectively

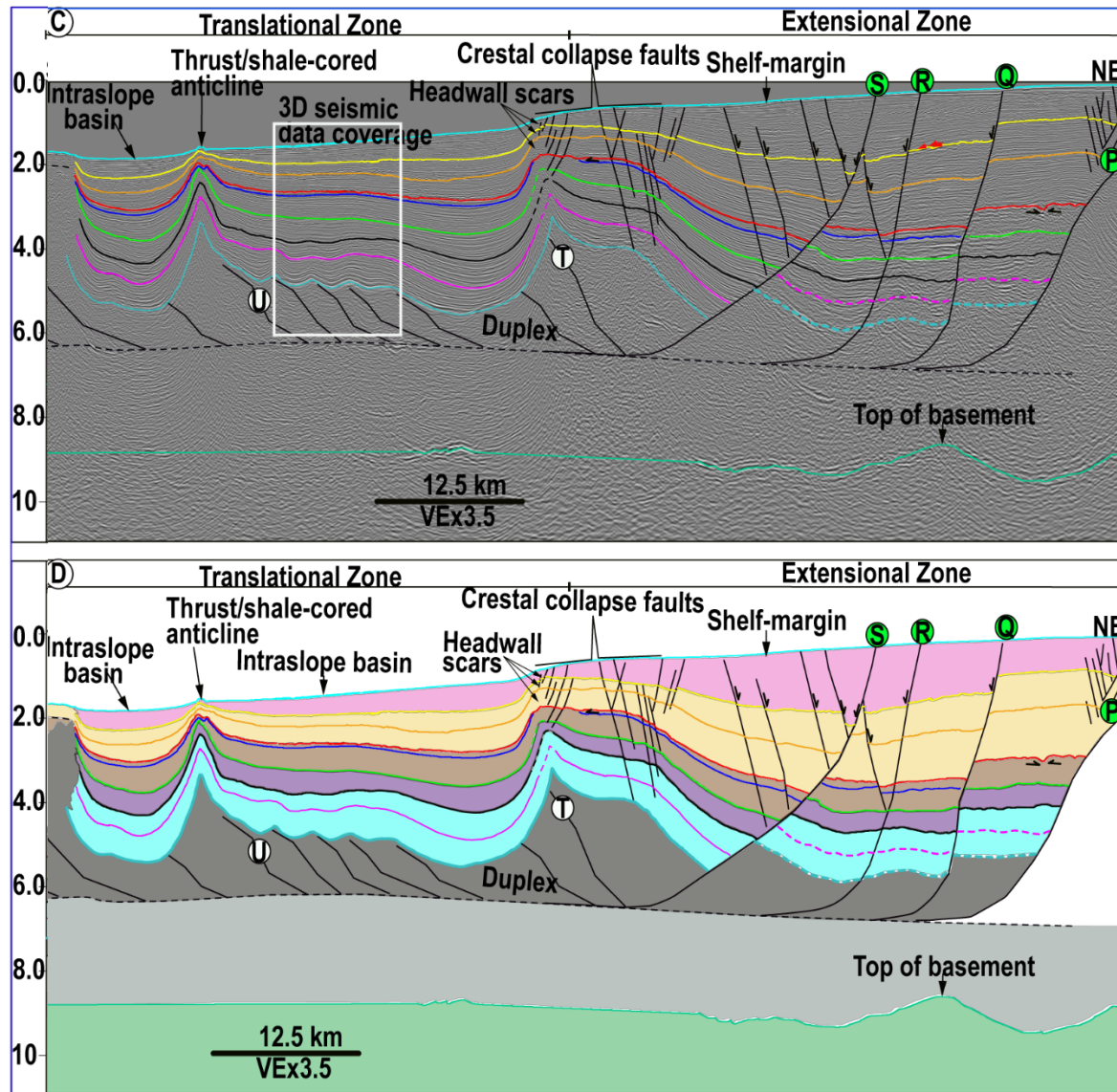


Fig. 4.5. C, D: Interpreted and seismic line drawing showing the detailed tectonostratigraphic architecture of the extensional and translational zones. Note the detachment of faults at the base of the upper dark grey unit. See text for a detailed explanation.

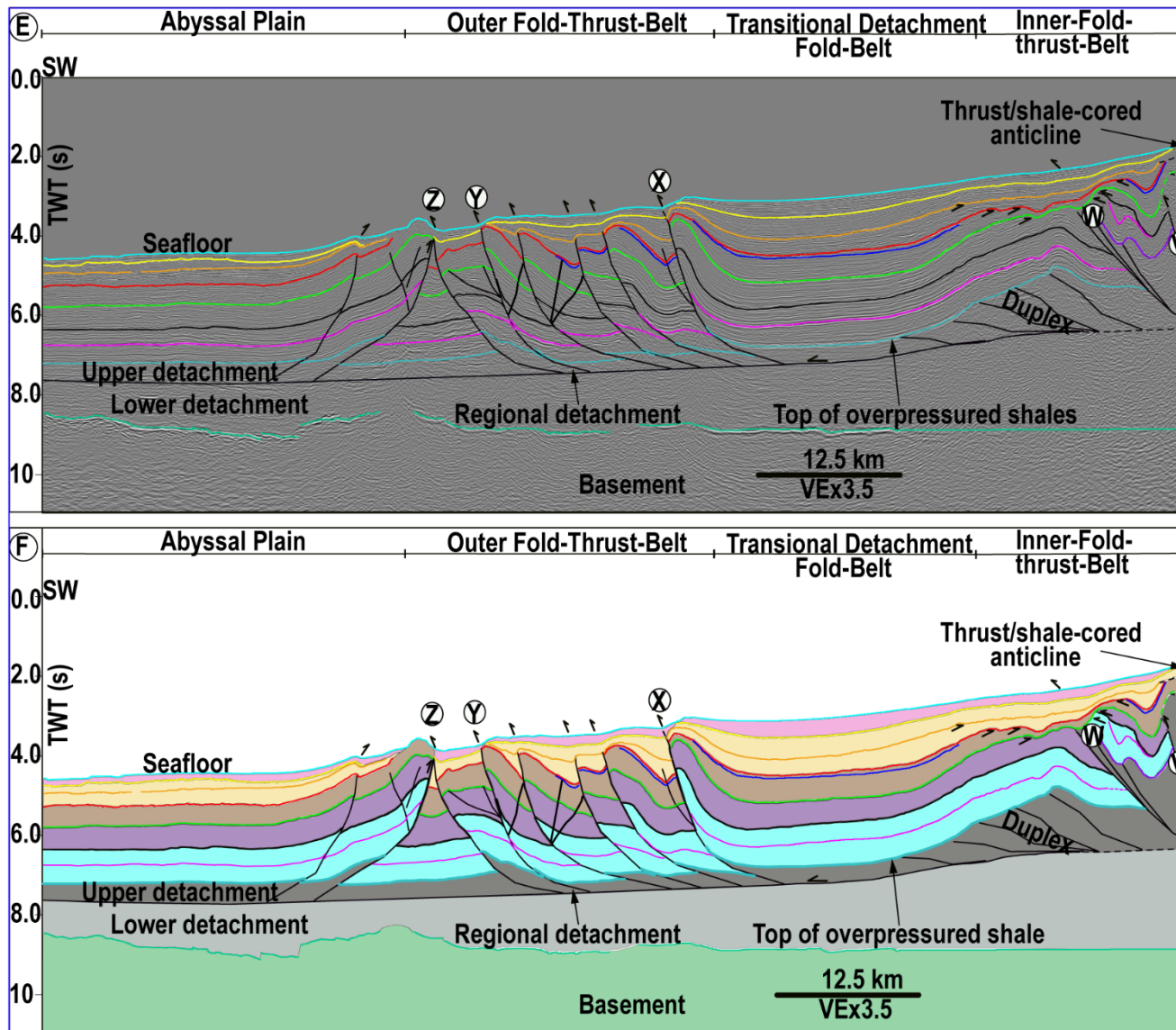


Fig. 4.5. E, F: Interpreted and seismic line drawing showing the detailed tectonostratigraphic architecture of the contractional zone. Note also the detachment of faults at the base of the upper dark grey unit. See text for a more detailed explanation.

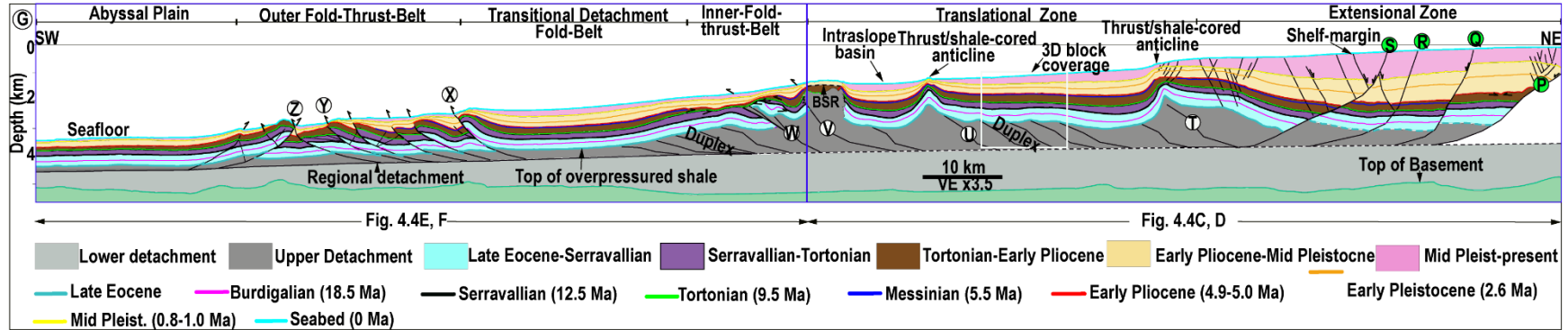


Fig. 4.5 G: Line drawing (the depth equivalent of panel A, B displayed with the same scale). Note the overall decrease in sediment thickness on this panel compared to panels A, B. Although vertically exaggerated, this depth section enabled us to build a more reliable tectonostratigraphic evolution of the western Niger Delta from the Cretaceous-present as presented in the discussion. See Fig. 4.1A for location of interpreted line.

4.4.1.2 The late Eocene-Serravallian

Description:

The late Eocene-Serravallian Unit (the interval shaded in blue in Figs. 4.4-4.6) is bounded at the base by the undulating seismic reflection, which corresponds to the late Eocene horizon described above, and at the top by an undulating seismic reflection (the black horizon, labelled the Serravallian in Figs. 4.4-4.6). The late Eocene-Serravallian Unit displays an overall uniform thickness within the extensional and contractional zones, but reaches a maximum thickness of 1 s within the intraslope/piggyback basins located basinward of the reverse faults (labelled T, U and W in Fig. 4.5A-F). The late Eocene-Serravallian Unit also displays an overall increase in the thickness on the hanging walls of the faults (labelled P, S in Fig. 4.4A, B and I, L in Fig. 4.6A, B). However, the unit thins at the top of

thrust/shale-cored anticlines (e.g. the reverse faults labelled T, U in Figs. 4.5A-D), and at the transition between the translational zone to the inner-fold-thrust belt, where it locally truncates below thrust/shale-cored anticline (e.g. Fig. 4.5A, B).

Interpretation:

The overall uniform thickness of the late Eocene-Serravallian Unit within the extensional zone (Figs. 4.4A, B; 4.5A-G; 4.6A, B), suggests that the normal faults were not active during the deposition of the unit. The increase in the thickness of the late Eocene-Serravallian Unit within the intraslope (piggyback) basins located basinward of the reverse faults (labelled T, U and W in Fig. 4.5A-G), was interpreted to record growth strata. This observation coupled with the corresponding thinning of the late Eocene-Serravallian Unit at the summit of thrusts/shale-cored anticlines, suggests the activity of the underlying thrusts/duplexes during the deposition of the unit. The undulating geometry of the late Eocene, Burdigalian and the Serravallian horizons within the intraslope/piggyback basins (e.g. Fig. 4.5A-D), further supports the activity of the underlying thrusts/duplexes during deposition of the unit. The abrupt truncation of seismic reflections e.g. the Burdigalian horizon below the Serravallian surface, within the inner-fold-thrust belt (e.g. Fig. 4.5E, F), suggests local erosion, probably triggered by the activity of the underlying duplexes and the reverse faults (labelled V, W in Figs. 4.5E, F).

4.4.1.3 The Serravallian-Tortonian (12.8 Ma-9.5 Ma).

Description:

The Serravallian-Tortonian Unit (shaded in purple; Figs. 4.4-4.7), is bounded at the base by the Serravallian horizon described above and at the top by the seismic reflection marked in light green (the Tortonian horizon). Seismic reflection truncations were observed below the Tortonian horizon at the summit of thrust/shale-cored anticlines within the inner-fold-thrust belt (e.g. Fig. 4.5A, B, E, F). Along a 500 km delta-wide strike line located on the Niger Delta continental shelf

(Fig. 4.1A), the Serravallian-Tortonian Unit displays uniform thickness in the eastern Niger Delta lobe, but increases locally within hanging walls in the western Niger Delta lobe (Fig. 4.7A, B), reaching a maximum thickness of 1.2 s within the hanging walls of listric growth faults located above the tilted part of the basement (see dashed blue polygon in Fig. 4.7A-D). Along the regional dip lines located further downdip of (Fig. 4.7), the Serravallian-Tortonian Unit displays lateral variation in thickness from the extensional zone to the abyssal plain (Figs. 4.4-4.6). The Serravallian-Tortonian Unit generally thickens on the hanging walls of the normal faults (labelled P, S in Figs. 4.4A, B; 4.5A-D; G and G-H in Fig. 4.6A, B). Also, while the Serravallian-Tortonian Unit displays overall uniform thickness within the outer-fold-thrust belt, it thins above thrusts/shale-cored anticlines and reaches a maximum of 1.2 s within piggyback basins located in the translational zone, inner-fold-thrust belt and transitional detachment fold (Figs. 4.4-4.6).

Interpretation:

The truncation of seismic reflections below the Tortonian horizon within the inner-fold-thrust belt, suggests the activity of the underlying duplexes and the thrust faults (labelled V, W e.g. Fig. 4.4A, B, E, F). The local increase in the thickness of the Serravallian-Tortonian Unit on the hanging walls of the normal faults (labelled P and S in Figs. 4.4, 4.5), was interpreted to document growth strata, suggesting the activity of the faults during the deposition of the unit. Similarly, the overall increase in the thickness of the Serravallian-Tortonian Unit within piggyback basins, interpreted as growth strata and the corresponding decrease at the top of thrust/shale-cored anticlines (Figs. 4.4-4.6), was interpreted to record the activity of the underlying thrusts/shale-cored anticlines during the deposition of the unit. The along-strike variation in thickness of the Serravallian-Tortonian Unit was interpreted to record differential subsidence and variation in the locations of sediment input to the Niger Delta (see also Jermannaud *et al.*, 2010; Rouby *et al.*, 2011; Figs. 4.1A; 4.7A, B).

4.4.1.4 The Tortonian-early Pliocene Unit (9.5-4.9 Ma)

Description

The Tortonian-early Pliocene Unit (the interval highlighted in brown; Figs. 4.4-4.7), is bounded at the base and the top by high-amplitude seismic reflections, characterized by irregular geometries (see light green and red horizons labelled Tortonian and early Pliocene respectively) in (Figs. 4.4-4.7). Seismic reflections within this unit locally terminate below the early Pliocene horizon, notably at the summit of the thrust/shale-cored anticline within the inner-fold-thrust belt (Fig. 4.5A, B, E, F) and also within the hanging wall of the normal fault (labelled P in Fig. 4.5A-D). The Tortonian-early Pliocene Unit displays an overall increase in thickness across the hanging walls of the normal faults (labelled P, Q, S in Figs. 4.5A, B; 4.5A-G and I and J in Fig. 4.7A, B). Along the delta-wide seismic line located further up-dip of the extensional zone (Fig. 4.1A), the Tortonian-early Pliocene Unit displays overall uniform thickness but locally thickened within hanging walls in the eastern, central and western Niger Delta lobes (Fig. 4.7A, B). Within the translational zone and the transitional detachment fold belt, the Tortonian-early Pliocene Unit displays moderate thickness within intraslope basins, but thins at the summit of thrust/shale-cored anticlines associated with the reverse faults (labelled T-W; Fig. 4.5A- D). While the Tortonian-early Pliocene Unit maintains uniform thickness within the abyssal plain, it displays erosional truncations on the folds associated with the thrust faults (labelled X, Y, Z in Fig. 4.5A, B; E-G) in the outer-fold-thrust belt.

Tectonostratigraphic Evolution of the western Niger Delta From Neogene to Present

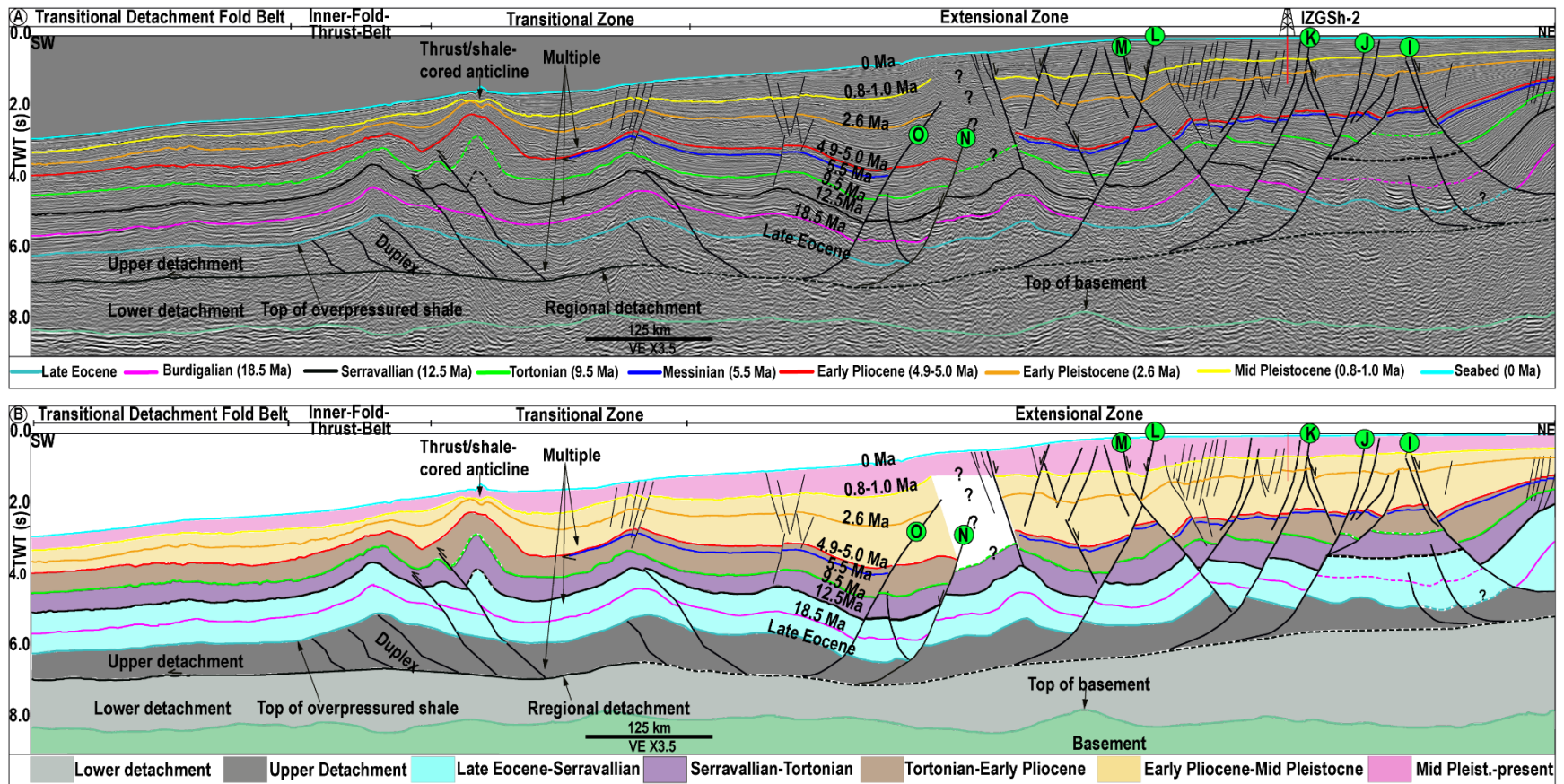


Fig. 4.6. A, B: Regional two-way-travel time (TWT) seismic line (interpreted and line drawing), about 40 km west of Fig. 4.2, shows the structural styles in the western part of the study area (see Fig. 1A). Note the overall uniform sediment thickness between the Late Eocene-Serravallian and a lateral variation in sediment thickness from Serravallian-present. Note also the overall increase in sediment thickness within the extensional zone (the early Pliocene-present). See Fig. 4.1A for location of interpreted line.

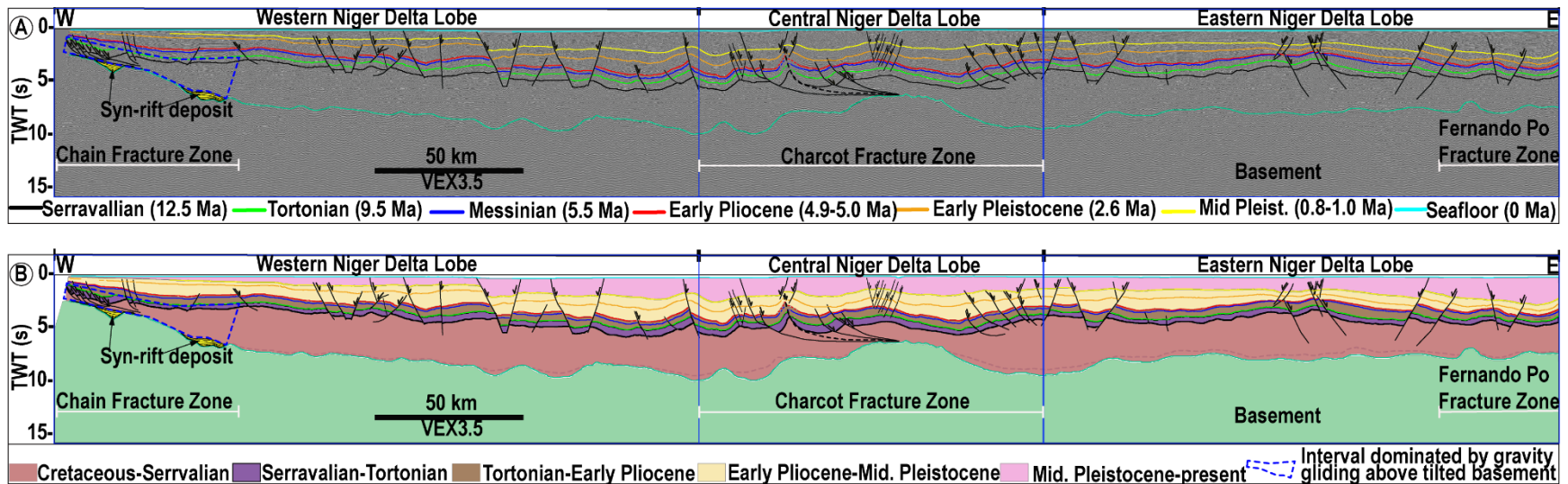


Fig. 4.7A, B: Delta-wide seismic strike line, showing the eastern, central and western Niger Delta lobes (see Fig. 4.1A). The structural high at the central part of the line corresponds to the Charcot Fracture Zone (CFZ), which divides the delta into the eastern and western lobes (see Fig. 4.1A). Note the tilt in the basement in the western Niger Delta lobe and the occurrence of listric normal faults that offset basin centre-dipping seismic reflections (dashed blue polygon in Fig. 4.7A-D). Note the non-uniform nature of the basement, the variation is stratigraphic thickness from the eastern to the western Niger Delta lobes, the overall thinning of the Cretaceous to Serravallian stratigraphy above the Charcot Fracture Zone compared to the Serravallian to present-day Unit. Note the overall thinning of the early Pliocene to present-day Unit to the western part of the delta compared to the eastern part, the reflection-free character of the Cretaceous-Serravallian Unit (Fig. 4.7C, E below) and the presence of syn-rift deposits in the western Niger Delta. See Fig. 4.1A for location of interpreted line

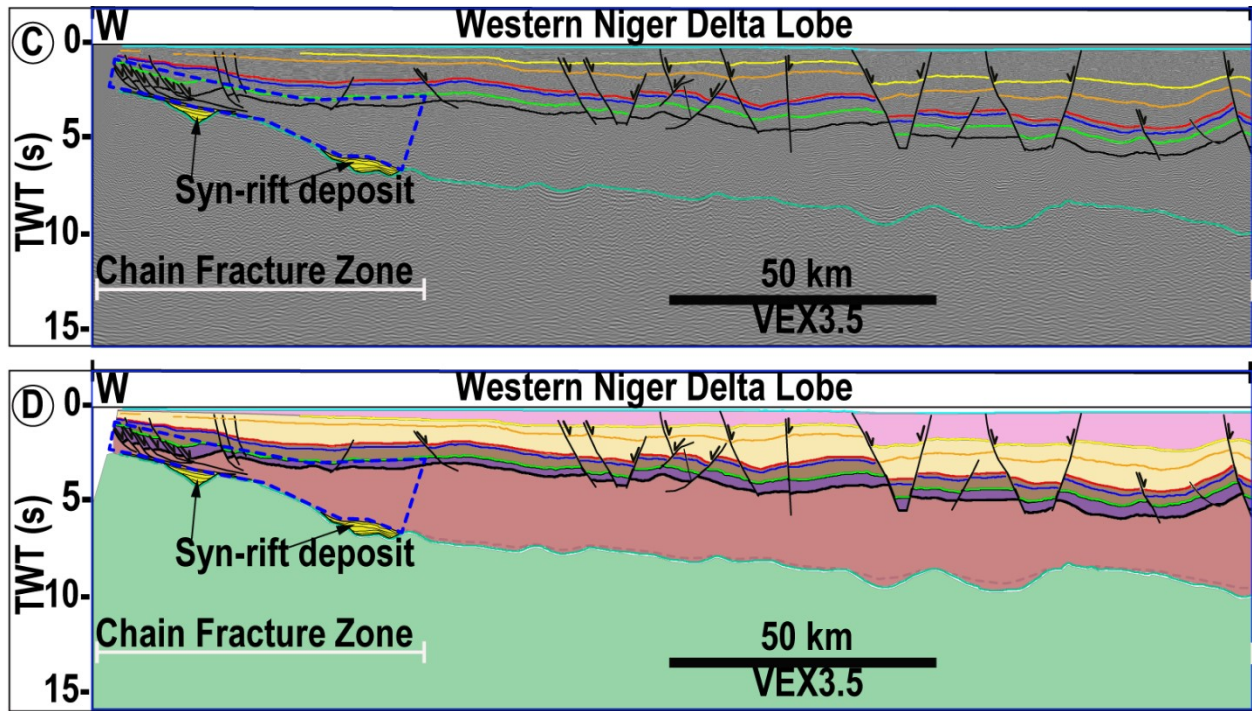


Fig. 4.7C, D: Interpreted seismic and line drawing of the western Niger Delta lobe illustrating the syn-rift deposits and stratigraphic interval dominated by gravity gliding (dashed blue polygon) above the tilted basement. See Fig. 4.7A, B above for legend to horizons and shaded intervals.

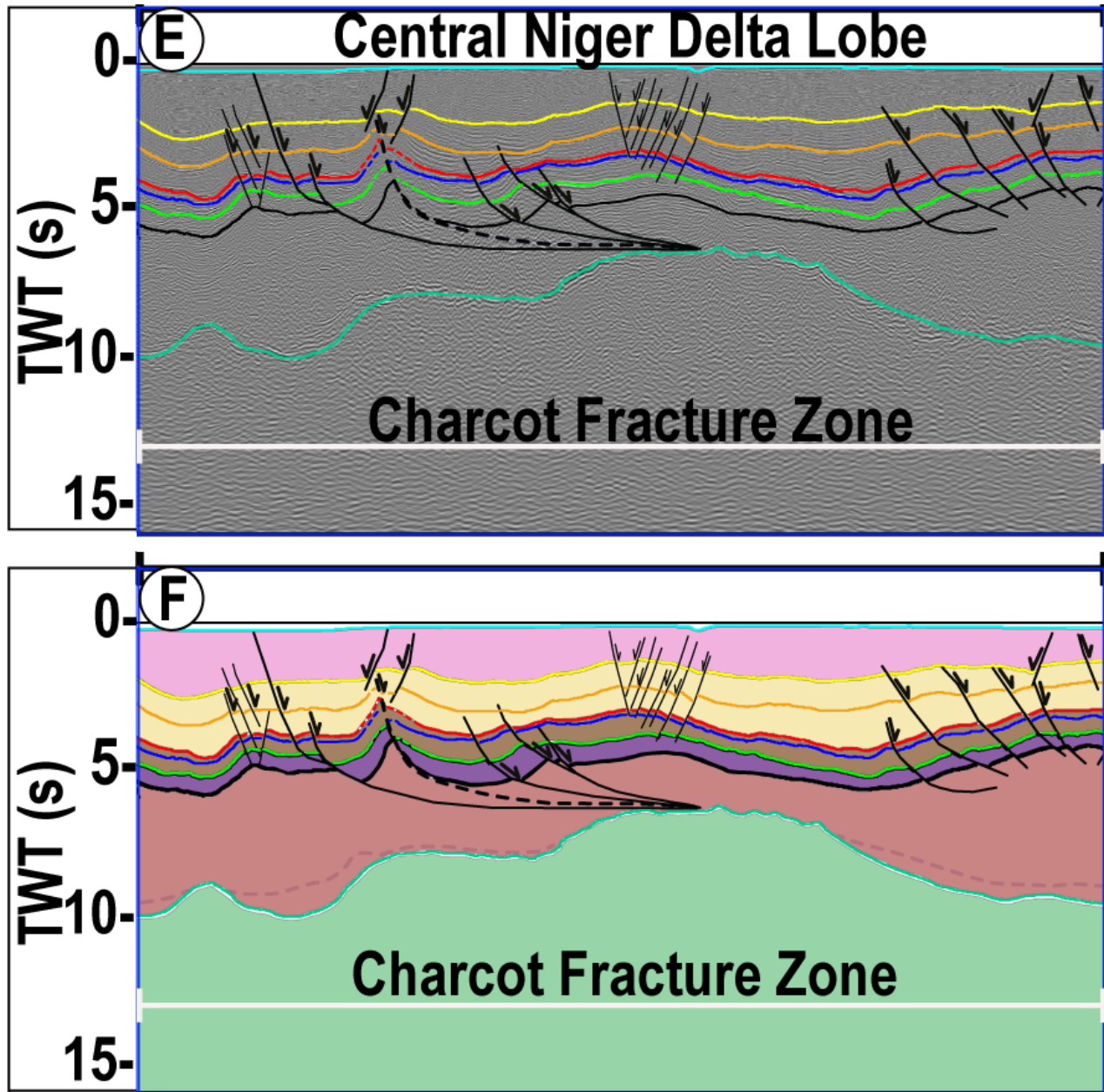


Fig. 4.7E, F. Central Niger Delta. Zoomed seismic and line drawing illustrating the overall thinning of the Cretaceous-Serravallian stratigraphy (red interval) above the CFZ (green interval) compared to the Serravallian-present (purple, orange, yellow and pink) intervals respectively. See Fig .4. 7A, B above for legend to horizons and shaded intervals.

Interpretation:

The local truncations of seismic reflections below Tortonian and early Pliocene horizons suggest their erosional character, linkable to the activity of the underlying thrust faults (labelled V and W in Fig. 4.5A-G). The overall thickening of the Tortonian-early Pliocene Unit across the hanging walls of the normal faults (labelled P, Q, S in Figs. 4.4A-D; 4.5A, B and G, H in Fig. 4.6A, B), record growth strata and is interpreted to record the activity of these normal faults during the deposition of the unit. The lateral variation in the thickness of the Tortonian-early Pliocene Unit along strike, with an overall increase within the hanging walls of normal faults distributed across the delta from the east to the west, was interpreted to record differential subsidence/gravity collapse in response to spatio-temporal changes in sediment input points (see also Sapin *et al.*, 2009; Jermannaud *et al.*, 2010; Rouby *et al.*, 2011; Figs. 4.1A; 4.7A, B). The general increase in the thickness of the Tortonian-early Pliocene Unit within piggyback basins in the translational zone and the transitional detachment fold belt (interpreted as growth strata), and the concomitant thinning at the summit of the thrust/shale-cored anticlines (Figs. 4.4-4.6), was interpreted document the activity of thrusts/shale-cored anticlines during the deposition of the unit. The smooth geometry of the Tortonian-early Pliocene horizons within the intraslope basin, seaward of the reverse fault (labelled T, U in Fig. 4.5A-D; G), compared to the underlying Serravallian, Burdigalian and the late Eocene horizons, suggests that the underlying duplexes were not active during the deposition of the unit. The erosional character of the early Pliocene horizon on the continental shelf (e.g. within the hanging of the normal fault labelled P in Fig. 4.5A-D; G), the slope (Figs. 3.3 A, B and 3.8C) and in the deep basin (within the inner-fold-thrust belt; Fig. 4.5A, B, E, F, G), coupled with its association with laterally extensive MTDs (e.g. Fig. 3.3A, B), suggests possible development of the early Pliocene horizon during relative sea-level fall (see Chima *et al.*, 2019 and Chima *et al.*, revised).

4.4.1.5 The early Pliocene-middle Pleistocene Unit (4.9 to ~1 Ma)

Description:

The early Pliocene-middle Pleistocene Unit (the interval shaded in yellow in Figs. 4.4-4.7), is bounded at the base by the early Pliocene horizon described above and at the top by a conformable/downlap surface (the yellow horizons labelled middle Pleistocene in Figs. 4.4-4.7). The early Pliocene-middle Pleistocene Unit marks the onset of a significant increase in sediment thickness across the western Niger Delta compared to the older stratigraphic intervals between the early Pliocene and the late Eocene (e.g. Figs. 4.4-4.7). On the delta-wide seismic line located further up-dip of (Figs. 4.4-4.7; see Fig. 4.1A), the early Pliocene-middle Pleistocene Unit displays lateral variation in stratigraphic thickness from the western to the eastern Niger Delta, reaching a maximum thickness of 2.3 s within hanging walls located within the central Niger Delta lobes, but thins at the edges of the delta (Fig. 4.7A, B). On regional dip lines located downdip of (Figs. 4.4-4.7), the early Pliocene-middle Pleistocene Unit generally increases in thickness within the hanging walls of the normal faults (labelled P, Q, S in Fig. 4.4A, B; 4.5 A-D; G and I, J, K, L, N in Fig. 4.6A, B). The early Pliocene-middle Pleistocene Unit also displays an overall increase in thickness within intraslope basins and concomitant thinning at the summits of thrust/shale-cored anticlines (Figs. 4.4-4.6). In the abyssal plain, the early Pliocene-middle Pleistocene Unit also shows an overall increase in thickness in the distal part compared to the proximal part, where it thins and onlaps the bathymetric relief associated with the imbricated thrusts (labelled Z in Fig. 4.5A, B; E-G).

Interpretation:

The remarkable increase in the thickness of the early Pliocene-middle Pleistocene Unit within the hanging walls of the normal faults (labelled P-S in Figs. 4.4A, B; 4.5A-D; G; and I-N in Fig. 4.6A), as well as on the upper slope, was interpreted to record growth strata and syn-depositional gravity collapse/accommodation creation on the continental shelf and slope regions over the early Pliocene-middle Pleistocene (Figs. 4.4-4.7). Similarly, the overall increase in the thickness of the early Pliocene-middle Pleistocene Unit within piggyback basins, the thinning at the summit of thrust/shale-cored structures within the translational and the contractional zones, and the onlapping of the unit on the bathymetric relief associated with the imbricated thrusts

(labelled Z in Fig. 4.5A, B; E-G), indicates that up-dip gravity collapse within the shelf and the upper slope was accommodated downslope by shortening and folding (Fig. 4.4-4.6).

4.4.1.6 The middle Pleistocene-present (~1-0 Ma)

Description:

The middle Pleistocene-present Unit (the interval highlighted in pink in Figs. 4.4-4.7), is the youngest stratigraphic unit identified in the western Niger Delta. It is bounded at the base by the downlap surface, which delimits the underlying unit, and at the top by the modern seafloor (Figs. 4.4-4.7). Along the delta-wide strike line displayed in (Fig. 4.7A, B), the middle Pleistocene-present Unit displays an overall increase in thickness from the western to the eastern Niger Delta lobes (Fig. 4.7A, B). Like the underlying early Pliocene-middle Pleistocene Unit, the middle Pleistocene-present Unit, displays a significant increase in thickness within the extensional zone, where it reaches a peak of 2s but, decreases remarkably from the translational zone to the abyssal plain, where it merely onlaps the bathymetric high associated with the imbricated thrusts (labelled Z), at the front of the contractional system (Fig. 4.5A, B; E-G). The Pleistocene-present Unit equally thins at the summit of thrust/shale-cored anticlines and folds associated with imbricated thrusts within the translational and contractional zones (Figs. 4A B; 4.5A, C, D; 4.6A, B).

Interpretation:

The overall thickening of the middle Pleistocene-present Unit within the hanging walls of normal faults in the extensional zone was interpreted to record syn-depositional gravity collapse/creation of accommodation on the shelf from the middle Pleistocene to present (Figs. 4.4-4.6). However, the overall basinward decrease in the thickness of the middle Pleistocene to present suggest that gravity collapse of normal faults on the shelf facilitated sediment sequestration in this region with relative decrease in sediment bypass to the deep basin (Figs. 4.4-4.6). The general thinning of the middle Pleistocene to present Unit at the summit of thrust/shale-cored anticlines

within the translational and contractional zones, indicates that thin-skinned deformation was accommodated downdip by shortening/folding (Figs. 4.4-4.6). The overall decrease in thickness of the middle Pleistocene-present towards the edge of the western Niger Delta lobe, compared to the eastern part, suggests an overall easterly increase in flexural subsidence (Figs. 7A, B).

4.5 Sedimentation rates (shelf and slope regions)

Based on a detailed seismic interpretation of 21 2D seismic lines located on the continental shelf and a high-resolution 3D seismic survey located on the continental slope (Fig. 4.1A), we estimated sedimentation rates since the Serravallian on the shelf and since the late Eocene on the slope (Fig. 4.8A, C). We could not estimate the sedimentation rates on the shelf within the late Eocene-Serravallian interval because seismic markers were completely buried beyond the resolution of seismic data (e.g. Fig. 4.7A, B). In addition, due to the limited coverage of the seismic data in the deepwater region, we could not estimate the sedimentation rate in this region.

4.5.1 Sedimentation rate (shelf region)

During the Serravallian-Tortonian, sedimentation rate on the continental shelf was 250 m/Ma but decreased to 150 m/Ma from the Tortonian to the early Pliocene (Fig. 4.8A). From the early Pliocene to the middle Pleistocene, the sedimentation rate was 460 m/Ma and increased gradually 470 m/Ma from the middle Pleistocene to present (Fig. 4.8A).

4.5.2 Sedimentation rate (slope region)

Sedimentation rate on the continental slope remained constant 25 m/Ma from the late Eocene to the Burdigalian but increased (doubled) to 55 m/Ma from the Burdigalian to the Serravallian (Fig. 4.8B). Similarly, from the Serravallian to the Tortonian, the sedimentation rate tripled to 160 m/Ma before decreasing to 80 m/Ma and 75 m/Ma over the Tortonian-early Pliocene

and early Pliocene-middle Pleistocene respectively (Fig. 4.8B). The sedimentation rate increased to 140 m/Ma from the middle Pleistocene to present (Fig. 4.8B).

We acknowledge some uncertainties associated with well and seismic data in the estimated sedimentation rates. We relied on published studies e.g. Bellingham *et al.* (2014; Fig. 4.1E) to fix the ages of the deeper stratigraphic surfaces as the Cretaceous and the late Eocene due to the lack of biostratigraphic data within the interval (Figs. 4.4-4.6). Similarly, although detailed cyclostratigraphic analysis combined with high-resolution 3D seismic geomorphology, allowed us to propose the early Pliocene, the early and middle Pleistocene over the younger stratigraphic intervals (see Chima *et al.*, revised; Figs. 3.3; 3.10), the absence of biostratigraphic data within these intervals, did not allow us to verify the proposed ages. Also, the depth conversion of stratigraphic surfaces was based on limited well control. The depth conversion of selected regional seismic lines (e.g. Fig. 4.5G), was based on relatively shallow well information with only the FMSL 1 (4,154 m) and FMSL 2 (3,627 m), sampling the Burdigalian horizon (e.g. Figs. 2.2, 2.5, 2.7). Hence, the extrapolation of velocity analysis beyond the Burdigalian to the Cretaceous-late Eocene Unit, resulted in the overall shallowing of the surfaces (up to 2 km) and a general reduction in sediment thickness (compare Fig. 4.5B and 4.5G). Despite the fact that the foregoing uncertainties may have led to underestimation or overestimation of the sedimentation rates presented in (Fig. 4.8), our results are consistent and provide a general understanding of the tectonostratigraphic evolution of the western Niger Delta since the late Eocene as discussed below.

4.6 Discussion

Detailed tectonostratigraphic analysis and interpretation of regional, depth-penetrating 2D seismic and 3D seismic data cube, calibrated with well information on the western Niger Delta, allow us to discuss at a regional scale, the interaction between paleo-topographies associated with the spreading of the margin, delta top tectonostratigraphic dynamics and gravity deformation of the margin's sedimentary cover from Cretaceous to present.

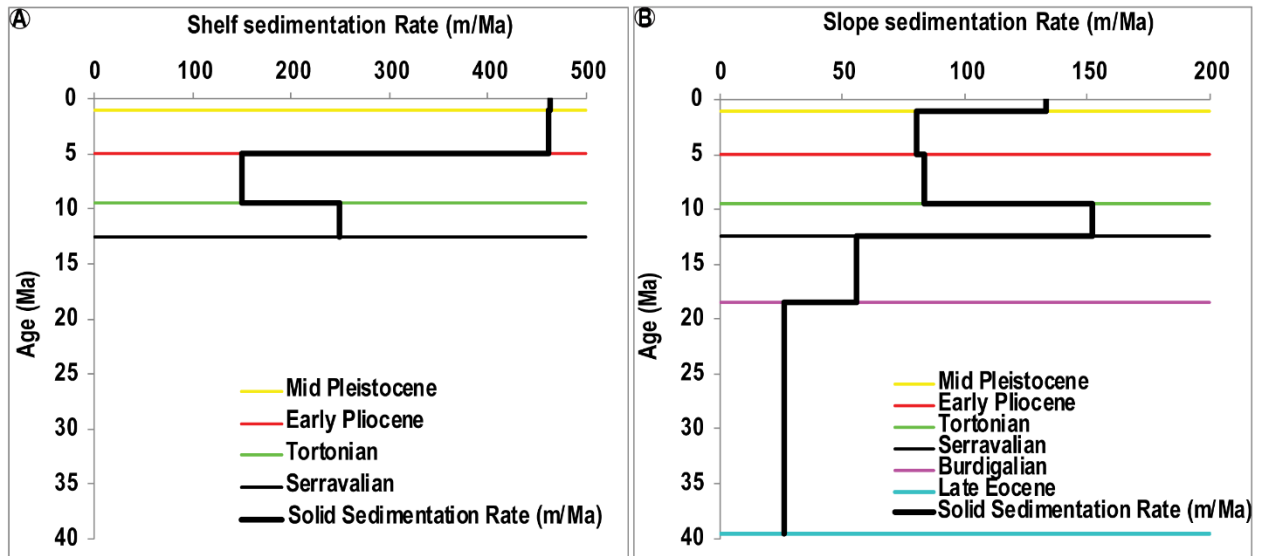


Fig. 4.8. Estimated sedimentation rates. A (shelf region); B (slope) region. Note the relatively high sedimentation rates from the Serravalian to the Tortonian and the early Pliocene to present. See text for a more detailed explanation.

4.6.1 Tectonostratigraphic evolution of the western Niger Delta

The Cretaceous-late Eocene Unit, sub-divided into the lower and upper detachments (Figs. 4.4-4.6), is inferred to be dominated by marine shales that were probably deposited during the Paleocene-Eocene high sea-levels and relative tectonic quiescence (see Cohen and McClay, 1996; Briggs *et al.*, 2006; Maloney *et al.*, 2010; Wiener *et al.*, 2010; Chardon *et al.*, 2016; Grimaud *et al.*, 2017; Figs. 4.4-4.6). The local rise of the upper detachment through stratigraphy, notably within the translational zone (Fig. 4.5A-D), coupled with the listric geometry of faults and their termination within the upper detachment, suggests the presence of overpressure within the unit (see Cohen and McClay, 1996; Maloney *et al.*, 2010; Wiener *et al.*, 2010; Figs. 4.4-4.6; 4.9A). The presence of shale withdrawal intraslope basins that root into the detachment unit, flanked by thrust/shale-cored anticlines within the translational zone and the inner-fold-thrust belt, compared to the outer-fold-thrust belt, dominated by imbricated thrusts and associated folds (e.g. Fig. 4.5A-G), suggests an overall basinward decrease in overpressure (see also Rowan *et al.*, 2004; Corredor *et al.*, 2005; Mourgues *et al.*, 2009; Sapin *et al.*, 2012; Wiener *et al.*, 2010; Rouby *et al.*, 2010; Restrepo-Pace, 2018; Figs. 4.4-4.6). Also, the observed tectonic thickening of the upper

detachment (duplexing), within the translational zone and the inner-fold-thrust belt, compared to the outer-fold-thrust belt, where imbricated thrust sheets and folds dominate (Fig. 4.5A-G), further supports a basinward decrease in fluid overpressure and a corresponding increase in shear strength/frictional resistance of the detachment (see also Rowan *et al.*, 2004; Corredor *et al.*, 2005; Billotti and Shaw, 2005; Maloney *et al.*, 2010; Figs. 4.4-4.6). The presence of syn-rift deposits (Fig. 4.7A-D), generally associated with lacustrine depositional environment, dominated by type I organic matter (e.g. Ekweozor and Daukouru, 1994; Fig. 4.7C, D), suggests the possible presence of Cretaceous-Paleogene petroleum play in the western Niger Delta. Syn-rift deposits have not been explored in the offshore Niger Delta but are known to contain oil show in the inland basins (see Ekweozor and Daukouru, 1994).

The overall uniform thickness of the late Eocene-Serravallian Unit within the extensional zone, suggests that the normal faults (labelled P-S in Figs. 4.4A, B; 4.5A, D), were not active during the deposition of the unit. However, the thinning of the unit at the summit of the thrust/shale-cored anticline associated with the reverse fault (labelled T in Fig. 4.9A), and the presence of growth strata within the piggyback basin associated with the reverse fault, support our interpretation that the movement of fault T, controlled the geometry of the late Eocene-Serravallian Unit (e.g. Fig. 4.5A-D). The undulating geometries of the late Eocene, Burdigalian and Serravallian horizons support the activity of the underlying duplexes during the deposition of the late Eocene-Serravallian Unit (Figs. 4.5A-D; 4.6A, B). Although a regional tectonic reorganization of the Niger catchment (~34-29 Ma; Fig. 4.1A) and associated increase in sediment supply to the delta (Chardon *et al.*, 2016; Grimaud *et al.*, 2017), is thought to have triggered deformation of the late Eocene-Serravallian Unit at a regional scale, the overall uniform thickness and relatively low sedimentation rate of 60 m/Ma on the slope (Fig. 4.8B), suggest that deposition was probably focused within fault-bounded accommodation in the onshore (Fig. 4.1A). This interpretation seems to agree with previous studies in the eastern Niger Delta, where deposition is reported to have been focused in the onshore, where the extensional zone was located between the Oligocene to the Tortonian (Billotti and Shaw, 2005; Wiener *et al.*, 2010).

During the Serravallian-Tortonian interval, the presence of growth on the hanging walls of the normal faults (labelled P-S in Figs. 4.4A, B; 4.5A-D; 4.9B and G-O in Fig. 4.6A, B), suggests the onset of thin-skinned deformation within the extensional zone. The overall thinning and local

erosion of the Serravallian-Tortonian sediment at the summit of the thrust/shale-cored anticlines, coupled with the local thickening of the unit within the piggyback basins associated with the reverse faults (labelled T-W in Fig. 4.5A-F), suggest that extensional deformation in the up-dip was accommodated by shortening/folding downdip. The relatively high sedimentation rates of 250 m/Ma on the shelf and 160 m/Ma on the slope (Fig. 4.8A, B), coupled with the basinward shift of deformation from the translational zone to the proximal part of the contractional zone (e.g. Fig. 4.5A-G), suggest the onset of sediment bypass on the onshore (Fig. 4.1A).

The presence of growth strata within the Tortonian-early Pliocene Unit, notably on the hanging wall of the normal fault (labelled S in Fig. 4.5A, B), indicates further thin-skinned deformation within the extensional zone. The relatively high sedimentation rates of 150 m/Ma on the shelf and 80 m/Ma on the slope (Fig. 4.8A, B), and basinward propagation of deformation to the outer-fold-thrust belt, evidenced by thinning as well as local erosion of the Tortonian-Pliocene Unit at the summit of the fold associated with the imbricated thrust (labelled X in Fig. 4.5A, B), further demonstrate that thin-skinned deformation was accommodated downdip by shortening/buckling (Figs. 4.5A-D; 4.6A, B; 4.9B). Also, the presence of growth strata within the piggyback basin associated with the reverse fault (labelled X in Fig. 4.5A, B; E-F), further supports basinward migration of the contractional front probably in response to inferred migration of the extensional zone from its initial position in the onshore to its modern position (see Fig. 4.1A). This interpretation seems to agree with the observation in the eastern Niger Delta, where basinward propagation of the contractional front to its present position between the Tortonian and the Messinian, was linked to the migration of the extensional zone from the onshore to its present position (see Billotti and Shaw, 2005; Wiener *et al.*, 2010). Although the foregoing observations point to the possible initiation of mobile shales activity on the western Niger Delta over the Tortonian-Pliocene, the overall thinning of the Burdigalian-Serravallian Unit at the peak of the thrust/shale-cored anticlines (e.g. Fig. 4.5A, B), suggests that shale tectonics could have commenced since the Burdigalian-Serravallian (see also Chima *et al.*, 2019; Fig. 2.5; Appendices 4, 5, 6).

The early Pliocene-middle Pleistocene interval not only marks the onset of a remarkable increase in sedimentation rate of 470 m/Ma on the western Niger Delta continental shelf and corresponding decrease to 80 m/Ma on the continental slope (Fig. 4.8A, B), but also the

intensification of thin-skinned deformation, evidenced by significant sediment thickening on the rapidly collapsing hanging walls of normal faults (Figs. 4.4A, B; 4.5A-D; G; 4.6A, B; 4.7A, B; 4.9C). The observed increase in sedimentation rates on the shelf compared to the slope (Fig. 4.8A, B), suggests the onset of sediment sequestration within the rapidly subsiding shelf and upper slope (Figs. 4.4-4.7; 9D). The regional nature of the erosional event associated with the early Pliocene horizon (e.g. Fig. 4.5C, E), suggests that the surface may be related to a lowering in the sea-level during the early Pliocene (see Chima *et al.*, 2019; Fig. 2.5; Chima *et al.*, *revised*; Figs. 3.3 and 3.10). The overall decrease in thickness of the Pliocene-middle Pleistocene Unit in the abyssal plain (Fig. 4.5A, B; E-F), where it onlaps a bathymetric relief associated with the imbricated thrust (labelled Z in Fig. 4.5A, B; E-F), the thinning and local erosion of the unit above thrusts/shale-cored anticlines within the outer-fold-thrust belts, suggest that extensional deformation was significantly accommodated in this region by shortening/folding.

The middle Pleistocene-present marks overall increase in sedimentation rates of 475 m/Ma on the shelf and 135 m/Ma on the slope, with a general reduction in sediment transfer to the deep basin, evidenced by remarkable thinning of stratigraphy in the abyssal plain (Figs. 4.4-4.7; 4.8A, B; 4.9E). The general thinning of the middle Pleistocene-present Unit above thrust/shale-cored anticlines from the translational zone to the abyssal plain, where the unit onlaps the bathymetric relief associated with the imbricated thrust (labelled Z in Fig. 4.5A, B; E-G), suggests that thin-skinned deformation was accommodated within the outer-fold-thrust belt by shortening/folding. The presence of bathymetric topographies on the modern seafloor suggests that the thrust/shale-cored anticlines distributed across the western Niger Delta are still active or were recently active (see also Chima *et al.*, 2019; Chima *et al.*, *revised*; Fig. 4.4A, B; 4.5A, B; E-G; 4.6A, B).

A schematic illustration of the tectonostratigraphic evolution of the western Niger Delta from the Cretaceous-present is presented below (Fig. 4.9).

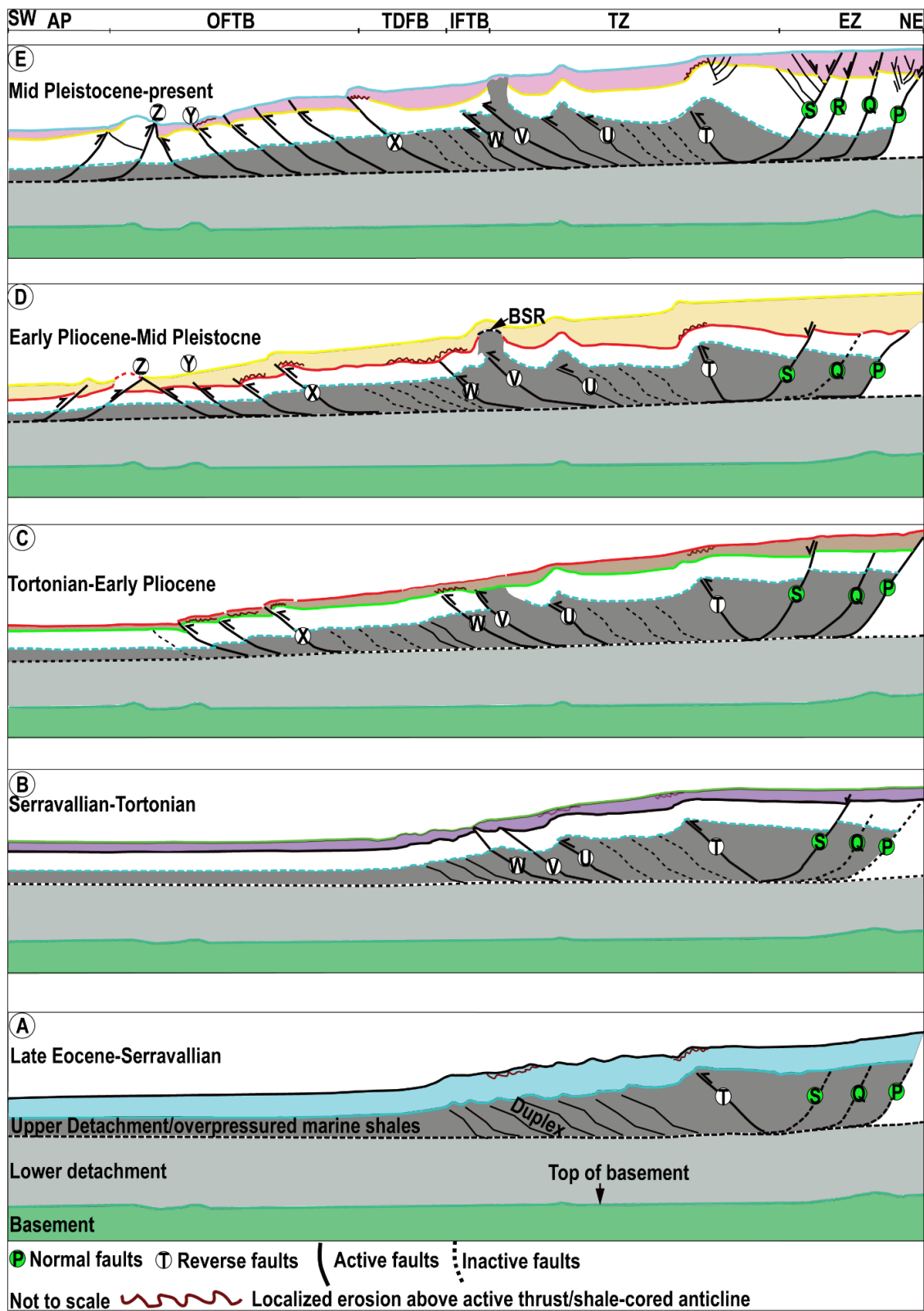


Fig. 4.9. Schematic illustration of the tectonostratigraphic evolution of the western Niger Delta. See text for a more detailed explanation.

4.6.2 Controls of paleo-topography and delta top tectonostratigraphic dynamics on gravity deformation of the western Niger Delta

Interpreted regional seismic strike line, which extends 500 km across the eastern and western Niger Delta (Fig. 7A, B), reveals that 3 major paleo-topographies namely; (i) the Fernando Po, (ii) the Charcot and (iii) Chain Fracture Zones (Fig. 4.1A), developed during the spreading of the margin in the Cretaceous (Short and Stauble, 1967; Evamy *et al.*, 1978; Doust and Omatsola, 1990), controlled sedimentation and gravity deformation of the margin. The lateral variation in thickness of the Cretaceous-Serravallian Unit (Fig. 4.7A, B), suggests that the topographies associated with the fracture zones, controlled the deposition of the unit. The ubiquity of listric normal faults above the tilted portion of the basement corresponding to the Chain Fracture Zone in the western Niger Delta (see dashed blue polygon in Fig. 4.7A, B), characterized by basin-centre dipping seismic reflections, suggests that gravity gliding dominated the region over the Cretaceous-Serravallian. Gravity gliding could also have been facilitated by mobile shales activity.

However, following the overall increase in sedimentation rates and structurally-induced accommodation on the western Niger Delta continental shelf and slope regions, notably over the Pliocene and the Pleistocene (Figs. 4.4-4.7; 4.8A, B), we infer that the margin switched from a gravity gliding-dominated to a gravity spreading dominated system (see also Rowan *et al.*, 2004). This interpretation is supported by the observed increase in structural collapse/sediment sequestration on the shelf and the upper slope over the early Pliocene and the Pleistocene, a prerequisite condition for the development of seaward-dipping bathymetric surface, which triggers the deformation of a system under its weight by gravity spreading (see Peel *et al.*, 2014; Figs. 4.4-4.7; 4.9).

4.6.3 Pliocene and Pleistocene stratigraphy of the western vs the eastern Niger Delta

Comparison of regional dip lines from the western and the eastern Niger Delta over the Pliocene and the Pleistocene (Figs. 4.1A, 4.10A, B), reveals differences in gravity deformational patterns and sediment partitioning from the continental shelf to the abyssal plain (Fig. 4.10A, B). The extensional, translational and contractional zones of the western Niger

Delta are respectively dominated by basinward dipping regional normal faults, thrust/shale-cored anticlines and imbricated thrusts and associated folds (Fig. 4.10A). While the extensional and translational domains of the eastern Niger Delta are characterized by landward as well as basinward dipping counter regional faults and thrust/shale-cored anticlines, the contractional domain display minor buckling (Fig. 4.10B).

The dominance of basinward dipping normal faults within the extensional domain of the western Niger Delta was interpreted to have facilitated overall sediment transfer from the continental shelf to the abyssal plain since the early Pliocene, with an overall increase in sediment thickness since the early Pleistocene (Fig. 4.10A). However, the presence of actively subsiding counter regional faults at the eastern Niger Delta continental shelf/slope boarder, was interpreted to have facilitated sediment sequestration on the shelf/upper slope with little or no deposition in the deep basin plain notably since the early Pleistocene (see Jermannaud *et al.*, 2010; Rouby *et al.*, 2011; 4.10B). Estimated sedimentation rates on the eastern Niger Delta continental shelf and slope regions over the middle Pliocene (3.7 Ma) and the early Pleistocene (2.6 Ma), ranges between 50-1000 m/Ma and 300-700 m/Ma, respectively (Jermannaud *et al.*, 2010; Rouby *et al.*, 2011). Similarly, estimated sedimentation rates both on the shelf and the slope from the early Pleistocene to present, ranges between 50-700 m/Ma (Jermannaud *et al.*, 2010; Rouby *et al.*, 2011). In the western Niger Delta, estimated sedimentation rates are 460 m/Ma on the continental shelf and 470 m/Ma on the slope over the early Pliocene-middle Pleistocene, and 75 m/Ma and 140 m/Ma, on the shelf and the slope since the middle Pleistocene (Fig. 4.8A, B). Although our estimated sedimentation rates are generally lower than in the eastern Niger Delta, the distribution of sediment from the shelf to the deepasin since the early Pliocene, suggests an overall increase in sedimentation in the western Niger Delta, compared to the eastern part of the delta, which is reported to undergo retrogradation and overall decrease in sediment fluxes since the early early Pleistocene (see Jermannaud *et al.*, 2010; Rouby *et al.*, 2011; Fig. 4.10A, B). If this interpretation is correct, the lack of biostratigraphic data over the Pliocene and Pleistocene coupled with decrease in sediment thickness upon the conversion of seismic interpretations from time to depth, could have led to the underestimation of the sedimentation rates presented in (Fig. 4.8A, B). In summary, given the spatio-temporal variation in gravity deformation and sediment partitioning observed in the western and the eastern Niger Delta since the early Pliocene (e.g. Figs. 4.7A-F and 4.10A, B),

a more regional seismic and well data are needed for a complete source-to-sink (isopach mapping of the western Niger Delta), that allows for a more quantitative comparison of these regions.

Tectonostratigraphic Evolution of the western Niger Delta From Neogene to Present

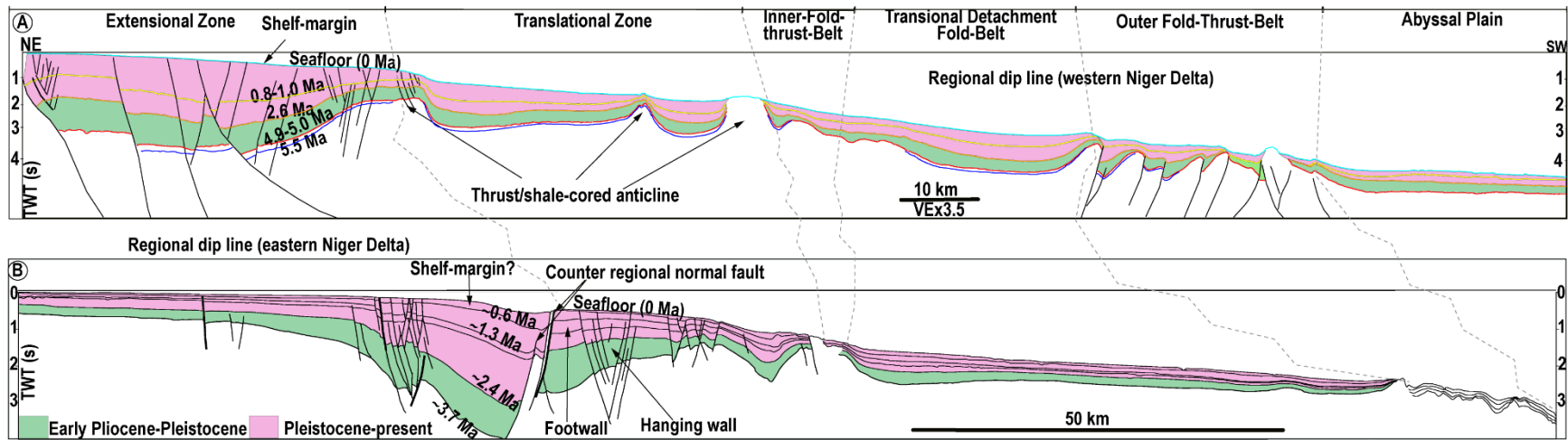


Fig. 4.10: Line drawing of the Pliocene and Pleistocene stratigraphic architecture of the western Niger Delta (A) and the eastern Niger Delta (B). Note the dominance of the western Niger Delta extensional and contractional zones by basinward dipping normal faults and imbricated faults folds respectively (Fig. 4.10A). Note the presence of actively subsiding counter regional normal faults at the eastern Niger Delta shelf/slope border and minor buckling in the contractional zone (Fig. 4.10B). Note also the overall distribution of sediment from the continental shelf to the abyssal plain in the western Niger Delta since the Pliocene (Fig. 4.10A), compared to the eastern part of the delta, where sediment is generally sequestered within collapsing normal faults with little or no deposition in the deep basin (Fig. 4.10B). See text for a more detailed explanation. See Fig. 4.1A for location of interpreted line.

4.7 Conclusions of chapter 4

- Paleo-topographies associated with (i) the Fernando Po, (ii) the Charcot and (iii) Chain Fracture Zones, developed during the Cretaceous oceanic spreading of the South Atlantic, controlled the geometry of the Niger Delta from the Cretaceous to the Serravallian, acting as sediment transfer zones. However, delta top tectonostratigraphic processes controlled the architectural evolution of the margin from the Serravallian to present.
- Tilting of the margin during the Cretaceous and the development of basin centre-dipping surface, characterized by listric normal faults and basin centre-dipping, seismic reflections over the Cretaceous-Serravallian, suggest the dominance of gravity gliding. However, the overall increase in syn-depositional gravity collapse on the continental shelf and upper slope from the Pliocene-present, suggest deformation of the margin under its weight by gravity spreading.
- Low sedimentary wedge deformation within the extensional and translational zones over the late Eocene-Serravallian, suggests up-dip location of the defunct extensional zone in the onshore, whereas the basinward propagation of deformation to the contractional zone over the Tortonian-Pliocene, seems to record the migration of the extensional zone to its present position, basinward of the modern coastline.
- Although the relatively high sedimentation rates on the western Niger Delta continental shelf and slope regions over the Serravallian-Tortonian, is inferred to have triggered shale tectonics in the area, the overall thinning of the Burdigalian-Serravallian Unit northeastward towards mobile shale and presence of growth strata within piggyback basins, suggest that shale tectonics could have been active since the Burdigalian.
- The dominance of actively subsiding basinward dipping normal faults on the western Niger Delta continental shelf since the early Pliocene facilitated the overall increase in sediment thickness within the extensional zone. Despite the relatively lower sedimentation rates estimated on the western Niger Delta continental shelf and slope regions since the early Pliocene, the overall increase in gravity collapse/accommodation, sediment thickness and distribution from the shelf to the deep basin, suggest an overall increase in sedimentation in this region. However, in the eastern Niger Delta, the actively subsiding counter regional normal faults and inferred delta lobe migration are thought to have contributed to the ongoing reduction in sedimentation notably in the deep basin since the Pleistocene.

- Given the spatio-temporal variation in gravity deformation and sediment partitioning across the western and the eastern Niger Delta structural zones since the early Pliocene, a more regional seismic and well data are needed for a complete source-to-sink (isopach mapping) of the former for a more quantitative comparison of these regions.
- This study not only improves our understanding of the tectonostratigraphic evolution of the western Niger Delta, highlighting the complex structural and stratigraphic trapping styles notably in the underexplored deepwater systems, but also shows the presence of syn-rift deposits that may host the Cretaceous-Paleogene petroleum play in the offshore western Niger Delta.

CHAPTER 5

General conclusions, Limitations and Perspectives

5.1 General conclusions

As the twelfth largest petroleum province in the world, the Cenozoic Niger Delta remains an ideal natural laboratory, globally both for the industry and academia for the study of (i) regional/global climate dynamics; (ii) sea-level variation (iii); gravity-tectonics; (iv) drainage evolution and (v) sediment supply, that control the stratigraphic architecture of a large progradational delta located on a passive margin. Based on detailed tectonostratigraphic studies on the western Niger Delta lobe from the Cretaceous to present, using the integration of regional 2D and high-resolution 3D seismic reflection data, calibrated with well data (see chapters 2, 3 and 4), we draw the following general conclusions:

1. Paleo-topographies (fracture zones), namely (i) the Fernando Po, (ii) the Charcot and (iii) Chain Fracture Zones, linked to the oceanic spreading of the South Atlantic during the Cretaceous, controlled the geometry of the Niger Delta from the Cretaceous to the Serravallian, followed onwards by delta top tectonostratigraphic processes that controlled architectural evolution of the margin to present.
2. Tilting of the margin in the Cretaceous resulted in the development of basin centre dipping regional seismic surface, which facilitated sedimentary wedge deformation mainly by gravity gliding up to the Pliocene, when a remarkable increase in sedimentation rate is thought to have switched the western Niger Delta to a gravity spreading-dominated system over the Pliocene and the Pleistocene.
3. The extensional, translational and contractional zones of the western Niger Delta, evolved through time and space in response to variation in sedimentation and delta top tectonics. Overall low sedimentary wedge deformation between the late Eocene and the Serravallian was interpreted to mark the up-dip location of the defunct extensional zone in the onshore, while onwards increase in delta wedge deformation notably from the Tortonian to present, mark the

basinward migration of the extensional zone, with the proper outer-fold-thrust belt becoming fully developed during the Pliocene.

4. Against the general opinion that mobile shales initiated during the late Miocene and were fossilised during the Pliocene, this research demonstrates that mobile shales have been active in the western Niger Delta since the Burdigalian, and continued up to the Pliocene and the Pleistocene, controlling the morphology, distribution and depositional patterns of submarine channels.
5. Detailed 3D seismic interpretation calibrated with high-resolution 3D seismic geomorphological analysis, revealed the occurrences on the western Niger Delta slope (i) regional MTDs that are generally triggered by failures at the shelf margin/upper slopes, and (ii) local MTDs that are generally derived from mobile shales.
6. The Pliocene and Pleistocene stratigraphy of the western Niger Delta intraslope basins were controlled by the interplay between allocyclic forcing linked to glacio-eustatic sea-level oscillations and basin tectonics associated with shale tectonics, with the latter being more active during the Pliocene and the middle Pleistocene.
7. This research for the first time, demonstrates through detailed cyclostratigraphic and 3D seismic geomorphological analyses, the presence of eccentricity sequences of 400 ka and 100 ka periodicities, linked to orbital (Milankovich) forcing over the Messinian-middle Pleistocene and the middle Pleistocene-present, respectively in the Deepwater Niger Delta.
8. Notwithstanding the relatively lower sedimentation rates estimated on the western Niger Delta continental shelf and slope regions since the early Pliocene, the overall increase in gravity collapse/accommodation, sediment thickness and distribution from the shelf to the deep basin, suggest an overall increase in sedimentation in this region. However, in the eastern Niger Delta, the actively subsiding counter regional normal faults and inferred delta lobe migration are thought to have contributed to the ongoing reduction in sedimentation notably in the deep basin since the Pleistocene.
9. Given the spatio-temporal variation in gravity deformation, shale tectonics and sediment partitioning across the western and the eastern Niger Delta structural zones since the early Pliocene, a more regional seismic and well data are needed for a complete source-to-sink (isopach mapping) of the former for a more quantitative comparison of these regions.

10. This PhD research not only improves our understanding of the tectonostratigraphic evolution of the western Niger Delta, highlighting the complex structural and stratigraphic trapping styles notably in the underexplored deepwater systems, but also shows the presence of syn-rift deposits that may host the Cretaceous-Paleogene petroleum play in the offshore western Niger Delta.

5.2 Research limitations

Although we carefully analyzed and interpreted our data, we note that uncertainties including but not limited to; (i) poor biostratigraphic resolution; (ii) low seismic resolution and seismic reflection continuity problems arising from faulting and mass wasting; (iii) interpretation bias and (iv) errors arising from time-to depth conversions, could have led to overestimation or underestimation of sedimentation rate.

In addition to the limited well information (e.g. absence of biostratigraphic data explained in section 4.5.2), inadequate seismic data coverage of the western Niger Delta continental shelf, slope and deep basin (Fig. 4.1A), did not allow us to carry out complete source-to-sink studies for a more quantitative comparison of these regions to their equivalents in the eastern Niger Delta. Also, the overall decrease in 3D and 2D seismic resolution below 13.7 m and 25 m, respectively at depths >3 seconds two way travel time (3 s TWT), coupled with acoustic blanking associated with the presence of mobile shales, growth/reverse faults and ubiquitous mass wasting on the slope, locally hampered horizon interpretation (see Fig. 4.7 and Appendix 7).

5.3 Perspectives

1. More regional seismic and well data are critical for a complete source-to-sink study of the western Niger Delta. This will not only be useful for the academia in regards of the tectonostratigraphic evolution of the area in comparison with the eastern Niger Delta, but also to the industry as it would facilitate a better understanding of the currently producing fields/discovery of new frontiers (e.g. the Cretaceous-Paleogene plays), that would add to the western Niger Delta offshore assets.

2. There is need for continuous biostratigraphic and lithological data acquisition on the western Niger Delta shelf, slope and the deepwater for a more robust age and lithological calibrations. Among the advantages of these data would be the verification of the presence of or absence of eccentricity cycles of 400 ka and 100 ka within the deepwater western Niger Delta over the Messinian-Middle Pleistocene Transition (MPT) and MPT to present, respectively (see Figs. 4.10).
3. Forward stratigraphic modelling will be critical in the investigation of the interplay between eustatic sea-level changes, sediment supply and gravity tectonics in the stratigraphic evolution of the western Niger Delta.

References Cited

- Adeogba, A.A., McHargue, T.R., and Graham, S.A. 2005, Transient fan architecture and depositional controls from near-surface 3D seismic data, Niger Delta continental slope. AAPG Bulletin 89, 627–643.
- Agnini, C., Fornaciari, E., Raffi, I., Catanzariti, R., Pälke, H., Backman, J., Rio, D., 2014. Biozonation and biochronology of Paleogene calcareous nannofossils from low and middle latitudes. *Newsletters on Stratigraphy* 47, 131–181. <https://doi.org/10.1127/0078-0421/2014/0042>
- Allen, J. R. L., 1965. Late Quaternary Niger Delta and adjacent areas: sedimentary environments and lithofacies. AAPG Bulletin 49, 547-600.
- Allen, J. R. L., 1970, Sediments of the modern Niger delta, *in* Deltaic sedimentation; modern and ancient, p. 138-151: Soc. Econ. Paleontologists and Mineralogists Spec. Pub. 15, 312p.
- Alves, T.M., Cartwright, J., Davies, R., 2009. Faulting of salt-withdrawal basins during early halokinesis: effects on the Palaeogene Rio Doce Canyons System (Espírito Santo Basin, Brazil). AAPG Bulletin 93, 617-652.
- Alves, T.M., Lourenço, S.D.N., 2010. Geomorphologic features related to gravitational collapse: submarine landsliding to lateral spreading on a Late Miocene-Quaternary slope (SE Crete, eastern Mediterranean). *Geomorphology* 123, (1-2), 13-33, <http://dx.doi.org/10.1016/j.geomorph.2010.04.030>
- Alves, T. M., 2015. Submarine slide blocks and associated soft-sediment deformation in deep-water basins: A review. *Marine and Petroleum Geology* 67, 262-285.
- Anthonissen, D.E., Ogg, J.G., 2012. Cenozoic and Cretaceous Biochronology of Planktonic Foraminifera and Calcareous Nannofossils, in: *The Geologic Time Scale*. Elsevier, pp. 1083-1127. <https://doi.org/10.1106/B978-0-444-59425-9-15003>
- Alexander, E. W., Schilager, W., 2000, Observations of experimental non-channelized turbidites: thickness variations around obstacles. *Journal of Sedimentary Research*, 64, 899-909.
- Avbovbo, A. A., 1978, Tertiary lithostratigraphy of the Niger Delta: AAPG Bulletin, 62, 295–300.
- Armitage, S.J., Bristow, C.S., Drake, N.A, 2015, West African monsoon dynamics inferred from abrupt fluctuations of Lake Mega-Chad. *PNAS* 112 (28), 8543-8548.

- Backman, J., Raffi, I., Rio, D., Fornaciari, E., Pälke, H., 2012, Biozonation and biochronology of Miocene through Pleistocene calcareous nannofossils from low and middle latitudes. *Newsl. Stratigr.* 45, 221–244. <https://doi.org/10.1127/0078-0421/2012/0022>.
- Bakare, O., Hurley, N., and McHargue, T., 2007, Effect of Growing Structures on Stratigraphic Evolution, Channel Architecture, and Submarine Fan Distribution, Niger Delta, West Africa. AAPG Conference Proceedings, California.
- Barker, C., 1990. Calculated volume and pressure changes during the thermal cracking of oil and gas in reservoirs, AAPG Bull., 74, 1254-1261.
- Bassinot, F.C., Labeyrie, L.D., Vincent, E., Quidelleur, X., Shackleton, N.J., and Lancelot, Y., 1994, The astronomical theory of climate and the age of the Brunhes-Matuyama magnetic reversal. *Earth and Planetary Science Letters* 126, 91–108.
- Bellingham, P., Connors, C., Haworth, R., Barbara, R., Danforth, Al, 2014. The deep-water Niger delta: an underexplored world class petroleum province. *Petrol. Geosci. Mag.* 11, 1–9.
- Benjamin, U. K., Huuse, M., and Hodgetts, D., 2015, Canyon-confined pockmarks on the western Niger Delta slope. *Journal of African earth Sciences* 107, 15-27.
- Benjamin, U. K., Huuse, M., 2017. Seafloor and buried mounds on the western Niger Delta Slope. *Marine and Petroleum Geology*, 83, 158-173.
- Bilotti, F. D., Shaw, J. H., Cupich, R.M., and Lakings, R.M., 2005, Detachment fold, Niger Delta, in J. H. Shaw, C. Connors, and J. Suppe, eds., *Seismic interpretation of contractional fault related folds: AAPG Studies in Geology* 53, 103-104.
- Birchwood, K. M., 1965, Mud volcanoes in Trinidad. *Institute of Petroleum Reviews*, 19 (221), 164–167
- Booth, J.R., Duvernay, A.E., Pfeiffer, D.S., and Styzen, M.J., 2000, Sequence stratigraphic framework, depositional models, and stacking patterns of ponded and slope fan systems in the Auger Basin: central Gulf of Mexico slope, in Weimer, P., Slatt, R.M., Coleman, J., Rosen, N.C., Nelson, H., Bouma, A.H., Styzen, M.J., and Lawrence, D.T., eds., *Deep-Water Reservoirs of the World: Gulf Coast Section SEPM Foundation, 20th Annual Bob F. Perkins Research Conference*, 82-103.
- Booth, J. R., Dean, M. C., DuVernay III, A. 2003. E., Styzen, M. J Paleo-bathymetric controls on

- stratigraphic architecture and reservoir development of confined fans in the Auger Basin: central Gulf of Mexico slope. *Journal of Marine and Petroleum Geology* 20, 563-586. doi:10.1016/i.marpetgeo.2003.03.008.
- Boulila, S., Galbrun, B., Miller, K. G., Pekar, S. F., Browning, V. B., Lasker, J., Wright, J. D., 2011., On the origin of Cenozoic and Mesozoic “third-order” eustatic sequences. *Earth-Sciences Reviews* (3-4), 94-112.
- Briggs, S. E., Cartwright, J., Davies, R., 2009, Crustal structure of the deepwater west Niger Delta passive margin from the interpretation of seismic reflection data. *Marine and Petroleum Geology* 26, 936-950.
- Briggs, S. E., Cartwright, J., Davies, R., 2009, Crustal structure of the deepwater west Niger Delta passive margin from the interpretation of seismic reflection data. *Marine and Petroleum Geology* 26, 936-950.
- Brooks, J.M., Bryant, W.R., Bernard, B.B., Cameron, N.R., 2000. The nature of gas hydrates on the Nigerian Continental slope. In: *Gas Hydrates: Challenges for the Future: Annals of the New York Academy of Sciences*, 912, 76-93.
- Brown, A.R., 1999. *Interpretation of Three-dimensional Seismic Data*. fifth ed. American Association of Petroleum Geologists, Oklahoma
- Brownfield, M.E., 2016. Assessment of undiscovered oil and gas resources of the Niger Delta Province Nigeria and Cameroon, Africa, in Brownfield, M.E., compiler, *Geologic assessment of undiscovered hydrocarbon resources of Sub-Saharan Africa: USGS Digital Data Series 69–GG, 5, 20*.
- Bruce, C. H., 1984. Smectite dishydration, its relation to structural development and hydrocarbon accumulation in the Northern Gulf of Mexico basin. *AAPG Bull* 68, 673-683.
- Brun, J.-P., Merle, O., 1985, Strain patterns in models of spreading-gliding nappes. *Tectonics* 4, 705–719.
- Burke, K., 1996. The African plate. *S. Afr. J. Geol.*, 99, 339-410.
- Burke, K., 1972. Longshore drift, submarine canyons and submarine fans in development of Niger Delta: *AAPG, Bulletin*, 56, 1975-1983
- Burke, K., D. S. Macgregor, and N. R. Cameron (2003), Africa’s petroleum systems: Four tectonic ‘aces’ in the past 600 million years. *Geol. Soc.*, 207, 21–60.

- Burbank, D.W., 1992, Causes of recent Himalayan uplift deduced from deposited patterns in the Ganges basin. *Nature*, 357, 680–683.
- Canals, M., Lastras, G., Urgeles, R., Casamor, J.L., Mienert, J., Cattaneo, A., De Batist, M., Haflidason, H., Imbo, Y., Laberg, J.S., Locat, J., Long, D., Longva, O., Masson, D.G., Sultan, N., Trincardi, F., Bryn, P., 2004, Slope failure dynamics and impacts from seafloor and shallow sub-sea geophysical data: case studies from the COSTA project. *Mar. Geol.* 213, 9–72.
- Carvajal, C. R., and Steel, R. J., 2006. Thick turbidite successions from supply-dominated shelves during sea-level highstand. *Geology*, 34, 665-668.
- Catuneanu, O., 2006, Principles of sequence stratigraphy. Elsevier, Amsterdam, 386.
- Catuneanu, O., Galloway, W. E., Kendall, C. G. St. C., Miall, A. D., Posamentier, H. W., Strasser, S., and Tucker, M. E., 2011, Sequence stratigraphy: Methodology and Nomenclature. *Newsletter on Stratigraphy*, 44 (3), 173-245.
- Chapin, M., Swinburn, P., van der Weiden, R., Skaloud, D., Adesanya, S., Stevens, D., Varley, C., Wilkie, J., Brentjens, E., and Blaauw, M., 2002, Integrated seismic and subsurface characterization of Bonga Field, offshore Nigeria. *The Leading Edge* 21, 1125-113.
- Chardon, D., Grimaud, J.-L., Rouby, D., Beauvais, A., Christophoul, F., 2016, Stabilization of large drainage basins over geological time scales: Cenozoic West Africa, hot spot swell growth, and the Niger River: hot spot swell growth and Niger River. *Geochemistry, Geophysics, Geosystems* 17, 1164-1181.
- Chima, K. I., Do Couto D., Leroux, E., Gardin, S., Hoggmasacall, N., Rabineau, M., Granjean, D., and Gorini, C., 2019, Seismic stratigraphy and depositional architecture of Neogene intraslope basins, offshore western Niger Delta. *Marine and Petroleum Geology* 109, 449-468. doi: 10.1016/j.marpetgeo.2019.06.030
- Chima, K. I., Gorini, C., Rabineau, M., Granjeon, D., Do Couto, D., Leroux, E., Hoggmascall, N., (*revised*), Pliocene and Pleistocene sedimentary evolution of the western Niger Delta: A record of glacio-eustatic sea-level and basin tectonic forcings. *Global and Planetary Change*.
- Chopra, S., and Marfurt, K.J., 2007, Seismic attributes for prospect identification and reservoir characterization. *Tulsa, Oklahoma*, 457.
- Choudhuri, M., Guha, D., Dutta, A., Sinha, S, Sinha, N., 2010, Spatiotemporal variations and

- kinematics of shale mobility in the Krishna-Godavari basin, India, in L. Wood, ed., *Shale tectonics: AAPG Memoir 93*, 91-109.
- Clark, I. R. and Cartwright, J. A., 2012, Interactions between coeval sedimentations and deformation from the Niger Delta deep-water fold belt. *SEPM* 3, 243-267.
- Clift, P.D., 2010, Enhanced global continental erosion and exhumation driven by Oligo-Miocene climate change. *Geophys. Res. Lett.*, 37, L09402.
- Cobbold, P. R., Szatmari, P., 1991, Radial gravitational gliding on passive margins: *Tectonophysics*, 188, 249-289.
- Cobbold, P. R., Clark., B. J., Løseth, H., 2009, Structural consequences of fluid overpressure and seepage forces in the outer thrust belt of the Niger Delta. *EAGE* 15, 3-15.
- Cobbold, P.R., Mourgues, R., Boyd, K., 2004, Mechanism of thin-skinned detachment in the Amazon Fan: assessing the importance of fluid overpressure and hydrocarbon generation. *Mar. Pet. Geol.* 21, 1013–1025.
- Cohen, H.A., and McClay, K., 1996, Sedimentation and shale tectonics of the northwestern Niger Delta front. *Marine and Petroleum Geology* 13, 313-328.
- Collins, J.A., Schefuß, E., Govin, A., Mulitza, S., Tiedemann, R., 2014, Insolation and glacial-interglacial control on southwestern African Hydroclimate over the last 140,000 years. *Earth and Planetary Science Letters* 398, 1-10.
- Connors, C. D., Denson, D. B., Kristiansen, G. and Angstadt, D. M., 1998, Compressive anticlines of the mid-outer slope, central Niger Delta (abs.) *AAPG Bulletin*, 82, 1903.
- Corredor, F., Shaw, J.H., and Bilotti, F., 2005, Structural styles in the deep-water fold and thrust belts of the Niger Delta. *AAPG Bulletin* 89, 753780. <https://doi.org/10.1306/02170504074>
- Crutchley, G.J., Klaeschen, D., Planert, L., Bialas, J., Berndt, C., Papenberg, C., Hensen, C., Hornbach, M., Krastel, S., Brueckmann, W., 2014, The impact of fluid advection on gas stability: investigation at sites on methane seepage, offshore Costa Rica. *Earth and Planetary Science Letters* 401, 95-109.
- Costa, E., and B. C. Vendeville, 2002, Experimental insights on the geometry and kinematics of fold-and-thrust belts above weak, viscous evaporitic decollement: *Journal of Structural Geology*, 24, 1729–1739, doi:10.1016 /S0191-8141(01)00169-9.
- Covault, J.A., 2011, Submarine fans and canyon-channel systems: a review of processes,

- products, and models. *Nature Education Knowledge* 3(10):4.
- Damuth, J. E., 1994, Neogene gravity tectonics and depositional processes on the deep Niger Delta continental margin: *Marine and Petroleum Geology*, 11, 320–346.
- Davies, R. J., 2003, Kilometer-scale fluidization structures formed during early burial of a deep-water slope channel on the Niger Delta. *GSA* 31 (11) 949-952.
- DeJong, K.A., Scholten, R., 1973, *Gravity and Tectonics*. John Wiley, New York. 502.
- De Landro Clarke, W., 2010, Geophysical aspects of shale mobilization in the deep water off the east coast of Trinidad, in L. Wood, ed., *Shale tectonics: AAPG Memoir 93*, 111-118.
- Deptuck, M.E., Steffens, G.S., Barton, M., Pirmez, C., 2003. Architecture and evolution of upper fan channel-belts on the Niger Delta slope and in the Arabian Sea. *Marine and Petroleum Geology* 20, 649-676.
- Deptuck, M.E., Sylvester, Z., O'Byrne, C., 2012, Pleistocene seascape evolution above a "simple" stepped slope-western Niger Delta, in: Prather, B.E., Deptuck, M.E., Mohrig, D., Van Hoorn, B., Wynn, R.B. (Eds.), *Application of the Principles of Seismic Geomorphology to Continental-Slope and Base-of-Slope Systems: Case Studies from Seafloor and Near-Seafloor Analogues*, pp. 199-222.
- Doust, H., and Omatsola, E., 1990, Niger Delta, in J. D. Edwards and P. A. Santogrossi, (Eds.); *Divergent passive margin basins. AAPG Bulletin* 48, 239-248.
- Duval, B., C. Cramez, and M. P. A. Jackson, 1992, Raft tectonics in the Kwanza Basin, Angola: *Marine and Petroleum Geology*, (9), 389-404.
- Einsele, G., Ricken, W., Seilacher, A., 1991, *Cycles and Events in Stratigraphy*. Springer-Verlag, Berlin, 955.
- Elsley, G., Graham, P., 2006, Mobile shale in the Mackenzie delta-the Pakota shale diapir Complex; in L. Wood, S. Wharton, R. Davies, F. Hossein, and C. Archie, conveners, *Mobile shale basins-Genesis, evolution, and hydrocarbon systems: Proceedings of the AAPG/Geological Society of Trinidad and Tobago Hedberg Conference, Port-of-Spain, Trinidad*
- Ekweozor, C. M., and Daukoru, E.M, 1994. Northern delta depobelt portion of the Akata-Agbada petroleum system, Niger Delta, Nigeria; *In: Magoon, L.B., and Dow, W.G., eds., The Petroleum System-From Source to Trap, AAPG Bulletin* 60, 599-614.
- Eldefield, H., Ferretti, P., Greaves, M., Crownhurst, S. J., McCave, I. N., Hodell, D. A.,

- Piotrowski, A. M., 2012, Stable Oxygen isotope record and Mg/Ca ratios at the Mid-Pleistocene Climate Transition, ODP Site 181-1123. Pangea. Doi: doi.org/10.1594/PANGAEA.786205.
- Elliott, T., 1975, the sedimentary history of a delta lobe from a Yoredale (Carboniferous) cyclothem. Yorkshire Geological Society, Proceedings 40, 505-536.
- Embly, R.W., 1976, New evidence for occurrence of debris-flows deposits in the deep sea. *Geology* 4, 371–374.
- Evamy, B.D., Haremboure, J., Kammerling, R., Knaap, W.A., Molloy, F.A., and Rowlands, P.H., 1978, Hydrocarbon habitat of Tertiary Niger Delta. *AAPG Bulletin* 62, 1-39.
- Fatoka, O.A., Bhattacharya, J.P., 2010, Controls on Depositional Architecture and Sequence Stratigraphy of the Pliocene-Pleistocene Strata of Eastern Niger Delta, Nigeria. AAPG, Abstract, Denver.
- Ferry, J. N., Mulder, J., Praize, O., and Raillad, S., 2005. The concept of equilibrium profile in Deep-water turbidite systems: effects of local physiographic changes on the natural sedimentary process and geometries of deposits. *The Geological Society of London* 244, 181-193.
- Friedman, G.M., Sanders, J.E., Kopaska-Merkel, D.C., 1992, Principles of sedimentary deposits-stratigraphy and sedimentology. Macmillan, New York.
- Frey Martinez, J., Cartwright, J., Hall, B., 2005. 3D seismic interpretation of slump complexes: examples from the continental margin of Israel. *Basin Research* 17, 83-108.
- Gamberi, F., Rovere, M., Marani, M.P., 2011. Mass-transport complex evolution in a tectonically active margin (Gioia Basin, Southeastern Tyrrhenian Sea). *Marine Geology* 279, (1-4), 98-110. 10.1016/j.margeo.2010.10.015
- Gamberi, F., M. Rovere, Marani, M.P., Dykstra, M., 2015. Modern deep-sea fan facies development along a tectonically active margin. *Geosphere*, 11, 307-319. 10.1130/GES01030
- Gamboa, D., Alves, T.M., 2016. Classifications of submarine confluences and implications for intra-canyon sediment distribution. GSA Annual Meeting, Denver, 2016. 10.1130/abs/2016AM-281380
- Frizon de Lamotte, D., Fourdan, B., Leleu, S., Leparmentier, F., and de Clarens, P., 2015, Style of rifting and the stages of Pangea breakup: *Tectonics*, 34, 1009–1029, doi: 10.1002

/2014TC003760

- Galloway, W. E., 2001, Cenozoic evolution of sediment accumulation in deltaic and shore-zone depositional systems, northern Gulf of Mexico Basin: *Marine and Petroleum Geology*, 18, 1031-1040.
- Garcia, M. H., Parker, G., 1989, Experiments on hydraulic jumps in turbidity currents near a canyon fan transition. *Science*, 245, 393-396.
- Gee, M.J.R., Uy, H.S., Warren, J., Morley, C.K., Lambiase, J.J., 2007, The Brunei slide: a giant submarine landslide on the North West Borneo Margin revealed by 3D seismic data. *Mar. Geol.* 246, 9–23.
- Genik, G. J., 1993, Petroleum Geology of Cretaceous-Tertiary Rift Basins in Niger, Chad, and Central African Republic, *AAPG Bulletin*, 77, 1405–1434,
- Gibbard, P. L., Head, M. J, Walker, J. C., 2010, Formal ratification of the Quaternary system Period and the Pleistocene Series/Epoch with a base at 2.58 Ma. *Journal of Quaternary Science* 25 (2), 96-102.
- Gibbard, P. L., Head, M.J., and Walker, M.J., 2014, Subcommission on stratigraphy Formal ratification of the Quaternary System/Period and Pleistocene Series/Epoch with a base at 2.5 Ma. *Quaternary Science* 245, 96-102.
- Gibbard, P.L., Lewin, J., 2016, Partitioning the Quaternary. *Quaternary Science Reviews* 151, 127-139.
- Gonçalves Souza, J. M., Cubas, N., Rabe, C., Letouzey, J., Divies, R., Praeg, D. B., Granjean, D., Cruz, A., M., Silva, C. G., Do Reis, A. T., Gorini, C., 2020. Controls on overpressure evolution during the gravitational collapse of the Amazon deep-sea fan. *Marine and Petroleum Geology* 121, 104576.
- Gorini, C., Haq, B.U., dos Reis, A.T., Silva, C.G., Cruz, A.M., Soares, E., and Grangeon, D., 2014, Late Neogene sequence stratigraphic evolution of the Foz do Amazonas Basin, Brazil. *Terra Nova*, 26, (3), 179-185. <https://doi.org/10.1111/ter.12083>.
- Goudie, A. S., 2005, the drainage of Africa since the Cretaceous. *Gemorphology* (3-4), 437-456.
- Govin, A., Varma, V., Prange, M., 2014, Astronomically forced variations in western African rainfall (21°N-20°S) during the Last Interglacial period. *Geophysical research Letters* 41, 2117-2125. doi:10.1002/2013GL058999.
- Graue, K., 2000. Mud volcanoes in deep-water Nigeria. *Marine and Petroleum Geology* 17, 959-974. [https://doi.org/10.1016/S0264-8172\(00\)00016-7](https://doi.org/10.1016/S0264-8172(00)00016-7)

- Grimaud, J.-L. 2014, Dynamique long-terme de l'érosion en contexte cratonique: l'Afrique de l'Ouest depuis l'Eocène. PhD Thesis, Toulouse University, Toulouse, France.
- Grimaud, J.-L., Rouby, D., Chardon, D., Beauvais, A., 2017. Cenozoic sediment budget of West Africa and the Niger delta. *Basin Research*, 1-18.
- Guliev, I. S. 1992. A review of mud volcanism. Translation of the report by: Azerbaijan Academy of Sciences Institute of Geology, 65.
- Gulick, S.P., Jaeger, J.M., Mix, A.C., Asahi, H., Bahlburg, H., Belanger, C.L., Berbel, G.B., Childress, L., Cowan, E., Drab, L., Forwick, M., 2015, Mid-Pleistocene climate transition drives net mass loss from rapidly uplifting St. Elias Mountains, Alaska. *Proc. Natl. Acad. Sci. Unit. States Am.* 112, 15042–15047.
- Hampton, M., Lee, H.J., Locat, J., 1996. Submarine landslides. *Rev. Geophys*, 34, 33–59.
- Hansen, L., Janocko, M., Kane, I., Kneller, B., 2017. Submarine channel evolution, terrace development, and preservation of intra-channel thin-bedded turbidites: Mahin and Avon channels, offshore Nigeria. *Mar. Geol.* 383, 146–167. <https://doi.org/10.1016/j.margeo.2016.11.011>.
- Haq, B.U., Hardenbol, J., Vail, P.R., 1987. Chronology of fluctuating sea levels since the triassic. *Science* 235, 1156-1167.
- Head, M.J., Gibbard, P.L., 2015a, Early-Middle Pleistocene transitions: linking terrestrial and marine realms. *Quat. Int.* 389, 7-46. <http://dx.doi.org/10.1016/j.quaint.2015.09.042>
- Head, M.J., Gibbard, P.L., 2015b, Formal subdivision of the Quaternary System/Period: past, present, and future. *Quat. Int.* 383, 1-32.
- Heiniö, P., and Davies, R. J. 2007, Knickpoint migration in submarine channels in response to fold growth, western Niger Delta. *Marine and Petroleum Geology* 24, 434-449. doi.org/10.1016/j.marpetgeo.2006.09.002.
- Hooper, R. J., Fitzsimmons, R. J., Neil, G., Vendeville, B. C., 2002, The role of deformation in controlling depositional patterns in the south-central Niger Delta, west Africa: *Journal of Structural Geology*, 24, 847–859, doi:10.1016/S0191-8141(01)00122-5.
- Hudec, M., R., Jackson, M. P. A., 2004, Regional restoration across the Kwanza Basin, Angola: Salt tectonics triggered by repeated uplift of a metastable passive margin. *AAPG Bulletin* 88 (7), 971-990.
- Hovland, M., Gallagher, J.W., Clennell, M.B., Lekvam, K., 1997, Gas hydrate and free gas

- volumes in marine sediments: example from the Niger Delta front. *Mar. Petroleum Geol.* 14 (3), 245-255.
- Imbrie, J., Berger, A., Boyle, E.A., Clemens, S.C., Duffy, A., Howard, W.R., Kukla, G., Kutzbach, J.E., Martinson, D.G., McIntyre, A., Mix, A.C., Molfino, B., Morley, J.J., Peterson, L.C., Pisias, N.G., Prell, W.L., Raymo, M.E., Shackleton, N.J., and Toggweiler, J.R., 1993, On the structure and origin of major glaciation cycles 2. The 100,000-year cycle. *Paleoceanography* 8, 699-735.
- Jackson, M.P.A., Vendeville, B.C., Schultz-Ela, D.D., 1994, Structural dynamics of salt systems. *Annu. Rev. Earth Planet. Sci.* 22, 93–117.
- Jermannaud, P., Rouby, D., Robin, C., Nalpas, T., Guillocheau, F., and Raillard, S., 2010, Plio-Pleistocene sequence stratigraphic architecture of the eastern Niger Delta: A record of eustasy and aridification of Africa. *Marine and Petroleum Geology* 27, 810-821.
- Jervey, M.T., 1988, Quantitative geological modelling of siliclastic rock sequences and their seismic expressions. In: Wilgus, C.K., Hastings, B.S., St Kendall, C.G., Ross, C.A., Van Wagoner, J.C. (Eds.), *Sea-level Changes: An Integrated Approach*. SEPM Special Publication, Tulsa, 47-69.
- Jobe, Z.R., Lowe, D. R., Uchytel, S.J., 2011, Two fundamentally different types of submarine canyons along the continental margin of Equatorial Guinea. *Marine and Petroleum Geology* 28, 843-860.
- Jobe, Z.R., Sylvester, Z., Parker, A.O., Howes, N., Slowey, N., Pirmez, and C., 2015, Rapid adjustment of submarine channel architecture to changes in sediment supply. *Journal of Sedimentary Research* 85, 729-753.
- Jobe, Z.R., Sylvester, Z., Howes, N., Pirmez, C., Parker, A., Cantelli, A., Smith, R., Wolinsky, M.A., O’Byrne, C., and Slowey, N., 2016, High resolution, millennial-scale patterns of bed compensation on a sand-rich intraslope submarine fan, western Niger Delta slope. *GSA Bulletin* 129, 23-37.
- Jolly, B.A., Lonergan, L., Whittaker, A.C., 2016. Growth history of fault-related folds and interaction with seabed channels in the toe-thrust region of the deep-water Niger Delta. *Mar. Pet. Geol.* 70, 58–76.
- Karner, G. D., 2000. Rifts of the Campos and Santos Basin, Southeastern Brazil: Distribution and timing. *AAPG memoir* 73, 301-315.

- Kehle, R.O., 1989, The origin of salt structures. In: Schreiber, C.B. (Ed.), *Evaporites and hydrocarbons*. Columbia Univ. Press, NY, pp. 345-404.
- Komar, P. D., 1971, Hydraulic jumps in turbidity currents. *Geological Society of America*, 82, 1477-1488.
- Kulke, H., 1995, Nigeria; *In: Kulke, H., ed., Regional Petroleum Geology of the World. Part II: Africa, America, Australia and Antarctica: Berlin, Gebrüder Borntraeger, 143-172.*
- Kneller, B., McCaffrey, W., 1999. Depositional effects of flow nonuniformity and stratification within turbidity currents approaching a bounding slope: deflection, reflection and facies variation. *Journal of Sedimentary Research*, 69(5), 980-991.
- Lehner, P., De Ruiter, P.A.C., 1977. Structural history of Atlantic margin of Africa. *AAPG Bulletin* 61, 961–981.
- Le Pichon, X., Hayes, D.E., 1971. Marginal offsets, fracture zones and the early opening of the South Atlantic. *Journal of Geophysical Research* 76 (26), 6283–6293.
- Leroux, E., Rabineau, M., Aslanian, D., Gorini, C., Droz, L. and Granjeon, D., 2014, Stratigraphic simulation on the shelf of the Gulf of Lions: testing subsidence rates and sea-level curves during Pliocene and Quaternary. *Terra Nova*, 26, 230-238.
- Leroy, S.A.G., Wrenn, J.H., Suc, J.P., 1999, Global setting to comparative charts of regional events. In: Wrenn, J.H., Suc, J.P., Leroy, S.A.G. (Eds.), *The Pliocene: Time of Change*. American Association of Stratigraphic Palynologist Foundation, 1-12.
- Lisiecki, L.E., and Raymo, M.E., 2005, A Pliocene-Pleistocene stack of 57 globally distributed benthic $\delta^{18}\text{O}$ records. *Paleoceanography* 20, PA1003. doi:10.1029/2004PA001071.
- Lisiecki, L.E., and Raymo, M.E., 2007, Plio-Pleistocene climate evolution: trends and transitions in glacial cycle dynamics. *Quaternary Science Reviews* 26, 46-69.
- Liu, L., Zhang, T., Zhao, X., Wu, S., Hu, J., Wang, X., Zhang, Y., 2013, Sedimentary architecture models of deepwater turbidite channel systems in the Niger Delta continental slope, West Africa. *Petroleum Science* 10, 139-148.
- Lézine, A-M., Bassinot, F., Peterschmitt, J-Y., 2014, orbitally-induced changes of the Atlantic and Indian monsoons over the past 20,000 years: New insights based on the comparison of continental and marine records.
- Løseth, H., Gading, M., Wensaas, L., 2009. Hydrocarbon leakage interpreted on seismic data. *Marine and Petroleum Geology* 26, 1304–1319.

- Løseth, H., Wensaas, L., Arntsen, B., Hanken, N.-M., Basire, C., Graue, K., 2011. 1000 m long gas blow-out pipes. *Mar. Pet. Geol.* 28, 1047, 10-60.
- Lowe, D.R., 1982. Sediment gravity flows: II. Depositional models with special reference to the deposits of high-density turbidity currents. *Journal of Sedimentary Petrology* 52 (1), 279-297.
- Madof, A.S., Christie-Blick, N., Anders, M.H., Febo, L.A., 2017, Unreciprocated sedimentation along a mud-dominated continental margin, Gulf of Mexico, U.S.A.: Implications for sequence stratigraphy in muddy settings devoid of depositional sequences. *Marine and Petroleum Geology* 80, 492-516.
- Masson, D.G., Watts, A.B., Gee, M.J.R., Urgeles, R., Mitchell, N.C., Le Bas, T.P., Canals, M., 2002. Slope failures on the flanks of the western Canary Islands. *Earth-Science Reviews* 57 (1-2), 1-35
- Maloney, D., Davies, R., Imber, J., Higgins, S., King, S., 2010, New insights into deformation mechanisms in the gravitationally driven Niger Delta deep-water fold and thrust belt. *AAPG Bulletin* 94, (9), 1401-1424.
- Maudit, T., Guerin, G., Brun, J.-P., Lecanu, H., 1997. Raft tectonics: the effects of basal slope angle and sedimentation rate on progressive extension. *J. Struct. Geol.* 19, 1219-1230.
- Mayall, M., 2000, Deep-water sedimentary systems: new models for the 21st century. *Marine and Petroleum Geology*, 17, 125–135.
- Mayall, M., Stewart, I., 2000. The architecture of turbidite slope channels, in: Weimer, P., Slatt, R.M., Coleman, J., Rosen, N.C., Nelson, H., Bouma, A.H., Styzen, M.J., and Lawrence, D.T., (Eds.), *Deep-Water Reservoirs of the World: SEPM, Gulf Coast Section, 20th Annual Research Conference*, 578-586.
- Mayall, M., Jones, E., Casey, M., 2006, Turbidite channel reservoirs – key elements in facies prediction and effective development: *Marine and Petroleum Geology*, 23, 677–690.
- McHargue, T., Pyrcz, M.J., Sullivan, M.D., Clark, J.D., Fildani, A., Romans, B.W., Covault, J.A., Levy, M., 2011. Architecture of turbidite channel systems on the continental slope: patterns and predictions. *Marine and Petroleum Geology*, 28, 728 –743.
- Miall, A.D., 2010, *The Geology of Stratigraphic Sequences*, second ed. Springer-Verlag, Berlin, 522.
- Middleton, G.V., Hampton, M.A., 1973, *Sediment gravity flows: mechanics of flow and*

- deposition. In: Middleton, G.V., Bouma, A.H., (Eds.), *Turbidites and Deep-water Sedimentation*. Los Angeles, CA: Society of Economic Paleontologists and Mineralogists, 1-38.
- Miller, K.G., Kominz, M.A., Browning, J.V., Wright, J.D., Mountain, G.S., Katz, M.E., Sugarman, P.J., Cramer, B.S., Christie-Blick, N., and Pekar, S.F., 2005, The Phanerozoic Record of Global Sea Level Change. *Science Magazine* 310, 1293-1298.
- Mitchum, R.M., and Vail, P.R., 1977, *Seismic Stratigraphy and Global Changes of Sea Level, Part 7: Seismic Stratigraphic Interpretation Procedure: Seismic Stratigraphy: Applications to Hydrocarbon Exploration*. AAPG Memoir 26, 135-143.
- Morgan, R., 2004, Structural controls on the positioning of submarine channels on the lower slopes of the Niger Delta, in: Davies, R.J., Cartwright, J., Stewart, S.A., Underhill, J.R., Lappin, M. (Eds.), *3D Seismic Technology: Application to the Exploration of Sedimentary Basins*. Geological Society of London Memoir 29, 45-51
- Molnar, P., 2004, Late Cenozoic increase in accumulation rates of terrestrial sediment: how Might Climate Change Have Affected Erosion Rates? *Annu. Rev. Earth Planet. Sci.*, 32, 67-89.
- Morley, C. K., and Guerin, G., 1996. Comparison of gravity-driven deformation styles and behavior associated with mobile shales and salt. *Tectonics* 15, 1155-1170.
- Morley, C. K., King, R., Hillis, R., Tingay, M., Backe, G., 2011, Deep-water fold and thrust belt classification, tectonics, structure and hydrocarbon prospectivity. *Earth Sciences Reviews* 104, 41-91.
- Mourgues, R., Lecomte, E., Vendeville, B., Raillard, S., 2009, An experimental investigation of gravity-driven shale tectonics in progradational delta. *Tectonics*, 474, 643-656.
- Moulin, M., Aslanian, D., Unterneher, P., 2010, A new starting point for the South and Equatorial Atlantic Ocean. *Earth-Science Reviews* (98), 1-37.
- Mulder, T., and Syvitski, J.P., 1995, Turbidity currents generated at river mouths during exceptional discharges to the world oceans: *The Journal of Geology*, 103, 285–299.
- Mutti, E., Normark, W.R., 1991, An integrated approach to the study of turbidite systems. In: Weimer, P., and Link, M.H., (Eds.), *seismic facies and sedimentary processes of modern and ancient submarine fans*. New York, Springer-Verlag, 75–106.
- Navarre, J-C, Claude, D., Liberelle, E., Safa, P., Vallon, G., Keskes, N., 2002, Deepwater turbidite

- system analysis, West Africa: Sedimentary model and implications for reservoir model construction. *The Leading Edge*, 21, 1132-1139. Nedeco River studies and recommendations on improvement of Niger and Benue: Amsterdam, 1000.
- Nelson, C.H., Escutia, C., Damuth, J.E., Twichell, D.C., 2009, Interplay of mass-transport and turbidite-system deposits in different active tectonic and passive continental margin settings: external and local controlling factors. In: Shipp, R.G., Weimer, P., Posamentier, H.W., (Eds.), *Mass-Transport Deposits in Deepwater Settings*, SEPM, Special Publication, 96, 39–66.
- Nurnberg, D., Muller, R.D., 1991. The tectonic evolution of the South Atlantic from Late Jurassic to present. *Tectonophysics* 191 (1–2), 27–53.
- Nwachukwu, S. O., 1972, The tectonic evolution of the southern portion of the Benue Trough, Nigeria: *Geological Magazine*, 109, 411–419
- Omosanya, K.O., Alves, T. M., 2013. A 3-dimensional seismic method to assess the provenance of Mass-Transport Deposits (MTDs) on salt-rich continental slopes (Espírito Santo Basin, SE Brazil). *Marine and Petroleum* 44, 223-239.
- Omosanya, K. O., Harishidayat, D., 2019. Seismic geomorphology of Cenozoic slope deposits and deltaic clinoforms in the Great South Basin (GSB) offshore New Zealand. *Geo-Marine Letters*, 39, 77-99. <https://doi.org/10.1007/s00367-018-00558-8>
- Peel, F. J., 2014, The engines of gravity-driven movement on passive margins: Quantifying the relative contribution of spreading vs. gravity sliding mechanisms. *Tectonophysics* 633, 126-142.
- Picot M., Marsset T., Droz L., Dennielou B., Baudin F., Hermoso M., De Rafelis M., Sionneau T., Cremer M., Laurent D., Bez M., 2019, Monsoon control on channel avulsions in the Late Quaternary Congo Fan. *Quaternary Science Reviews*, 204, 149-171.
- Piper, D.J.W., Pirmez, C., Manley, P.L., Long, D., Flood, R.D., Normark, W.R., Showers, W., Z, 1997. Mass-transport deposits of the Amazon Fan, in: Flood, R.D., Piper, D.J.W., Klaus, A., and Peterson, L.C., (Eds.), *Proceedings ODP, Scientific Results*, 155, 109–146.
- Pälike, H., Frazier, J., Zachos, J.C., 2006. Extended orbitally forced palaeoclimatic records from the equatorial Atlantic Ceara Rise. *Quaternary Science Reviews* 25, 3138–3149.
- Porebski, S.J., and Steel, R.J., 2003. Shelf-margin deltas: their stratigraphic significance and

- relation to deep-water sands: *Earth-Science Reviews* 62, 283–326.
- Posamentier, H.W., Jervey, M.T., and Vail, P.R., 1988, Eustatic controls on clastic deposition I. Conceptual framework. In: Wilgus, C.K., Hastings, B.S., Kendall, C.G.S.C., Posamentier, H.W., Ross, C.A., Van Wagoner, J.C. (Eds.), *Sea-Level Changes-an Integrated Approach*. SEPM Special Publication 42, 102-124.
- Posamentier, H.W., and Kolla, V., 2003, Seismic geomorphology and stratigraphy of depositional elements in deep-water settings. *Journal of sedimentary research* 73, 367–388.
- Prather, B.E., Booth, J.R., Steffens, G.S., Craig, P.A., 1998, Classification, Lithologic Calibration and Stratigraphic Succession of Seismic Facies of Intraslope Basins, Deep- Water Gulf of Mexico. *AAPG Bulletin* 82 (5A), 701-728.
- Prather, B. E. 2000. Calibration and visualization of depositional process models for above-grade slopes: a case study from the Gulf of Mexico. *Marine and Petroleum Geology*, 17(5), 619-638.
- Prather, B.E., 2003, Controls on reservoir distribution, architecture and stratigraphic trapping in slope settings. *Mar. Petrol.* 20, 529-545.
- Prather, B.E., Pirmez, C., Sylvester, Z., and Prather, D. S., 2012 Stratigraphic Response to Evolving Geomorphology in a Submarine Apron Perched on the Upper Niger Delta Slope. *SEPM* 99, 145-161.
- Pulham, A.J., 1989, Controls on internal structure and architecture of sandstone bodies within Upper Carboniferous fluvial-dominated deltas, County Clare, western Ireland. In: Whateley, M.K.G., Pickering, K.T. (Eds.), *Deltas: Sites and Traps for Fossil Fuels*. Geological Society, Special Publication, 41, 79-203.
- Qin, Y., Alves, T. M., Constantine, J., and Gamboa, D., 2016. Quantitative seismic geomorphology of a submarine channel system in SE Brazil (Espírito Santo Basin): Scale comparison with other submarine channel systems. *Marine and Petroleum Geology* 78, 455-473. <https://doi.org/10.1016/j.marpetgeo.2016.09.024>
- Raffi, I., Agnini, C., Backman, J., Catanzariti, R., and Pälke, H., 2016. A Cenozoic calcareous nannofossil biozonation from low and middle latitudes: A synthesis
- Rabineau, M., Berné, S., Olivet, J-L., Aslanian, D., Joseph, P., and Guillocheau, F., 2006, Paleosea levels reconsidered from direct observation of paleo-shoreline position during Glacial Maxima (for the last 500 000 yr). *Earth and Planetary Science Letters*, 252 (1-2), 119-137 DOI: 10.1016/j.epsl.2006.09.033

- Rabineau, M., Leroux, E., Aslanian, D., Bache, F., Gorini, C., Moulin, M., Molliex, S., Droz, L., Dos Reis, T., Rubino, J-L., Olivet, J-L., 2014. Quantifying subsidence and Isostasy using paleobathymetric markers : example from the Gulf of Lion, EPSL, vol. 388, p. 353-366.
- Rainbowitz, P.D., LaBrecque, J., 1979. The Mesozoic South Atlantic Ocean and evolution of its continental margins. *Journal of Geophysical Research* 84 (B11), 5973-6002.
- Raillard, S., Vendeville, B. C., Guérin, G., 1997, Causes and structural characteristics of thin-skinned inversion during gravity gliding or spreading above salt or shale [abs.]: AAPG Annual Convention Official Program, A95.
- Ramberg, H., 1981, Gravity, deformation and the Earth's crust in theory, experiments and geological application (2nd Edition): London, Academic Press, 452.
- Raymo, M. E., Kozdon, R., Evans, D., Lorraine, E., Lisiecki, L., Ford, H. L., 2018, The accuracy of mid-Pliocene $\delta^{18}\text{O}$ based ice volume and sea level reconstructions. *Earth Science Reviews* 177, 291-302.
- Reijers, T. J. A., S. W. Petters, and C. S. Nwajide, 1997. The Niger Delta basin, in R. C. Selley, ed., *African basins: Amsterdam, Elsevier Science, Sedimentary Basins of the World* 3, 151–172.
- Reijers, T. J. A., 2011, Stratigraphy and sedimentology of the Niger Delta. *Geologos* 17 (13), 133-162.
- Reis, A. T., Araujo, E., Silva, C. G., Cruz, A. M., Gorini, C., Droz, L., Migéon, S., Perovano, R., King, I., bache, F., 2016, Effects of a regional décollement level for gravity tectonics on late Neogene to recent large-scale slope instabilities in the Foz do Amazonas Basin, Brazil. *Marine and Petroleum Geology*, 75, 29-52.
- Restrepo-Pace, P., 2018, Ductile v. Brittle'-Alternative structural interpretations for the Niger Delta. *Geological Society of London Special Publication* 46, 1-12.
- Riboulot, V., Cattaneo, A., Lanfumey, V., Voisset, M., Cauquil, E., 2011, Morphological Signature of Fluid Flow Seepage in the Eastern Niger Submarine Delta (ENSD). *Offshore Technology Conference*.
- Riboulot, V., Cattaneo, A., Berné, S., Schneider, R.R., Voisset, M., Imbert, P., Grimaud, S., 2012, Geometry and chronology of late Quaternary depositional sequences in the Eastern Niger Submarine Delta. *Marine Geology*, 319-322, 1-20.

- Richardson S.E.J, Davies R. J, Allen M.B., Grant S.F., 2011 Structure and evolution of mass transport deposits in the South Caspian Basin, Azerbaijan. *Basin Research* 23:702-719.
- Ricketts, B.D., and Evenchick, C.A., 1999, Shelf break Gullies; Products of Sea-level Lowstand and Sediment Failure: Examples from Bowser Basin, Northern British Columbia. *Journal of Sedimentary Research* 69 (6), 1232-1240.
- Ridente, D., Trincardi, F., Piva, A., Asioli, A., Cattaneo, A., 2008, Sedimentary response to climate and sea level change during the past ~400 kyr from borehole PRAD1-2 (Adriatic Margin). *Geochemistry, Geophysics, and Geosystems*. 20 doi: <http://dx.doi.org/10.1029/2007GC0017839/9Q09R04>,
- Robin, C., F. Guillocheau, S. Jeanne, F. P., and Calve's, G., 2011. Cenozoic siliciclastic fluxes evolution around Africa, *Geophys. Res. Abstr.*, 13, EGU, 2011-5659.
- Rouby, D., Nalpas, T., Jermannaud, P., Robin, C., Guillocheau, F., and Raillard, S., 2011, Gravity driven deformation controlled by the migration of the delta front: The Plio-Pleistocene of the Eastern Niger Delta. *Tectonophysics* 513, 54-67. <https://doi.org/10.1130/GEOSO1426.1>
- Rowan, M. G., Peel, F. J., Vendeville, B. C., 2004, Gravity-driven fold belts on passive margins: In: McClay, K. R. (Ed.), 2004. *Thrust Tectonic and Hydrocarbon Systems*, AAPG Memoir 82, 157-182.
- Ruddiman, W.F., Raymo, M.E., Martinson, D.G., Clement, B.M., and Backman, J., 1989, Pleistocene evolution: northern hemisphere ice sheets and North Atlantic Ocean. *Paleoceanography* 4, 353-412.
- Rovere, M., Gamberi, F., Mercorella, A., leidi, Elisa., 2014. Geomorphometry of a submarine mass-transport complex and relationships with active faults in a rapidly uplifting margin (Gioia Basin, NE Sicily margin). *Marine Geology*. <http://dx.doi.org/10.1016/j.margeo.2013.06.003>
- Sapin, F., Ringenbach, J-C., Rives, T., Pubellier, M., 2012, Counter-regional faults in shale-dominated deltas: origin, mechanism and evolution. *Marine and Petroleum Geology* 37, 121-128.
- Shackleton, N.J., 2000, The 100,000-year Ice-Age cycle identified and found to lag temperature, carbon dioxide, and orbital eccentricity. *Science* 289.
- Shanmugam, G., 2016, Sumarine fans: A critical retrospective. *Journal of Paleogeography*, 5(2),

110-184.

- Shepard, F.P., McLoughlin, P.A., Marshall, N.F., Sullivan, G.G., 1977. Current-meter recordings of low speed turbidity currents. *Geology*, 5, 297– 301.
- Short, K. C., and Stauble, A. J. 1967. Outline of geology of Niger Delta: AAPG Bulletin, 51, 761–779.
- Schultz-Ela, D. D., 2001, Excursus on gravity gliding and gravity spreading. *Journal of Structural Geology*, 23 (5), 725-731
- Smith, W. H. F., and Sandwell, D. T., 1997, Global seafloor topography from satellite altimetry and ship depth soundings: *Science*, (277), 1957-1962.
- Snead, R. E., 1972, Mud volcanoes of the Makran coast. *Exploration Journal*, 50 (1), 22–28.
- Soto, J. I., Fernandez-Ibanez, F., Talukder, A.R., Martinez-Garcia, P., 2010, Miocene shale tectonics in the northern Alboran Sea (western Mediterranean), in L. Wood, ed., *Shale tectonics: AAPG Memoir 93*, 119-143.7
- Sprague, A.R.G., Garfield, T.R., Goulding, F.J., Beaubouef, R.T., Sullivan, M.D., Rossen, C., Campion, K.M., Sickafoose, D.K., Abreu, V., Schellpeper, M.E., Jensen, G.N., Jennette, D.C., Pirmez, C., Dixon, B.T., Ying, D., Ardill, J., Morhig, D.C., Porte, M.L., Farrel, M.E., Mellere, D., 2005, Integrated slope channel development models: The key to successful prediction of reservoir presence and quality in offshore west Africa. CIPM, cuarto E1214 Exitep, Veracruz, Mexico, 1-13.
- Stow, D.A.V., and Piper, D.J.W., 1984, Deep-water fine-grained sediments: facies models. In: Stow, D.A.V., Piper, D.J.W. (Eds.), *Fine-grained Sediments: Deep-Water Processes and Facies*. Geological Society of London Special Publication, 15, 611-645.
- Stow, D.A.V., Sultan, N., Ribolout, V, Ker., S, Marsset, B, Tary, J. B., Voisset, M., Lanfumey, V, Ifremer, J. L., Colliat, J., Adamy, J., and Grimaud, T., 2012. Pore pressure monitoring of active faults- Fluid Hydrate System in Deep Water, Nigeria. *Offshore Technology conference*, 1-9.
- Suter, J.R., and Berryhill, H.L., J. R., 1985. Late Quaternary shelf margin deltas, northwest Gulf of Mexico, AAPB, Bulletin 69, 77–91.
- Tari, G., Molnar, J., Ashton, P., 2003, Examples of salt tectonics from West Africa: a comparative approach. *In: Doyle, P., Gregory, F.J., Griffiths, J.S., Hartley, A.J., Holdsworth, R.E., Morton, A.C., Robins, N.S., Stocker, M.S., Turner, J.P. (Eds.), Petroleum Geology of*

- Africa: New Themes and Developing Technologies: Geol. Soc. London Special Publication, 207, 85-104.
- Taner, M.T., Schuelke, J.S., O'Doherty, R., and Baysal, E., 1994, Seismic attributes revisited. In: SEG technical program expanded abstracts 1994. <https://doi.org/10.1190/1.1822709>.
- Thornton, S.E., 1984. Hemipelagites and Associated Facies of Slopes and Slope Basins. In: Geological Society of London, Special Publications, 15, 377-394.
- Tuttle, W.L.M, Brownfield, E.M., Charpentier, R.R., 1999, The Niger Delta Petroleum System Chapter A: Tertiary Niger Delta (Akata-Agbada) Petroleum System, Niger Delta Province, Nigeria, Cameroon and Equatorial Guinea, Africa. USGS, Open File Report. 99-50-H, 4-44.
- Urvoy, Y., 1942, Les Bassins du Niger. Etude de géographie physique et de paléogéographie: Mem. De l'Institut Français de l'Afrique Noire, no. 4.
- Van Rensbergen, P., C. K. Morley, D. W. Ang, T. Q. Hoan, and N. T. Lam, 1999, Structural evolution of shale diapirs from reactive rise to mud volcanism: 3-D seismic data from the Baram Delta, offshore Brunei Darussalam: Journal of the Geological Society, v. 156, p. 633–650, doi:10.1144/gsjgs.156.3.0633.
- Vendeville, B.C., 2005. Salt tectonics driven by sediment progradation: Part 1-Mechanisms and kinematics. AAPG Bull. 89, 1071–1079.
- Voute, C., 1962, Geological and morphological evolution of the Niger and Benue Valleys: Actes IVe Congrès Panafricain de Préhistoire et de l'étude du Quaternaire, 8, (40), 89-205.
- Warren, J. K., Cheung, A., Cartwright, I., 2010, Organic geochemical, isotopic, and seismic indicators of fluid flow in pressurized growth anticlines and mud volcanoes in modern deep-water slope and rise sediments of offshore Brunei Darussalam: Implications for hydrocarbon exploration in other mud-and salt-diapir provinces, in L. Wood, ed., Shale tectonics: AAPG Memoir 93, 161-194.
- Weimer, P., Buffler, R., 1992, Structural geology and evolution of the Mississippi Fan Fold Belt, deep Gulf of Mexico. AAPG Bulletin 76, 225-251.
- Weldeab, S., Frank, M., Stichel, T., Haley, B., Sangen, M., 2011, Spatio-temporal evolution of the West African monsoon during the last deglaciation. Geophysical Research Letters, 38, L13703. doi:10.1029/2011gl047805.
- Whiteman, A.J., 1982. Nigeria: Its petroleum geology resources and potential Parts II and I:

- Edinburgh/London, Graham and Trotman, 39.
- Wiener, R.W., Mann, M. G., Angelich, M. T., and Molyneux, J. B., 2010, Mobile shale in the Niger Delta: Characteristics, structure, and evolution. AAPG, 93, 145-161.
- Wood, L.J., 2000, Chronostratigraphy and tectonostratigraphy of the Columbus Basin, eastern eastern offshore Trinidad. AAPG Bull. 84, 1905–1928.
- Worrall, D. M., Snelson, S., 1989, Evolution of the northern Gulf of Mexico, with emphasis on Cenozoic growth faulting and the role of salt, in A. W. Bally and A. R. Palmer, eds., *The Geology of North America: an overview*: Geological Society of America, *The Geology of North America*, A, 97-138.
- Wu, S., Bally, A. W 2000. Slope tectonics. Comparisons and contrasts of structural styles of salt and shale tectonics of the northern Gulf of Mexico with shale tectonics of offshore Nigeria in Gulf of Guinea, in W. Mohriak and M. Talwani, eds., *Atlantic rifts and continental margins*: Washington, D.C., American Geophysical Union, 151-172.
- Wu, J. E., McClay, K., Frankowicz, E., 2015, Niger Delta gravity-driven deformation above the relict Chain and Charcot fracture zones, Gulf of Guinea: Insights from analogue models. *Marine and Petroleum Geology* 65, 43-62.
- Wu, N.N., Jackson, C. A-L., Johnson, H. D., Hodgson, D. M., Nugraha, H. D., 2020, Mass-transport complexes (MTCs) document subsidence patterns in 1 a northern Gulf of Mexico salt minibasin. *Basin Research*, 1-28. DOI: 10.1111/bre.12429
- Wynn, R.B., Masson, D.G., Stow, D.A.V., Weaver, P.P.E., 2000a. Turbidity current sediment waves on the submarine slopes of the western Canary Islands. *Marine Geology*, 163, 185-198.
- Ye, J., Chardon, D., Rouby, D., Guillocheau, F., Dall’asta, M., Ferry, J.-N., Broucke, O., 2017. Paleogeographic and structural evolution of northwestern Africa and its Atlantic margins since the early Mesozoic. *Geosphere* GES01426.1.
- Yoo, D-G., Kim, K-Y., Kang, N-K., Yi, B-Y., Cho, M-H., 2017, Plio-Quaternary seismic stratigraphy and depositional history of the Ulleung Basin, East Sea: Association with debris-flow activity. *Quaternary International*, 459, 69-88
- Zecchin, M. 2007, The architectural variability of small-scale cycles in shelf and ramp clastic systems: the controlling factors. *Earth-Sci. Rev.*, 84, 21-55.
- Zecchin, M., Caffau, M., Tosi, L., Civile, D., Brancolini, G., Rizzetto, F., and Roda, C., 2010,

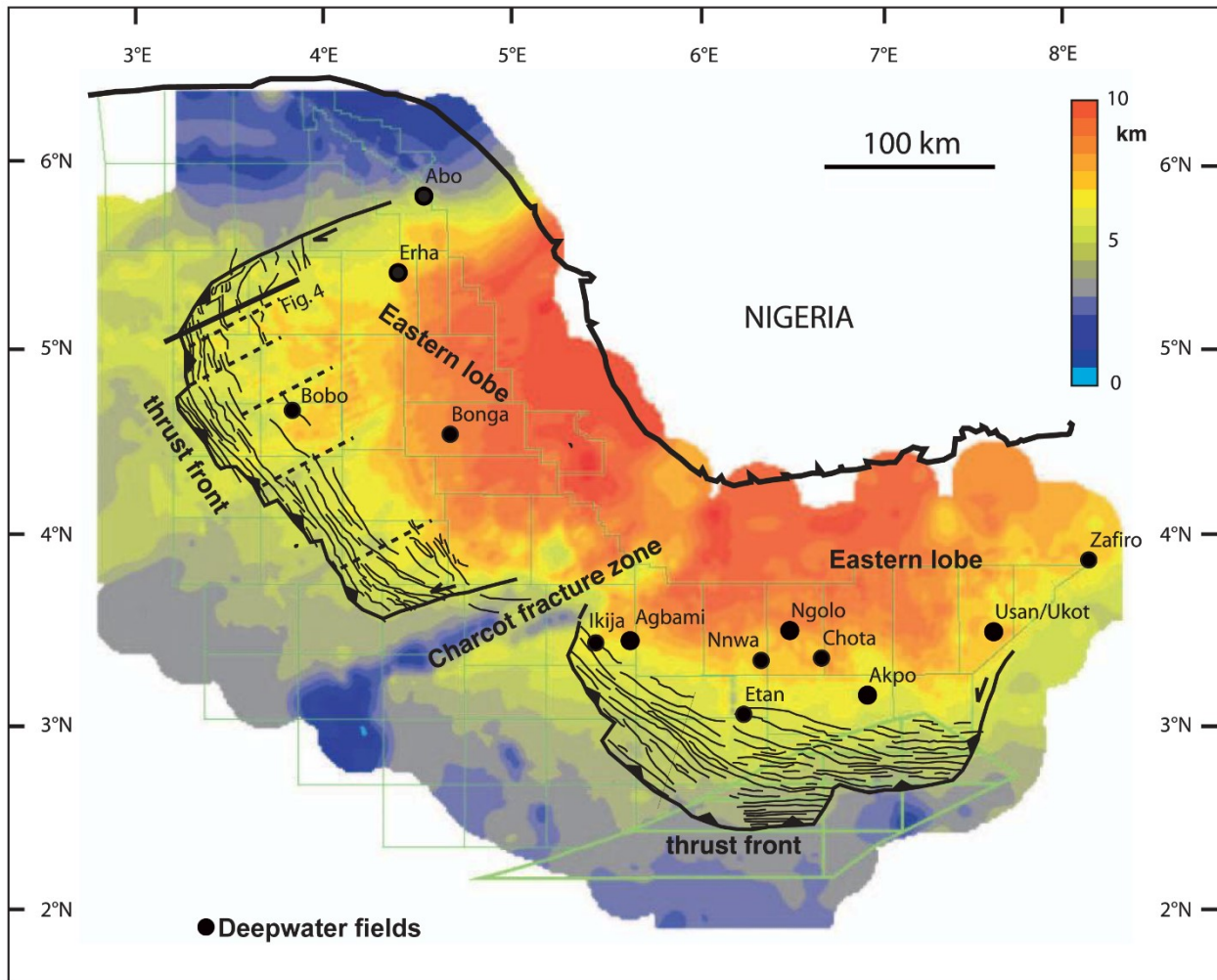
The impact of Late Quaternary glacio-eustasy and tectonics on sequence development: evidence from uplifting and subsiding settings in Italy. *Terra Nova* 22, 324-329. doi: 10.1111/j.1365-3121.2010.00953.

Zecchin, M., Catuneanu, O. 2012, High-resolution sequence stratigraphy of clastic shelves I: units and bounding surfaces. *Marine and Petroleum Geology* 39, 1-25.

Zhao, X., Qi, K., Patacci, M., Tan, C., Xie, T., 2019, Submarine channel network evolution above an extensive mass-transport complex: A 3D seismic case study from the Niger delta continental slope. *Marine and Petroleum Geology* 104, 231-248.

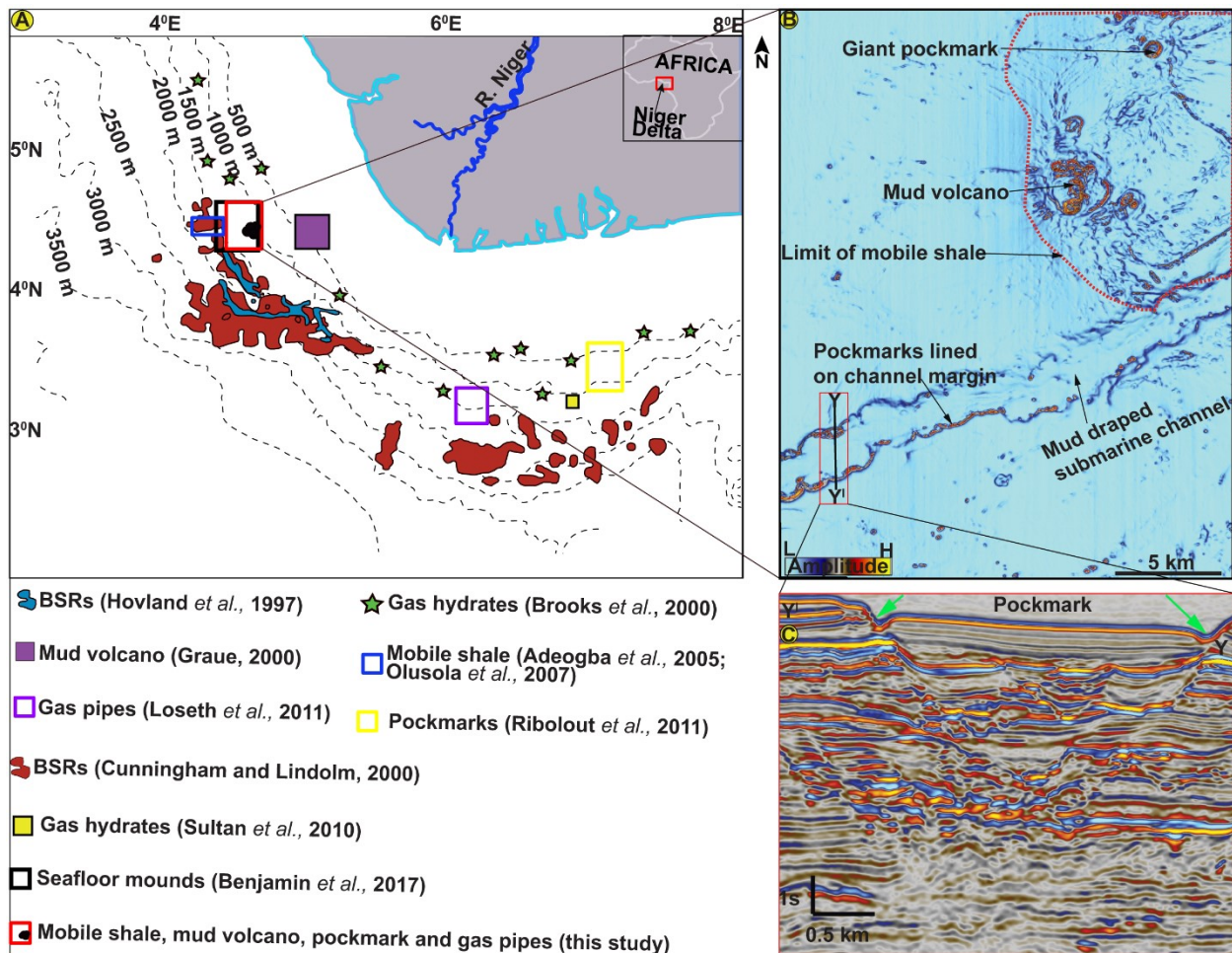
Zhang, J., Wu, S., Hu, G., Fan, T-E, Yu, B., Lin, P., Jiang, S., 2019, Sea-level control on the submarine fan architecture in a deep-water sequence of the Niger Delta Basin. *Marine and Petroleum Geology* 94, 179-197.

Appendix 1



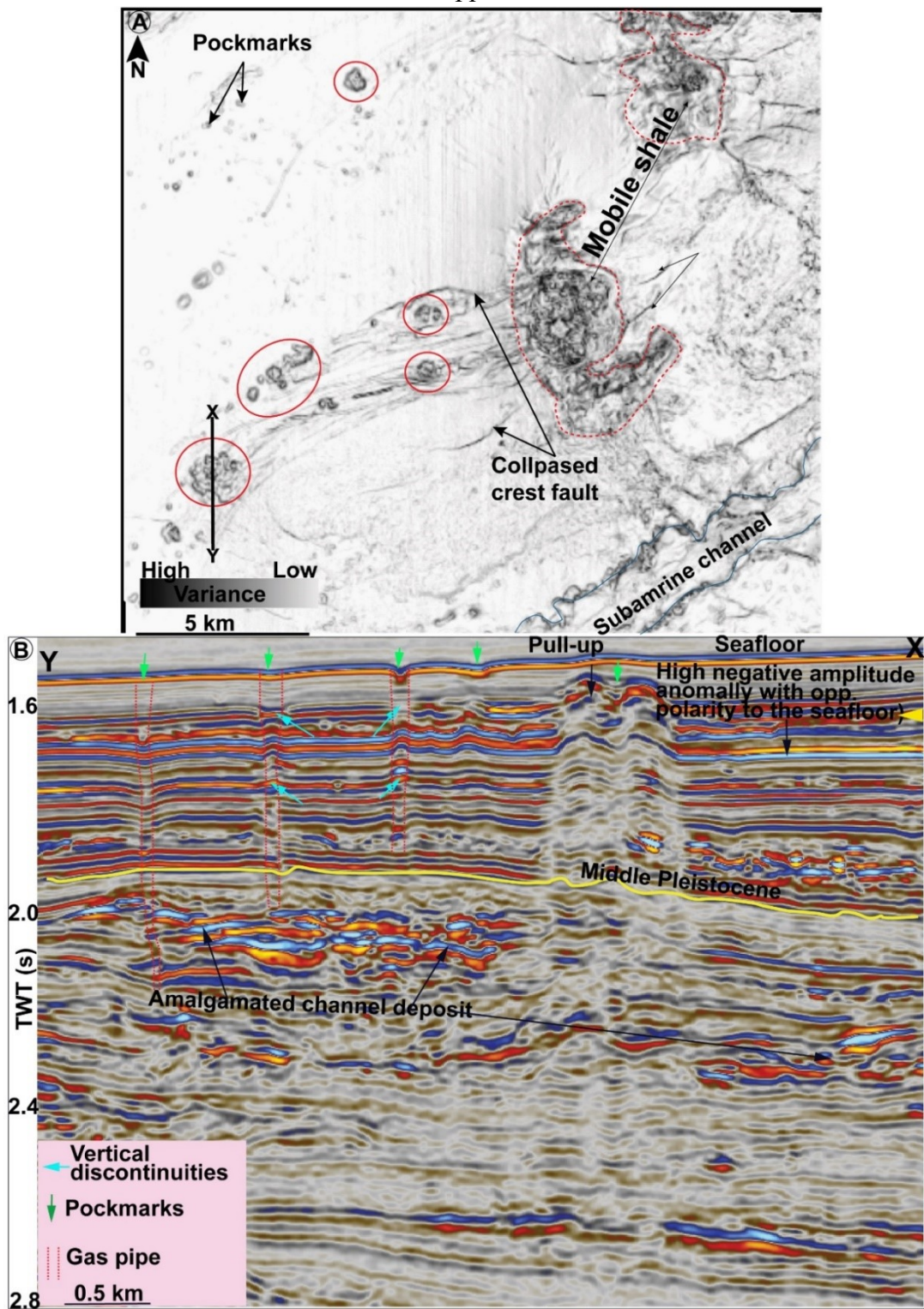
Regional thickness map of the Niger Delta showing the dominance of the currently producing deepwater fields in the eastern Niger Delta (from Cobbold *et al.*, 2009).

Appendix 2



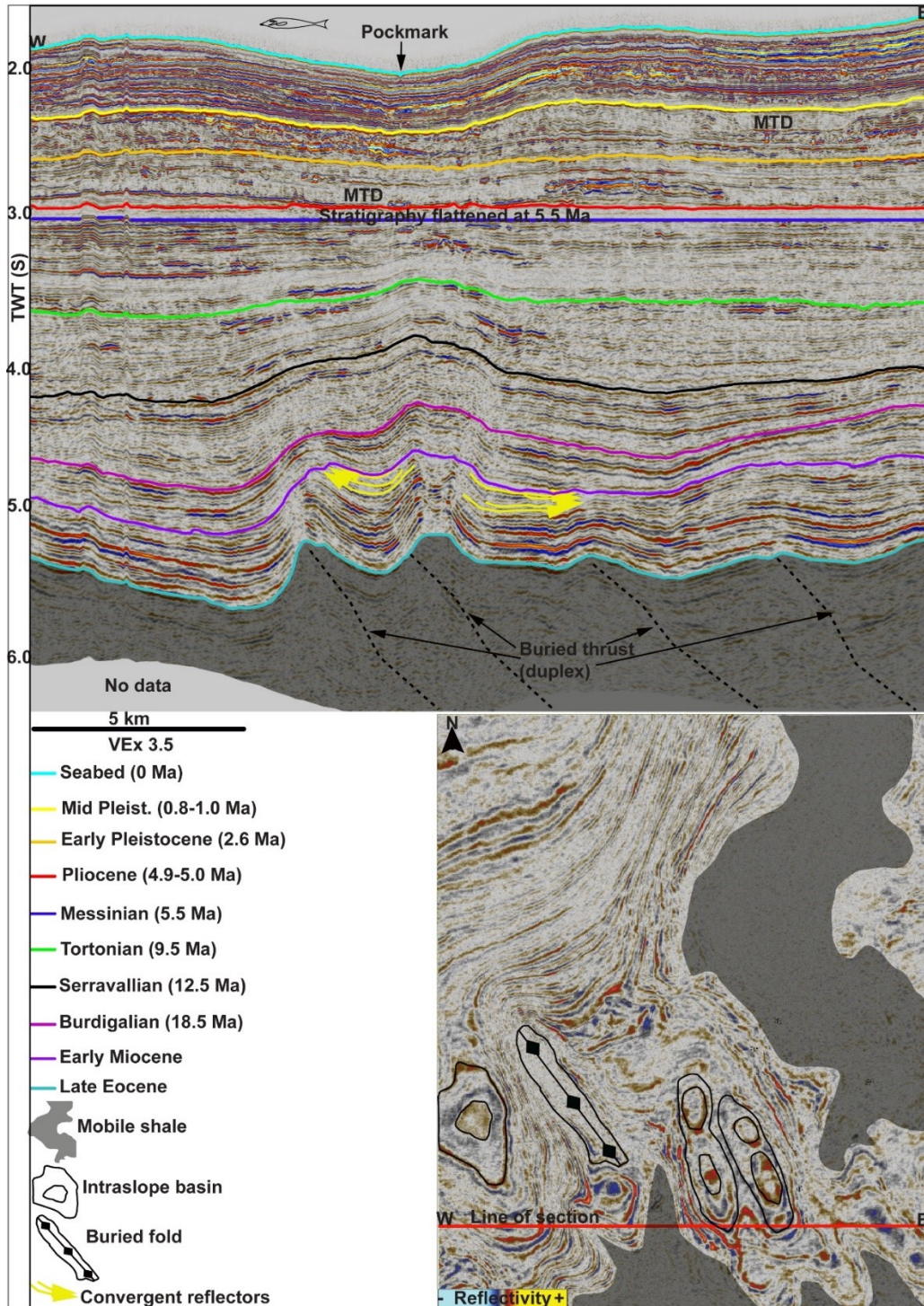
Bathymetry map of the Niger Delta showing the regional distribution of fluid-flow features in the deepwater (A); RMS amplitude map of the modern seafloor illustrating mobile shale, mud volcano and pockmarks (B); Close up of the pockmarks aligned on the margin of submarine channel (C).

Appendix 3

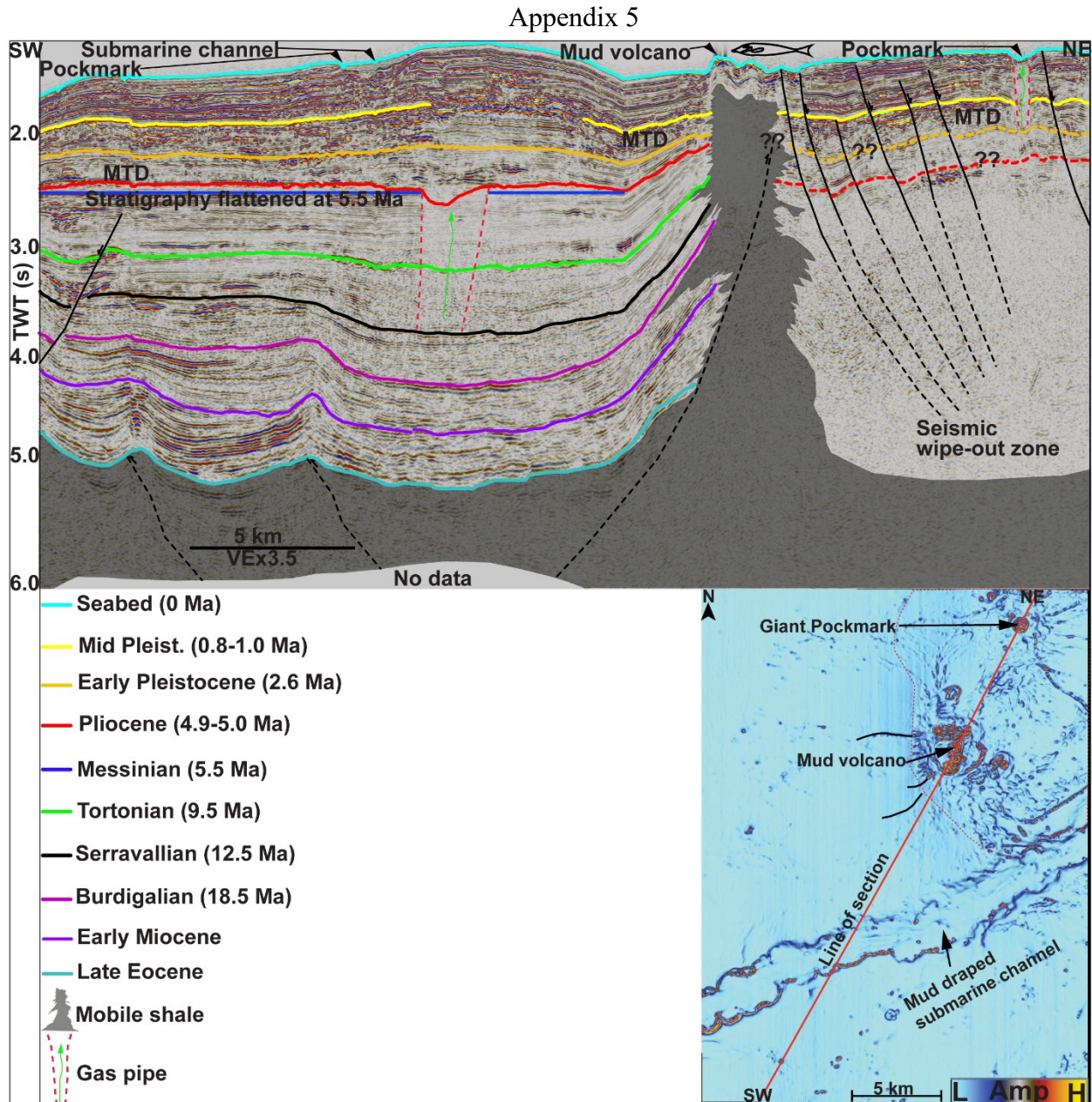


Horizon/variance attribute slice (see yellow arrow in panel B for stratigraphic level), illustrating mobile shales, pockmarks, gas pipes and pull-up zones associated with fluid flow seepage (A); Seismic illustration (YY¹) (B).

Appendix 4

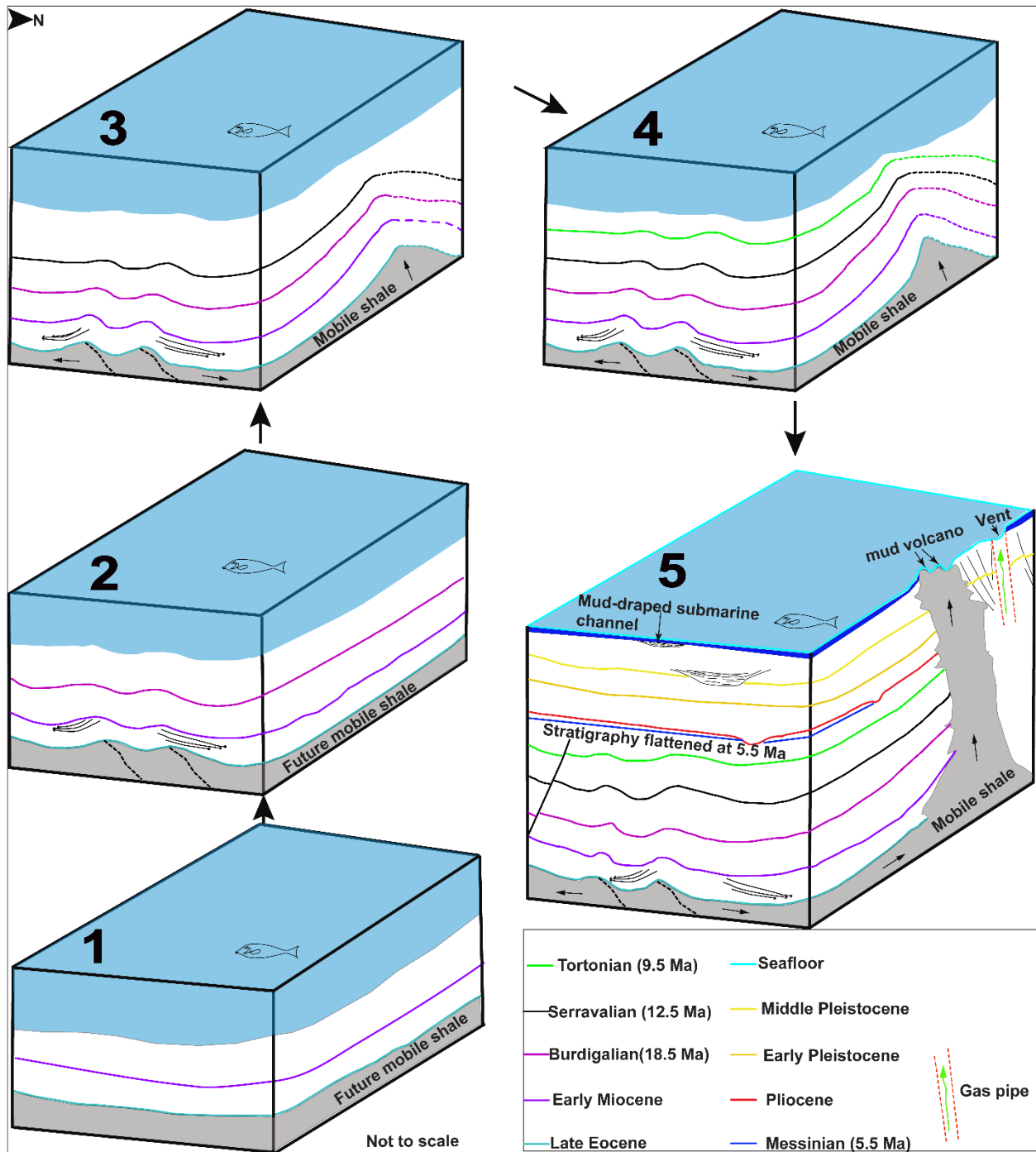


Seismic strike line (stratigraphy flattened at the base of hemipelagic drape, 5.5 Ma), illustrates a lateral variation in stratigraphic thickness linked to the onset of shale tectonics between the Burdigalian-Serravallian. Thickening within the underlying seismic units linked to duplexing.



Northeast-southwest seismic line (stratigraphy flattened at the base of hemipelagic drape, 5.5 Ma), illustrates the overall thinning of the Burdigalian-Serravallian stratigraphic Unit from the SW-NE, linked to the onset of shale tectonics. between the Burdigalian-Serravallian. Slight thickening to SW of the underlying seismic units is linked to the activity of the underlying duplexes. Note the presence of seismic wipe-out zone to the NE and central. Note also the presence of narrow vertical, seismic wipe-out zones (dashed red arrows), corresponding to gas pipes. The central gas pipe has buried while its NE counterpart (giant pockmark) is still active.

Appendix 6



Stage 1: Deposition of the first pre-shale kinematic (the late Eocene-early Miocene) Unit, above mud-rich unit (shaded in grey) in panels 1-5. The presence of convergent seismic geometries coupled with minor thickening of the late Eocene-early Miocene Unit from west to east in

(Appendix 4), and from southeast to northwest in (Appendix 5), is attributed to activity of the duplexes within the future mobile shale.

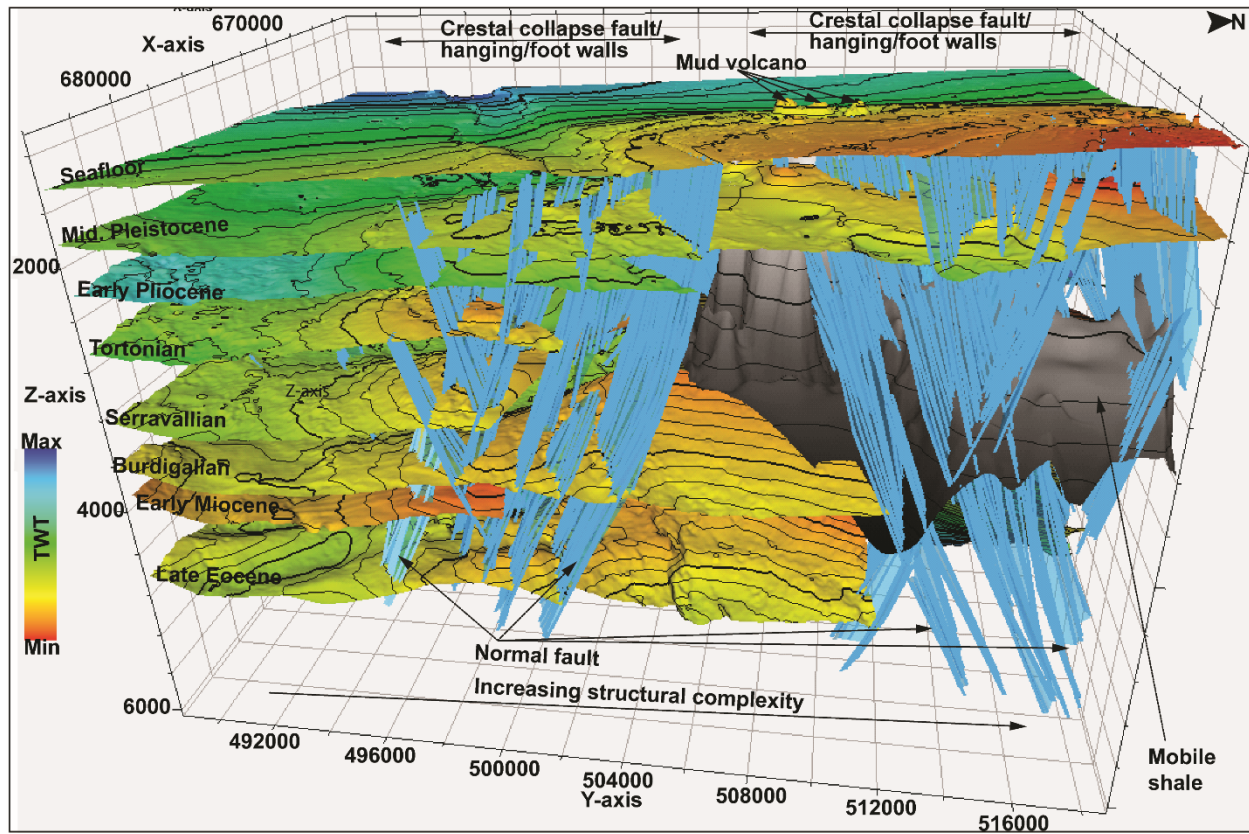
Stage 2: Deposition of the second pre-shale kinematic (the early Miocene-Burdigalian) Unit, where minor thickening in stratigraphy from the northeast to the southwest is attributed to the continued activity of the underlying duplexes.

Stage 3: Onset of mobile shale activity following the deposition of the Burdigalian-Serravallian Unit, characterized by lateral variation in stratigraphic thickness (Appendix 4) and remarkable thinning from the southwest, towards the active mobile shale in the northeast (Appendix 5).

Stage 4: Continued mobile shale activity evidenced by lateral variation in stratigraphic thickness (Appendix 4) and overall thinning of the Serravallian-Tortonian Unit towards mobile shale in the north (Appendix 5).

Stage 5: The overall thinning of the Tortonian-Pliocene and the early Pliocene-middle Pleistocene Units from southwest to northeast (Appendix 5; Figs. 3.3A, B), the deflection of erosional submarine channel from the north (stage 2 in Fig. 3.11B) towards the south (stage 3 in Fig. 3.11B), the overall increase in the gradient of channel levee system downstream of mobile shale within the middle Pleistocene stratigraphy (Fig. 3.11B) and the presence of mud volcanoes on the modern seafloor (Appendices 5, 6, 7; Figs. 2.5A, B, 3.3AB), all support the activity of the mobile shale from the Tortonian to present.

Appendix 7



3-D perspective view of horizons and faults within 3D block coverage (see Fig. 4.1A), illustrating structural configuration with an overall increase in structural complexity from south to north toward mobile shale zone in the north (vertical mound highlighted in grey). Note the presence of mud volcanoes on the modern seafloor. The mobile shale could not be confidently interpreted beyond 3.7 s due to acoustic blanking.